HAL
open science

Thermodynamic and structural investigations on the interactions between actinides and phosphonate-based ligands

Gaoyang Ye

To cite this version:

Gaoyang Ye. Thermodynamic and structural investigations on the interactions between actinides and phosphonate-based ligands. Radiochemistry. Université Paris-Saclay, 2018. English. NNT : 2018SACLS286 . tel-02169209

HAL Id: tel-02169209

https://theses.hal.science/tel-02169209

Submitted on 1 Jul 2019

HAL is a multi-disciplinary open access archive for the deposit and dissemination of scientific research documents, whether they are published or not. The documents may come from teaching and research institutions in France or abroad, or from public or private research centers.

L'archive ouverte pluridisciplinaire **HAL**, est destinée au dépôt et à la diffusion de documents scientifiques de niveau recherche, publiés ou non, émanant des établissements d'enseignement et de recherche français ou étrangers, des laboratoires publics ou privés.

université PARIS-SACLAY

NNT : 2018SACLS286

Thèse de doctorat

UNIVERSITÉ PARIS SUD

Comprendre le monde, construire l'avenir

Thermodynamic and structural investigations on the interactions between actinides and phosphonate-based ligands

Thèse de doctorat de l'Université Paris-Saclay
Préparée à l'Université Paris-Sud

École doctorale n°576 Particules Hadrons Energie et Noyau : Instrumentation, Image, Cosmos et Simulation (PHENIICS)
Spécialité de doctorat: Aval du cycle nucléaire, Radioprotection et Radiochimie

Thèse présentée et soutenue à Orsay, le 19 septembre, par

Gaoyang YE

Composition du Jury :

M. David Aitken Professeur, Université Paris-Sud	Président
M. Jean Aupiais Professeur, CEA/DAM bruyère le Chatel	Rapporteur
M. Gilles Montavon Professeur, SUBATECH - MINES Nantes	Rapporteur
M. Loic Charbonniere Professeur, CNRS Strasbourg	Examinateur
M. Christophe Den Auwer Professeur, Université de NICE	Examinateur
M. Wangsuo Wu Professeur, University of Lanzhou	Examinateur
M. Eric Simoni Professeur, Université Paris-Sud	Directeur de thèse

Acknowledgement

This thesis work was done at l'institut de physique nucléaire d'orsay in the group of Radiochemistry, Université Paris-Sud.

This work was funded by Chinese Science council.

I want to thank in the first place my thesis director Eric Simoni for the trust he has given me throughout these three years, for enlightened advice whether at the lab or for the project. Thank you for your patience and your availability.

I would like to thank Gilles Montavon and Jean Aupiais who accepted to be rapporteurs of my work, Loic Charbonniere, Christophe Den Auwer, Wangsuo Wu and David Aitken for having accepted to participate in my thesis jury.

I would also like to thank the groupe of Synthèse Pour l'Analyse (SynPA) and more particularly Câline Christine and Alexandre Lecointre for the advice on organic synthesize, Raphael Gillet, Soumaya Khalfallah and Mohamadou Sy for the French language training, Anne Boos and Jérémy Brandel for your kindles help for the ligand characterization.

I would like to thank l'équipe de Radiochimie Humaine et Environnementale (RHE). Special mention for Gaëlle, thank you for your support and your advice that often allowed me to avoid the traps of the IR,

Many thanks for the help on EXAFS study of Jérome Roques (Groupe Radiochime), Christophe Den Auwer (RHE) and Pier-Lorenzo Solari as well as to the members of the MARS line.

I also thank my 'greater groupe radiochime family': Florian Brulfert, Davide Rodrigues, Thi-Kim-Khanh Le, Gabriela Duran-Klie, Quentin Le Moëne, Céline Cannes, Sylvie Delpech, Romuald Drot, Elisabeth Seibert, Vladimir Sladkov and Véronika Zinovyeva, as well as Mingjian He, Thanks to you, these three years are filled with good memories. I would also like to express my thanks to Nicole Barre-Boscher, who help me fixed the instrument problem.

Finally, I thank my family and friends for supporting me during these three years. First of all, my sincere gratitude to my parents who encouraged and advised me throughout my studies. I also thank to my friends to eat and drink together sometimes to pass the hard time.

Content

General introduction 4

Chapter 1: Bibliographic study

1 Conception of actinides decorporation 8
2 General introduction of actinides 8
2.1 Generality 8
2.2 Uranium 9
2.2.1 Uranium in the industry and environment 9
2.2.2 Physic-chemical properties of uranium 11
2.3 Americium/curium 12
2.3.1 Americium/curium in the industry and environment 13
2.3.2 Physic-chemical properties of americium and curium, europium use as the chemical analogue 13
3 Toxicology 16
3.1 The contamination mode 16
3.1.1 Main entry routes 17
3.1.2 Main excretion routes 18
3.2 The factor which influences the toxicity 19
3.3 The bio-distribution of actinides 19
3.3.1 Uranium 21
3.3.2 Americium/curium 22
3.4 Human Health Effects 23
3.4.1 Uranium 23
3.4.2 Americium/curium 24
3.5 Conclusion 24
4 Chelation therapy 24
4.1 Actinides chelating agents under studies 26
4.1.1 The poly-amino-carboxylic ligands 27
4.1.2 Siderophores analogues: CAM & HOPO 28
4.1.3 Phosphonate ligands 31
4.2 Methods for *in vitro* study 34
4.3 Conclusion 34
5 Chelation study for biology simulation with calmodulin 35
5.1 Description of the protein 35
5.2 Interaction between calmodulin and calcium 36

5.3 Interactions between calmodulin and actinides 37

Chapiter 2: synthesis of polyaminophosphonates ligands

1 General strategy 42
2 Synthesis of precursor 42
2.1 Synthesis of pyridinic platform 43
2.2 Synthesis of amine monophosphonate 43
3 Synthesis of bisphosphonate ligand L^1 44
4 Synthesis of bisphosphonate ligand L^2 44
5 Synthesis of bisphosphonate ligand L^3 45
6 Conclusion 47
7 Experimental part 48

Chapiter 3: structural and thermodynamic study of uranyl with polyaminophosphonates ligands

1 Acid-base properties of polyaminophosphonates ligands 56
1.1 Potentiometric study 56
1.2 Spectrophotometric study according to the pH 60
1.3 Conclusion 62
2 Uranium/ligands interactions studied by Time-resolved laser fluorescence spectroscopy (TRLFS) and UV-visible spectroscopy 62
2.1 Time-resolved laser fluorescence spectroscopy (TRLFS) and UV-visible spectroscopy 62
2.2 Experimental conditions selection 62
2.3 Solubility test with uranyl-ligand complex 63
2.4 Stability test with uranyl-ligand complex for sample preparation 64
2.5 Stability test of uranyl-ligand complex with TRLFS 69
2.6 Study of uranyl-ligand complex 72
2.7 Conclusion 77
3 IR characterization of two ligands with uranium in aqueous solution 77
3.1 IR spectra of ligands 77
3.2 IR spectra of uranyl-ligand complexation 80
3.3 Conclusion 83
4 Structural study of uranyl-ligand complexes 83
4.1 Possible structure of uranyl-ligand complexes 83
4.2 Possible structure optimized by DFT 83
4.3 EXAFS data analysis 86
4.4 EXAFS data analysis of the uranyl-ligand complex 86
4.4.1 Uranyl-ligand study at pH 3 86

4.4.2 Uranyl-ligand study at pH 7.4 88
4.4.3 Comparison of uranyl-ligand study at two pHs 91
4.5 Conclusion 91
5 Thermodynamics study by displacement titration 92
5.1 Fast screening 92
5.2 Determination of the ligand complexation constants 93
6 Selectivity study with cation 95
7 Chelation affinity of ligand towards Calmodulin - uranyl complex 96
8 Conclusion 98

Chapiter 4: thermodynamic study of uranyl with polyaminophosphonates ligands

1 Thermodynamics study of europium-L^3 complex 102
2 Europium/ligands interactions studied by Time-resolved laser fluorescence spectroscopy (TRLFS) and UV-visible spectroscopy 103
2.1 Experimental conditions selection 103
2.2 Study of europium-ligand complexes 104
2.3 Conclusion 107
3 IR characterization of two ligands with europium in aqueous solution 108
3.1 IR spectra of europium -ligand complexation 108
4 Structural study of europium-ligand complexes 109
4.1 Possible structure of europium-ligand complexes 109
4.2 Possible structure optimized by DFT 109
4.3 EXAFS data analysis of the europium-ligand complex 111
4.3.1 Eu-L^3 complex study at pH 3 111
4.3.2 Eu-L^4 complex at pH 7.4 112
5 Conclusion 112

Chapter 5: General conclusion

General conclusion 116
Perspectives 117

Appendix I: materials

1 Experiment conditions 119
2 Preparation of stock solutions 119

Annexe II: Experimental methods

1 Potentiometry 121
1.1 Preparation of solutions 121
1.2 Potentiometric titrations 121

2 UV-visible spectrophotometry 122
2.1 Titration for free ligand L^3 species 122
2.2 Displacement titration of uranyl-ligand complex 122
2.2.1 The solutions 122
2.2.2 Procedure for the fast screening 122
2.2.3 Procedure for the titration 122
3 Time-resolved laser fluorescence spectroscopy (TRLFS) 123
3.1 Principle 123
3.2 Luminescence property of europium 124
3.3 Luminescence properties of uranium 125
3.4 Instrumentation 126
3.5 Samples 126
4 ATR-IR Spectroscopy 126
4.1 Principle 126
4.2 General 127
4.3 IR measurements of the uranyl-L^3 complex 127
4.4 IR measurements of the uranyl-L^4 complex 127
4.5 IR measurements of the Eu-ligand complex 128
5 Functional Theory of Density (DFT) 128
6 EXAFS Spectroscopy 128
6.1 The uranyl-L^3 complex sample for EXAFS measurements 128
6.2 The uranyl-L^4 complex sample for EXAFS measurements 129
6.3 The Eu-ligand complex sample for EXAFS measurements 129
Annexe III: Thermodynamic data 130
Reference 131
Résumé 131

Table of illustrations

Figure 1 : periodic table of actinide elements[17] 8

Figure 2 : illustration of nuclear fuel cycle[20] 10

Figure 3 : Pourbaix diagram of uraniumin a non-complexing aqueous medium calculate by Hydra/Medusa Chemical Equilibrium Database and Plotting Software. [U]= 10 **µM**; T=25.0 °C. 11

Figure 4 : Pourbaix diagram of americium a non-complexing aqueous medium. [Am]= 10E-10 **M**; T=25.0 °C.[29] 14

Figure 5 : Cohesive energy for the rare earths (full. curves) and actinides (dashed curves). The smooth curves denote the cohesive energy in case these elements had remained divalent in their metallic modification, the jagged curves the cohesive energy of their trivalent metallic state.[36] 16

Figure 6 : The main routes of intake, transfer and excretion of radionuclides in the body (ICRP 130). 17

Figure 7 : Uranium particles during inhalation contamination (ICRP 66). 17

Figure 8 : Systemic model of the bio-distribution of uranyl ion in human body (ICRP 72). .. 22

Figure 9 : Systemic model of the bio-distribution of the bone-surface seekers, americium and curium, in human body (ICRP 72). 23

Figure 10 : Structures, abbreviated names, and pKa values of metal-binding units of different chelation ligands. Carboxylic acid; phosphoate acid; catecholate (CAM); hydroxypyridinonate (HOPO). 25

Figure 11 : Chemical structure of EDTA and DTPA. 27

Figure 12 : Binding unit's structures and abbreviated names of siderophores. catecholate (CAM); hydroxypyridinonate (HOPO). 29

Figure 13 : Crystal structures of uranyl 5-LIO(Me-3,2-HOPO) complex[107] and Gd(III) 30

Figure 14 : chemical structures of 3,4,3-LI(1,2-HOPO), 5-LIO(Me-3,2-HOPO) and 5-LICAM(S). 30

Figure 15 : Structure of phosphonate group and bisphosphonate group. 31

Figure 16 : Structure of 1-hydroxyethane-1,10-diphosphonic acid (HEDP), three bisphosphonate sequestering ligands (2H, 3C, 7B) and polyaminophosphonates ligand (L^4).[75] 32

Figure 17 : Proposed Structure of the Uranyl-HEDP Complex. 32

Figure 18 : Example of displacement method: Displacements (%) of the uranyl SCP complex are presented in a color-coded format for clarity reason. $\log K_{cond}$ (estimates) were calculated by using the HYSS program supposing that the complex competitive uranyl/ligand is 1:1.[123] 33

Figure 19 : Structure illustration of actinides chelation agents 35

Figure 20 : Schematic of the calcium binding site 1 of Paramecium tetraurelia calmodulin.[146] 36

Figure 21 : Fractional species calculation for **Cax2** +(calmodulin) as a function of [Ca^{2+}]. The total calmodulin concentration is 15**µM**.[155] 37

Figure 22 : Theoretical models and electronic density of the U(VI) interaction sites on the CaMWT calculated by DFT (oxygen: red, carbon: blue, nitrogen: light green, uranium: yellow and neptunium: dark green).[151] 38

Figure 23 : Chemical structure of ligands L^1, L^2, $L^3$and L^4. 42

Figure 24 : Chemical structure of precursors. 43
Figure 25 : ^{1}H RMN spectrum of ligand L^2 (D_2O, 400 MHz, t.a.). 46
Figure 26 : ^{13}P RMN spectrum of ligand L^2 (D_2O, 161.9 MHz, t.a.). 47
Figure 27 : Chemical structures of ligands L^2 and L^3 (fully deprotonated forms). 56
Figure 28 : Potentiometric curve of ligand L^3. Solvent: H_2O; I = 0.1 M ($NaClO_4$); T = 25.0(2) °C; $[L^3]_{tot}$ = 8.168E-4 M. 56
Figure 29 : Chemical structure of the analogue pyridine tetracarboxylate (noted L^C). 57
Figure 30 : Distribution curves of protonated species of ligands L^2, L^3 and L^4. Solvent : H_2O; T = 25,0 °C ; I = 0.1 M ($NaClO_4$) ; $[L_2]_{tot}$, $[L_3]_{tot}$ and $[L_4]_{tot}$ = 1E-4 M. 60
Figure 31 : Spectrophotometric titration of L^3 as a function of pH. Solvent: H_2O; T = 25.0 (2) °C; I = 0.1M ($NaClO_4$); l = 1 cm; $[L^3]$ tot = 1.02E-4 M. 61
Figure 32 : Electronic spectra of the protonated species of ligand L^3. Solvent: H_2O; T = 25.0 (2) °C; I = 0.1M ($NaClO_4$); l = 1 cm. 61
Figure 33 : Species diagram of uranyl ion; [U] = 5E-5 M in 0.1M $NaClO_4$. 63
Figure 34 : Fluorescence study of uranyl in each ionic solution at different pH; a [U] = 5E-5 M, pH 3, 0.1M NaCl; b [U] = 5E-5 M, pH 7.4, 0.1M NaCl; c [U] = 5E-5 M, pH 7.4, 0.1M $NaClO_4$. 64
Figure 35 : Study of uranyl-L^3 complex, absorption measure (left); TRLFS measure (right); $[L^3]$ = 5E-5 M, [U] 0-1 eq, pH 3, 0.1M NaCl. 65
Figure 36 : Study of uranyl-L^3 complex, absorption measure (left); TRLFS measure (right); $[L^3]$ = 5e-5 M, [U] 0-1 eq, pH 7.4, 0.1M $NaClO_4$. 65
Figure 37 : Study of uranyl-L^3 complex, absorption measure (left); TRLFS measure (right); $[L^3]$ = 5e-5 M, [U] 0-1 eq, pH 7.4, 0.1M NaCl. 66
Figure 38 : Steps in the photocatalyzed H-atom abstraction from hydrocarbons by the uranyl dication.[189] 66
Figure 39 : HPLC chromatograms of air-saturated solutions of 0.5 mM $\mathbf{UO22+}$ and 5 mM $PhCH_3$ in 0.01M H_3PO_4 after irradiation with visible light in 15 min intervals. The monitoring wavelength was 254 nm.[193] 67
Figure 40 : Plot showing increase in [PhCHO] with irradiation time. Data from Figure 13.[193] 67
Figure 41 : Sunlight spectrum in space as a function of wavelength. Public Domain Image, image source: Christopher S. Baird, data source: American Society for Testing and Materials Terrestrial Reference. 68
Figure 42 : Solubility of oxygen in water 68
Figure 43 : Comparison of uranyl-L^3 complex by two preparation method, absorption measure (left); TRLFS measure (right); $[L^3]$ = 5E-5 M, [U] 0.8&1 eq, pH 3, 0.1M NaCl. 69
Figure 44 : Study of uranyl-L^3 complex, absorption measure (left); TRLFS measure (right); $[L^3]$ = 5E-5 M, [U] 0-1 eq, pH 3, 0.1M NaCl. 70
Figure 45 : Study of uranyl-L^3 complex under 430nm laser excitation, absorption measure (left); TRLFS measure (right); $[L^3]$ = 5E-5 M, [U] 0.8 &1eq, pH 3, 0.1M NaCl. 70
Figure 46 : Study of uranyl-L^2 1:1 complex under 430nm laser excitation, absorption measure (left); TRLFS measure (right); $[L^2]$ = 5E-5 M, [U] = 5E-5 M, pH 7.4. 72
Figure 47 : Study of uranyl-L^3 complex, absorption measure (left); TRLFS measure (right); $[L^3]$ = 5E-5 M, [U] 0-1 eq, pH 3, 0.1M NaCl. 73
Figure 48 : Evolution of the absorption ratio at 262nm (left) and the emitted intensity at 522 nm

(right) as a function of uranyl/L^3; [L^3] = 5E-5 M, [U] 0-1 eq, pH 3, 0.1M NaCl. 73
Figure 49 : Study of uranyl-L^4 complex, absorption measure (left); TRLFS measure (right); [L^4] = 5E-5 M, [U] 0-1 eq, pH 3, 0.1M NaCl. 74
Figure 50 : Evolution of the absorption ratio at 262nm (left) and the emitted intensity at 520 nm (right) as a function of uranyl/L^4; [L^4] = 5E-5 M, [U] 0-1 eq, pH 3, 0.1M NaCl. 74
Figure 51 : Study of uranyl-L^3 complex, absorption measure (left); TRLFS measure (right); [L^3] = 5E-5 M, [U] 0-1 eq, pH 7.4, 0.1M $NaClO_4$..... 75
Figure 52 : Evolution of the absorption ratio at 263nm as a function of uranyl/L^3; [L^3] = 5E-5 M, [U] 0-1 eq, pH 7.4, 0.1M $NaClO_4$..... 75
Figure 53 : Study of uranyl-L^4 complex, absorption measure (left); TRLFS measure (right); [L^4] = 5E-5 M, [U] 0-1 eq, pH 7.4, 0.1M $NaClO_4$..... 76
Figure 54 : Evolution of the absorption ratio at 263nm as a function of uranyl/L^4; [L^4] = 5E-5 M, [U] 0-1 eq, pH 7.4, 0.1M $NaClO_4$..... 76
Figure 55 : FT-IR spectra of pH in H_2O. Spectra of L^4 in red and L^3 in black. Difference spectra L^3 minus half L^4 (blue). 78
Figure 56 : FT-IR spectra of pH 7.4 in H_2O. Spectra of L^4 in red and L^3 in black. Difference spectra L^3 minus half L^4 (blue). 78
Figure 57 : FT-IR spectra of difference spectrum at pH 3(red) and 7.4(black). Difference spectra L^3 minus half L^4 at each pH. 79
Figure 58 : FT-IR spectra of L^4 in H_2O. Spectra recorded at pH 7.4 (red) and pH 3 (black). Difference spectrum pH 7.4 minus pH 3 (blue). 79
Figure 59 : FT-IR spectra of L^3 in H_2O. Spectra recorded at pH 7.4 (red) and pH 3 (black). Difference spectrum pH 7.4 minus pH 3 (blue). 80
Figure 60 : FT-IR spectra of uranyl-L^3 at pH 3 in H_2O. Spectra of uranyl-L^3 in red and L^3 in black. Difference spectrum uranyl-L^3 minus L^3 (blue). 81
Figure 61 : FT-IR spectra of uranyl-L^4 (right) at pH 3 in H_2O. Spectra of uranyl-L^4 in red and L^4 in black. Difference spectrum uranyl-L^4 minus L^4 (blue). 81
Figure 62 : FT-IR spectra of of uranyl-L^3 at pH 7.4 in H_2O. Spectra of uranyl-L^3 in red and L^3 in black. Difference spectrum uranyl-L^3 minus L^3 (blue). 82
Figure 63 : FT-IR spectra of uranyl-L^4 (right) at pH 7.4 in H_2O. Spectra of uranyl-L^4 in red and L^4 in black. Difference spectrum uranyl-L^4 minus L^4 (blue). 82
Figure 64 : Theoretical models optimized by DFT and electronic density of L^3 & L^4 interaction sites with uranyl at pH 3 (Oxygen: red, carbon: blue, nitrogen: light green, uranium: yellow). 84
Figure 65 : Theoretical models optimized by DFT and electronic density of L^4 interaction sites with uranyl at pH 7.4 (Oxygen: red, carbon: blue, nitrogen: light green, uranium: yellow). .. 85
Figure 66 : U L_{III} edge k^3–weighted EXAFS spectra (left) and the corresponding Fourier transforms (right) of the L^3-U complex (lower traces) and L^4-U (upper traces) complex formed at pH 3. The experimental spectra are given in dash line and the fits are given in line. 88
Figure 67 : U L_{III} edge k^3–weighted EXAFS spectra (left) and the corresponding Fourier transforms (right) of the L^3-U-OH complex (lower traces) and L^4-U-OH (upper traces) complex formed at pH 7.4. The experimental spectra are given in dash line and the fits are given in line. 90
Figure 68 : Theoretical models optimized by DFT and electronic density of L^3 & L^4 interaction sites with uranyl at pH 3 and 7.4 (Oxygen: red, carbon: blue, nitrogen: light green, uranium: yellow). 91

Figure 69 : Structure of three ligands. 93
Figure 70 : Screening results of three ligands; [ligand] = 8E-5 M, [SCP] = [U] =4E-5 M, HEPES buffer=12.5 mmol, [$nBu_4N^+Cl^-$] =112.5 mmol at pH 7.4. 93
Figure 71 : Competition displacement titration of uranyl-SCP complex by L^2; [SCP] = [UO] =4e-5 M, [L^2] 0-8E-4 M, HEPES buffer=12.5 mmol, [$Bu_4N^+Cl^-$] =112.5 mmol. 94
Figure 72 : Competition displacement titration of uranyl-SCP complex by L^3; [SCP] = [U] =4e-5 M, [L^3] 0-8E-4 M, HEPES buffer=12.5 mmol, [nBu_4N+Cl-] =112.5 mmol. 94
Figure 73 : Selectivity study of 1:1 uranyl-L^3 complex by Ca^{2+}, absorption spectrum (left); fluorescence spectrum (right); [L^3] = [U] =5E-5 M; [Ca^{2+}] =0-350 eq; [$NaClO_4$]=0.1 M. 95
Figure 74 : Selectivity study of 1:1 uranyl-L^3 complex by Mg^{2+}, absorption spectrum (left); fluorescence spectrum (right); [L^3] = [U] =5E-5 M; [Mg^{2+}] =0-150 eq; [$NaClO_4$]=0.1 M. 96
Figure 75 : Species diagram of Ca-UO_2-CaM complex from pH 5 to 8; [CaM] = [U] =5E-5 M; [Ca^{2+}] =2E-4 M; [$NaClO_4$]=0.1 M. 96
Figure 76 : Chelation study of L^3 towards Ca-UO_2-CaM complex, absorption spectrum (left); fluorescence spectrum (right); [CaM] = [UO_2^{2+}] =2.5E-5 M; [Ca^{2+}] =2E-4 M; [MES]=0, 1 and 5eq ; [$NaClO_4$]=0.1 M ; [MES]= 5 mmol ; pH 5.5. 97
Figure 77 : Devolution study of L^3 towards Ca-UO_2-CaM complex, 1eq L^3 (left); 5eq L^3 (right). [CaM] = [UO_2^{2+}] =2.5E-5 M; [Ca^{2+}] =2E-4 M; [MES]=0, 1 and 5eq ; [$NaClO_4$]=0.1 M ; [MES]= 5 mmol ; pH 5.5. 98
Figure 78 : Comparison of CaM spectra from two devolutions. CaM1 in black; CaM5 in red; UO2-CaM in blue. 98
Figure 79 : Chemical structures of bis-phosphonated ligand L^3 & L^{3*} and tetra-phosphonated ligand L^4 102
Figure 80 : Species diagram of europium ion, [Eu] = 5E-5 M in 0.1M $NaClO_4$ (left); [Eu] = [L^4] = 1e-4 M in 0.1M $NaClO_4$ (right). 103
Figure 81 : Study of europium-L^4 complex, absorption measure; [Eu] = [L^4] = 1E-4 M , pH 3, 0.1M $NaClO_4$. 104
Figure 82 : Study of europium-L^3 complex, absorption measure; [Eu] = [L^3] = 1E-4 M , pH 3, 0.1M $NaClO_4$. 105
Figure 83 : Study of europium-L^4 complex, absorption measure; [Eu] = [L^4] = 1E-4 M, pH 5, 0.1M $NaClO_4$. 105
Figure 84 : Study of europium-L^3 complex, absorption measure; [Eu] = [L^3] = 1E-4 M, pH 5, 0.1M $NaClO_4$. 106
Figure 85 : Study of europium-L^4 complex, absorption measure; [Eu] = [L^4] = 1E-4 M, pH 7.4, 0.1M $NaClO_4$. 107
Figure 86 : Study of europium-L^3 complex, absorption measure; [Eu] = [L^3] = 1E-4 M , pH 7.4, 0.1M $NaClO_4$. 107
Figure 87 : FT-IR spectra of europium-L^4 at pH 7.4 in H_2O. Spectra of europium–L^4 in red and L^4 in black. Difference spectrum europium-L^4 minus L^4 (blue). 108
Figure 88 : FT-IR spectra of europium−L^3 at pH 3 in H_2O. Spectra of europium -L^3 in red and L^3 in black. Difference spectrum europium−L^3 minus L^3 (blue). 109
Figure 89 : Theoretical models optimized by DFT and electronic density of L^3/Eu^{3+} with 6 H_2O at pH=3 (right) and L^4/Eu^{3+} with 1 H_2O at pH=7.4 (left) (Oxygen: red, carbon: blue, nitrogen: light green, uranium: yellow) 110
Figure 90 : Eu L_{III} edge k^3–weighted EXAFS spectra (left) and the corresponding Fourier transforms (right) of the L^3-Eu complex at pH 3. The experimental spectra are given in line and

the fits are given in dash line. 111
Figure 91 : Eu L_{III} edge k^3–weighted EXAFS spectra (left) and the corresponding Fourier transforms (right) of the L^4-Eu complex at pH 7.4. The experimental spectra are given in line. 112
Figure 92 : Chemical structures of bis-phosphonated ligand L^2 & L^3 and tetra-phosphonated ligand L^4 116
Figure 93: Chemical structures of bis-phosphonated pyridine ligand..... 118
Figure 94 : Perrin–Jablonski diagram[253] 123
Figure 95 : Energy diagram and degeneracy lift for an Ln^{3+} ion 124
Figure 96 : Partial energy diagram of Eu^{3+} ($4f^6$) showing the relative magnitude of the interelectronic repulsion (terms), spin–orbit coupling (levels) and crystal-field effects (sublevels). The downward arrows indicate the excited states $^5D_0$ and $^5D_1$ from which luminescence occurs.[254]..... 124
Figure 97 : Energy levels of the aqueous Eu ion (III) and associated transitions 125
Figure 98 : Fluorescence emission of uranyl..... 125
Figure 99 : Energy levels for a molecule. 127

List of tables

Table 1：Main treatments used in decorporation therapies versus the type of incorporation. iv, Intravenous; ip, intraperitoneal; im, intramuscular[16] 8

Table 2：Oxidation States and electronic configurations for the Actinide Elements,[18] [a]In bold font are the most stable oxidation states under aqueous conditions, and in italics are those that were obtained under very specific conditions. 9

Table 3：World uranium production from mining in tons U (*Data from the World Nuclear Association). 10

Table 4：Main isotopes of uranium. Trace: natural isotope in trace amount; syn: synthetic isotope. 11

Table 5：Main isotopes of americium. syn: synthetic isotope. 13

Table 6：Main isotopes of curium. syn: synthetic isotope. 13

Table 7：Ionic radii (Å) of Eu and Am in different coordination numbers (CN) and at oxidation states.[31,32] 15

Table 8：Main isotopes of europium. 16

Table 9：Default absorption parameters for Type F, M and S materials. 19

Table 10：Biokinetic data on actinides. Data on the distribution of Np(IV) and Np(V) in rat and mouse.[41,42] 20

Table 11：Main families of ligands tested for decontamination/decorporation of Pu ,U and Am.[5,16] 27

Table 12：Stabilities of some metal complexes relevant to therapeutic actinide removal. a Log K_{ML}, measured at 0.1 to 0.3 mol/L ionic strength and 20 to 25°C, values rounded to two significant figures. Numerical average is shown for two suitable values. Median is shown for three or more suitable values; b[80]; c[79]; d[78]; e[84]; f[83]; g[77]; h[85]; i[86]; j[82]; k[81]. 28

Table 13：pKa of the catechol and hydroxypyridinone groups.[39] 29

Table 14：Effect of a prompt injection of bisphosphonate ligands on the biodistribution and excretion of $^{233}U(VI)$. Ligands were injected ip (30 mmol/kg, molar ratio 100) 5 min after injection of 9.2 kBq of $^{233}U(VI)$; animals were sacrificed 5 days later. Data are expressed as % of injected radioactivity, discrepancies are due to rounding. Bold means are significantly different than control mean.[75] 33

Table 15：Major actinide ligands (M) present in selected in vivo human biological media.[135] 34

Table 16：Summarizes the values of the protonation constants determined by potentiometry of ligands L^2 and L^3 represented in their logarithmic form (log K_{LHx} with $1 \leq x \leq 7$). 57

Table 17：Successive protonation constant (log K_{LHx}) of derivatives polyaminophosphonates from the literature compared to data measured for L^2 and L^3. 59

Table 18：Spectral characteristics of protonated species of ligand L^3. 62

Table 19：Distances calculated by DFT for the four complexes 84

Table 20：Distances calculated by DFT for the two complexes. 85

Table 21：Description of the paths used to fit the EXAFS data of the L^3-U complex determined at pH 3. S_0^2 = 1.19; ΔE_0 = 6.50 eV. R = 0.03; $\chi^2_{i\ ln}$ = 115.8. 87

Table 22 : Description of the paths used to fit the EXAFS data of the L^4-U complex determined at pH 3. S_0^2 = 1.27; ΔE_0 = 5.67 eV. R = 0.02; $\chi^2_{i\ ln}$ = 4.35. 87

Table 23 : Description of the paths used to fit the EXAFS data of the L^3-U-OH complex determined at pH 7.4. S_0^2 = 1.20; ΔE_0 = 7.20 eV. R = 0.01; $\chi^2_{i\ ln}$ = 5.22. 89

Table 24 : Description of the paths used to fit the EXAFS data of the L^4-U-OH complex determined at pH 7.4. S_0^2 = 1.22; ΔE_0 = 3.62 eV. R = 0.01; $\chi^2_{i\ ln}$ = 27.3. 89

Table 25 : Displacements (%) of the uranyl-SCP complex with $\log K_{cond}$ (estimates) at pH 7.4 were calculated by using the HYSS program supposing that the complex competitive uranyl-ligand is 1:1. For details on the procedure, see the appendix. 93

Table 26 : Thermodynamic stability constants and protonation constants for the complexes formed with ligands L^2 and L^4 and various Ln^{III} cations along the series and corresponding values of pLn. [a] pLn values are defined by $pLn=-\log[Ln^{III}]_{free}$ at pH 7.0 for $[Ln^{III}]$=1 **µm** and [L]=10 **µm**;[242] [2] According to reference [13]. [c] Precipitationof the complexes precludes accurate determination. The hydrolysis con- stants of the free Ln^{3+} cations have been taken into account in the statistical processing ($\log K_{LaOH}$=-8.83; $\log K_{NdOH}$=-8.20; $\log K_{EuOH}$=-7.78; $\log K_{GdOH}$=-7.85; $\log K_{TbOH}$=-7.66; $\log K_{ErOH}$ =-7.54; $\log K_{LuOH}$=-7.29). 102

Table 27 : Distances calculated by DFT for the Eu-L^3 complex at pH 3 110

Table 28 : Distances calculated by DFT for the Eu-L^4 complex at pH 7.4 110

Table 29 : Description of the paths used to fit the EXAFS data of the Eu-L^3 complex at pH 3. S_0^2 = 1; ΔE_0 = 4.69 eV. R = 0.01; $\chi^2_{i\ ln}$ = 23.6 111

Table 30 : Formation constant which used in this study 130

General introduction

During the military and industrial application of enriched uranium in the middle of the 20th century, the properties of uranium, plutonium and most of the fission product were not well studied. The large amount of radioactive materials which produced in this period could be considered equal to tons of radium[1].Therefore, with the development of nuclear energy industry, especially industrial accidents (Mayak, Chernobyl, Fukushima), the manipulation and accumulation of actinides lead to consider the dispersion, fate and health effect of these radioactive materials[2–4]. Nowadays the contamination is still happened for the nuclear workers, scientist and soldiers.[5]

After an external or internal contamination, the solubilized actinides could be distributed to the target organs *via* the bloodstream. Uranium, which is in $[UO_2]^{2+}$ form and americium/curium, which are in Am^{3+} and Cm^{3+} form, preferentially transfer to the skeletal, liver and kidneys tissues and are retained at these target organs. Due to the chemo-toxicity and radio-toxicity of these elements, the acute effect on health could cause death and the long-term effect could result in cancer, anemia and necrosis[6].

In order to limit sequence damage to organs by promoting the actinides excretion, chelating agents was used to serve this purpose. Diethylenetriaminepentaacetic acid (DTPA) presents particularly affinity towards actinides(IV), and it is currently used in clinics in case of contamination[7,8]. Polyphosphonates (HEDP[9]) is also used in clinics for uranium(VI) decorporation. 3,4,3-Li(1,2-HOPO), a siderophore derivative under investigation, has shown strong affinities for actinides (III), (IV), (V) and (VI)[10,11]. With the development of actinide chelating agents, several properties for agents are enrolled to have strong affinity and selectivity towards actinides, low toxicity, high excretion rate, etc.

The decorporation agents are toxic because of both the nature of ligand and the large amount injection for chelation therapy in a biological medium. Essential elements such as iron and calcium are also chelated just like actinides considering the concentration of essential elements. Therefore, good molecular designs are required for several important aspects among the other demands: 1) to distribute the chelating agents to the target organs; 2) to excrete the complex of target toxic element with chelating agents by urine or bile; 3) high selectivity and binding affinity with the target toxic element over the other metal ion to decrease the injection amount of chelating agents. The polyaminophosphonates ligands in this study are originally designed for magnetic resonance imaging (MRI) contrast and Single-Photon Emission Computed Tomography (SPECT) study[12,13]. From the ^{99m}Tc ligand complex SPECT study, a large amount of ^{99m}Tc with four phosphonate groups ligand could be fast excrete and part of the complex accumulated in bone tissues after 4 h. While for ^{99m}Tc with two phosphonate groups ligand complex, due to the more lipophilic character, fast excretion and much less retention in the joints could be found. And lanthanides could forms tight binding with four phosphonate groups ligand with similar high stability constants like DOTP[14], the phosphonated analogue of DOTA, than those with DOTA[15]. The coordination of lanthanides by the four phosphonate groups ligand is composed by 1 nitrogen atom from pyridine group, 2 nitrogen atoms from amine parts, 4 oxygen atoms from phosphonate groups and 1 oxygen atom from water molecular. Meanwhile two of the methylene-phosphonate groups are lie close to that plane of the pyridyl fragment and form 5 coordination at equatorial planar, the other two methylenephosphonate groups are placed above and below the mean plane of the pyridyl fragment.[13] Due to the similarity of actinides ligand complex with ^{99m}Tc ligand complex and lanthanides ligand complex, we supposed the possible bio-distribution and excretion of four phosphonate groups ligand and two phosphonate groups ligand will show similar behaviors with the complex of ^{99m}Tc with ligands. According to the molecular design, high selectivity and binding affinity with actinides could be reached. Therefore the potential application on chelation therapy should be promising.

This thesis project is a preliminary investigation on the polyaminophosphonates ligands, a series ligand designed for MRI contrast and SPECT agents, to chelate the actinides which are deposited in the target organs in order to increase their excretion.

This PhD work has focused on the synthesis of polyaminophosphonates ligands and on the structural and affinity study of the complexes form with uranium(VI) and europium(III) as americium/curium(III) analogue. The sphere of coordination of these cations could be observed by UV-visible spectroscopy, TRLFS, FT-IR and Extended X-Ray Absorption Fine Structure (EXAFS).The affinity study will be done with UV-visible spectroscopy, and in the case of europium complexes, potentiometry measurement could be done in addition. Finally, the UV-visible spectroscopy and TRLFS will be used to test the stability of uranyl ligand complex with competition metal ion in biology conditions and to reveal the interaction between the ternary system, uranyl ion, ligand, calmodulin.

This project was conducted as following:

- Synthesize polyaminophosphonates ligands which capable to complex uranium (VI) and americium/curium(III) in a biological medium.
- Characterize the structures of uranyl ligand complex formed by synthesized polyaminophosphonates ligands. Estimate affinities of these uranyl ligand complexes to compare with 5-LICAMS and 3,4,3-LI(1,2-HOPO), which have good potential application on chelation therapy. Competition mechanisms study with uranyl calmodulin complex and ligand and with uranyl ligand complex and competition metal ion will be done to reveal possible effect in biology conditions.
- Characterize the structures of europium, as the americium/curium analogue, ligand complex formed by synthesized polyaminophosphonates ligands.

This dissertation is articulated around four chapters:

The first chapter is devoted to the description of the fate and health effect of actinides, uranium (VI) and americium/curium(III), in the human body. The actinide chelation agent current and those in development are also referenced.

The second chapter details the synthesize of polyaminophosphonates ligands which designed for decorporation of actinides, uranium (VI) and americium/curium(III), that we wish to have a strong affinity with actinides.

The third and fourth chapters will focus on the study of the affinity between the protein and the metals of interest (UV-visible spectroscopy, TRLFS and FT-IR) and on the determination of the coordination sphere of the uranyl ions and europium(IV) when they are complexed by synthesized polyaminophosphonates ligands (EXAFS and DFT calculations). Once the complexation proved and the sphere of coordination of the metals defined, the simulation test in biology conditions will be done with uranyl calmodulin complex to determine the chelation affinity of ligand and with uranyl ligand complex and competition metal to test the complexation stability.

A conclusion of this work proposing a reflection on the applicability of this strategy based on polyaminophosphonates ligands will be approached to define and present the numerous problems that remain to be solved.

The appendixes grouped at the end of the manuscript are related to the preparation of the solutions and the description of the principles of each experimental technique used.

Chapter 1: Bibliographic study

Conception of actinides decorporation

Decorporation is the method which is dedicated to remove the radioactive and toxic elements which has been incorporated in target organs from human body. The main treatments used in decorporation therapies were listed in table 1 concerninig actinide contamination. However, in reality, this strategy faces many obstacles: often difficult to transfer to the target organ, hard to withdraw radioactive and toxic elements deposited in the target organ, related to the complexity of a living organism. In practice, a very good *in vitro* ligand can be totally ineffective, and sometimes even harmful, *in vivo* evaluations.

Type of incorporation	Treatment
Inhalation	Lung washing Blood chelation (iv, ip, im)
Ingestion	Gastric dressing Precipitation Purge
Wound	Washing Surgical excision, dressing Blood chelation (iv, ip, im)

Table 1：Main treatments used in decorporation therapies versus the type of incorporation. iv, Intravenous; ip, intraperitoneal; im, intramuscular[16].

Thus to better understand and investigate effective methods to remove actinides deposited in human body, three fundamental aspects related with this question need to be studied: the chemical and physical properties of actinides (uranium and americium/curium in this study); the toxicology of actinides (uranium and americium/curium in this study); countermeasures after contamination (chelation therapy in this study).

For this project, we focus on synthesis chelation ligands for uranium and americium/curium by using europium as the chemical analogue.

General introduction of actinides

1.1 Generality

The actinide elements are the 15 chemical elements with atomic numbers 89 through 103 which are naturally occurring or artificial metallic elements (Fig. 1). The first member of actinide elements is actinium and the last member is lawrencium. The generation of these radionuclides mainly comes from accelerator driven, nucleo-synthesis, nuclear weapon development, decayed isotopes and civilian nuclear power plants. Owing to the radioactivity, actinides can be used as fuels in nuclear plants, leading to lanthanide isotopes and trans-uranium elements as the fission products in spent fuels.

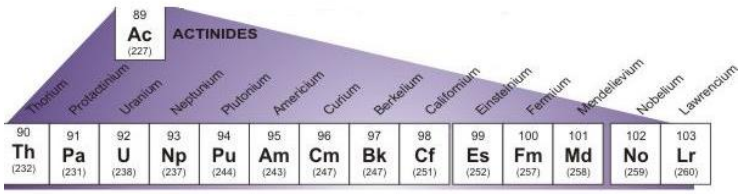

Figure 1： periodic table of actinide elements[17].

The chemical properties of actinide elements are governed by their outermost electronic

subshells. The actinides are the transition elements that fill the 5f subshell (Table 2). Hence there are some unique properties for actinide:

- All actinide isotopes are radioactive;
- The radii of actinides and actinide cations are very large;
- Many of the actinide elements have a large number of oxidation states.

element	Electronic configuration outside the [Xe] core		low oxidation	high oxidation	very high oxidation
	An	An^{3+}	states	states	states
Ac	$6d^17s^2$	$5f^0$	**III**		
Th	$6d^27s^2$	$5f^1$	**IV**		
Pa	$5f^26d^17s^2$	$5f^2$	IV	**V**	
U	$5f^36d^17s^2$	$5f^3$	III, IV	V, **VI**	
Np	$5f^46d^17s^2$	$5f^4$	III, IV	V, **VI**	VII
Pu	$5f^67s^2$	$5f^5$	III, **IV**	V, VI	VII, *VIII*
Am	$5f^77s^2$	$5f^6$	**III,**IV	V,VI	*VII*
Cm	$5f^76d^17s^2$	$5f^7$	**III**,IV		
Bk	$5f^97s^2$	$5f^8$	**III**,IV		
Cf	$5f^{10}7s^2$	$5f^9$	**III**,IV		
Es	$5f^{11}7s^2$	$5f^{10}$	II,**III**		

Table 2：Oxidation States and electronic configurations for the Actinide Elements,[18] [a]In bold font are the most stable oxidation states under aqueous conditions, and in italics are those that were obtained under very specific conditions.

For the biological point of view, actually actinides are the chemical elements which have no essential or beneficial for life. Due to the radioactivity (radio-toxic) and chemical behavior (chemo-toxic), the actinides are considered toxic. However at normal environmental levels, this toxicity could be managed by human body itself, by excretion and/or retention of the metal in a biochemically inactive form. But the nuclear weapon tests and industrial exploitation of the actinides with actinides, mainly uranium and plutonium, initiate societal and environmental questions because of the pollution and human contamination risk. Therefore the need to understand the behaviors of actinides with human is essential to elucidate their mechanisms of toxicity. Then the request for therapeutic actinide chelation agents is also urgent.

1.2 Uranium

Uranium is a chemical element with symbol U and atomic number 92. The Prussian chemist Martin Heinrich Klaproth was the first to isolate uranium from pechblende in its oxide form in 1789. Then in 1841, Eugene-Melchior Péligot obtained the pure uranium metal by reducing uranium tetrachloride (UCl_4) with potassium metal. In 1896 its radioactivity was found by Henri Becquerel and further proved by the work on the radioactivity of Pierre and Marie Curie.

1.2.1 Uranium in the industry and environment

Before the Second World War, interest in uranium was limited. Uranium has been used since ancient Rome as a pigment for faience and ceramics. It is abundant on Earth (about 3 g/t in granitic or sedimentary soils and 3 mg/m^3 in seawater). After the discovery of the U-235 fission by the Enrico Fermi team in December 1942, uranium has been used in military weapon

(uncontrolled nuclear energy) and nuclear power plant (controlled nuclear energy). The energy released during the complete fission of the U-235 is about 2E7 kWh/kg. Also the high-density and high-melting properties of this metal (U-235 depleted uranium in this case) are also used for tank armor, anti-tank ammunition, missiles and other projectiles.

year	2010	2011	2012	2013	2014	2015	2016
total	53,671	53,493	58,489	59,331	56,041	60,496	62,366
% of demand*	78%	85%	86%	92%	85%	90%	98%

Table 3：World uranium production from mining in tons U (*Data from the World Nuclear Association).

Although nuclear industry suffered a crisis due to the Fukushima accident in 2011, the uranium industry is actually growing within recent years (Table 3). Every year, tens of thousands tons of uranium are chemically produced and enriched. While safety is the priority in the nuclear industry and can be considered excellent, several accidents have occurred in the past.[19] In such accidents, the radiological risk may be significant due to the relatively high radioactive isotopes, ^{232}U, ^{233}U, ^{234}U and ^{235}U, especially during the mining and reprocessing processes.

Many forms and different abundance of uranium are produced and manipulated by the nuclear industry along the complex and multi-stage processes of the fuel cycle (Fig. 2). These forms have very different physicochemical properties and therefore different dangerousness. An important parameter is the aqueous solubility of different forms of uranium; the biological transferability of species depends on this parameter. These main chemical species are:

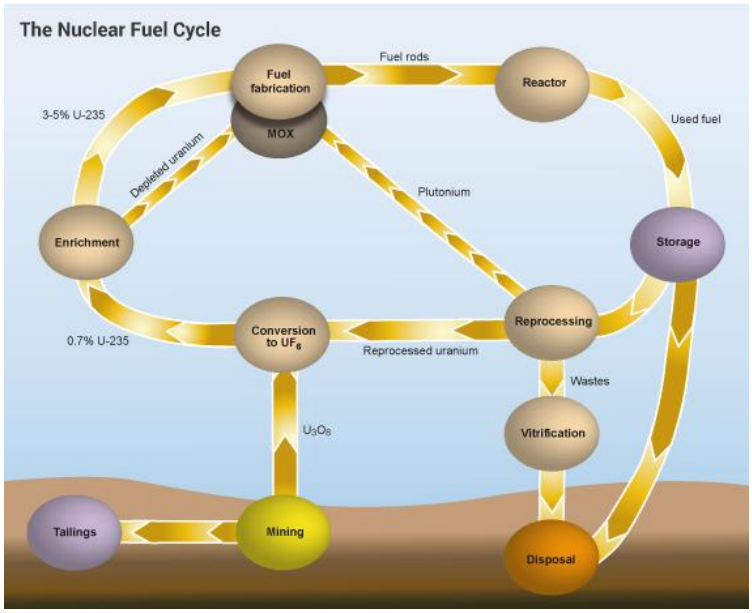

Figure 2 : illustration of nuclear fuel cycle[20].

- Soluble forms: $UO_2(SO_4)_n^{(2n-2)-}$, $UO_2(CO_3)_n^{(2n-2)-}$ (produced during the first stage of the chemical treatment in mining); $UO_2(NO_3)_2$;

- Non or slightly soluble forms: UF_4; UO_2; UO_3; U_3O_8 (the main form found after the explosion of a depleted uranium ammunition); $(NH_4)_2U_2O_7$ (Yellow cake);

- "Reactive" forms: uranium metal (pyrophoric) reacts with water to give UO_2 and H_2; UF_6 reacts with H_2O to give UO_2F_2 (soluble).

Four types of uranium UO_x, varying according to their isotopic compositions, are produced industrially: depleted uranium (-0.2% ^{235}U) which is the secondary product of uranium enrichment, moderately enriched uranium (3-5% ^{235}U) used in nuclear reactors, highly enriched

uranium (20 to 90% U-235) for research use and highly enriched uranium (> 90% ^{235}U) which is used in the construction of nuclear weapons.

1.2.2 Physic-chemical properties of uranium

Until now 24 uranium isotopes, all radioactive, have been identified. Natural uranium is composed of three isotopes: U-238, U-235 and U-234 (Table 4) but a total of 24 isotopes of uranium could be produced, from U-217 to U-242. The three natural isotopes are all radioactive. U-238 and U-235, the abundant isotopes, are the ascendants of the 4n+2 and 4n+3 decay families.

Isotope	Half-life (year)	Abundance	Decay mode
U-238	4,47E+09	99,28%	α/SF
U-236	2,34E+07	trace	α/SF
U-235	4,04E+08	0,72%	α/SF
U-234	2,45E+05	0,01%	α/SF
U-233	1,59E+05	trace	α/SF
U-232	68,9	syn	α/SF

Table 4 : Main isotopes of uranium. Trace: natural isotope in trace amount; syn: synthetic isotope.

^{234}U, ^{235}U, ^{238}U could decays and generate alpha-particle with a mean energies about 4.2-4.8 MeV. Due to the relatively short half-life of ^{234}U, the specific activity of ^{235}U, 2.3E8 Bq/g, is 2880 times higher than that of ^{235}U, 8.0E4 Bq/g and 19200 times higher than that of ^{238}U, 1.2E4 Bq/g. Due to the relatively long half-life for two isotopes, the power output per unit mass is low enough, so the heat generation after contamination could be neglected.

The uranium atom has the following external electronic configuration: $5s^2 5p^6 5d^{10} 5f^3 6s^2 6p^6 6d^1 7s^2$. The six outermost electrons of levels 5f, 6d and 7s form the uranium valence electron system. Uranium, like all actinides, has several stable or unstable oxidation states depending on the conditions: +III (U^{3+}), +IV (U^{4+}), +V (UO_2^+), +VI (UO_2^{2+}) and 0 (U) in metallic form.

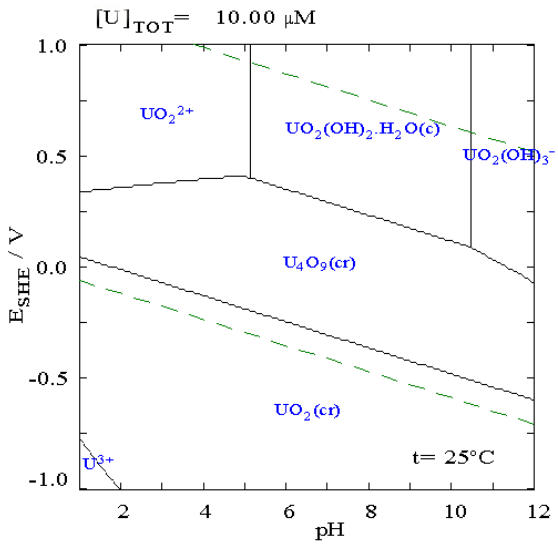

Figure 3 : Pourbaix diagram of uraniumin a non-complexing aqueous medium calculate by Hydra/Medusa Chemical Equilibrium Database and Plotting Software. [U]= 10 µM; T=25.0 °C.

The thermodynamic and hydrolytic properties of uranium can be represented in the form

of a Pourbaix diagram (Fig. 3). It shows the E/pH diagram of uranium for a total concentration of U (VI) equal to 10E-5 M at the temperature of 298 K in a non-complexing aqueous medium. This diagram shows: 1) the dominance species U (VI) (aq); 2) the instability of U(III) (aq) with respect to oxidation by H^+ (aq); 3) the inexistence of the thermodynamic stability domain of U (V) (aq).

The redox properties of uranium in an aqueous medium illustrates the thermodynamic instability of U^{3+} with respect to protons in the solution and the thermodynamic instability of UO_2^+ with respect to U^{4+} and UO_2^{2+} disproportionation (Scheme 1).

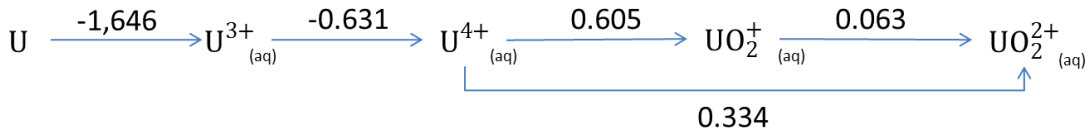

Scheme 1 : Latimer diagram of uranium in aqueous solution (potentials are expressed in a 1 M perchloric acid medium (in V/SHE).

Among the four oxidation states of uranium in aqueous solution, U (IV) and in particular U (VI) are the most important. Indeed, it is these species that are found in the vast majority in the environment and in biological environments. *In vivo*, U (IV) is rapidly oxidized to U (VI). It is therefore this single degree of oxidation that focuses the interest for projects such as the *in vivo* decorporation of uranium.

In an aqueous medium, uranyl (UO_2^{2+}) is predominate species. Uranyl is a very stable linear system $[O=U=O]^{2+}$. As indicated by Denning et al.,[21] several symmetrical overlaps occur between uranium atomic orbital (OA) 6d and oxygen OA 2p to form binding OMs $3\sigma_g$ and $2\pi_g$. Plutonium, neptunium, and americium, under oxidizing conditions can also be found in their actinyl form ($AnO_2^{+,2+}$). This trans-oxo form is specific to actinides because of the presence of fz^3 orbitals.

Like all other actinide cations, uranyl is a hard acid according to the Pearson classification. So it has strong affinity for hard bases like carboxylates or phosphonates. Because of the steric hindrance caused by the oxo groups, the metal/ligand orbital recovery will be in the equatorial plane and the electronic transfers will preferentially be ligand to the OAs d or f. The effect of a donor ligand on uranyl results in the weakening of the bond O=U=O, by formal reduction of the binding order. Thus this weakening of the bond O=U=O is observable in infrared spectroscopy. Indeed the antisymmetric vibrating band of the U-O bond, only IR active, will shift from 950 cm^{-1} for a hexaaquo complex[22] to about 920 cm^{-1} in the case of coordination by phosphonate functions[23,24].

Due to the presence of axial "yl"-Oxygen of uranyl ion, normally five water molecules at equatorial plane could be found for the uranyl ion coordination for the non-complexation cases.[25,26] But for the uranyl carbonate complexes in solution or solid, six coordination number was found.[27] This mode of coordination is a peculiarity of the uranyl ion which can be used in the design of selective ligands.

The fluorescence spectrum of the aqueous uranyl ion reflects the symmetrical vibration of the U-O bond. The observed emission bands correspond to the electronic transition $S_{11} \rightarrow S_{00}$ (473 nm) and $S_{10} \rightarrow S_{0v}$ with n=0–4 (488, 510, 535, 560, and 587 nm).[28] The free uranyl ion UO_2^{2+} is taken as a reference in terms of spectroscopic scale since it is very likely that all the other species present a bathochromic shift due to complexation and a broadening due to the addition of new vibrational modes.

1.3 Americium/curium

Americium is a synthetic chemical element with symbol Am and atomic number 95.

Curium is also a synthetic chemical element with symbol Cm and atomic number 96. The discovery of americium and curium in 1944 was closely related to the Manhattan Project. These two elements were produced by the group of Glenn T. Seaborg at the University of California, Berkeley.

1.3.1 Americium/curium in the industry and environment

Due to the short half-life of americium and curium, any primordial americium (americium that was present on Earth during its formation) should have decayed by now. Existing americium and curium are concentrated in the areas used for the atmospheric nuclear weapons tests conducted between 1945 and 1980, as well as at the sites of nuclear incidents, such as the Chernobyl disaster. However, on a global scale these large releases resulted in very small concentrations of americium and curium in the environment.

Americium and curium are produced mostly artificially in small quantities, for research purposes. The main source of americium and curium are from the nuclear industry. ^{241}Am and ^{243}Am are the americium isotopes which could be formed by ^{238}U (the major uranium isotope used in nuclear power reactor fuel) or ^{238},^{239}Pu (primarily used in nuclear weapons). ^{242}Cm and ^{244}Cm are the curium isotopes which could be formed by ^{238}U (the major uranium isotope used in nuclear power reactor fuel) or ^{241}Am (the fission product in nuclear power reactor fuel). By bombarding uranium or plutonium with neutrons in nuclear reactors, about 100 g of americium and 20 g of curium could be obtained in one ton of spent nuclear fuel. The oxidation states of these two elements are +III in the reprocessing process.

For now, the americium and curium were mainly used for research interests. Due to the high radioactivity, separation of these two elements is the aim for the reprocessing process in order to reducing the difficulty for storage.

1.3.2 Physic-chemical properties of americium and curium, europium use as the chemical analogue

All the isotopes of these two elements are radioactive (Table 5 & 6). All of them are synthetic isotope. The americium atom has the following external electronic configuration: $5f^7 7s^2$, which is $5f^7 6d^1 7s^2$ for curium. The charge for the stable or unstable oxidation states depending on the conditions: +III (Am^{3+}, Cm^{3+}), +IV (Am^{4+}, Cm^{4+}).

Isotope	Half-life($t_{1/2}$)	Abun-dance	Decay mode
Am-241	432.2 y	syn	α
Am-242	141 y	syn	IT/α
Am-243	7370 y	syn	α

Table 5：Main isotopes of americium. syn: synthetic isotope.

Isotope	Half-life(year)	Abundance	Decay mode
Cm-242	160 d	syn	α
Cm-243	29.1 y	syn	α/ε
Cm-244	18.1 y	syn	α

Table 6：Main isotopes of curium. syn: synthetic isotope.

^{241}Am, ^{244}Cm could decays and generate alpha-particle with a mean energies about 4.8–6.1MeV. Due to the relatively short half-life of ^{244}Cm, the specific activity of ^{244}Cm, 1.3E12 Bq/g, is 23 times higher than that of ^{241}Am, 1.3E11 Bq/g. Among the actinides, ^{241}Am, ^{243}Cm and ^{244}Cm have high power output per unit mass, 0.115, 1.81 and 2.83 in W/g respectively, the

power could result in a very large heat releases in the case of these isotopes ,especially for ^{243}Cm and ^{244}Cm.

The redox properties of americium in an aqueous medium illustrates the thermodynamic instability of Am^{4+} with respect the very high redox potential of couple Am(IV)/Am(III) (about 2.34 V/SHE) which makes the element highly unstable in oxidation state +IV (Scheme 2).

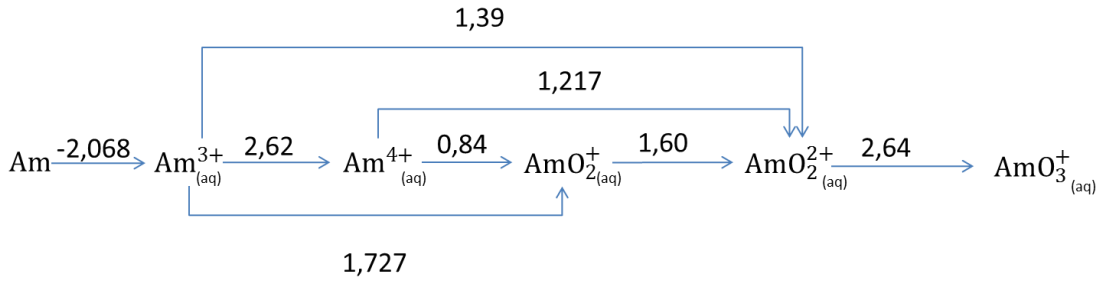

Scheme 2 : Latimer diagram of americium in aqueous solution (potentials are expressed in a 1 M perchloric acid medium (in V/SHE).

The thermodynamic and hydrolytic properties of americium can be represented in the form of a Pourbaix diagram (Fig. 4). It shows the E/pH diagram of americium for a total concentration of Am^{3+} equal to 10E-10 M at the temperature of 298 K in a non-complexing aqueous medium. This diagram shows: 1) the dominance species Am^{3+} (aq) in the acidic condition; 2) the instability of Am^{4+} (aq).

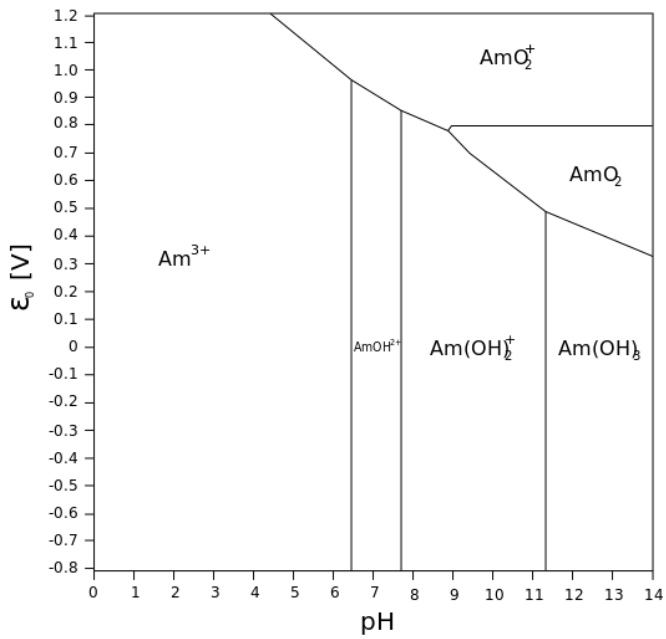

Figure 4 : Pourbaix diagram of americium a non-complexing aqueous medium. [Am]= 10E-10 M; T=25.0 °C.[29]

Cm(III) oxidation state is very stable due to the half-filled ($5f^7$) configuration. Because Cm^{4+} only exist in the strongest oxidizing conditions, the redox potential for the Cm(IV)/Cm(III) couple is 3.1V in a 1 M perchloric acid medium (in V/SHE).

Among the two oxidation states of americium and curium in aqueous solution, Am(III) and Cm(III) are the most important. Indeed, it is these species that are found in the vast majority in the environment and in biological environments. *In vivo*, Am^{3+} and Cm^{3+} are the major species. It is therefore this single degree of oxidation that focuses the interest for projects such as *in vivo* decorporation of americium and curium. Am(IV) and Cm(IV) are hard acids according to the

Pearson classification.

The aquatic chemistry of trivalent 4f- and 5f-elements has been demonstrated to be very similar. Trivalent 4f-elements have a coordination number of 8 to 9 while trivalent 5f-elements have the similar number for that in the dilute non-complexation solution.[30]

	Eu	**Am**
	3+	3+
CN=6	0,947	0,975
CN=8	1.066	1.109
CN=9	1.120	-

Table 7：Ionic radii (Å) of Eu and Am in different coordination numbers (CN) and at oxidation states.[31,32]

For americium, the location in the periodic table is under the lanthanide element europium. Meanwhile the ionic radii of Eu^{3+} and Am^{3+} in coordination numbers equal to 8 and 9 were list in table 7.[31,32] It is clear that these two elements in di-and trivalent ionic state have similar ionic radii. In Fig. 1.5, there is a similar trend that the cohesive energies of the divalent and trivalent rear earth elements and actinides. Especially, compared to other rare earth elements Yb-No and Eu-Am have significantly low cohesive energy for trivalent form. With the help of ground state configuration of $f^n s^2$ and $f^n d^1 s^2$, the same trend could be found for Eu and Am.[33] Due to the similarity in chemical and physical properties, ionic radii, cohesive energy and relative energy relationship, Eu^{3+} could be used as analogue of Am^{3+} in the chemical study. By observing the behaviors of natural analogue like the rare-earth metals for trivalent actinides, it is possible to reduce the uncertainty in the geochemical study.[34] Because americium has radio-toxicity and chemo-toxicity, it is difficult to understand the impact of americium in ecotoxicology study. And it is pretty hard to do ecological experiments with americium. The much less toxic metal europium is also used as chemical analogue in the ecotoxicology investigations to study the behavior of americium.[35] The metabolisms of ^{152}Eu and ^{241}Am have been measured in both carbs and crayfish revealed that it is reliable in the biological study to use europium as a chemical analogue of americium.

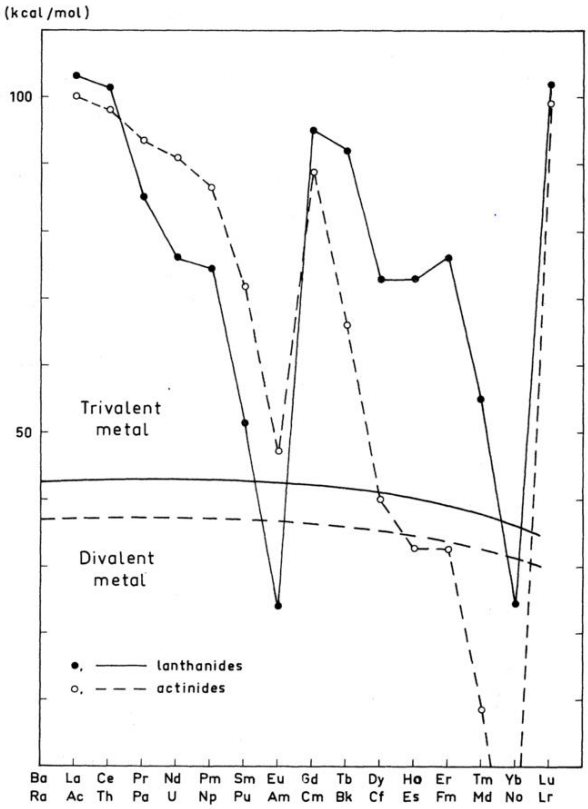

Figure 5 : Cohesive energy for the rare earths (full. curves) and actinides (dashed curves). The smooth curves denote the cohesive energy in case these elements had remained divalent in their metallic modification, the jagged curves the cohesive energy of their trivalent metallic state.[36]

Isotope	Half-life (year)	Abundance	Decay mode
Eu-151	5×10^{18}	47.8%	α
Eu-153	stable	52.2%	-

Table 8：Main isotopes of europium.

Europium is a chemical element with symbol Eu and atomic number 63. It was isolated in 1901 and is named after the continent of Europe. Europium is composed of 2 isotopes, ^{151}Eu and ^{153}Eu, in nature condition (Table. 8). ^{153}Eu is the most abundant, 52.2%. The europium atom has the following external electronic configuration: $4f^7 6s^2$. The charge for the stable or unstable oxidation states depends on the conditions: +II (Eu^{2+}), +III (Eu^{3+}). Eu^{3+} is the main species in the acidic condition, then starts to form the hydroxide in the neutron range.

Toxicology

The collection of data on the bio-distribution of actinides in the body began with the Manhattan project in the late 1940s. It first focused on plutonium and then expanded its interest circle to other actinides strategic (uranium, thorium, neptunium ...).

1.4 The contamination mode

Depending on these modes of contamination (Fig. 6), the biological path of actinides will be different. There are four main entry routes and four excretion route for actinides in the body.

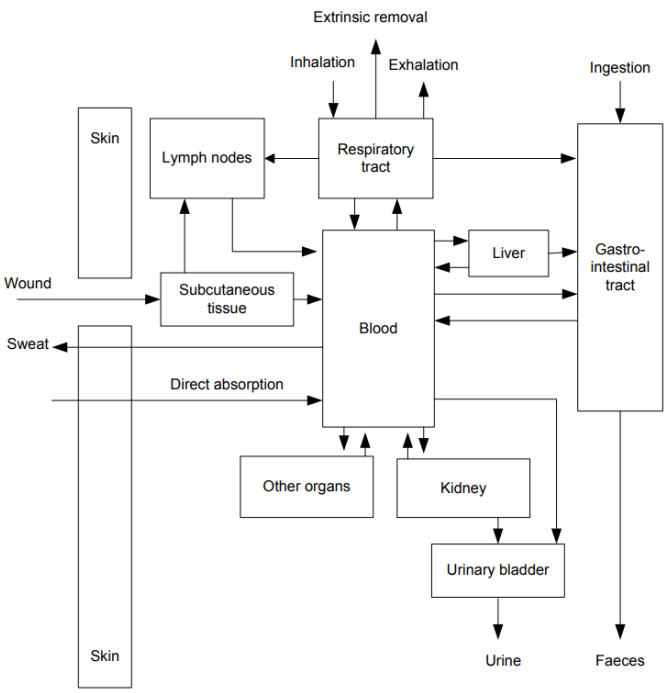

Figure 6 : The main routes of intake, transfer and excretion of radionuclides in the body (ICRP 130).

1.4.1 Main entry routes

1.4.1.1 Inhalation, when inhaling dust, aerosols or gases containing uranium compounds or particles.

The inhalation is the main gateway into the body of radionuclides, whether in the form of dust, aerosol or gas. The fate of the inhaled contaminant in the lungs is strongly conditioned by physical parameters such as: the physical state (gas, liquid, solid); the physico-chemical form (degree of oxidation and solubility); particle size and surface appearance for solids.

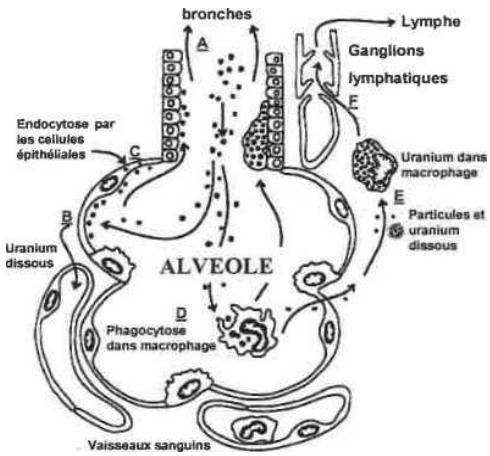

Figure 7 : Uranium particles during inhalation contamination (ICRP 66).

Depending on the actinide physicochemical properties, the fate of this particle in the lung can be multiple: 1) dissolution and released in the bloodstream (Fig. 7, B) 2) endocytosis by the epithelial cells (Fig. 7, C); 3) phagocytosis by macrophages (Fig. 7, D); 4) transport as free or phagocytic particles and deposition in the lymph nodes until dissolution and transport to the lymph (Fig. 7, E, F).

The purpose of chelating agents is to limit toxicity of soluble forms of actinides by increase

the excretion after complex with the chelating agents.

1.4.1.2 The digestive tract (when ingesting contaminated food), the bloodstream (during an accidental injury), the skin (when in contact with the skin).

The uptake of actinides by the digestive system is mainly performed in intestinal. The absorption rate is strongly depending on the element. Studies in humans have shown that this absorption is very low (1 to 2.4%) for soluble forms of uranium. This absorption is 10 to 100 times lower for poorly soluble forms such as U_3O_8 and UO_2. Uranium that has not been absorbed is eliminated in the feces in 24 hours. The toxicity of uranium during ingestion contamination is therefore very low; the LD_{50} (in the rodent) is of the order of 114-136g / kg.[37]

1.4.1.3 Contamination following injury

During an injury, the soluble products will very quickly enter the bloodstream. Absorption is usually complete after 24 hours. For moderately or poorly soluble products, such as metal particles, the entry of uranium into the bloodstream is gradual. For this kind of contamination washing the wounds with a solution containing a chelating agent of uranium may be interesting.

1.4.1.4 Entry through intact skin

The contact with the skin of soluble forms is one of the ways of entry of actinides into a human body. Animal experiments have shown that the application of soluble forms of uranyl ion can cause renal toxicity that can lead to death of the animal.[38] In contrast, insoluble forms do not induce a toxic effect when these are applied to the skin. In the latter case, a simple washing is likely to eliminate any risk of intoxication.

The mode of airways is considered as the most common way of contamination in the industry. After a fire accident or an explosion, a dispersion of radionuclides in the atmosphere could be possible then the inhalation of radionuclides will cause an internal contamination. The modes of contamination following injury and cutaneous contamination are considered as the second most common way of contamination in the industry. After an explosion or improper handling of contaminated tools or sharps inside a glove-box, the skin can also be contaminated by contact with aerosols or by contact with surfaces contaminated with radionuclides.

Following internal exposure, the radionuclide is incorporated into the body and the damage induced by irradiation of cells or tissues at the vicinity of the element can be of concern, whatever the radiation type, and especially in the case of highly ionizing alpha particles which transfer their energy more rapidly and at shorter range than gamma radiation for instance. Hence, since the major isotopes of the actinides U and Pu are mostly alpha emitters, the toxicological consequences related to the incorporation of these elements can be quite concerning. This mode of exposure to both actinides mainly depends on the industrial or military uses of the different compounds.

1.4.2 Main excretion routes

There are four possible excretion routes for human: exhalation, faces excretion, urine excretion and sweat. The removal of the actinides which has deposited from the human body normally occurs by faces excretion and urine excretion.

There are two origins of actinides which are excreted by faces. 1) Systemic (endogenous) faecal excretion: due to secretions along the alimentary tract and biliary secretion from the liver, actinides could be removed with systemic material *via* the alimentary tract; 2) Direct (exogenous) faecal excretion: strictly elimination of the actinides which are unabsorbed through the alimentary tract after ingestion and clearance to the throat from the respiratory system after inhalation. Urinary excretion is the removal in urine of radionuclides from blood following filtration by the kidneys.

1.5 The factor which influences the toxicity

The toxicity of the uranium and americium/curium, are different from normal poison due to the radioactivity. It is important to separate chemo-toxicity that acts on all target organs from radiation-induced toxicity which is related to the issuer properties and radioactive isotopes that concerns the storage organs.

In order to compare the dose coefficients, or dose per unit intake for radionuclides, ICRP classified the compounds into three types according to the absorption rates from the lungs to blood , fast (Type F), moderate (Type M) and slow (Type S) in ICRP-66. The default absorption parameter values are given in Table 1.9. Generally those soluble compound (Type F &M) could rapidly be transferred into the blood as uranyl ion (transfer kinetics of a few minutes to a few days) and develop their chemical toxicity on the various target organs while the weakly transferable forms (type S) will stay for a long time at the place of contamination. The chemical form and solubility are the main factors influencing the chemo-toxicity.

ICRP -66 absorption type		**F (fast)**	**M (mod.)**	**S (slow)**
Model parameters:				
Initial dissolution rate (d^{-1})	s_p	100	10	0,1
Transformation rate (d^{-1})	s_{pt}	0	90	100
Final dissolution rate (d^{-1})	s_t	-	0,005	0,0001
Fraction dissolved rapidly	f_r	1	0,1	0,001
Approximate dissolution rates:				
Rapid (d^{-1})	s_r	100	100	100
Slow (d^{-1})	s_s	-	0,005	0,0001
Fraction to bound state	f_b	0	0	0
Uptake rate from bound state (d^{-1})	s_b	-	-	-100

Table 9：Default absorption parameters for Type F, M and S materials.

For the radiation-induced toxicity, the isotopic composition and the chemical form of the contaminant are also the main factors. For example, only the chemical toxicity of the metal will be taken into account during contamination with depleted uranium. While for americium/curium, both toxicities need to be considered.

1.6 The bio-distribution of actinides

Scientist, nuclear workers and soldiers are the people under risk of contamination with actinides. Also a major event (nuclear accident, conflict, terrorism) which could lead to a large-scale contamination of the civilian population should be taking into account.

The bio-distribution of actinides is determined by two main factors; the nature of the contaminant and the mode of contamination. No matter the exposure route, the pathway for actinides transport in human body is similar (Fig. 5). After the transfer *via* blood, unlike ^{3}H as tritiated water which seems uniformly throughout the body and ^{131}I selectively deposit in the thyroid, actinides are prefer to concentrate in a few different target organs: the bones, liver and kidneys, which present the largest proportion of actinides present in the body for most case.[39]

The behavior of an actinide which is a non-essential element after the transfer to blood (e.g., ^{232}Th, ^{238}U, ^{239}Pu, or ^{241}Am) depends on a number of function of human body to which it can be sequestered by the reticuloendothelial (RE) system, its affinity for specific biological ligands,

its filterability by the kidneys, and the ability of the body to eliminate it in liver bile or other secretions into the gastrointestinal tract. In some cases, the biokinetics of actinides which is a non-essential element may showing some similarities with those essential elements due to similar chemical affinities for some but not all components of tissues and fluids. For example, the behavior of uranium in the skeleton presents some similarities to that of calcium because uranium can replace calcium to some extent in bone. While in other tissue or fluid the biokinetic behaviors of uranium show greater differences compared with calcium. Nevertheless, the use of chemical or biological analogues has its limits.[40]

Actinides		**Thorium**	**Uranium**	**Neptunium***		**Plutonium**	**Americium**	**Curium**
Biological form		Th^{4+}	UO_2^{2+}	Np^{4+}	NpO_2^{+}	Pu^{4+}	Am^{3+}	Cm^{3+}
Ionic radius (Å)		1.00	2.80	0.95	2.90	0.93	1.00	0.98
Blood stay		10% 1 day 0.3% 10 days	25% 5 min 1% 1 day	20% 1 h	< 1% 1 h	< 1% 1 day	< 1% 1 day	
Blood complexes		100% Tf	50% HCO3 –, 30% Tf, 20% red cells	< 1% 1 day 80% Tf	70% free	100% Tf	100% Tf	
Organ retention								
Bone		70%	10–15%	30–50%	30–50%	50%	30%	
Liver		5%	/	2–10%	2–10%	30%	50%	
Kidneys		3%	12–25%	/	1%	/	/	
Soft tissues		4%	5%	5%	5%	10%	/	
Urinary		4–6% 5 days	65% 1 day	3–4% 1 h	15–20% 1 h	0.4% 1 day	< 1% 1 day	
Excretion		7–9% 20 days	70% 6 days	15% 1 day	20–40% 1 day	1.4% 14 days		
ICRP model	Type M	5×10^{-4}	2×10^{-2}	5×10^{-4}		5×10^{-4}	5×10^{-4}	
	Type S	2×10^{-4}	2×10^{-3}			1×10^{-5}		
		69	69	67 *		67	67	

Table 10：Biokinetic data on actinides. Data on the distribution of Np(IV) and Np(V) in rat and mouse.[41,42]

When the radioactivity is low (the case of ^{238}U and ^{232}Th), chemical toxicity is the main concern. But for the high radioactivity isotopes, apart from the chemical toxicity, radioactive toxicity also needs to be considered due to the radiation damage for the living cell [43] and heat generation. In both cases, the prolonged duration of internal exposure causes damage at the cellular level which is carcinogenicity. Table 10 summarizes the biokinetics and bioinorganic chemistry of some actinides in ICRP Publications 67 and 69, the proportions of actinides in the blood and each target organ with the residence time.[44,45]

For the Systemic model which is proposed by ICRP (Fig. 6 & 7), two compartments representing short- and long-term retention are considered for the liver. The short-term compartment (Liver 1) represents the actinides which enter the liver and may transfer back to

blood or intestines by biliary secretion. The actinides which belong to long-term compartment (Liver 2) could slowly returns to blood. For kidneys, two compartments, urinary path and other kidney tissue, are omitted. Urinary path represents the actinides loses to urine over a period of hours or days which other kidney tissue shows slowly returns actinides to blood. Three compartments, ST0, ST1 and ST2, were considered for remaining soft tissue other than bone marrow. ST0, ST1 and ST2 are the paths of rapid, intermediate, and slow return of actinides to blood, respectively. ST0 is the sign to count the actinides rapid build-up of in soft tissues and also regarded as part of the actinides circulating in body fluids. After acute input of actinides to blood, the rapid feedback to blood is also treating as ST0. The skeleton is separating into cortical and trabecular fractions and each of these fractions could be attributing to bone surface, bone volume, and bone marrow. Actinides which entering the skeleton is assigned to bone surface and subsequently gradually transfer to bone marrow and bone volume by bone remodelling processes. Also actinides in bone volume are transferred gradually to bone marrow by bone remodelling. Actinides could be lost from bone marrow to blood over a period of months. And the subsequently redistributed is in the same mode similar to the original input to blood. The transfer from cortical and trabecular bone compartments to all destinations are related with the turnover rate of cortical and trabecular bone. The rates from cortical and trabecular bone compartments to all destinations are assumed to be 3% and 18% per year, respectively. Other parameter values in the model are depends on the nature of each element. After reaching bone volume, these elements may migrate back to plasma (*via* bone surface in the model) or they may become fixed in bone volume and are then gradually removed to blood at the rate of bone remodelling. For example, the bone-surface seekers (thorium, neptunium, plutonium, americium, and curium) diffuse throughout bone volume within hours or days after depositing in bone (Fig. 7).

1.6.1 Uranium

In nature, uranium which is an inhomogeneous distribution on the planet occurs in granite, metamorphic rock, lignite, monazite sand, and phosphate deposits at concentrations on the order of 0.5 to 5 ppm. Through food and water mainly[46], a large part of population in the world absorbs uranium about 1- 5μg/d daily in uncontaminated regions which is 13-18μg/d daily or more in uranium mining areas. A 70 kg, non-occupationally exposed 'Reference Man' living in Europe has an estimated total body uranium content of about 22μg. Since the quantity of uranium which is present in the human body is small, the health risk is negligible.

Uranium is the most widely used actinide element in the world, therefore plenty study which focus on potential risk on health has revealed the bio-distribution of uranium *in vitro* or *in vivo* on small animals (rats, dogs, *etc.*) or on the man. [47,48] However, most of the biological mechanisms related with uranium are only partially known.

Besides the other non-soluble or less soluble form of uranium, the contamination by uranyl ion is of the interest in this study. The elimination of uranium from human body will be favored in this form and the majority of the uranium retained in human body will result from the bio-distribution of uranyl ion.[49] Generally uranyl ion forms complexes with citrate, carbonate, or protein in plasma.[40] The stability of the carbonate complex and concentration of carbonate depends on the pH and nature of the solution which will differ in different parts of the body. The bicarbonate uranyl complex can be filtered at the renal glomerulus due to the low molecular weight, then depend on the urine pH be excreted in urine (70%).[50] The uranium which is bounded to the protein in blood (mainly plasma proteins, 30%)[51] is harder to filtered due to the larger size, thus this part of uranium prefers to remain in blood at the early stage of the uranium bio-distribution. The blood serves as the vector which transfers the solubilized uranium to all target organs (Fig. 1.8). The bio-distribution of uranium is rapid. After a few hours, the majority of uranium in uranyl ion form leaves the blood to be either excreted by the urine (70%) or

directed to the skeleton (10-15%) and to the kidneys (12-25%) (Table 10). Although for uranium retention, soft tissues could only retain 5% which should also be considered.

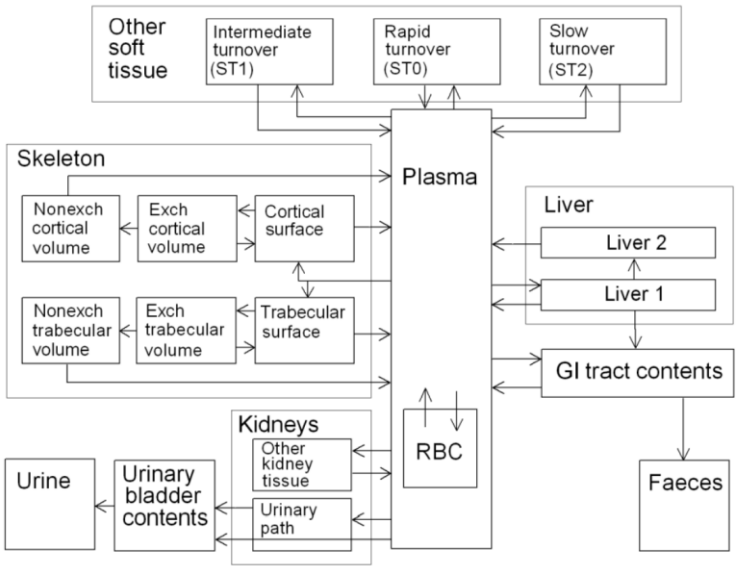

Figure 8 : Systemic model of the bio-distribution of uranyl ion in human body (ICRP 72).

1.6.2 Americium/curium

Normally americium and curium could be found in the spent fuel, reprocessing process and laboratory. Similarly, the elimination of americium and curium will be favored and the majority of the americium and curium retained will result from its dissolution in trivalent form. Concerning the soluble form of americium and curium, they will bind with proteins and also form complex with various inorganic anions, such as carbonate and phosphate, and carboxylic acids, such as citrate and lactate (Table 9). These types of interactions would be expected for all routes of exposure.

In the blood, americium and curium is totally complexes with plasma protein, transferrin (Table 10). The bio-distributions of americium and curium are rapid. The blood compartment is also the vector which distributes americium and curium in all target organs (Fig. 1.9). Bio-distribution is also rapid. After one hour[52], only a few amounts of americium and curium excreted by the urine (10%) due to the complexation with transferrin. the majority of the americium and curium leaves the blood directed to the skeleton (30%) and to the liver (50%). Kidneys (0.9%), gonads (0.045% for ^{244}Cm, 0.037 for ^{241}Am), spleen (0.7% for ^{244}Cm, 0.35% for ^{241}Am) and other soft tissues, which may also be affected to a lesser extent (5%) by americium and curium retention, should also be considered.[52,53]

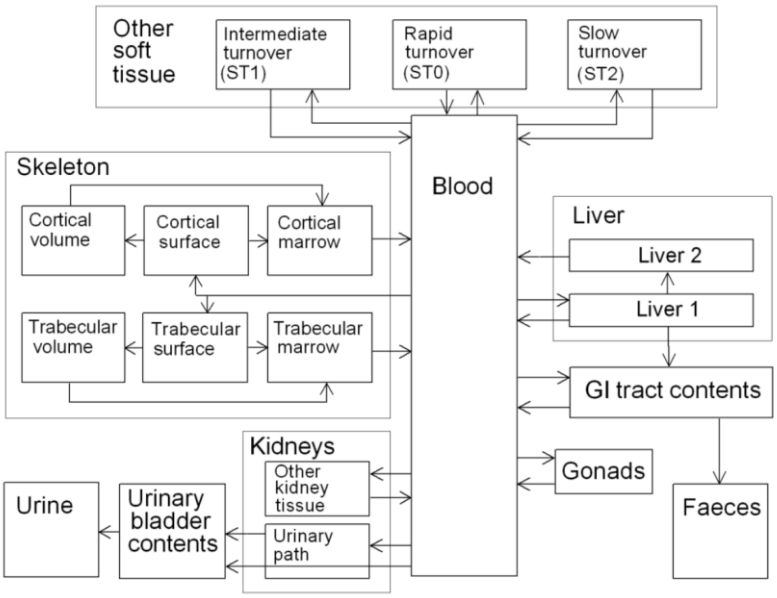

Figure 9 : Systemic model of the bio-distribution of the bone-surface seekers, americium and curium, in human body (ICRP 72).

1.7 Human Health Effects

1.7.1 Uranium

According to the radioactivity, the uranium could be separate into 2 classes, low radioactive uranium (e.g., natural and depleted uranium); high radioactive uranium (e.g., ^{232}U, ^{233}U, ^{234}U and ^{235}U). Chemical toxicity is the major concern for low radioactive uranium contamination. For high radioactive uranium contamination, both chemical and radiological toxicity need to be considered. It is hard to distinguish the two toxicities due to the overlap of etiology and manifested effects.

1.7.1.1 Acute effects

8.3 and 20.4 mg/kg were found for median lethal dose (LD_{50}) within 14 days continually administration for rats and mice, respectively; 204 and 242 mg/kg were found for oral LD_{50} and the death is mainly due to the renal toxicity which is caused by intake of uranyl acetate.[54]

1.7.1.2 Long-term effects significant

As shown in table 8, a majority of uranium will be excreted by urine and then part of the uranium will be retained in the kidneys for several months.[55] Thus the renal toxicity is the major concern for uranium human health effects. The uranium-induced renal toxicity could be explained by the following mechanism: the uranyl ion could occupy the binding sites of adenosine-5'triphosphate (ATP) which normally provides Mg^{2+} and Ca^{2+}, and subsequent energy transport will be disrupted in the cells of the proximal tubule and associated structures.[55] Besides uranium also has toxic effects on the cardiovascular system, liver, muscle and nervous system as well.[56]

The toxic effects observed on the bone after the injection of uranyl nitrate has shown that the bone activity decreased and in turn the bone resorption increased, and the different doses studies indicated that the degree of damage is proportional to the dose employed which means the nature of toxicity effect was the same for different radioactivity.[57]

Internalized radionuclides that emit alpha-particles are carcinogenic to humans (Group 1), so high activity of uranium could also cause cancer. The accumulation of uranium in bone is similar to that of radium; therefore the emitting alpha particles would assume to be nearly as

effective in the osteogenic sarcomas generation. After exposures to high dose of ^{232}U and ^{233}U, sarcomas have been found in mice.[58] For the toxicity in the lungs, it mainly related with alpha radiation from inhalation of insoluble forms of uranium which is retained in the lungs. Chronic uranium exposure during 30 days could cause theneurophysiological perturbations as the uranium likely accumulated in the brain.[59] An excess of lung cancer deaths among 18,869 white male workers and an excess of death from central nervous system (CNS) cancer were found in a uranium enrichment factory.[58]

International Agency for Research on Cancer considers that inadequate evidence in humans was found for the carcinogenicity of natural uranium. And limited evidence in experimental animals was found for the carcinogenicity of natural uranium. There is inadequate evidence in experimental animals for the carcinogenicity of ^{233}U.[60] While American Conference of Governmental Industrial Hygienists confirmed that natural uranium ether in soluble or insoluble compounds is human carcinogen.

1.7.2 Americium/curium

Few studies on the toxicity of the americium and curium radionuclides were done. Due to the very high specific activities of all americium and curium isotopes, compared to chemo-toxicity, the radio-toxicity seems to be main concern for human health.

1.7.2.1 Acute effects

LD_{50} within 60 days study with rat is 2220 Bq/g for ^{241}Am and ^{244}Cm which is equal to about 80 mg ^{244}Cm into a 70kg human for acute effects. The damage to the bone marrow by the high dose is the main reason for the death.[61]

1.7.2.2 Long-term effects

The damage to other organ than bone marrow could also cause death or cancer. The study with animals was done to prove the carcinogenicity of mixed alpha-particle emitters (^{241}Am, ^{244}Cm).[60] There are two reasons for the carcinogenicity: 1) the alpha-particles emitted by americium and curium, 2) secondary ionizations and the same pattern of localized damage. Both effects could damage biological molecules which results in DNA doublestrand breaks, chromosomal aberrations, gene mutations and cell transformation. The risk coefficients of bone tumors after injection of ^{241}Am and ^{244}Cm were increased.[62,63]

1.8 Conclusion

The toxicity of U(VI), Am(III) and Cm(III) has been illustrated in this part. In the case of contamination, after transferred by blood, the solubilized actinides are widely distributed to the target organs: bone, liver and kidneys, and then these actinides could cause serious damage to human health. Since the human body is a dynamic system, the actinides retained in the target organs can be released into the bloodstream and then possibly excreted by urine. Chelation therapy is considered as the most effect way to decorporate actinides from human body. In the next part, several works of chelation agents for decorporate actinides will be described.

Chelation therapy

Chelation therapy is focused on reduce the solubilized actinide entered by inhalation, intact skin or wound (Table 1) which will decrease acute radiation damage, long-term chemo-toxicity and long-term radio-toxicity, hence risks of death, induction of cancer and other diseases could be reduced.

The investigations of actinides chelation therapy till now could be separate into 3 stages:

1. Starting stage 1938-1950: The investigations to improve actinide excretion began with

methods to increase radium excretion.[64] Except administration of bicarbonate to reduce uranium in human body from acute exposures,[65] no effective method was found for actinides.[66]

2. Early stage 1950-1960: Toxicities of plutonium and other actinides were recognized in the middle of the 20th century with the development of Manhattan project. Thus the study to find effective decorporation methods began.[67,68] Three tasks were enrolled: the metabolism of fission products and heavy elements; the acute and long-term toxicity of ionizing radiation from external and internal sources; the methods to remove internal deposited radioelements from the body.[65,68] There are huge improvement on evaluate the first two tasks in the following years.[69,70] But the investigations on the removal of radioelements from human body met plenty of problems. In the early stage (1940s), chelation study was focus on hormones, common carboxylic acids or complexing agents, or colloidal zirconium citrate, and the rat test with these compound proved little effect on the plutonium excretion.[67,71] EDTA, synthesis in 1947 as calcium analytical agent, and DTPA synthesis in 1954 for multivalent cations, were used in the radioelement decontamination study (Fig. 1.10).

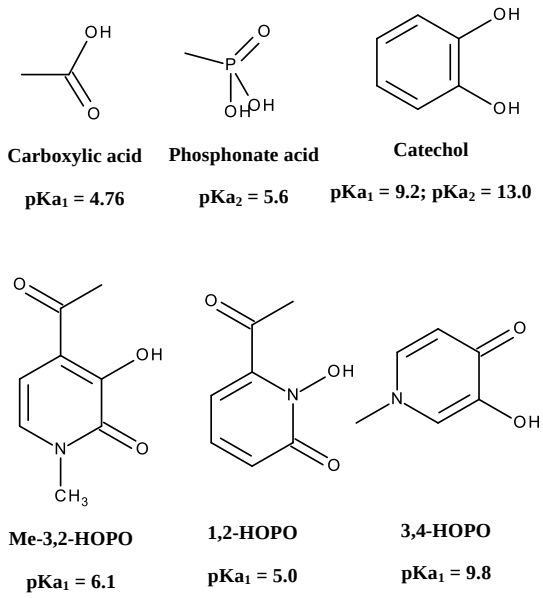

Figure 10 : Structures, abbreviated names, and pKa values of metal-binding units of different chelation ligands. Carboxylic acid; phosphoate acid; catecholate (CAM); hydroxypyridinonate (HOPO).

3. Recent stage 1960 to now: Then steady improvement has been made by focusing on the design ligands with structural and coordination to have better chelation affinity with actinides. As iron (III) and trivalent or tetravalent actinides have similar coordination and these cations could defined as hard Lewis acid metals, siderophores which are highly selective chelating agents for essential element iron were tested for actinides chelation therapy due the presence in the bacterial and well microorganisms study. The catecholates derived from enterobactin, the hydrozamic acid derived from desferriozamine and the hydroxypyridinones (HOPOs) derived from cepabactin were the most widely used function groups from siderophores (Fig. 10). Plenty of chelation agents based on siderophore derives were synthesized after 1960s. Numerous works with siderophore on actinides chelation therapy, mainly for plutonium (IV), were done by the KN Raymond and PW Durbin groups at Berkeley. The affinities of the ligands which originally developed for plutonium (IV) were tested also with uranium. Decorporation for uranyl decorporants focused on testing the affinity of ligands developed for plutonium (IV) such as DTPA or derivatives of HOPO functions and catecholates. Unfortunately in case of contamination with uranium, the toxicity of these ligands, especially at the renal level, prevents

their use for the decoration of uranyl.[72–74] The bisphosphonate moiety, a structural analogue of pyrophosphate, could form strongly binding with hard Lewis acid metals at physiological pH. And bisphosphonates are also known to target bones and generally display low toxicity. The group of Frédéric Taran at CEA-Saclay synthesized a lot of bisphosphonate ligands which were found to be the best uranyl chelation agents among the other actinides chelation agents (Fig. 10).[75]

The main idea is to use those ligands to complex the actinides which has already been deposited in the target organs in the complexation form. Therefore the actinide ligand complexes as xenobiotics could be transfered by blood from the target organs due to the high hydrophilic and water solubility and finally be excreted *via* urine and bile[76]. Three important points need to be considered: 1) the bio-distribution of chelating agent *via* different intake methods; 2) the chelation affinity of chelating agent with target actinide under physiological conditions; 3) the excretion route of actinides ligand complex.

Therefore several properties for an effective actinide chelating agent under physiological conditions were proposed by different authors[5,39,40]:

1) Design of the chelating agent: molecular mass limit of chelating agent due to different intake methods; bio-distribution of chelating agent in the target organs; the binding affinity of metal-binding unit based on Pearson acid-base concept for the actinide of interest; sufficient deprotonation of metal-binding unit under biological conditions to chelate the actinide of interest; good geometry of chelating ligand for the coordination of the actinide of interest to ensure the high selectivity over the other essential elements.

2) Interaction between agent and organs: low toxicity of the ligand; high bioavailability of ligand for different drug delivery system (Intravenous, intraperitoneal, oral, lung, etc); bio-distribution of sufficient ligand which could transfer to the target organs due to the ligand bio-distribution; high excretion rate and short retain duration of the actinide-chelating ligand according to the lipophilic properties of the chelating ligand.

3) Practical use of chelating agent: low cost; easy and quickly to be used; high stability under normal reserve condition.

1.9 Actinides chelating agents under studies

The main families of ligands synthesized and some chelating agents tested for the *in vivo* decorporating efficiency with actinides are listed in table 11. Some of their important properties are also referenced. 1) polyaminocarboxylic acids: diethylenetriaminepentaacetic acid (DTPA) is effective for Pu; 2) siderophores: catecholates (CAM), hydroxamates, hydroxypyridonates (HOPO) are mainly effective for U, Pu and Am; 3) phosphonates ligands :1-hydroxyethane-1,1′-diphosphonic acid (HEDP) is effective for U, and tris-Bisphosphoniqes displaying a high affinity for U; 4) macrocyclic compounds: calixarenes displaying a high affinity for U.

Thus three families, polyaminocarboxylic acids, siderophores and phosphonates ligands, will be illustrating in the following section.

Ligand family	Chelating agents	Elements	Toxicity or side effects	State of clinical development
Polyaminopolycarboxylics	(Ca,Zn,Na) DTPA	Pu(IV), Am(III)	Nephrotoxicity, teratogenicity, embryotoxicity, suppressed hematopoiesis	In clinics by parenteral and lung administration
Siderophores	3,4,3-LI-CAM	Pu(IV), Am(III)	Nephrotoxicity	Preclinical
	3,4,3-LI(1,2-HOPO)	Pu(IV), U(VI), Am(III)	Low acute toxicity in mice and	Phase I clinical trial
	5-LIO(Me-3,2-HOPO)	Pu(IV), U(VI)	Low acute toxicity in mice and	Preclinical
Macrocycles	para-tert-butyl calix [6]arene	U(VI)	Not tested	Preclinical
Bisphosphonics	HEDP	U(VI), Np(IV)	Nephrotoxicity, Serum calcium drop	In clinics
Polyphosphonates	tris-Bisphosphoniqes	U(VI)	Not tested	Preclinical

Table 11：Main families of ligands tested for decontamination/decorporation of Pu ,U and Am.[5,16]

1.9.1 The poly-amino-carboxylic ligands

The family of poly-amino-carboxylates (EDTA, DTPA, etc.) is known for its ability to complex metals. The multi-dentistry and the strong electron donor character of the carboxylate functions (HSAB-based solid bases), makes it possible to form stable complexes with numerous cations.

1.9.1.1 Chemical behaviors of EDTA and DTPA

H_4-EDTA (Fig. 11), a hexadentate amino-carboxylic ligand, has been applied in chemical industry since 1949 which has shown much greater stabilities of its metal chelates comparing to their complexes with polycarboxylic acids (Table 12).[77–80]

Due to the defects of $CaNa_2$-EDTA, H_5-DTPA (Fig. 11), an octadentate amino-carboxylic ligand, was designed and synthesized. The stabilities of Ca(II) with EDTA and DTPA are similar, while the stabilities of the actinides with EDTA complexes are lower than those of their DTPA complexes(Table 12).[77,78,80–83]

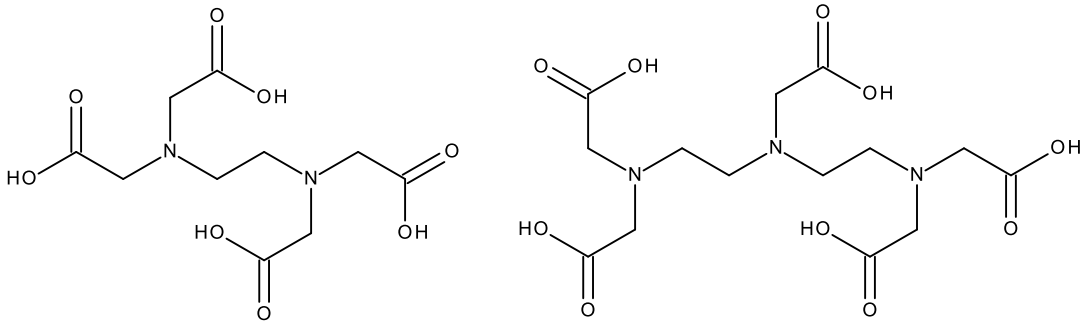

Ethylenediaminetetraacetic acid (EDTA) diethylenetriaminepentaacetic acid

Figure 11 : Chemical structure of EDTA and DTPA.

	Log K_{ML}[a]							
Metal ion (M)	Ca(II)	Zn(II)	Fe(III)	Am(III)	Np(IV)	Pu(IV)	Np(V)	U(VI)
Ligand (L)								
Oxalate	2.5[b]	2.9[c]	7.5[d]	5.0[e]	11[f]	11[c]	3.7[c]	6.1[c]
Citrate	3.4[b]	4.8[b]	11[d]	7.8[c]	15[h]	16[e]	3.0[e]	7.4[c]
EDTA	11[b]	16[b]	25[d]	17c	24f	26c	7.2c	11[c]
DTPA	11[i]	18[i]	28[d]	23[b]	29[i]	37[j]	11[f]	16[k]

Table 12：Stabilities of some metal complexes relevant to therapeutic actinide removal. a Log K_{ML}, measured at 0.1 to 0.3 mol/L ionic strength and 20 to 25°C, values rounded to two significant figures. Numerical average is shown for two suitable values. Median is shown for three or more suitable values; b[80]; c[79]; d[78]; e[84]; f[83]; g[77]; h[85]; i[86]; j[82]; k[81].

1.9.1.2 *In vivo* tests of EDTA and DTPA

For H_4-EDTA, due to the rapid depletion of serum Ca(II), 100% lethal was reached with 1.4 mmol/kg injected ip in rats. Because toxicity could be reduced by substituting by the metal ion, $CaNa_2$-EDTA, the acute LD_{50} of one ip injection in mice is 17.4 mmol/kg. Repeated injections of $CaNa_2$-EDTA was toxic for renal because the depletion of essential trace metals by forming more stable EDTA chelates [e.g., Zn(II), Mn(II)].[87,88] $CaNa_2$-EDTA enhanced excretion of Pu(IV), and Am(III).[71,89,90]

For $CaNa_3$-DTPA, the acute LD_{50} of one ip injection in mice is 12.5 mmol/kg. So $CaNa_3$-DTPA is slightly more toxic than $CaNa_2$-EDTA. Although the absorption of $CaNa_3$-DTPA and $ZnNa_3$-DTPA from the Gastrointestinal (GI) tract by oral uptake is low (3 to 5%),[91] the actinide could be removed by protracted oral administration of a high dosage chelaters. Like $CaNa_2$-EDTA repeated injections of $CaNa_3$-DTPA lead kidneys and intestinal epithelium toxicities. By using $CaNa_3$-DTPA and $ZnNa_3$-DTPA the retention of ^{238}Pu, ^{239}Pu, ^{241}Am, ^{242}Cm, ^{252}Cf, and ^{253}Es could be reduced in experimental animals and for treating actinide-contaminated radiation workers.[92] Although somewhat less effective for decorporation of foreign metal ions than $CaNa_3$-DTPA, the reduced toxicity of $ZnNa_3$-DTPA allows frequent injections and continuous infusion over extended time [93–98]

1.9.1.3 Deficiencies of polyaminopolycarboxylic acids.

Due to the low absorption, $CaNa_3$-DTPA and $ZnNa_3$-DTPA are not orally effective at the recommended clinical dosage. DTPA couldn't remove Pu(IV) from bone mineral. Octadentate DTPA satisfies the coordination requirements of An(III), thus DTPA could be used as chelation agents for Pu(IV), Am(III).[39,99] But DTPA does not satisfy the coordination requirements of An(IV). They are not effective chelation agents for Th(IV), U(VI), or Np(IV,V).[39,92,99–103] And hexadentate EDTA couldn't satisfy the coordination requirements of An(III) and An(VI). The stabilities of EDTA with An(III) and An(VI) (Table 1.12) are not large enough to compete successfully at the recommended clinical dosage with the bio-ligands which could bind metal ion in the tissues and bone.

1.9.2 Siderophores analogues: CAM & HOPO

Siderophores are the iron chelating agents which normally exist in the bacteria. Siderophores have high binding affinity and selectivity with iron.

1.9.2.1 Chemical behaviors of siderophores analogues

Hydroxamic acid is the binding unit which could be found in desferrioxamine, the linear hexadentate trishydroxamic acid. Catecholamide (CAM) is the binding unit which presents in enterobactin, the hexadentate triscatecholate. Hydroxypyridinonate (HOPO) is the binding unit

which was discovered in a few siderophores and plant products. Binding units' structures of siderophores were presented in Fig. 12.

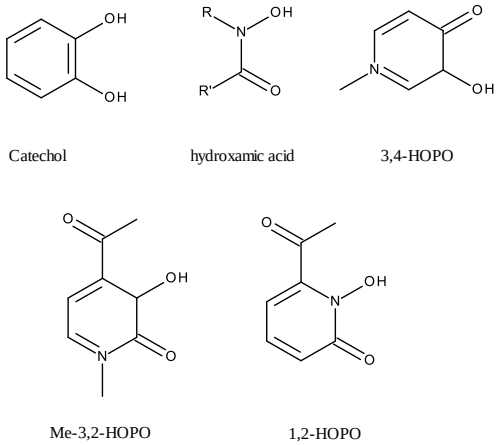

Figure 12 : Binding unit's structures and abbreviated names of siderophores. catecholate (CAM); hydroxypyridinonate (HOPO).

	pKa1	pKa2
Catechol	9,2	13
1, 2 HOPO	-0,8	5,8
3, 2 HOPO	0,1	8,7
3, 4 HOPO	3,4	9

Table 13：pKa of the catechol and hydroxypyridinone groups.[39]

The three units, hydroxamic acid, CAM and HOPO, could provide "hard" oxygens as the electron donors for the coordination which preferred by actinide ions.[104] 1,2-HOPO and 3,2-HOPO (Fig. 12), HOPO isomers, are structural and electronic analogs of hydroxamic acid and catechol, respectively. The amides of two isomers could deprotonate at pH 6.1 (Table 13), and the stability constants of two isomer with Fe(III) is higher than those of divalent cations complexes. For this reason, they considered as the promising binding unit for An(III) and An(IV) in the range of physiological pH.[105]

The group of Professor Kenneth N. Raymond synthesized fifty-five multidentate ligands which are composed by the molecular backbones as linear or cyclic and binding groups from siderophores. The affinities of these ligand with Pu(IV) or U(VI) were evaluated *in vivo*.[39,106]

The crystal structures of uranyl 5-LIO(Me-3,2-HOPO) complex and Gd(III) TREN(Me-3,2-HOPO) complex were show in Fig. 13. The crystal structures of uranyl 5-LIO(Me-3,2-HOPO) complex has similarities with the U(VI) complexes with several linear tetradentate Me-3,2-HOPO ligands. The coordination of uranyl ion is composed by the ligand molecule and one water molecular.[107] The uranyl ion has five coordination numbers in the equatorial plan. Due to the similar coordination properties of Am(III) and Gd(III), the structures of Am(III) TREN-(Me-3,2-HOPO) complex are similar to one of their respective Gd(III) analogs. The stability constant log K_{110} of Am(III) TREN-(Me-3,2-HOPO) complex is 20.3.[108]

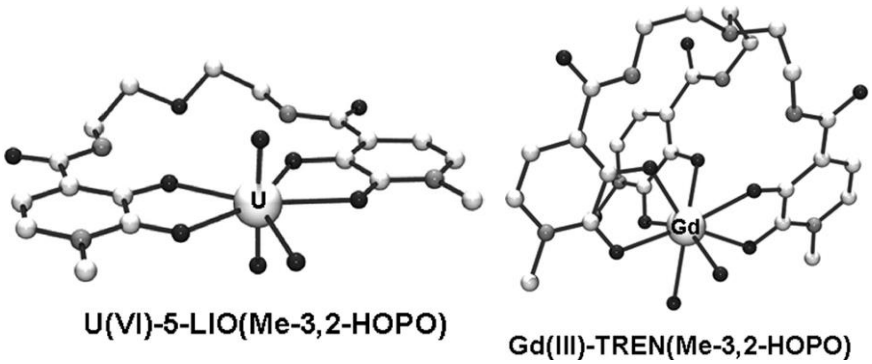

Figure 13 : Crystal structures of uranyl 5-LIO(Me-3,2-HOPO) complex[107] and Gd(III)

***In vivo* tests of siderophores analogues**

For the siderophores analogues, the acute toxicities in mice of the most effective HOPO ligands are different depending on the structure of ligand. Acute toxicity was primarily due to chemical nephrosis.[102,106] It ranges from absent or very mild [5-LIO(Me-3,2-HOPO), 5-LI(Me-3,2-HOPO), TREN-(Me-3,2-HOPO)], to moderate [(3,4,3-LI(1,2-HOPO), 3,4,3-LI(1,2-Me-3,2-HOPO)] to severe [4-LI(Me-3,2-HOPO)]. The efficient removal of actinides which are deposited in the liver by the HOPO ligands is due to the direct access to the hepatic cells, after the actinide HOPO ligand complex could be substantial fecal excreted.[106,109,110] the toxicity of ligand was further proved by the 24 hours renal residence times of moderately toxic, 3,4,3-LI(1,2-HOPO) and 3,4,3-LI(1,2- Me-3,2-HOPO), which are about midway between those of the least and most toxic ligands.[111]

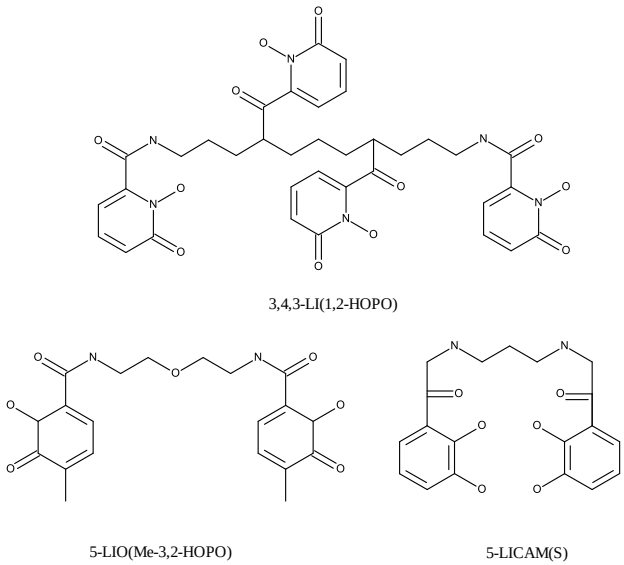

Figure 14 : chemical structures of 3,4,3-LI(1,2-HOPO), 5-LIO(Me-3,2-HOPO) and 5-LICAM(S).

For U(VI) *in vivo* decoporation tests, tetradentate 5-LICAM(S) and 5-LIO(Me-3,2-HOPO) and octadentate 3,4,3-LI(1,2-HOPO) (Fig 14) are the three ligands which have good performance among the twenty multidentate ligands which consist with 1,2-HOPO, Me-3,2-HOPO and CAM. The U(VI) in kidney and body could deceased 24 and 54% of control. With 5-LIO(Me-3,2-HOPO) and 3,4,3-LI(1,2-HOPO) the best reductions of U(VI) in kidney could be reached. With 5-LICAM(S) U(VI) in skeleton was reduced to half of control. Cocktail chelation investigations were done by different ligands which more efficient for kidney and skeleton respectively. Equal mole ration of 5-LIO(Me-3,2- HOPO) and 5-LICAM(S) are more effective for reducing U(VI) in all tissues which is about twice as much of either ligand alone.

For Am(III) *in vivo* decoporation tests, the first attempts were done with multidentate ligands containing catecholate or hydroxamate. The results shown that these ligands are not effective for Am(III) decorporation,[112,113] The reason is due to the low charge density of Am(III) (30.8 e nm^{-1}) which hardly deprotonates sufficient numbers of the OH groups of binding units at physiological pH.[41,112,114] Then four HOPO ligands were tested *in vivo*. Octadentate 3,4,3-LI(1,2-HOPO) has shown the best reduction of Am(III) in the skeleton and tissues which is as effective as $CaNa_3$-DTPA. Due to the insufficient denticity, the other ligands are not as good as 3,4,3-LI(1,2-HOPO).[115,116]

Mixed oxide (MOX) particles was injected im into rats, after 3,4,3-LI(1,2-HOPO) was repeatedly injected into the wound site. The retention of ^{241}Am, the decay product of ^{241}Pu, in bone and tissues are translocated from the wound. The amount of ^{241}Am, which has been removed, was more important than the one obtained by the same treatment with $CaNa_3$-DTPA.[11]

1.9.2.2 Deficiencies of siderophores analogues

The linear octadentate catecholates offer the advantages of oral activity and effectiveness at low dosage, but they are defective. It dissociates at the reduced pH of the kidneys depositing Pu(IV), and a stable Pu(IV) chelate may not form in the slightly acidic environment of the lungs.[95,113,117–120] The charge density (e nm^{-1}) of Pu(IV) is not great enough to deprotonate more than six of the eight OH groups of the octadentate catecholate ligands at pH 7.4.[112,113] For the hydroxypyridinonate, special care need to be considered due to the ligand toxicity.

1.9.3 Phosphonate ligands

1.9.3.1 Chemical behaviors of phosphonate ligands

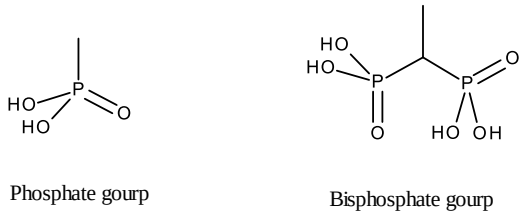

Figure 15 : Structure of phosphonate group and bisphosphonate group.

Phosphonate group and bisphosphonate group also provide “hard” oxygen and form monodentate bond with actinides under biological conditions (Fig. 15).

1-hydroxyethane-1,10-diphosphonic acid (HEDP) (Fig. 16) could inhibits bone resorption, and was used for some skeletal disorders treatment. The group of Frédéric Taran synthesized fifty-three multidentate ligands for uranyl chelation therapy which are composed by the molecular backbones and bisphosphonate binding group groups from HEDP.[75]

The stability constant of uranyl with HEDP 1:1 complex is 7.7 at pH 7. The structures of the uranyl HEDP complex were proposed (Fig. 17).[121] For the bisphosphonate ligands which were synthesized by the group of Frédéric Taran, a displacement method of the uranyl sulfochlorophenole (scp) complex by competition ligand (bisphosphonate ligands in this case) with UV-visible spectroscopy was developed for fast conditional stability constant determination of the uranyl ligand complex at pH 5.5 and 7.4 which are the pH of kidneys and blood respectively.[122] The example of displacement method was listed in Fig 18. This method provides the estimation of chelation affinity of ligand with uranyl ion at the pH of kidneys and blood by adding two equivalence of candidate ligand to uranyl SCP 1:1 complex in 112.5 mmol $nBu_4^+Cl^-$ solution with respect buffer, CHES for pH 5.5, HEPES for pH 7.4, to maintain the pH. Due to the complexation of sulfochlorophenole with sodium ion, it is important to use the ionic

liquid as the ionic strength.

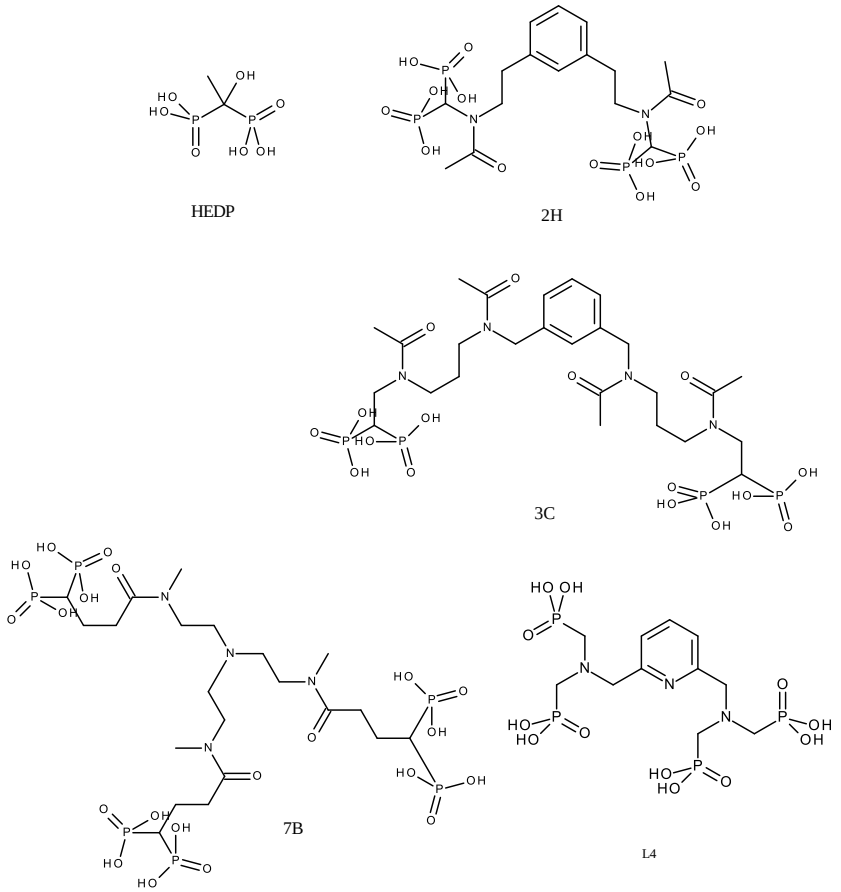

Figure 16 : Structure of 1-hydroxyethane-1,10-diphosphonic acid (HEDP), three bisphosphonate sequestering ligands (2H, 3C, 7B) and polyaminophosphonates ligand (L^4).[75]

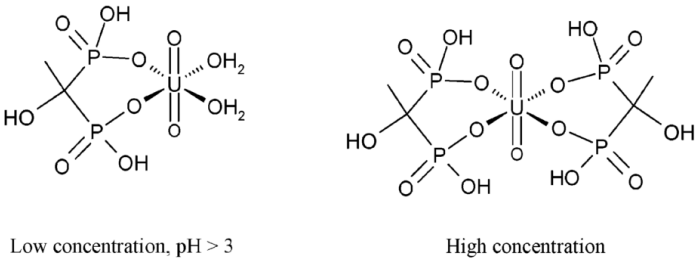

Figure 17 : Proposed Structure of the Uranyl-HEDP Complex.

Polyaminophosphonates ligands have proved to be efficient chelating agents for ^{64}Cu and ^{99m}Tc which are widely used in Positron Emission Tomography (PET) and Single Photon Emission Computed Tomography (SPECT).[12,123–125] A series of ployphosphonated pyridine ligands were synthases by the group of Prof. Loïc J. Charbonnière in Université de Strasbourg.[12,13,126–130] The test with polyaminophosphonates ligand **L^4** and europium proved the high stability in aqueous solution which $\log K_{EuL}$ is 25.7. The coordination of europium is composed by 3 nitrogen atoms and 4 oxygen atoms from the ligand and 1 oxygen atom from the water molecular.[13] As europium is the chemical analogue of americium, this ligand could be used as the actinides(III) chelating agents.

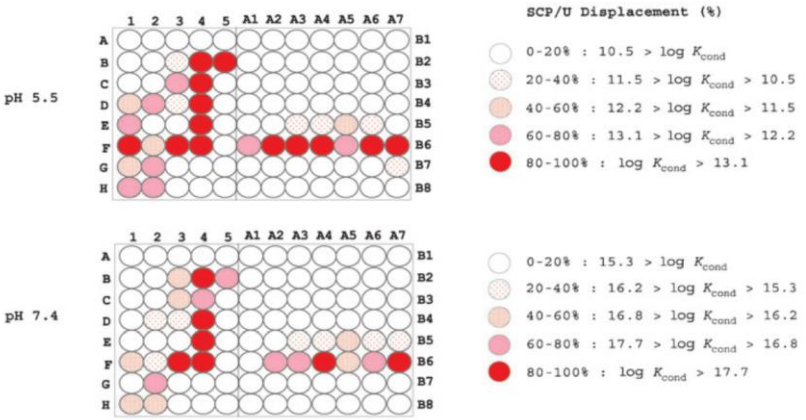

Figure 18 : Example of displacement method: Displacements (%) of the uranyl SCP complex are presented in a color-coded format for clarity reason. logK_{cond} (estimates) were calculated by using the HYSS program supposing that the complex competitive uranyl/ligand is 1:1.[122]

1.9.3.2 *In vivo* tests of phosphonate ligands

Twenty polyphosphonic or phosphinic acids and derivatives were injected at t=30 min (molar ratios 1.6/104) in rats that had been injected with ^{233}U(VI) nitrate. Immediate injection of the compounds DTPMP, EDTMP, or HMTMP reduced ^{233}U in kidneys and enhanced urinary ^{233}U excretion. Compounds DDMT, CDTT, or BCPBP injected at 30 min reduced ^{233}U in kidneys and body, and compound E enhanced ^{233}U excretion.[131]

Rats, injected with a 50% lethal amount of U(VI) nitrate, were promptly injected with HEDP (molar ratio 124). Survival was 100% at 60 d, and kidney structure was within normal limits.[132] Rats were injected im with ^{233}U(VI) nitrate, and EHBP was injected im at the wound site at 5 or 30 min (molar ratio 5,000) or injected ip (molar ratio 2,500). Injection of HEDP im or ip at 5 min significantly reduced ^{233}U in kidneys and increased urinary ^{233}U excretion.[133] The bio-distribution of uranyl with 25 bisphosphonate ligands, dipodal bisphosphonates with $K_{cond}>10^{17}$ and tripods with Kcond>10^{18} at pH 7.4, was investigate (Table 14). Among them, three bisphosphonate ligands, 2H, 3C, and 7B, could increase the uranyl ligand complex excretion. This result might suggest that this hepatic deposition is avoided when N-methyl-amide moieties are present. A uranium removal study was done with HEDP, 5-LICAM(S), 2H, 3C, and 7B in mice. Only 3C have the similar ability like HEDP to promote the uranyl excretion about 50% in the 5 days after ^{233}U(VI) injected ip.

Ligand	**Percent of injected ^{233}U(VI)±SD at 5 days**				
	Retention			Excretion	
	Kidneys	Skeleton	Liver	Urine	Feces
No (controls)	**8.0**±2.3	**34.2**±4.5	**0.4**±0.0	**40.7**±3.4	**1.8**±1.0
HEDP	**5.5**±0.5	30.2±1.2	0.4±0.1	**50.1**±4.3	2.9±1.7
5-LICAM(S)	6.3±0.8	**22.8**±4.7	0.5±0.1	**48.0**±5.7	2.2±1.2
2H	6.7±1.3	**41.8**±3.9	2.8±0.5	31.6±7.8	**4.9**±1.3
3C	**3.6**±0.6	32.4±1.5	0.3±0.0	**53.5**±2.7	2.3±0.5
7B	**3.4**±0.6	**23.9**±0.5	1.5±0.6	**29.7**±5.1	1.4±0.6

Table 14 : Effect of a prompt injection of bisphosphonate ligands on the biodistribution and excretion of ^{233}U(VI). Ligands were injected ip (30 mmol/kg, molar ratio 100) 5 min after injection of 9.2 kBq of ^{233}U(VI); animals were sacrificed 5 days later. Data are expressed as % of injected radioactivity, discrepancies are due to rounding. Bold means are significantly different than control mean.[75]

The ^{99m}Tc SPECT/CT of mice images shown that the complex of ^{99m}Tc with four phosphonate groups ligand **L^4** rapidly accumulated in the kidneys after 5 minutes, and part of complex could be found in the bladder after 2 h. But part of the complex is accumulated in bone tissues after 4 h. For the case of complex of ^{99m}Tc with two phosphonate groups ligand, part of the complex could be found in the kidneys after 7 min, and then transferred to the bladder after 1 h 10 min.

1.10 Methods for *in vitro* study

In order to perform study under the bio-conditions, a number of biology-relevant actinide ligands, minerals, organics, proteins and amino acids, and metals, present in a few media within the human body (saliva and blood serum) and their concentrations are listed in table 15, together with the composition of a cell culture medium used for *in vitro* experiments that simulate actinide behavior.

Components (M)	Blood serum	Saliva
pH	7.4	5.6–7.6
E (mV)	200–300	200–300
"Mineral"		
Carbonate	2.5×10^{-2}	6.6×10^{-3}
Phosphate	1.1×10^{-3}	3.7×10^{-3}
SCN^-		2.1×10^{-3}
F^-		7.3×10^{-6}
SO_4^{2-}	3.3×10^{-4}	3.3×10^{-4}
Cl^-	9.0×10^{-2}	2.9×10^{-2}
NH_4^+		2.6×10^{-3}
"Organic"		
Ascorbate		8.0×10^{-6}
Citrate	1.6×10^{-4}	5.4×10^{-5}
Lactate	1.5×10^{-3}	1.4×10^{-6}
Oxalate	9.2×10^{-6}	
"Proteins + amino-acids"	10^{-4} to 10^{-5}	10^{-4} to 10^{-5}
Albumin	6.3×10^{-4}	
Transferrin	3.7×10^{-5}	
Urea		3.0×10^{-3}
HEPES buffer "Metals"		
Ca^{2+}	1.4×10^{-3}	1.5×10^{-3}
Mg^{2+}	5.6×10^{-4}	2.7×10^{-4}
Na^+	9.0×10^{-2}	1.0×10^{-2}
K^+	4.9×10^{-4}	2.0×10^{-2}
Fe^{2+}	3.0×10^{-5}	

Table 15：Major actinide ligands (M) present in selected in vivo human biological media.[134]

1.11 Conclusion

Due to the affinity difference of the binding groups at the biological pH of blood and kidneys, 7.4 and 5.5 respectively, the actinide ion which are complexed by the chelation agent

could be dissociated, e.g. Pu(IV) catecholates complex. Carboxylic group, HOPO and phosphonate group showed the affinity to complex the actinide ions under different biological pHs.

For the actinides chelation agents which have been studied in the past, the structure contains two parts, the binding group and the backbone. The binding group can be carboxylic group, CAM & HOPO or phosphonate group which have been reviewed in the previous chapter. The backbone influences the stability of the metal chelate by the spatial arrangement of the binding groups.[66] It has no ability to coordinate the metal ion, and impact the solubility and toxicity. This phenomenon confirmed be the study of different siderophore analogues[39,74,102,110,112] and bisphosphonate ligands[75,122].

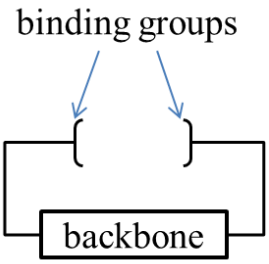

Figure 19 : Structure illustration of actinides chelation agents

Phosphonated pyridine ligands, new design of chelation agents, have offered another possibility with structural and coordination properties suitable for actinide chelation. The binding group is a phosphonate group which could complex the actinide ion at biological pH. By using pyridine group as the backbone, the ligand structure is more compact which promotes the selectivity.

For this study, polyaminophosphonates pyridine ligands with 5 donors from phosphonate groups, amine part and pyridine group at the equatorial planar will be synthesized for uranium decorporation investigations.

Chelation study for biology simulation with calmodulin

It is important to understand to possible behavior of the ligand in the actinide chelation therapy. Because plenty of work on the interactions between uranyl ion and calmodulin was done by Dr. Florian BRULFERT from Institut de Physique Nucléaire d'Orsay, a ternary system with uranyl ion, ligand and calmodulin was chosen for a preliminary test for the chelation study for biology simulation.

1.12 Description of the protein

Intracellular calcium, a secondary messenger, is playing an important role in extracellular stimulus. The increasing of calcium in the cytoplasmic could lead to the complexation between this metal and the intracellular regulatory protein. One of the many proteins responsible for the regulation of Ca^{2+} is calmodulin (CaM). It is a ubiquitous, multifunctional protein which can active several enzymes such as phosphodiesterase, ATPase, calmodulin kinases.[135]

Calmodulin is a small globular protein consisting of a peptide chain of 148 amino acids for a total mass of about 16700 Da by amino acid sequence.[136] It contains a large proportion of aspartate and glutamate (35%) which provides plenty of acidic amino acid carboxylate groups. Thus it is a relatively acidic protein. This amino acid sequence forms two similar globular ends

which contain two calcium binding domains. Each complexation site is described as helix-loop-helix "EF-Hand" region (EF-1, EF-2, EF-3 and EF-4 numbered from the N-terminal domain). The EF-3 and EF-4 binding domains of the C-terminal domain have an affinity for calcium 10-20 times higher than the EF-1 and EF-2 binding domains of the N-terminal domain.[137–139] The complexation affinity of calcium by each pair of binding domains is cooperative.[140,141]

Calmodulin (CaM) is found in almost all eukaryotic cells.[142,143] It believed to be involved in intracellular Ca^{2+} homeostasis, cell proliferation, smooth muscle contraction, microtubular function, exocytotic secretion of cellular products, and cell motility.[144] The primary structure has been remarkably conserved which suggest that each binding domains of calcium and each structural parameter of the protein is useful for its various functions. Thus different occupation degrees of the binding domains can translate a quantitative calcium concentration difference into a qualitatively different cellular response by interaction with different types of enzymes or molecules depending on the calcium concentration.[140]

Calmodulin, thanks to its various roles in the human body, represents a subject of study of particular interest in the radioactive decontamination investigation.

1.13 Interaction between calmodulin and calcium

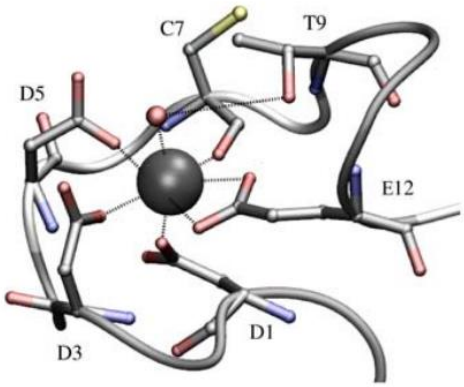

Figure 20 : Schematic of the calcium binding site 1 of Paramecium tetraurelia calmodulin.[145]

Calcium is a divalent ion which preferentially forms bonds with oxygen donor ligands. The preferential coordination of the ion comprises seven ligands arranged either in distorted octahedron or bipyramidal pentagon. The main-EF motif is responsible for the complexation of calcium in proteins.[146] It is composed of two orthogonal α-helices that flanks a flexible complexation site that provides the residues involved in coordination at positions 1, 3, 5, 7, 9 and 12 (Fig. 20).

In CaM site 1 (Fig. 20), the coordination sphere of calcium is composed of three monodentate aspartates at positions 1, 3, 5, a bidentate glutamate at position 12, a carbonyl from the main chain at position 7 and a water molecule stabilized by threonine at position.[147,148] The composition of the calcium coordination site (hard and acid ligands) could form complexation with other metals such as uranyl or minor actinides[148,149]. Meanwhile a competition between uranyl and calcium for the occupation of the calcium binding domains of certain proteins has been confirmed .[150,151] Lanthanides could occupy the calcium binding domains also.[146] Ln^{3+} binds to the N-terminal of calmodulin first, while Ca^{2+} binds to the C-terminal domain of the protein first.[152]

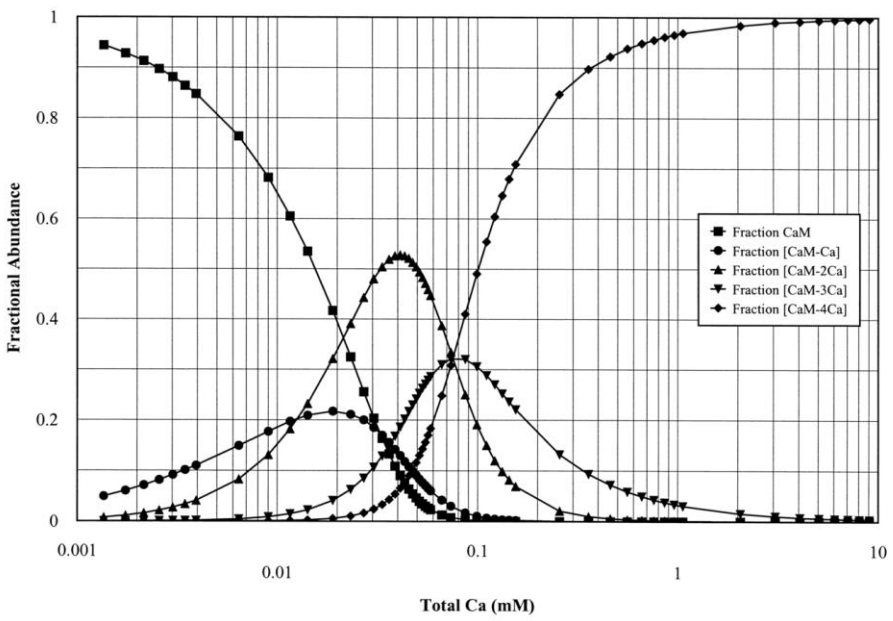

Figure 21 : Fractional species calculation for Ca_x^{2+}(calmodulin) as a function of [Ca^{2+}]. The total calmodulin concentration is 15µM.[153]

The four similar binding domains of calcium present some different ability on calcium complexation. The sequential stability constants are as follows: K_1 = 1.3E5 M^{-1}, K_2 = 3.7E5 M^{-1}, K_3 = 3.2E5 M^{-1}, K_4 = 3.2E5 M^{-1}.[153] A large excess of calcium is required for the four sites of the protein to be loaded (Fig. 21).

1.14 Interactions between calmodulin and actinides

There isn't sufficient information over the complexation of actinides by CaM. However, Pu(III) could be complexed by this protein, and also occupy the complexation site of calcium and therefore can replace it in case of internal contamination.[154] Uranyl ion has been the subject of several affinity studies and the results obtained show that it also present a high affinity for CaM (K_d = 32 ± 7 nM[145]). Uranyl also occupies the calcium site[149], as is the case of other proteins[150,155], which it is therefore required to replace in case of internal contamination. The EXAFS data could fit well with the DFT calculations for the synthesized CaM motif (Fig 22).[149]

Further work on trivalent ions (such as lanthanides which are americium analogs) has shown that these lanthanides have a high affinity and even greater than calcium for CaM. The ionic radius of these ions is similar to calcium.[156] And a study by Song et al[157] showed that complexation of these lanthanides by CaM could also active the target enzymes which is similar when complexed with calcium.

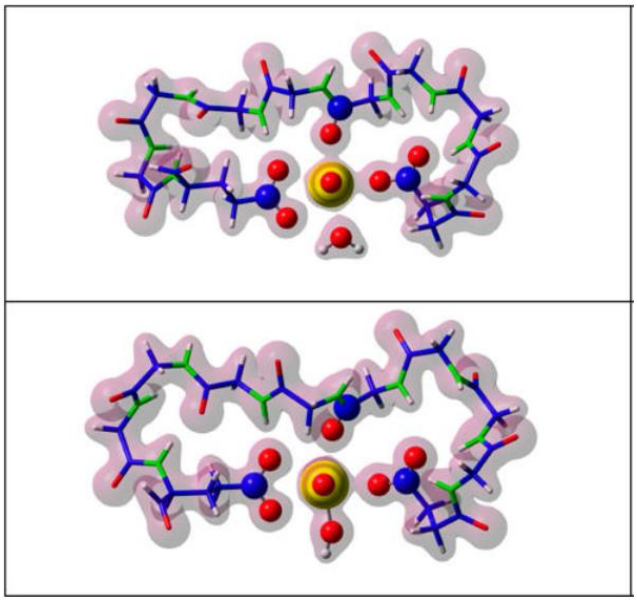

Figure 22 : Theoretical models and electronic density of the U(VI) interaction sites on the CaMWT calculated by DFT (oxygen: red, carbon: blue, nitrogen: light green, uranium: yellow and neptunium: dark green).[149]

Calmodulin with a relatively high affinity towards uranyl, is therefore chosen on decorporation study.[155,157] In this study, fluorescence study on uranyl, while the chelation agent and calmodulin are present, was done to investigate the evolution of decorporation rate.

Chapiter 2: synthesis of polyaminophosphonates ligands

1 General strategy

Although uranium is used as colorants since Roman times[158], and widely used in the nuclear industry and for military applications for now, there is only a few people which contaminated by this metal. Consequently, uranium poisoning is not currently a major public health issue. Thus, the development of ligands which has a strong affinity towards uranium is slowly promoting. The groups of Prof. K. N. Raymond of the University of Berkeley and Frédéric Taran of CEA Saclay, reweld by some teams all over the world, are the main actors which focus on the uranyl decoperation agent research. There are a few ligands which could effective complex uranyl *in vivo*.

Based on this situation, the ligand for the MRI contrast which has been extensively studied is a promising candidate.[130,159–163] Normally these ligands, molecular mass is between 300 and 600, could provide 7-8 coordination for lanthanide and have a really strong complexation affinity. Meanwhile the excretion of metal ligand complex is pretty fast, hours to days. The toxicity is relatively low.

Among all the MRI contrast ligands, polyaminophosphonates ligands have been chosen for this study. The synthesis of polyaminophosphonates ligands was developed by the group of Prof. Loïc Charbonniaire from IPHC.[12] The main idea is by using phosphonated groups which shown hard base character and high negative charge to functionalized the position 2 and 6 of pyridine. In this way the stability of uranyl-ligand complex could be increased.

Due to the different coordination of uranyl and lanthanide, several synthesis routes have been tested to have a new polyaminophosphonates ligand with 5 coordinations (Figure 23). Three new ligands **L^1-L^3** with 2 phosphonated groups were successfully synthesized. In order to understand the coordination processes of **L^1**, another analogue (**L^4**), synthesis by the group of Loïc Charbonniaire, has been used for the further study. The structures of the **L^1**, **L^2, L^3** and **L^4** are shown in figure 23.

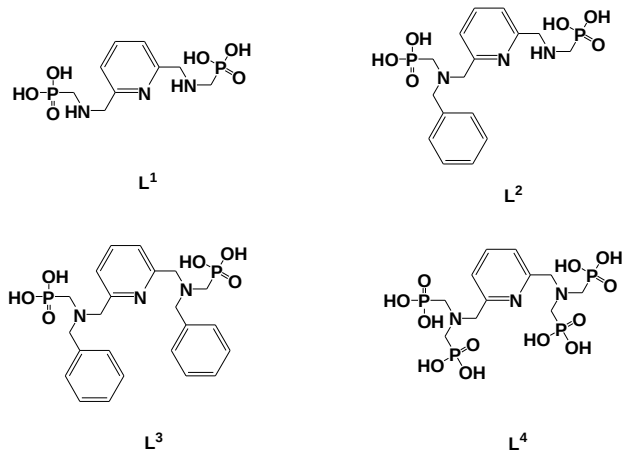

Figure 23 : Chemical structure of ligands L^1, L^2, L^{3}and L^4.

Synthesis of precursor

To get polyaminophosphonate ligands **L^1-L^3**, is required prior synthesis of the pyridinic platform **1** which carry the phosphonate arms (Figure 24). The phosphonate arms precursors are compounds **3** and **5** (Figure 24).

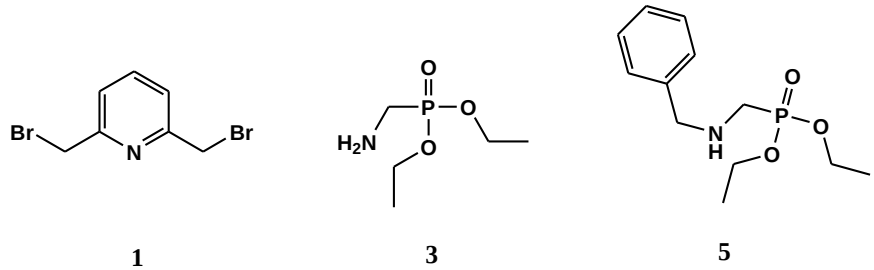

Figure 24 : Chemical structure of precursors.

1.1 Synthesis of pyridinic platform

2,6-dibromomethylpyridine **1** was obtained in a single step by reaction of PBr_3 with 2,6-hydroxymethyl-pyridine in DMF at 0°C (scheme 3).[164]

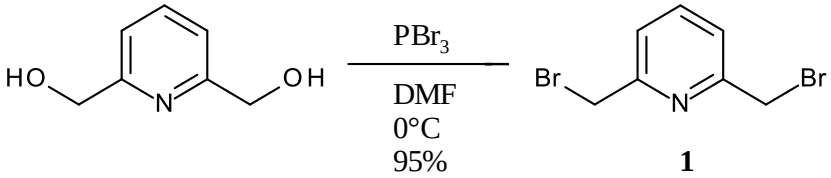

Scheme 3 : Synthesis of 2,6-dibromomethylpyridine.

1.2 Synthesis of amine monophosphonate

Diethyl (aminomethyl)phosphonate **3** was obtain from diethyl phosphate by the Kabachnik−Fields reaction in a two steps reaction (scheme 4).[165] The first step is by adding dibenzylamine and formaldehyde to a solution of diethyl phosphite in THF to get Diethyl ((dibenzylamino)methyl)phosphonate **2**. Then a palladium-carbon catalyzed hydrogenation reaction has been performed to yield the desired compound **3** (scheme 4).[166]

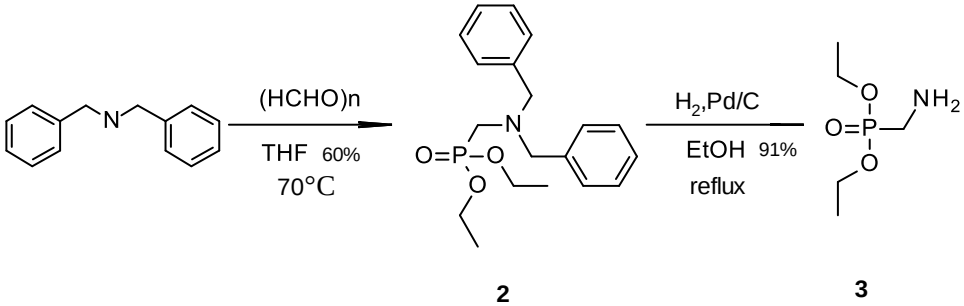

Scheme 4 : Synthesis of diethyl (aminomethyl)phosphonate.

Diethyl ((benzylamino)methyl)phosphonate **5** was obtain from benzylamine in two step (scheme 5). To a stirred solution of benzylamine, formaldehyde was added to get 1,3,5-Tribenzylhexahydrotriazine **4**.[167] The desired compound **5** was synthesized by react with diethylphosphite.[168]

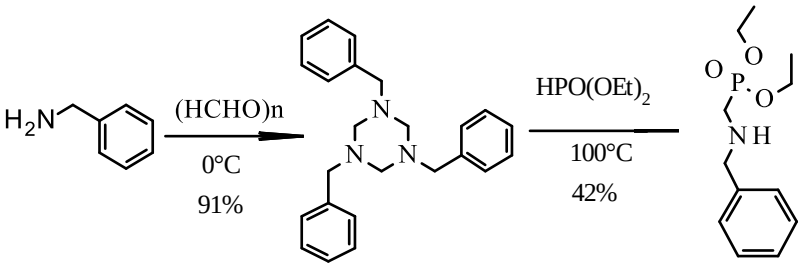

4 **5**

Scheme 5 : Synthesis of diethyl ((benzylamino)methyl)phosphonate.

Synthesis of bisphosphonate ligand L^1

The ligand $\mathbf{L^1}$ was synthesized in 2 different routes. But due to low yield and byproduct, two synthesized routes were not possible to get the precursor. The synthesis of ligand $\mathbf{L^1}$ cannot be done.

First synthesized route:

In this synthesis route (Scheme 6), precursor compound **6** was obtained by reacting dibrominated pyridine **2** with compound **3** in acetonitrile in the presence of K_2CO_3. But due to the polynuclear reaction between the residues N-H with bromine, the yield was below 10% for various conditions. So that we tried the second route to get $\mathbf{L^1}$.[12]

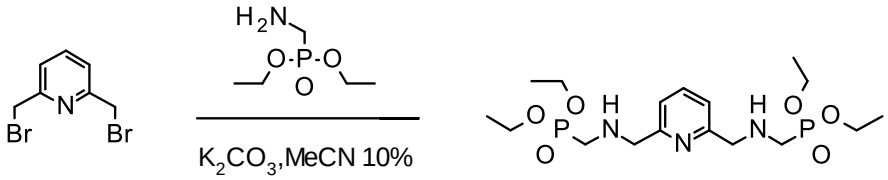

1 **6**

Scheme 6 : First synthesized route of bisphosphonate ligand L^1.

Second synthesized route:

In this synthesis route (Scheme 7), compound **7** was obtained by dibrominated pyridine **2** with compound **5** in acetonitrile in the presence of K_2CO_3. Then a palladium-carbon catalyzed hydrogenation reaction has been performed to yield the precursor compound **6.** Due to the cleavage of the carbon chain between nitrogen with benzyl group, there are several ways to break carbon chain which could form different byproduct; this route was not acceptable.

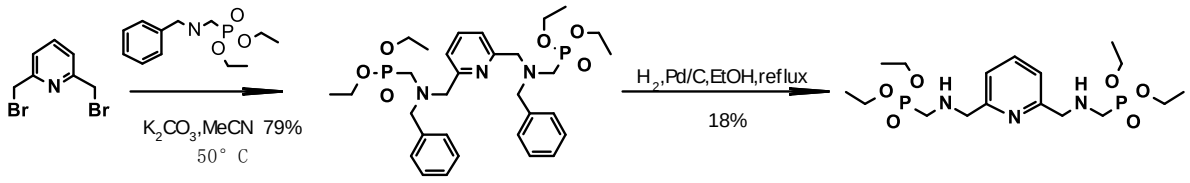

1 **7** **6**

Scheme 7 : Second synthesized route of bisphosphonate ligand L^1.

Synthesis of bisphosphonate ligand L^2

Compound **8** was obtained by dibrominated pyridine **2** with less equivalence compound **5** in acetonitrile in the presence of K_2CO_3 (Scheme 7). Precursor compound **9** was obtained by

compound **8** with compound **3** in acetonitrile in the presence of K_2CO_3. The yield of two steps reaction to get precursor was low (10%). Thus the synthesis of bisphosphonate ligand $\mathbf{L^2}$ was abandoned.

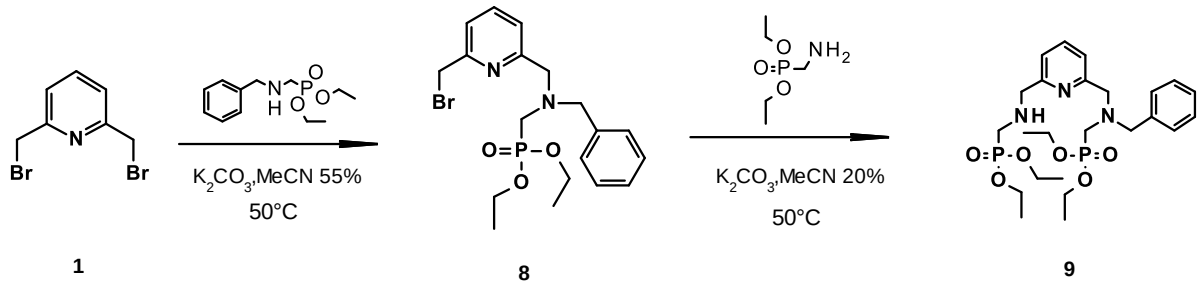

Scheme 8: Synthesized route of bisphosphonate ligand L^2.

Synthesis of bisphosphonate ligand L^3

Compound **7** was getting in the same way in second synthesized route of bisphosphonate ligand $\mathbf{L^1}$. In this synthetic route, the deprotection of the ethyl groups is carried out in concentrated HCl medium. There are three ligands, $\mathbf{L^1}$, $\mathbf{L^2}$ and $\mathbf{L^3}$ which were found in the crude after purified with revise phase chromatography. The yields for each compound are 9% for $\mathbf{L^1}$, 13% for $\mathbf{L^2}$ and 52% for $\mathbf{L^3}$. The total efficiency of this deprotection is 74%. The reason of generation of $\mathbf{L^1}$ and $\mathbf{L^2}$ was not found in the literature.

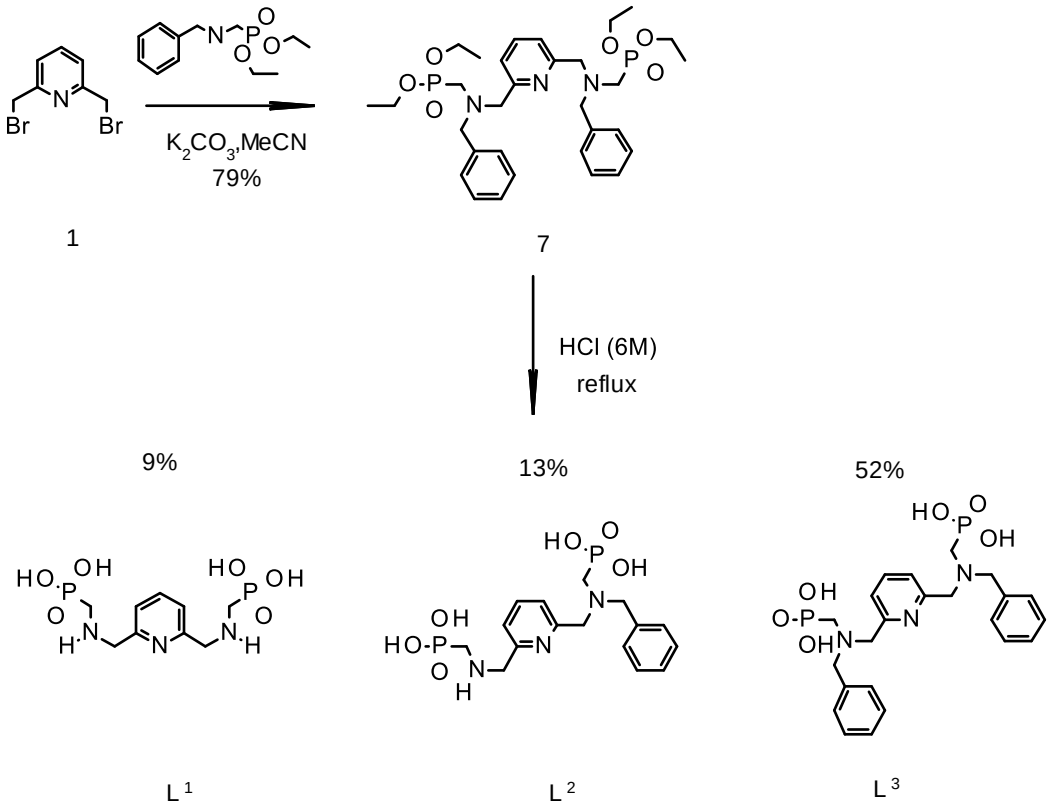

Scheme 9: Synthesized route of bisphosphonate ligand L^3.

The $\mathbf{L^1}$-$\mathbf{L^3}$ ligands synthesized were all characterized by ^{1}H NMR, ^{13}C NMR and ^{31}P NMR. $\mathbf{L^2}$ and $\mathbf{L^3}$ were further analyzed by elementary analysis and ESI-MS mass spectrometry in negative mode.

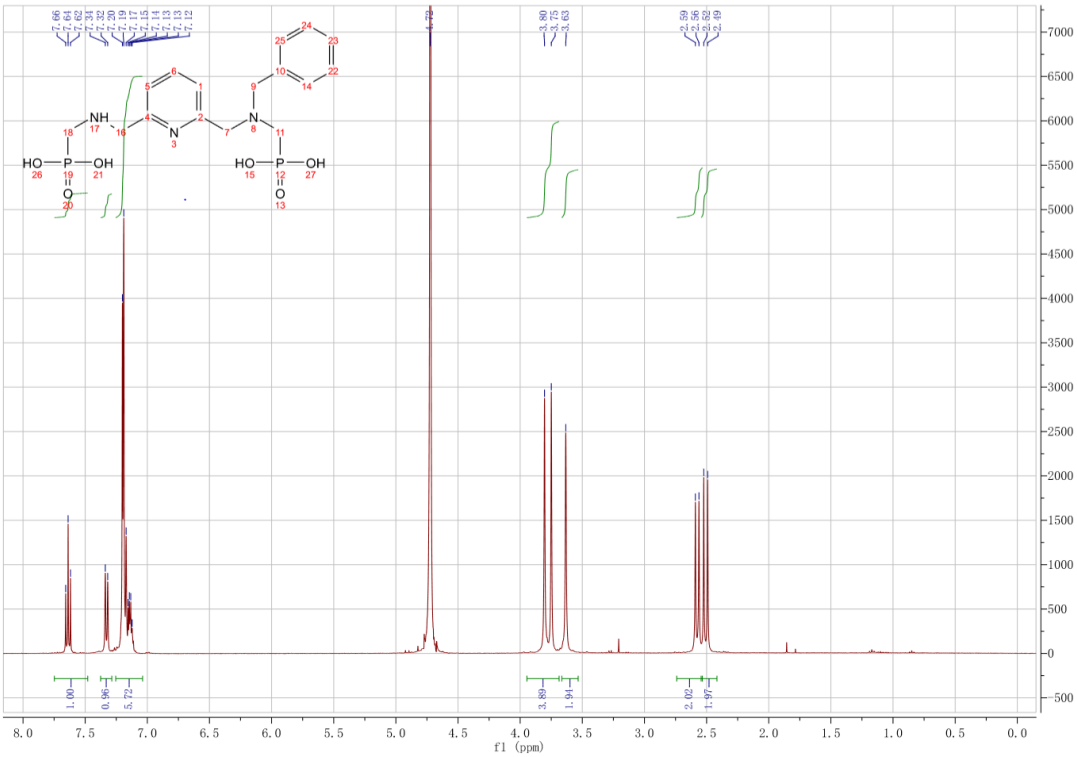

Figure 25 : ^{1}H RMN spectrum of ligand L^{2} (D_2O, 400 MHz, t.a.).

The ^{1}H NMR spectra of the **L^{1}-L^{3}** ligands are characterized by a splitting of the alpha phosphorus proton signals explained by a coupling with the phosphorus atom ^{31}P of spin S = 1/2. By the example above, we perform the attribution of proton spectrum of ligand **L^{2}** (Figure 25). The 3 protons of pyridine appear in the form of two doublets associated with a triplet with weak fields. The protons of benzyl group appear as multiple peaks at high chemical shift range. The -CH_2 protons of gamma phosphonates are come out in the form of a doublet from 2.3 to 2.7 ppm.

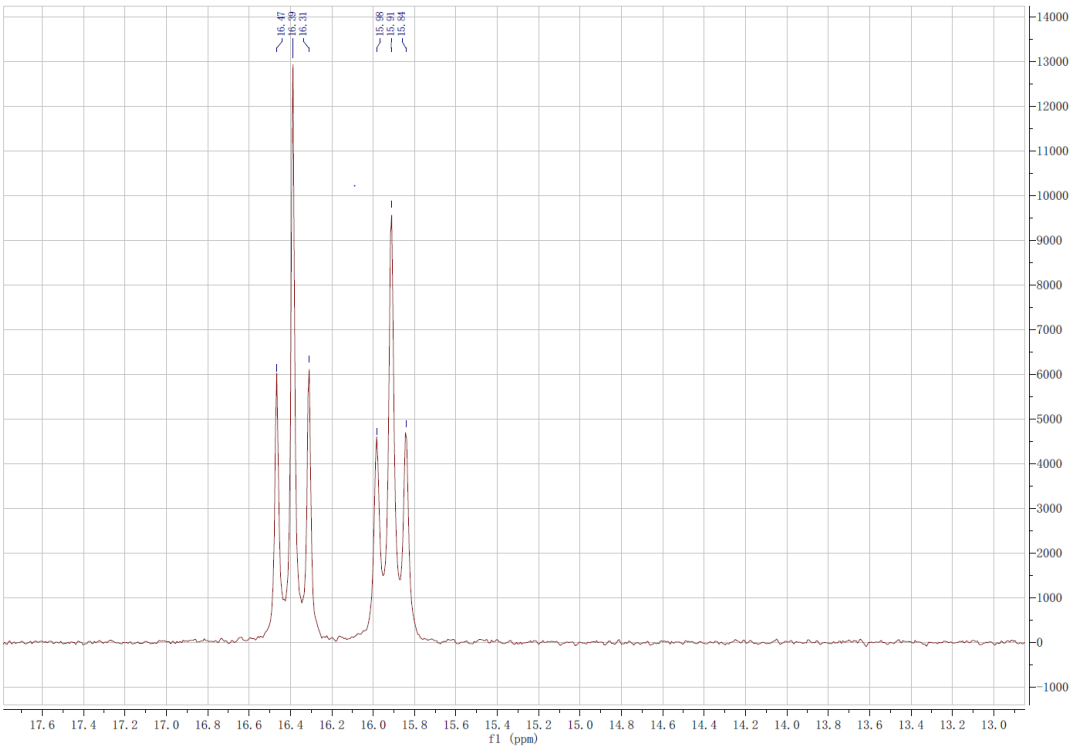

Figure 26 : ^{13}P RMN spectrum of ligand L^2 (D_2O, 161.9 MHz, t.a.).

The NMR spectrum of phosphorus exhibits two triplet peaks at 16 and 16.4 ppm respectively for the ligands $\mathbf{L^2}$ because of the asymmetric (Figure 26). In contrast to the $\mathbf{L^2}$, the ^{31}P NMR spectra of the $\mathbf{L^1}$ and $\mathbf{L^3}$ ligands, which are symmetric, have only one triplet peak at 16.5 ppm and 8.5 ppm respectively.

Conclusion

In this chapter, the synthesis of a new family of acyclic polyaminophosphonate ligands is shown. This ligand family is based on the pyridine platform which carries two phosphonate groups.

The synthesis of these ligands is based on three main reactions: the first is the N-alkylation with amino-methylphosphonate groups and ((benzylamino)methyl)phosphonate on a dibromed derivative of pyridine. The second is the palladium-carbon catalyzed hydrogenation reaction to remove the benzyl group. The third is the deprotection reaction of the phosphonic esters in HCl (6M).

It is interesting to note that the benzyl group will be removed while the deprotection of the phosphonic esters in HCl (6M) to get the final product. Ligand $\mathbf{L^3}$ is obtained with acceptable yield. $\mathbf{L^1}$ and $\mathbf{L^2}$ were obtained as byproduct.

To obtain these polyaminophosphonate ligands, the prior synthesis of two diphosphonate precursors is required. Sequently three acyclic ligands, synthesized from a pyridinic chromophore and phosphonate groups, could provide sufficient donors for the equatorial complexation of uranyl (UO_2^{2+}). The next chapter will be devoted to the determination of the coordination properties and thermodynamic constants in aqueous medium of uranyl complexes for chelation therapies. The structural studies of Eu^{3+}, as analogue of Am^{3+}, with ligands also investigated in the following chapter.

Experimental part

Synthesis of ligand L[1]

First route:

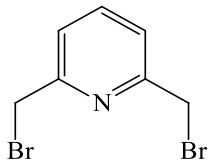

1

2,6-Bis(bromomethyl)pyridine 1. To a solution of 2,6-pyridinedimethanol (3.36 g, 24.1 mmol) in DMF (20 mL) at 0 °C, PBr_3 (5.22 mL, 55.6 mmol) was added dropwise. The mixture was stirred at room temperature for 6 h, then water was added (300 mL) to solubilize the formed solid. After extraction with CH_2Cl_2 (3 × 100 mL), the organic layer was dried with Na_2SO_4 and the solvent was removed *in vacuo* to yield a yellow solid. The crude product was purified by flash chromatography (CH_2Cl_2) to give compound **1** as a pure white solid (5.26 g, 82 %).

^{1}H NMR (400 MHz, $CDCl_3$): δ 7.64 (t, J = 7.7 Hz, 1H), 7.31 (d, J = 7.7 Hz, 2H), 4.47 (s, 4H).

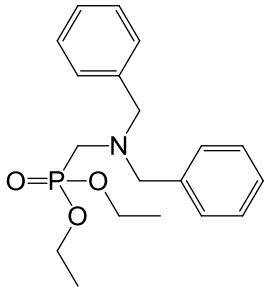

2

Diethyl ((benzylamino)methylphosphonate 2. To a solution of diethyl phosphate (5.07 g, 36.7 mmol) in THF (15.7 mL), dibenzylamine (6.09 g, 30.8 mmol) and formaldehyde (1.81 g, 60.3 mmol) were added. The mixture was heated to 60 °C for 16 h. The solvent was removed *in vacuo* and the crude oil was dissolved with cyclohexane (150 mL). The solution was washed three times with water (75 mL). After evaporation of the solvent, compound **2** was obtained as a colorless oil (5.26 g, 60 %).

^{1}H NMR (400 MHz, $CDCl_3$): δ 7.21 (m, 5H), 3.97 (qd, J = 7.2 Hz, J = 7.2 Hz, 4H), 3.69 (s, 4H), 2.80 (d, J = 10.4 Hz, 2H), 1.20 (t, J = 7.1 Hz, 6H). **^{31}P NMR** (162 MHz, $CDCl_3$): δ 25.7.

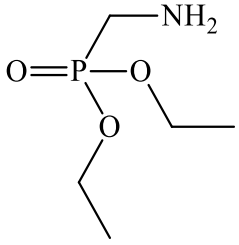

3

Diethyl aminomethylophosphonate 3. A solution of compound 2 (5.26 g, 15.7 mmol) in dry EtOH (200 mL) was hydrogenated in presence of Pd/C catalyst (280 mg, 5% Pd). After 16 h at reflux, the reaction was complete. After filtration, the solvent was evaporated to dryness to afford compound **3** as an oily product (2.3 g, 91 %).

^{1}H NMR (400 MHz, $CDCl_3$) δ: 4.17 – 3.99 (m, 4H), 2.95 (d, J = 10.3 Hz, 2H), 1.40 (s broad, 2H), 1.28 (t, J = 7.1 Hz, 6H).

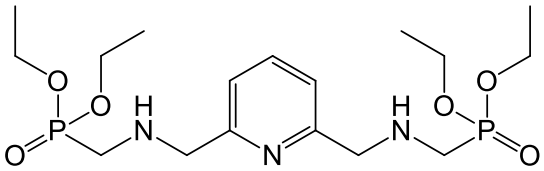

6

Tetraethyl (((pyridine-2,6-diylbis(methylene))bis(azanediyl))bis(methylene))bis(phosphonate) 10. To a solution of amine **8** (3.5 g, 21 mmol) in MeCN (40 mL), under a nitrogen atmosphere, freshly flame-dried K_2CO_3 (3.4 g, 26 mmol) was added. The mixture was heated to 70 °C. And then a solution of 2,6-bis(bromomethyl)pyridine **2** (1.4 g, 5.3 mmol) in MeCN (100 mL) was added dropwise over a *3 hours period*. The reaction mixture was monitored by TLC (CH_2Cl_2/MeOH 95/5). After filtration, the solvent was removed *in vacuo* and the crude oil was purified by flash chromatography (CH_2Cl_2/MeOH 100/0 to 95/5). Compound **10** was obtained as an oily product (230 mg, 10 %).

^{1}H NMR (400 MHz, $CDCl_3$): δ 7.55 (t, J = 7.7 Hz, 1H), 7.13 (d, J = 7.7 Hz, 2H), 4.16 – 4.03 (m, 8H), 3.90 (s, 4H), 2.95 (d, J = 12.6 Hz, 4H), 2.23 (s, 2H), 1.28 (t, J = 7.1 Hz, 12H). **^{13}C NMR** (101 MHz, $CDCl_3$): δ 158.5, 137.1, 120.8, 62.3 (d, J = 6.6 Hz), 56.0 (d, J = 15.5 Hz), 44.7 (d, J = 156.1 Hz), 16.6 (d, J = 5.7 Hz). **^{31}P NMR** (162 MHz, $CDCl_3$): δ 26.

<u>Second route:</u>

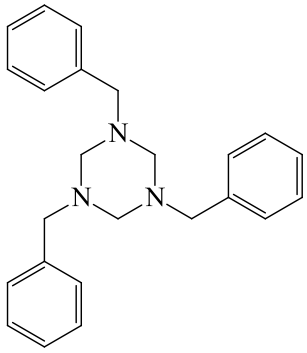

4

1,3,5-Tribenzylhexahydrotriazine 4. To a stirred solution of benzylamine (20.7 g, 193 mmol) at 0 °C, 37 % aqueous formaldehyde solution (19.4 mL, 60.7 mmol) was slowly added keeping the temperature below 5 °C. 1M aqueous sodium hydroxide solution (5 mL) was added to the resulting precipitated gum and the mixture was under ultrasonic treatment for 1 h at 0 °C. Diethyl ether (190 mL) was added and then the aqueous phase was extracted with diethyl ether (3 × 50 mL). The organic layer was dried with Na_2SO_4 and the solvent was removed under reduced pressure to yield a colorless oil. The crude product was purified by flash chromatography (Cyclohexane/Ethyl Acetate 100/0 to 85/15). Compound **4** was obtained as a colorless oil (21.1 g, 91%).

^{1}H NMR (300 MHz, $CDCl_3$): δ 7.33 – 7.05 (m, 15H), 3.59 (s, 6H), 3.34 (s broad, 5H).

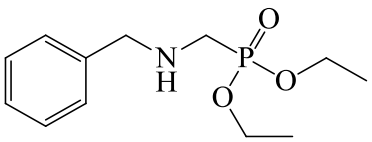

5

Diethyl ((benzylamino)methyl)phosphonate 5. Compound **4** (4 g, 11.2 mmol) was added

to diethyl phosphite (5.1 g, 36.9 mmol), under nitrogen and the mixture was heated at 100°C for 16 h. The resulting product was purified by flash chromatography (Ethyl Acetate) to give compound **5** as an oily product (3.65 g, 79 %).

^{1}H NMR (300 MHz, $CDCl_3$): δ 7.33 – 7.09 (m, 5H), 4.07 (m, 4H), 3.80 (s, 2H), 2.88 (d, J = 12.6 Hz, 2H), 1.61 (s broad, 1H), 1.26 (t, J = 7.1 Hz, 6H). **^{31}P NMR** (162 MHz, $CDCl_3$) δ: 25.7.

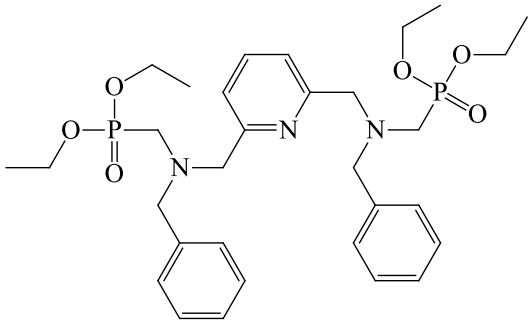

7

tetraethyl (((pyridine-2,6-diylbis(methylene))bis(benzylazanediyl))bis(methylene))bis(phosphonate) 7. Under a nitrogen atmosphere, amine **5** (1.1 g, 4.3 mmol) and freshly flame-dried K_2CO_3 (1.2 g, 9.1 mmol) were added to a solution of 2,6-bis(bromomethyl)pyridine **2** (600 mg, 2.26 mmol) in MeCN (20 mL). The mixture was heated for 16h at 70 °C. After filtration, the solvent was removed *in vacuo* and the crude oil was purified by flash chromatography (Ethyl Acetate/MeOH 100/0 to 90/10). Compound **7** was obtained as an oily light-yellow product (1.1 g, 79 %).

^{1}H NMR (400 MHz, $CDCl_3$): δ 7.59 (t, J = 7.7 Hz, 1H), 7.38 (d, J = 7.7 Hz, 2H), 7.34 – 7.10 (m, 10H), 4.05 – 3.93 (qd, J = 7.2 Hz, J = 7.2 Hz, 8H), 3.85 (s, 4H), 3.73 (s, 4H), 2.88 (d, J = 10.6 Hz, 4H), 1.21 (t, J = 7.1 Hz, 12H). **^{13}C NMR** (100 MHz, $CDCl_3$): δ 158.6, 138.6, 137.0, 129.2, 128.4, 127.3, 121.5, 61.9 (d, J = 6.7 Hz), 61.2 (d, J = 8.3 Hz), 59.8 (d, J = 9.0 Hz), 49.1 (d, J = 161.5 Hz), 16.6 (d, J = 6.0 Hz). **^{31}P NMR** (162 MHz, $CDCl_3$): δ 25.4. **ESI$^+$/MS** (CH_2Cl_2): m/z = 618.3 ([M + H]$^+$, 100 %).

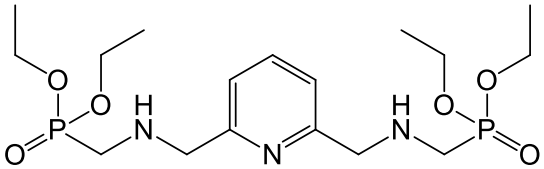

6

Tetraethyl (((pyridine-2,6-diylbis(methylene))bis(azanediyl))bis(methylene))bis(phosphonate) 10. A solution of compound 7 (0.2 g, 1.52 mmol) in dry EtOH (30 mL) was hydrogenated in presence of Pd/C catalyst (20 mg, 10 % Pd). After 6h at reflux, the reaction was stopped. After filtration, the solvent was evaporated to dryness to afford compound **10** as an oily product (25 mg, 18 %).

^{1}H NMR (400 MHz, $CDCl_3$): δ 7.55 (t, J = 7.7 Hz, 1H), 7.13 (d, J = 7.7 Hz, 2H), 4.16 – 4.03 (m, 8H), 3.90 (s, 4H), 2.95 (d, J = 12.6 Hz, 4H), 2.23 (s, 2H), 1.28 (t, J = 7.1 Hz, 12H). **^{13}C NMR** (101 MHz, $CDCl_3$): δ 158.5, 137.1, 120.8, 62.3 (d, J = 6.6 Hz), 56.0 (d, J = 15.5 Hz), 44.7 (d, J = 156.1 Hz), 16.6 (d, J = 5.7 Hz). **^{31}P NMR** (162 MHz, $CDCl_3$): δ 26.

<u>Synthesis of ligand L^2</u>

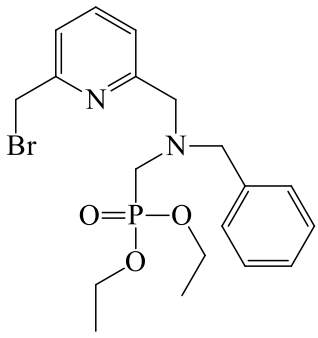

8

Diethyl ((benzyl((6-(bromomethyl)pyridin-2-yl)methyl)amino)methyl)phosphonate 11. To a solution of 2,6-*bis*(bromomethyl)pyridine **2** (1.09 g, 4.1 mmol) in MeCN (20 mL), amine **5** (1.17 g, 4.5 mmol) in MeCN (20 mL) and freshly flame-dried K_2CO_3 (1.07 g, 8.3 mmol) were added under a nitrogen atmosphere. The reaction mixture was heated at 70 °C for 16 h. After filtration, the solvent was removed *in vacuo* and the crude oil was purified by flash chromatography (Ethyl Acetate/MeOH 100/0 to 90/10) to give compound **13** as an oily product (1 g, 55 %).

^{1}H NMR (400 MHz, $CDCl_3$): δ 7.67 (t, J = 7.7 Hz, 1H), 7.51 (d, J = 7.8 Hz, 1H), 7.41 – 7.20 (m, 5H), 4.52 (s, 2H), 4.12 – 4.03 (m, 4H), 3.94 (s, 2H), 3.82 (s, 2H), 2.97 (d, J = 10.6 Hz, 2H), 1.29 (t, J = 7.1 Hz, 6H). **^{13}C NMR** (101 MHz, $CDCl_3$): δ 159.5, 155.9, 138.3, 137.6, 129.2, 128.4, 127.4, 122.6 121.9, 62.0 (d, J = 6.7 Hz), 60.8 (d, J = 8.0 Hz), 59.8 (d, J = 8.6 Hz), 49.0 (d, J = 158.7 Hz), 34.0, 16.6 (d, J = 6.1 Hz). **^{31}P NMR** (162 MHz, $CDCl_3$): δ 25.3. **ESI$^+$/MS** (CH_2Cl_2): *m/z* = 441.1 ([M + H]$^+$, 98 %), *m/z* = 443.1 ([M + H]$^+$, 100 %), *m/z* = 463.1 ([M + Na]$^+$, 50 %), *m/z* = 465.1 ([M +Na]$^+$, 50 %), *m/z* = 479.0 ([M + K]$^+$, 19 %), *m/z* = 481.0 ([M + K]$^+$, 19 %).

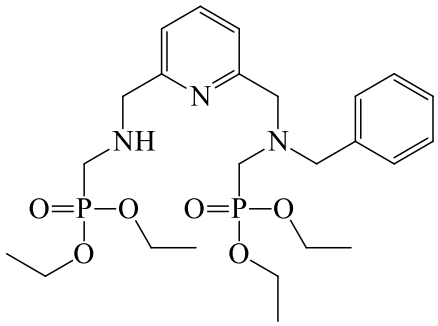

9

Diethyl ((((6-((benzyl((diethoxyphosphoryl)methyl)amino)methyl)pyridin-2-yl)methyl)amino)methyl)phosphonate 12. Under a nitrogen atmosphere to a solution of compound **11** (809 mg, 1.83 mmol) in MeCN (10 mL), amine **8** (734 mg, 4.4 mmol) in MeCN (10 mL) and freshly flame-dried K_2CO_3 (720 mg, 5.5 mmol) were added. The reaction mixture was heated at 70 °C for 16 h. After filtration, the solvent was removed *in vacuo* and the crude oil was purified by flash chromatography (CH_2Cl_2/MeOH 100/0 to 95/5). Compound 11 was obtained as an oily product (200 mg, 20 %).

^{1}H NMR (400 MHz, $CDCl_3$): δ 7.56 (t, J = 7.7 Hz, 1H), 7.40 (d, J = 7.6 Hz, 1H), 7.34 – 7.13 (m, 5H), 7.10 (d, J = 7.5 Hz, 1H), 4.13 – 3.95 (m, 8H), 3.90 (s, 2H), 3.88 (s, 2H), 3.73 (s, 2H), 2.96 (d, J = 12.6 Hz, 2H), 2.91 (d, J = 10.6 Hz, 2H), 1.28 (t, J = 7.0 Hz, 6H), 1.23 (t, J = 7.0 Hz, 6H).**^{13}C NMR** (101 MHz, $CDCl_3$): δ 158.8, 157.7, 138.2, 136.7, 128.9, 128.1, 127.0, 121.3, 120.4, 61.9 (d, J = 6.6 Hz), 61.6 (d, J = 6.7 Hz), 60.8 (d, J = 8.2 Hz), 59.5 (d, J = 9.0 Hz), 55.7 (d, J = 15.9 Hz), 48.7 (d, J = 161.4 Hz), 44.4 (d, J = 156.3 Hz), 16.3 (d, J = 5.6 Hz). **^{31}P NMR** (162 MHz, $CDCl_3$): δ 26.0, 25.2. **ESI$^+$/MS** (CH_2Cl_2): *m/z* = 528.3 ([M + H]$^+$, 100 %),

m/z = 550.2 ([M +Na]$^+$, 33 %), *m/z* = 566.2 ([M + K]$^+$, 19 %).

Synthesis of ligand L^3

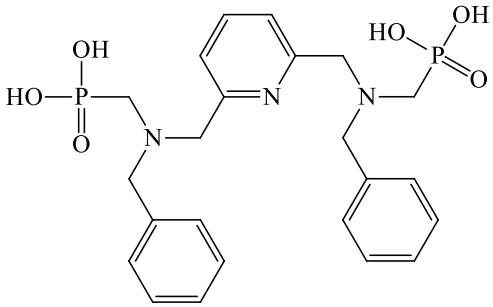

L^3

(((pyridine-2,6-diylbis(methylene))bis(benzylazanediyl))bis(methylene))diphosphonic acid L^3. Compound **7** (1.7 g, 2.79 mmol) was dissolved in 6 M HCl (36.5 mL) and the mixture was heated at reflux for 16 h. The solvent was removed under reduced pressure. After completion of the reaction, the mixture was evaporated to dryness, and the crude product was purified by flash chromatography with a C18 reverse phase column (eluent system H_2O/ACN 0.1 % TFA), to give ligand **L^3** (0.74 g, 52 %).

^{1}H NMR (400 MHz, MeOD) δ 7.84 (t, J = 7.8 Hz, 1H), 7.74 – 7.64 (m, J = 8.6, 3.8 Hz, 4H), 7.49 – 7.38 (m, 6H), 7.34 (d, J = 7.8 Hz, 2H), 4.76 (s, 4H), 4.67 (s, 4H), 3.37 (d, 4H).**^{13}C NMR** 13C NMR (101 MHz, MeOD) δ 150.07 (s), 139.18 (s), 131.98 (s), 130.01 (s), 128.95 (s), 128.63 (s), 122.85 (s), 59.42 (d), 57.05 (d, J = 6.1 Hz), 50.30 (d, J = 136.4 Hz). **^{31}P NMR** (162 MHz, MeOD) δ 8.48. **ESI$^+$/MS** (CH_2Cl_2): *m/z* = 506.2 ([M + H]$^+$, 100 %), *m/z* = 1011.3 ([2M + H]$^+$, 23. **Calc.** for $C_{23}H_{29}N_3O_6P_2$·TFA: C, 50.5; H, 5.64; N, 7.43; Found: C, 48.5; H, 4.88; N, 6.78.

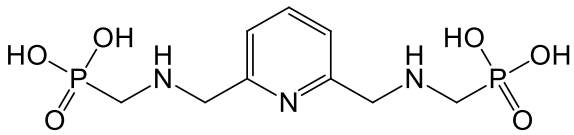

L^1

(((pyridine-2,6-diylbis(methylene))bis(azanediyl))bis(methylene))bisphosphonic acid L^1. The crude product was purified by flash chromatography with a C18 reverse phase column (eluent system H_2O/ACN 0.1 % TFA), to give ligand **L^1** (0.08 g, 9 %).

^{1}H NMR (400 MHz, D_2O) δ 7.74 (t, J = 7.8 Hz, 1H), 7.27 (d, J = 7.8 Hz, 2H), 3.82 (s, 4H), 2.53 (d, J = 12.5 Hz, 4H).**^{13}C NMR** (101 MHz, D_2O) δ 158.13, 138.76, 121.34, 48.31, 46.95. **^{31}P NMR** (162 MHz, D_2O) δ 16.50.

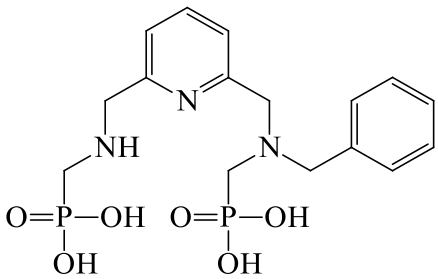

L^2

((((6-((benzyl((diethoxyphosphoryl)methyl)amino)methyl)pyridin-2-yl)methyl)amino)methyl) diphosphonic acid L^2. The crude product was purified by flash chromatography with a C18 reverse phase column (eluent system H_2O/ACN 0.1 % TFA), to

give ligand **L²** (0.15 g, 13 %).

^{1}H NMR (400 MHz, D_2O) δ 7.64 (t, J = 7.8 Hz, 1H), 7.33 (d, J = 7.7 Hz, 1H), 7.25 – 7.04 (m, 6H), 3.78 (d, J = 21.9 Hz, 4H), 3.63 (s, 2H), 2.58 (d, J = 11.6 Hz, 2H), 2.51 (d, J = 12.7 Hz, 2H).**^{13}C NMR** (101 MHz, D_2O) δ 163.10 (s), 158.72 (s), 138.56 (s), 138.56 (s), 129.86 (s), 128.18 (s), 127.08 (s), 122.89 (s), 120.84 (s), 60.28 (d), 59.24 (d, J = 8.2 Hz), 55.19 (d, J = 12.8 Hz), 54.12 (d, J = 140.4 Hz), 47.70 (d, J = 137.0 Hz).**^{31}P NMR** (162 MHz, D_2O) δ 16.39, 15.91.**ESI$^+$/MS** (CH_2Cl_2): *m/z* = 416.1 ($[M + H]^+$, 100 %); *m/z* = 831.2 ($[2M + H]^+$, 15 %). **Calc.** for $C_{16}H_{23}N_3O_6P_2$·TFA: C, 41.6; H, 5.77; N, 8.66; Found: C, 40.9; H, 4.57; N, 7.94.

Chapiter 3: structural and thermodynamic study of uranyl with polyaminophosphonates ligands

1 Acid-base properties of polyaminophosphonates ligands

It is important to know the acid-base properties of organic ligand before any thermodynamic study of metal-ligand complexation. There is a competition between the protons and the metal during the complexation at the basic donor sites such as the phosphonate and amine groups of polyaminophosphonates ligands in this study. Thank to potentiometric titration, it is possible to precisely determine the protonation constants of synthesized ligands whose structures are shown in figure 27.

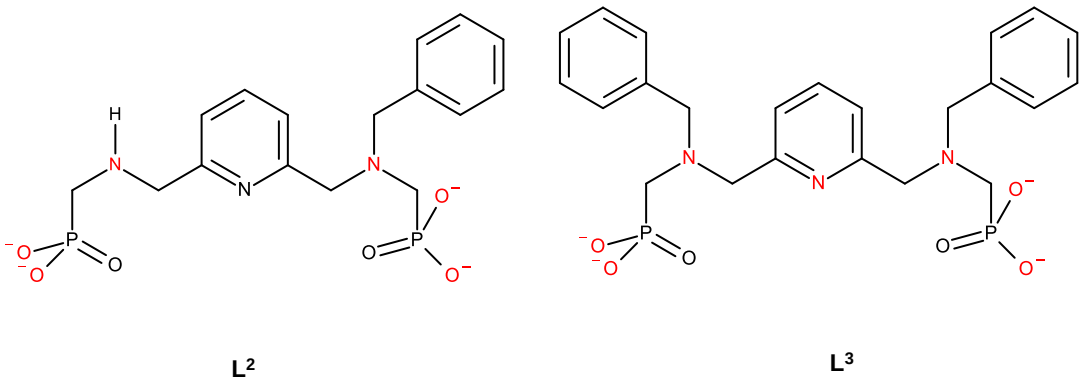

Figure 27 : Chemical structures of ligands L^2 and L^3 (fully deprotonated forms).

1.1 Potentiometric study

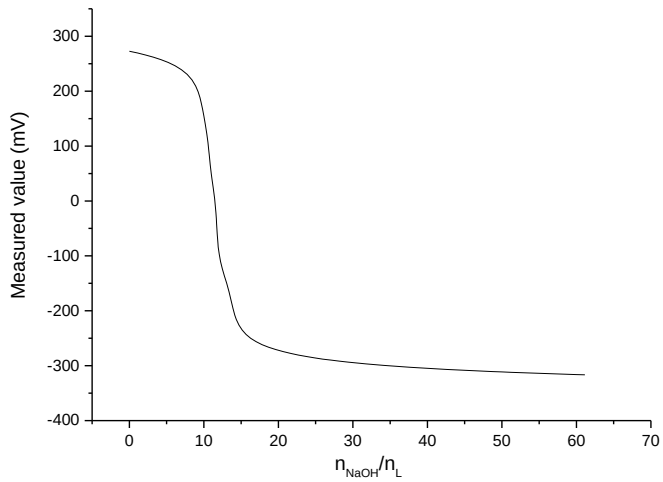

Figure 28 : Potentiometric curve of ligand L^3. Solvent: H_2O; I = 0.1 M ($NaClO_4$); T = 25.0(2) °C; $[L^3]_{tot}$ = 8.168E-4 M.

The determination of the stability constants of the metal complexes requires the characterization of the acid-base properties of the $\mathbf{L^2}$ and $\mathbf{L^3}$ ligands. The synthesized polyaminophosphonate ligands were consist by a pyridinic chromophore and two tertiary amines. $\mathbf{L^2}$ and $\mathbf{L^3}$ ligands have two phosphonic acid groups respectively. A potentiometric titration of ligand $\mathbf{L^3}$ which carried out in water with 0.1 M $NaClO_4$ as ionic strength at 25 ° C was shown in figure 28.

Four protonation constants on the seven possible could be determined for $\mathbf{L^2}$ and $\mathbf{L^3}$

respectively in the studied pH range (2<pH <12). Thus the other non-characterized ionizable sites are associated with much lower protonation constants (log K_{LHx} << 2) which couldn't be detected under our experimental conditions. The two most basic protonation constants K_{LH} and K_{LH2} for **L²** and **L³** can be attributed to tertiary amines, in agreement with data that exist in the literature for many polyaminomethanephosphonate analogues (Table 16).[12,126,169–174] The following protonation constants determined for the **L²** and **L³** ligands are associated with the first protonation constants for each of the methanephosphonate groups.

Equilibrium	log K_{LHx} (3σ)	
	L²	**L³**
$L + H^+ \overset{K_{LH}}{\Longleftrightarrow} LH$	9,5(1)[a]	9,28(5)[a]
$LH + H^+ \overset{K_{LH_2}}{\Longleftrightarrow} LH_2$	9,15(1)[a]	8,91(6)[a]/8,80[b]
$LH_2 + H^+ \overset{K_{LH_3}}{\Longleftrightarrow} LH_3$	6,17(6)[a]	6,36(8)[a]
$LH_3 + H^+ \overset{K_{LH_4}}{\Longleftrightarrow} LH_4$	4,6(2)[a]	4,45(5)[a]

Solvent: H_2O; I = 0.1 M; T = 25.0 (2) °C. Error = 3 σ with σ = standard deviation. K_{LHx} = [LH_x] / [[L_{Hx-1}] [H]. The charges have been omitted for reasons of clarity. [a] Potentiometric titrations. [b] Spectrophotometric titrations vs. pH.

Table 16 : Summarizes the values of the protonation constants determined by potentiometry of ligands L² and L³ represented in their logarithmic form (log K_{LHx} with 1 ≤ x ≤ 7).

The log K_{LH} and log K_{LH2} values of the synthesized **L²** and **L³** ligands are more than one order of magnitude higher than those measured for the **L^C** analogue (log $K_L{}^C{}_H$ = 8.95 and log $K_L{}^C{}_{H2}$= 7.85) which have terminal carboxylate units (Figure 29).[174] Meanwhile due to the interfere of benzyl group, the log K_{LH} and log K_{LH2} values is about two orders of magnitude lower than those measured for the **L^F, L^G** and **L⁴**.[12]

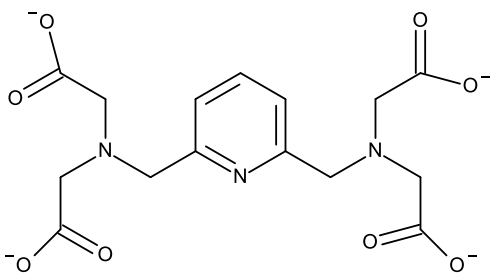

L^C

Figure 29 : Chemical structure of the analogue pyridine tetracarboxylate (noted L^C).

There are more electrostatic effects in doubly negatively charged phosphonate units($-PO_3^{2-}$) than negatively charged carboxylate groups ($-CO_2^-$) which could explain the increase of basicity. The electrostatic effects may predominate over inductive factors.[173] Furthermore, the length of the spacer which connects the two symmetrical sites amino-N,N-bis (methanephosphonate) (ligands: **L^B**, **L^C**, **L^D** and **L^E**, Table 3.2) could affect the values of the protonation constants of the amine functions for a series of polyaminomethanphosphonate

derivatives. Actually, there is a strong interactions when a short spacer is present (**EDTPA** or **L^{B}**, n = 2). Hydrogen bond inter-units between the ammonium unit and the amine unit ($NH^{+} \cdots N$) take place within the monoprotonated species.[173] As a result, the ($\Delta \log K_{LHx}$) difference of tertiary amine sites indicates this phenomenon. The difference between the protonation constants between the two tertiary amine functions decreases and tends towards a value close to statistical processes when the length of the spacer increases (n = 3 for **L^{C}** or 6 for **L^{D}**, Table 17) and these interactions flexibility increases consequently.[169]

name	**Ligand structure**	**Tertiary Amines**		**methanephosphonate**		
		log K_{LHx}	Δlog K_{LHx}	log K_{LHx}	log $K_{LHx\ avg}$	Δlog K_{LHx}
L^{A}	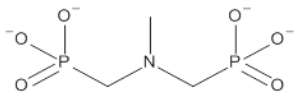	12,1	-	6,1/4,95/1,3	5,52	1,15
L^{B}	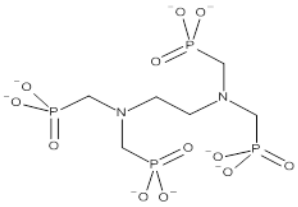	13,5 10,2	3,3	8,08/6,41/5,08 / 2,71	5,59	1,67/ 1,33/ 2,37
L^{C}	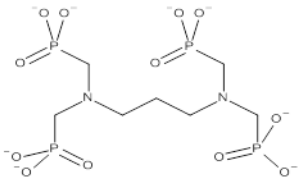	13,0 11,15	1,85	6,99/6,07/5,18 / 4,37	5,65	0,92/ 0,89/ 0,81
L^{D}	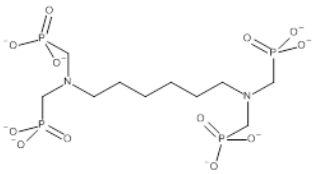	13,3 13,0	0,3	6,88/6,13/5,29 / 4,61	5,73	0,75/ 0,84/ 0,68
L^{E}	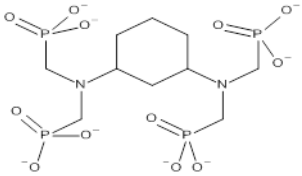	10,89 9,38	1,5	7,69/6,97/6,46 /5,32	6,61	0,72/ 0,51/ 1,14
DO2P	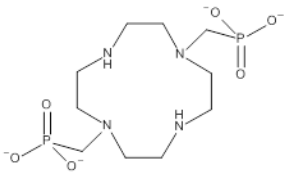	12,80(8) 10,92(2)		8,47(2)/ 6,39(2)	7,43	2,08
L^{F}	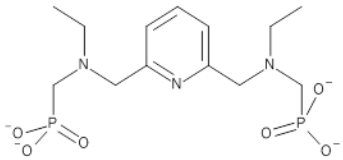	11,04(1) 10,4(1)	0,64	6,9(2)/5,7(3)/ 4,5(3)	5,7	1,2/1,2

L^{G}	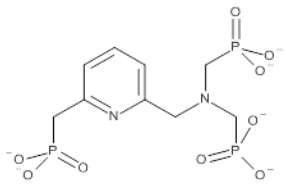	11,8(2)		8,3(3) /6,5(5)/ 5,1(6)	6,63	1,8/1,4
L^{2}	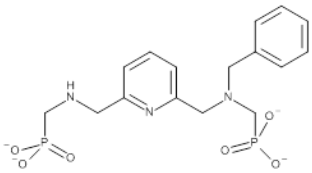	9,5(1) 9,15(1)	0,35	6,17(6)/4,6(2)	5,4	1.54
L^{3}	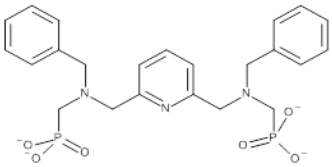	9,28(5) 8,91(6)	0,36	6,36(8)/ 4,45(5)	5,4	1,92
L^{4}	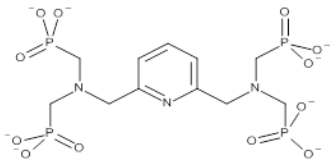	11,21(2) 10,29(2)	0,39	8,04/6,49/ 5,53/4,19	6,06	1,55/ 0,96/ 1,34

Table 17 : Successive protonation constant (log K_{LHx}) of derivatives polyaminophosphonates from the literature compared to data measured for L^{2} and L^{3}.

Because of their long alkyl spacer (n = 6), the two amino units N,N-bis (methanephosphonate) **L^{D}** ligand behave than of one another. The value of $(\Delta \log K_{LHx} = 0.3)$ is close to the expected statistical deviation $(\Delta \log K_{LHx} = 0.6)$ for two identical and independent sites for the derivative **L^{D}** ((hexamethylenedinitrilo) tetra (methanephosphonate)).[169] Pyridyl groups (**L^{2}**, **L^{3}**, **L^{F}**, **L^{G}** and **L^{4}**)[12] or cyclohexyl (**L^{E}**)[171] are inserted as rigid spacers which constraint structure and geometry. As a result the hydrogen bonds ($NH^{+} \cdots N$) is weaken compare to previous molecules. The values of $\Delta \log K_{LHx}$ associated with tertiary amines deviate significantly from the statistical value, but are nevertheless attenuated.

The hydrogen bridges between pyridine nitrogen and protonated tertiary amines has been found by the sharp increase in the acidity of pyridine.[12] The protonation constant of pyridine and the second constants of protonation of phosphonate groups could not be determined under our experimental conditions (log K << 2). The first protonation constants for each methanephosphonate group are the least basic protonation constants which determined from this series of ligands studied. These values are comparable to those determined for the **L^{A}** and **L^{F}** (Table 17).

The average basicity does not vary significantly for **L^{2}** and **L^{3}**, the $\Delta \log K_{LHx}$ for both ligands are the same due to structure and geometry similarity. These differences reflect inter-unit interactions by hydrogen bridges that may exist between the methanephosphonate group of one tertiary amine unit and the ammonium site of the other adjacent unit for the deprotonated species (the two amines tertiary are protonated). A solid-state structure of **EDTPAH$_{8}$** demonstrates solid-state inter-unit hydrogen bonds.[175] Thus, the $\Delta \log K_{LHx}$ values of the phosphonate functions decrease with length of the spacer and indicate the attenuation of these interactions by hydrogen bridges when the spacer is longer and more flexible within the polyaminomethanephosphonate series (Table 17). The deviations $\Delta \log K^{H}$ then tend towards expected statistical values for four identical and independent sites ($\Delta \log K^{H}$= 0.35 and 0.43).[169] The log $\Delta \log K_{LHx}$values obtained for **L^{2}** and **L^{3}** seem to indicate strong inter-unit interactions

in accordance with the topology of our systems. For the four systems studied, the other protonation constants (protonation of $-PO_3H^-$ and protonation of pyridine units) could not be determined under these experimental conditions and their logarithmic values were estimated << 2, in agreement with data from literature.[176–178]

The distribution diagrams of protonated species of ligands **L²**, **L³** and **L⁴** were calculated using the HYSS[179] software and are presented in Figure 30. Negatively charged species ($\mathbf{L^2}H_3^-$ and $\mathbf{L^2}H_2^{2-}$), ($\mathbf{L^3}H_3^-$ and $\mathbf{L^3}H_2^{2-}$) and ($\mathbf{L^4}H_3^{4-}$ and $\mathbf{L^4}H_2^{5-}$) coexist under conditions of physiological pH.

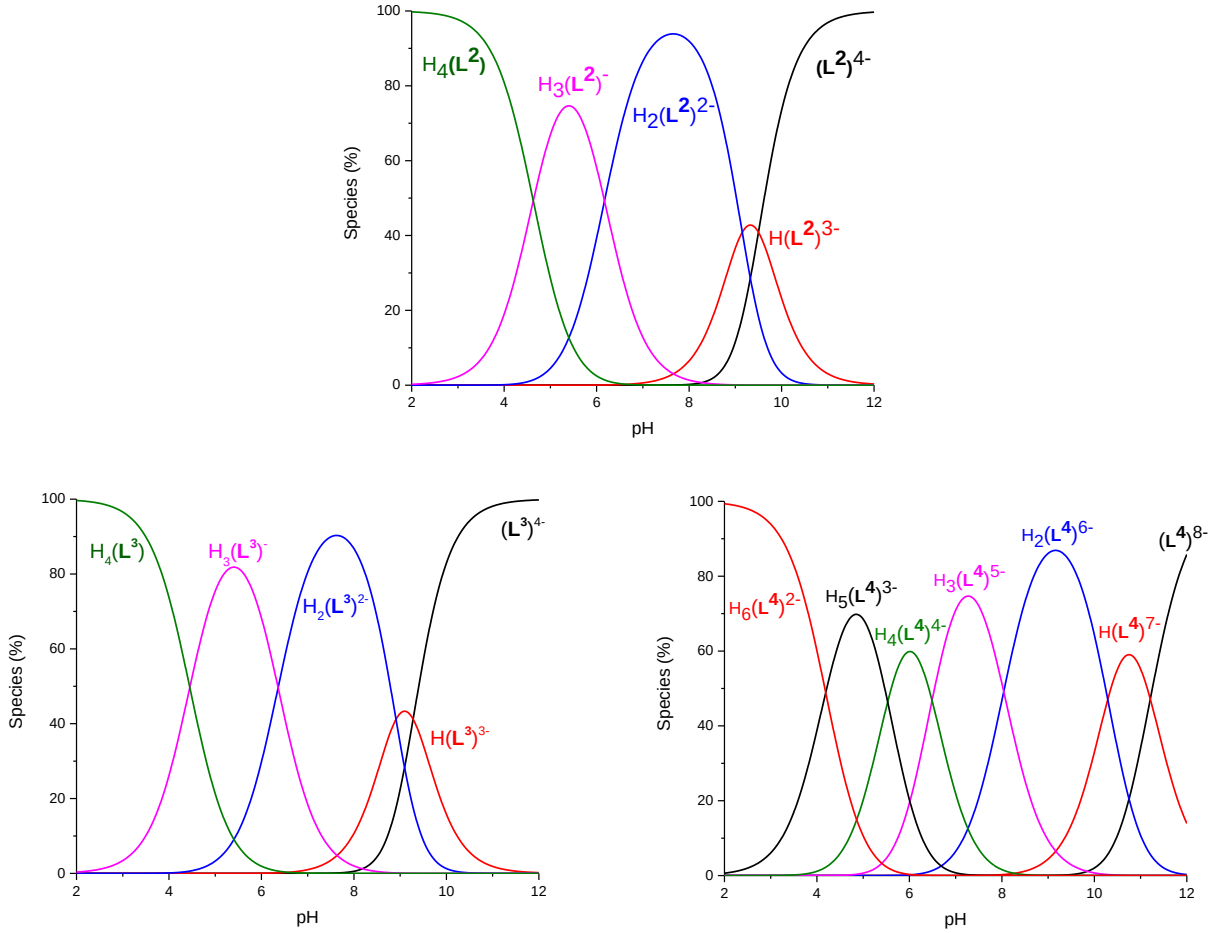

Figure 30 : Distribution curves of protonated species of ligands L², L³ and L⁴. Solvent : H_2O; T = 25,0 °C ; I = 0.1 M ($NaClO_4$) ; $[L_2]_{tot}$, $[L_3]_{tot}$ and $[L_4]_{tot}$ = 1E-4 M.

1.2 Spectrophotometric study according to the pH

A spectrophotometric titration (220 nm <λ <350 nm) as a function of the pH was done to evaluate the spectrophotometric properties of polyaminophosphonates ligand **L³** and protonated species. The obtained variation spectral is shown in figure 31. Pyridine is the main chromophore of the synthesized ligand.

We observe that the titration of ligand **L³** as a function of the pH exhibit similar behavior of ligand **L^F**.[12] A hyperchromic effect is observed on the absorption spectra after pH 7. This effect can be explained by the presence of hydrogen bond between the pyridine nitrogen and the different protonated units formed by protonation of the first two methanephosphonate units. The processing of the data by HypSpec[180,181] allowed us to determine a single protonation constant for the **L³** bisphosphonate ligand. The values obtained are in very good agreement with those determined by potentiometry (Table 16).

These data thus confirm the values determined previously by pHmetry and suggest that the aforementioned hydrogen bonding networks also involve the pyridinic chromophore. Indeed, the nitrogen of pyridine is likely to interact by hydrogen bonding with protonated ammonium sites, which leads to the most significant effects (hypochromic effect of π-π* transitions under the effect of protonation) and allows to explain its low protonation constant that could not be determined under our experimental conditions. The involvement of methanephosphonate units in the establishment of "cross" hydrogen bonds also seems to influence the chromophore but in a more modest way.

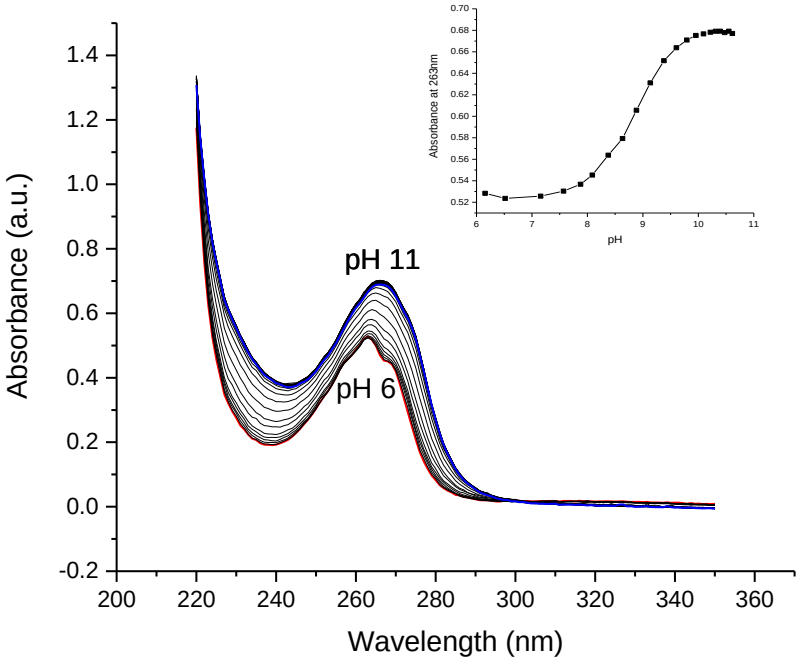

Figure 31 : Spectrophotometric titration of L^3 as a function of pH. Solvent: H_2O; T = 25.0 (2) °C; I = 0.1M ($NaClO_4$); l = 1 cm; [L^3] tot = 1.02E-4 M.

The calculated electron spectra of protonated species of ligands $\mathbf{L^3}$ is shown in figure 32.

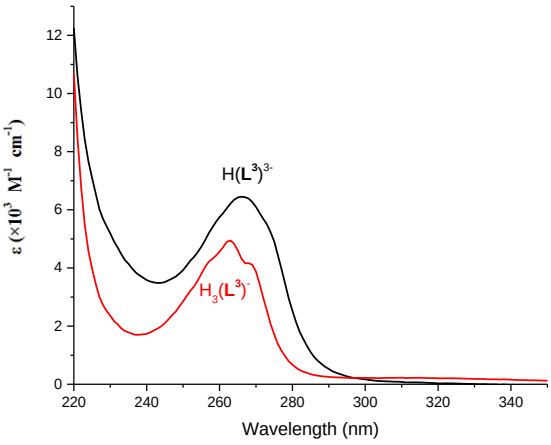

Figure 32 : Electronic spectra of the protonated species of ligand L^3. Solvent: H_2O; T = 25.0 (2) °C; I = 0.1M ($NaClO_4$); l = 1 cm.

The spectrophotometric characteristics of protonated species of ligand $\mathbf{L^3}$ is presented in

Table 18.

	λ_{max}(nm)	$\varepsilon_{max}(\times 10^3\ M^{-1}\ cm^{-1})$
$H(\mathbf{L^3})^{3-}$	266	6.45
$H_3(\mathbf{L^3})^{-}$	263	4.95

Table 18：Spectral characteristics of protonated species of ligand L^3.

1.3 Conclusion

With the help of potentiometric and spectrophotometric study, it is possible to calculate and determine different values of protonation constants for the synthesized ligands $\mathbf{L^2}$ and $\mathbf{L^3}$. The two tertiary amine functions are the most basic sites. Pyridine, main chromophore, is the most acidic site in synthesized ligand $\mathbf{L^2}$ and $\mathbf{L^3}$. Due to the π-π * transitions centered on pyridine and benzene, the ligands have an absorption band at about 266 nm. The deprotonation constants variations are mainly due to the change of hydrogen bonding between pyridine nitrogen, protonated tertiary amines and methanephosphonate group for the deprotonated species.

The formation of hydrogen bridges between pyridine nitrogen and tertiary amines protonated has been evidenced by a sharp increase in the acidity of pyridine. The protonation constant of pyridine, secondary amine and the second constants of protonation of phosphonate groups could not be determined under our experimental conditions (log K << 2). The protonation constants determined by spectrophotometry are in very good agreement with those determined by potentiometry.

2 Uranium/ligands interactions studied by Time-resolved laser fluorescence spectroscopy (TRLFS) and UV-visible spectroscopy

2.1 Time-resolved laser fluorescence spectroscopy (TRLFS) and UV-visible spectroscopy

Photoluminescence process consists by phosphorescence and fluorescence. After the absorption of a photon by a molecule, a complex or an ion, phosphorescence and fluorescence occur. Fluorescence is particularly interesting for our study because of its significant selectivity and its very low detection limit (μM). The lifetimes of the fluorescence species are modified according to the environment of the metal studied (here uranyl). Moreover, the lifetime, although sensitive to the temperature and the composition of the solution (ionic strength, buffer) [182–184], are generally specific to the desired species [185,186]. Therefore it is possible to follow the evolution of uranium complexation with the ligand and to determine its speciation. The detailed principle, the specificities of the systems studied and the experimental parameters are listed in Appendix. The lifetime and spectral characteristics specific to each species will also be reported in Appendix.

The samples were also measured with UV-visible spectrometer to verify the ligand absorption change which reflects the change on uranyl coordination and uranyl-ligand complex.

2.2 Experimental conditions selection

Due to the hydrolysis of uranium (Fig. 33), it is important to have the measurement for the

uranyl alone to have a preliminary idea over the complexation without uranyl hydroxide. There is mainly hydrogen phosphonate at pH 3, and free uranyl ion is major species at this pH, the measurement at pH 3 was chosen for the free uranyl-ligand study.

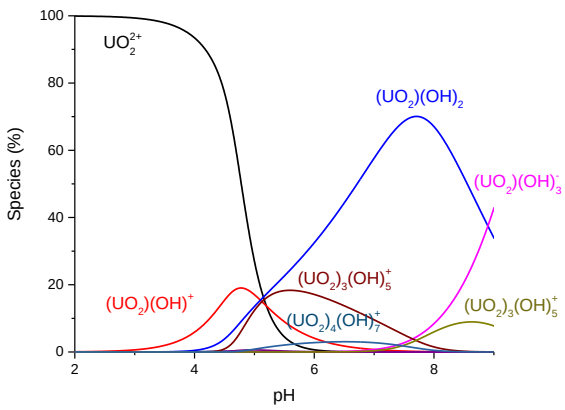

Figure 33 : Species diagram of uranyl ion; [U] = 5E-5 M in 0.1M $NaClO_4$.

According to the biochemical condition of human, the pH range is from 7 to 7.5 for most organs. For saliva, blood, bone, all have a pH of about 7.4. The kidney is an important organ for long-term regulation of pH. The pH of urine is between 4.0 and 8.0. Then it is hard to define the pH of kidney. As the uranyl ion is transferred by blood after contamination, meanwhile bone and kidney are the main target organ for resist uranyl ion, the measurement at pH 7.4 was chosen to simulate the possible complexation between uranyl ion and ligand at biochemical condition.

For the Study, the ligand concentration is fixed at 5E-5M, the uranyl concentration is from 0 to 1eq. Normally the decorporation agent was much over equivalence in the biology study, ~100eq.[75] Moreover there is polynuclear species after 1eq of europium which forms base on the study of similar ligand.[13] The polynuclear species could also formed with uranyl ion because of the complexation affinity difference of different donors from the multidentate ligands.

2.3 Solubility test with uranyl-ligand complex

Because of the low solubility of metal-phosphonate complex at acidic condition in H_2O, different ionic strength solutions, NaCl, $NaClO_4$ and $NaNO_3$, were prepared. Different ionic strength solutions with different concentration were used to solubilize 5e-5M uranyl-ligand complex at pH 3 and 7.4. The solubility of complex was checked after preparation and 12 hours with the help of bright light. There is no problem with the samples at pH 7.4 in different ionic strength solution. But for test at pH 3, the uranyl-ligand compound only solubilize in NaCl solution.

Another solubility test was done for $\mathbf{L^3}$ and $\mathbf{L^4}$ to test the solubility at pH 3. The method is to decrease the uranyl-ligand complex sample pH in $NaClO_4$ from 7.4 to 3 to verify the possible complexation mode difference. Indeed, for the uranyl-ligand complexation, the first step should be the interaction between uranyl ion with phosphonate group, then the uranyl ion is moved into the pocket part of the ligand, take place of the proton which attach to the nitrogen atom of the amine part and finally form complexation with the 3 nitrogen atoms and 2 oxygen atoms from the ligand. For the sample at pH 7.4, the uranyl ion has already located in the pocket part, after decrease the pH the complexation mode should remain the same. The sample doesn't form precipitation after decrease pH, after 12 hours, the precipitation presented.

The uranyl-ligand complex precipitation in different concentration of $NaClO_4$ and $NaNO_3$ at pH 3 is might due to the neutral charge of complex. $\mathbf{L^3}$ and $\mathbf{L^4}$ is mainly hydrogen

phosphonate at pH3. Then the complex charges are 0 for uranyl- $\mathbf{L^3}$ and -2 for $\mathbf{L^4}$. The uranyl-ligand complex is solubilized in 0.1M NaCl at pH 3. It might due to the complexation of chloride which changed the charge of uranyl-ligand complex. At pH 7.4, the uranyl-ligand complex is soluble in all ionic solution at different concentration.

For this study, sample with 0.1M NaCl was selected for the study at pH 3 and 7.4; sample with 0.1M $NaClO_4$ was selected for pH 7.4 study for comparison.

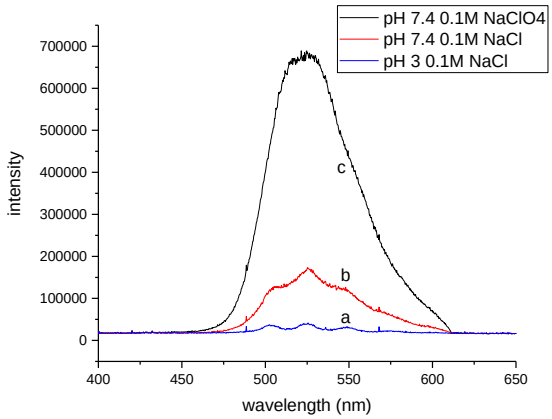

Figure 34 : Fluorescence study of uranyl in each ionic solution at different pH; a [U] = 5E-5 M, pH 3, 0.1M NaCl; b [U] = 5E-5 M, pH 7.4, 0.1M NaCl; c [U] = 5E-5 M, pH 7.4, 0.1M $NaClO_4$.

The TRLFS test was done for the uranyl ion at each condition (Fig. 34). The center peak position of uranyl fluorescence in 0.1M NaCl at pH 3 (Fig. 34 a) is at 524nm. It is different from the center peak position of free uranyl which is at 510nm. So the uranyl ion is complexed with chloride ion. For the measurement at pH 7.4, the fluorescence is much lower in 0.1M NaCl (Fig. 34 b) compare to the one in 0.1M $NaClO_4$ (Fig. 34 c). And the shapes of spectra are different. This is due to the quenching and complexation by chloride ion. The center peak position at pH 7.4 is at 525nm for sample with 0.1M NaCl and 522nm for sample 0.1M $NaClO_4$.

2.4 Stability test with uranyl-ligand complex for sample preparation

The first slope tests at pH 3 and 7.4 were done by mixing the ligand, ionic strength solution and uranyl solution in sequence, then the pH was adjusted to corresponding pH, the volume was fixed at 2 mL by adding ionic strength solution, the final pH was recorded, then samples were reserved for 12 hours and measured with UV-Vis absorption spectroscopy and time-resolved laser fluorescence spectroscopy.

a. Study of uranyl-$\mathbf{L^3}$ complex at pH 3 in 0.1M NaCl

Owning to the benefit of nitrate present in the uranyl solution, it is pretty easy to identify uranyl concentration in each sample by the UV absorption at 220nm of nitrate. The trend of the aromatic absorption (Fig. 35 left) is hard to verify with the uranyl concentration increased. The shapes of curves remain the same for the titration.

For the fluorescence spectra (Fig. 35 right), the intensity was increasing for the first four samples. The center peak position is at 522nm which is a sigh for the tight complexation. The intensity was decreased for the 0.99eq sample after excited the sample for a period under the beam.

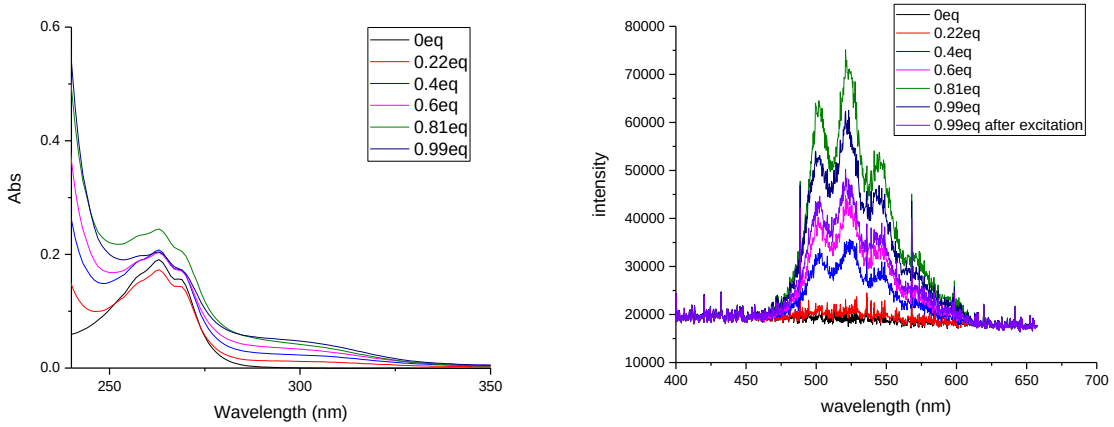

Figure 35 : Study of uranyl-L^3 complex, absorption measure (left); TRLFS measure (right); [L^3] = 5E-5 M, [U] 0-1 eq, pH 3, 0.1M NaCl.

There might be decomposition in the solution after preparation. And after excitation with the beam, there might be quenching happening; the lifetime measurement is not reliable in this case.

The same test with **L^4** was done and has the same phenomenon.

b. Study of uranyl-**L^3** complex at pH 7.4 in 0.1M NaCl and $NaClO_4$

The aromatic absorption (Fig. 3.36 left) is keep increasing with the uranyl concentration increase. Meanwhile the shapes of the curves are changed from multipeaks to a broadband absorption. The fluorescence spectrum (Fig. 3.36 right) was remain the same which shown the uranyl-**L^3** complex in 0.1M $NaClO_4$ is non-fluorescence.

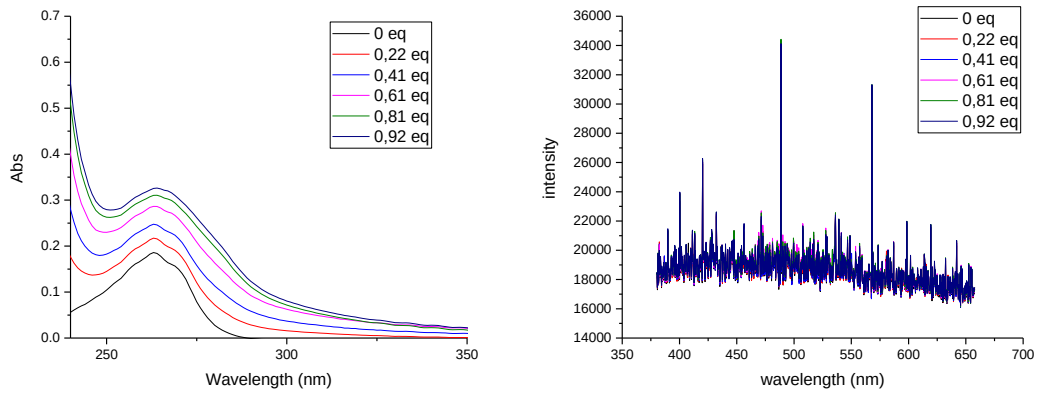

Figure 36 : Study of uranyl-L^3 complex, absorption measure (left); TRLFS measure (right); [L^3] = 5e-5 M, [U] 0-1 eq, pH 7.4, 0.1M $NaClO_4$.

Similar study was done in 0.1M NaCl ionic strength solution (Fig. 37). The absorption evolution and fluorescence change of uranyl-**L^3** complex have the same trend and shape with the measurement in 0.1M $NaClO_4$.

For this reason, there is no degradation happened for the samples at pH 7.4 after sample preparation. And for the samples at pH 7.4, the preparation will remain the same without any further improvement.

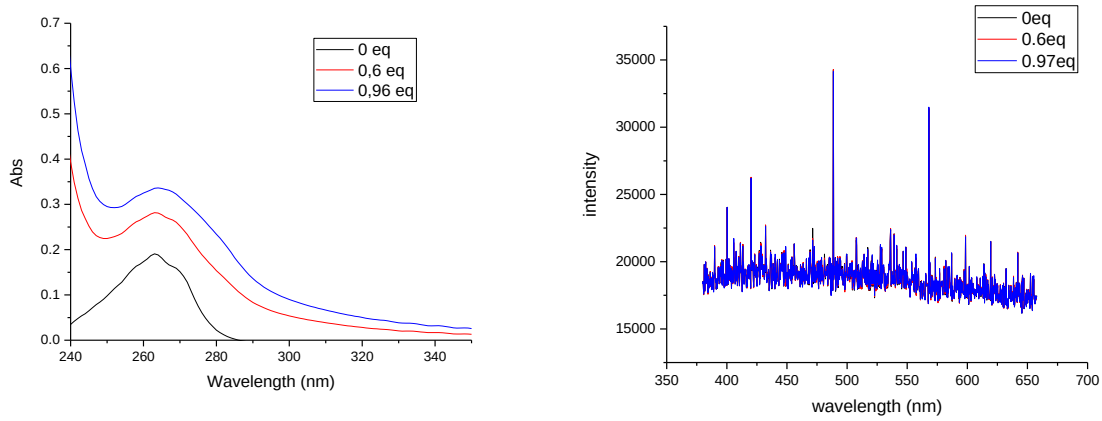

Figure 37 : Study of uranyl-L^3 complex, absorption measure (left); TRLFS measure (right); [L^3] = 5e-5 M, [U] 0-1 eq, pH 7.4, 0.1M NaCl.

The same test with **L^4** was done and has the same phenomenon.

At the beginning of the nineteenth century, the photochemistry of the uranyl ion has enrolled the curiosity of researchers.[178,179] The figure 38 shows the mechanism which could happen for uranyl photolysis.

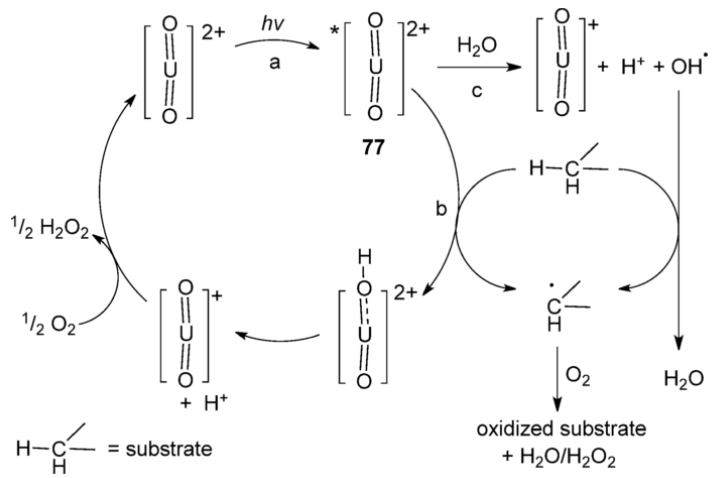

Figure 38 : Steps in the photocatalyzed H-atom abstraction from hydrocarbons by the uranyl dication.[187]

The UO_2^{2+} absorbs visible light (λ_{max} 414 nm, $\varepsilon_{max} = 7.70\ M^{-1}\ cm^{-1}$ in 0.1M$HClO_4$)[188,189] to form *UO_2^{2+} which is unreactive towards O_2. The reaction rates for the quenching of *UO_2^{2+} by aliphatic compounds respond to the energy of the weakest C-H bond(s) in these molecules.[190] The bond dissociation energy (BDE) of the PhC(H_2)-H bond (368 kJ/mol) is lower than BDE of the C-H bonds in several reactive aliphatic compounds studied so far.[190] UO_2^{2+} serves as a selective catalyst for the oxidation of organic substrates by molecular oxygen in presence of visible light (Fig. 39 & 40).[191]

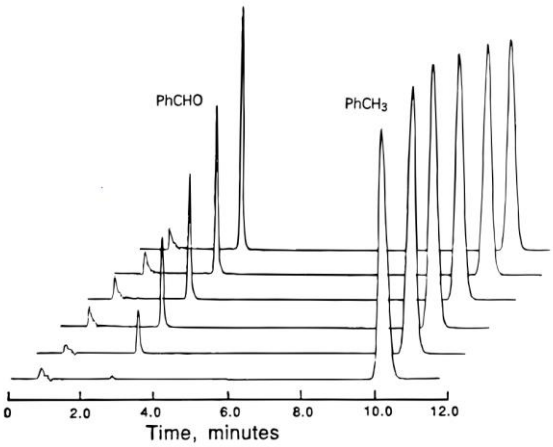

Figure 39 : HPLC chromatograms of air-saturated solutions of 0.5 mM UO_2^{2+} and 5 mM $PhCH_3$ in 0.01M H_3PO_4 after irradiation with visible light in 15 min intervals. The monitoring wavelength was 254 nm.[191]

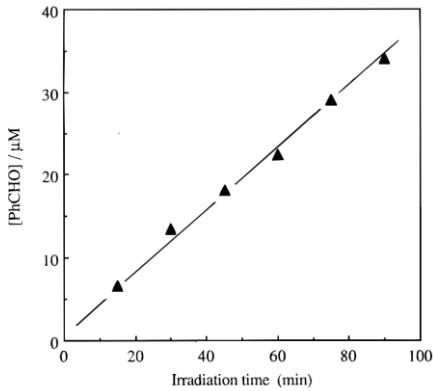

Figure 40 : Plot showing increase in [PhCHO] with irradiation time. Data from Figure 13.[191]

The sunlight spectrum is present in figure 41. The spectral irradiance of sunlight in the range from 300 to 500nm is relatively high. And the absorption of photon by uranyl in this energy range could form $*UO_2^{2+}$. Then H atom abstraction with $*UO_2^{2+}$ by (eq 1) generates UO_2^{2+} and C-centered radicals, both of which react with molecular oxygen (eq 2 and 3). There are about 5e-4M molecular oxygen in the fresh water and ~ 4E-4M molecular oxygen in the seawater (Fig. 42). Reaction 3 regenerates UO_2^{2+}, and the photooxidation of RH becomes catalytic. This scheme has been proved for a number or organic compounds, including alkanes, alkenes, and side-chain aromatics.[192] Benzene, on the other hand, reacts with $*UO_2^{2+}$ exclusively by exciplex formation and no oxidation took place when O_2 was used as oxidant. A different reaction scheme, in effect a photoinduced Fenton-like reaction, was devised to oxidize benzene to phenol with use of H_2O_2 as terminal oxidant.[193] Normally the substrate activation reactions are generally carried out in water. So any hydrocarbon will have limited solubility, and be competing directly with the solvent water molecules in the reaction.

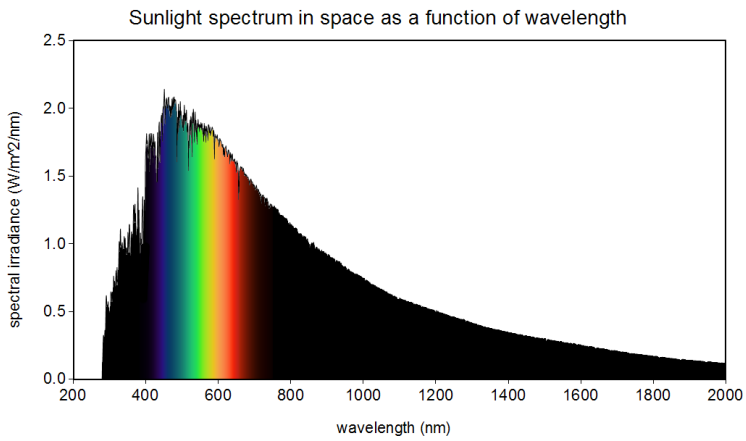

Figure 41 : Sunlight spectrum in space as a function of wavelength. Public Domain Image, image source: Christopher S. Baird, data source: American Society for Testing and Materials Terrestrial Reference.

$$^{*}\mathbf{UO_2^{2+}} + RH \rightarrow \mathbf{UO_2^{+}} + R\bullet + H^{+} \qquad \text{Equation 1}$$

$$R\bullet + O_2 \rightarrow RO_2\bullet \rightarrow \text{products} \qquad \text{Equation 2}$$

$$2\mathbf{UO_2^{+}} + O_2 + 2H^{+} \rightarrow 2\mathbf{UO_2^{2+}} + H_2O_2 \qquad \text{Equation 3}$$

For this study, the possible reason for the uranyl-ligand degradation at pH 3 is due to ligand degradation by uranyl ion with the presence of molecular oxygen in the solution and light. Meanwhile the uranyl-ligand complex slope test at pH 7.4 doesn't suffer from this phenomenon. The possible reason might relate with the fluorescence property difference at pH 3 and 7.4. The uranyl-ligand complex doesn't fluorescence at pH 7.4 which means the uranyl coordinations for pH 3 and 7.4 are not the same. The quenching of uranyl fluorescence minimize degradation of ligand by restrict H atom abstraction (eq 1). For study at pH 7.4, only the absorption spectra before the TRLFS study will be used for the Study. The fast fluorescence spectra will be recorded for the Study. The lifetime measurement cannot be done due to non-fluorescence uranyl-ligand complex.

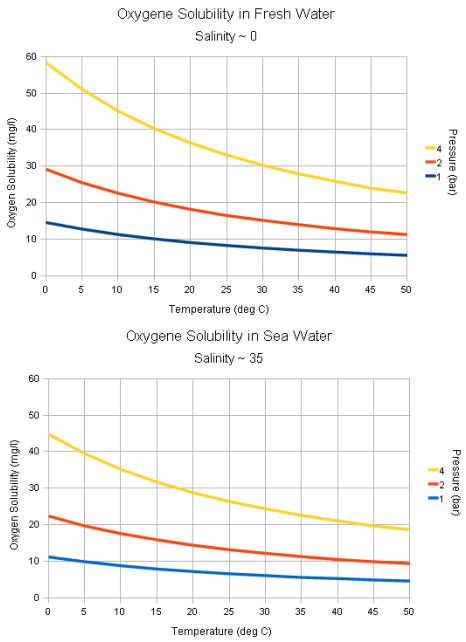

Figure 42 : Solubility of oxygen in water

2.5 Stability test of uranyl-ligand complex with TRLFS

Another sample preparation method was used to prepare the uranyl-ligand sample at pH 3 which aims to avoid the degradation during the sample preparation. First the NaCl ionic strength solution was degased with argon flow to remove the molecular oxygen. Then mixing the ligand, ionic strength solution and uranyl solution in sequence in a small brown bottle to minimize the effect of sunlight in a room with weak light, the pH was adjusted to neutral pH first, and reserve for 12hours. After the pH was adjust to 3 and the volume was fixed at 2 mL by adding ionic strength solution, the final pH was recorded. After 30mins, the samples were measured with UV-Vis absorption spectroscopy before and after the TRLFS test. And the time-resolved laser fluorescence spectra was recorded twice, the first measure was done just after the UV-Vis absorption spectroscopy measurement, the second was done after exciting the sample for 10mins with 430nm laser beam. This test is to confirm the effectiveness and feasibility of time resolve study of the uranyl species.

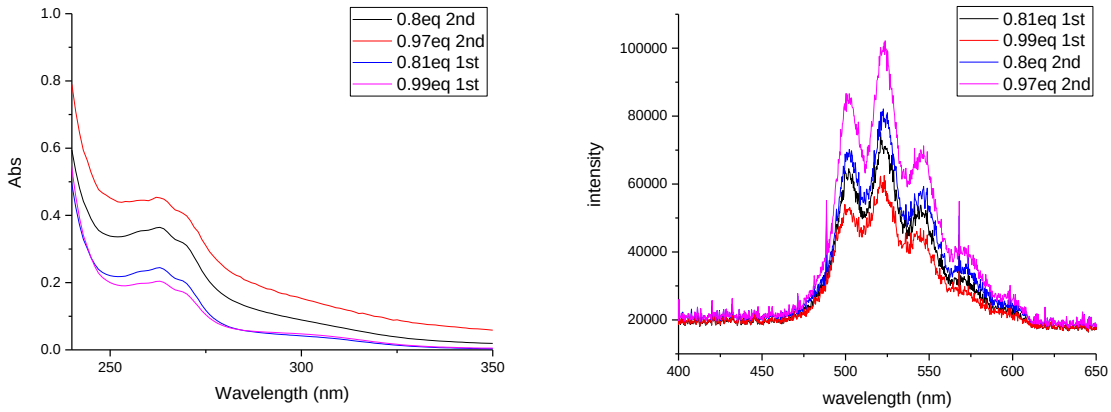

Figure 43 : Comparison of uranyl-L^3 complex by two preparation method, absorption measure (left); TRLFS measure (right); [L^3] = 5E-5 M, [U] 0.8&1 eq, pH 3, 0.1M NaCl.

A Study was done to determine the effectiveness of new sample preparation method. The results of absorption spectra and TRLFS spectra at 0.8eq and 1eq are shown below (Fig. 43). The samples which were prepared by minimize the impact of molecular oxygen and sunlight present higher absorption rate, about 2 times, on the ligand absorption range compare to the sample which prepared by previous method. Meanwhile the fluorescence intensity is also higher at 2 different equivalences. The degradation during the sample preparation has been minimizing by the new sample preparation method.

The comparison with **L^4** was done and has the same phenomenon.

a. Study of uranyl-**L^3** complex at pH 3 in 0.1M NaCl

The evolution of ligand absorption in the UV range (Fig. 44 left) is reasonable in this study. The absorption at 262nm was increasing with the increase of uranyl equivalence. The intensity of uranyl fluorescence (Fig. 44 right) was also increasing. Degradation by uranyl photolysis with molecular oxygen and sunlight was minimized. The samples preparation for uranyl-ligand complex at pH 3 will remain the same without any further improvement.

The same test with **L^4** was done and has the same phenomenon.

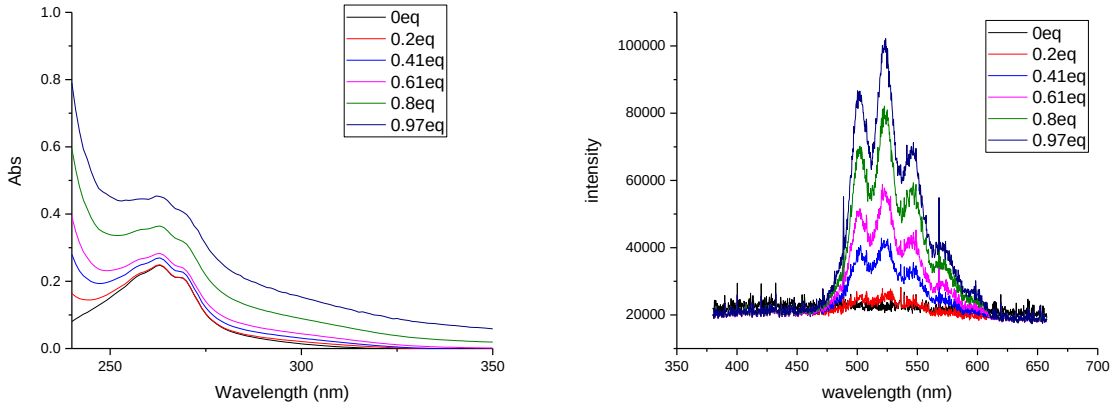

Figure 44 : Study of uranyl-L^3 complex, absorption measure (left); TRLFS measure (right); [L^3] = 5E-5 M, [U] 0-1 eq, pH 3, 0.1M NaCl.

Then the stability under the laser excitation has been evaluated (Fig. 45). It is clear that both the absorption rate of aromatic part (Fig. 45 left) and fluorescence intensity (Fig. 45 right) decreased after 10mins under 430nm laser excitation. So the uranyl-ligand complex was changed. The uranyl-ligand complex lifetime measurement cannot be done for this reason.

The same test with **L^4** was done and has the same phenomenon.

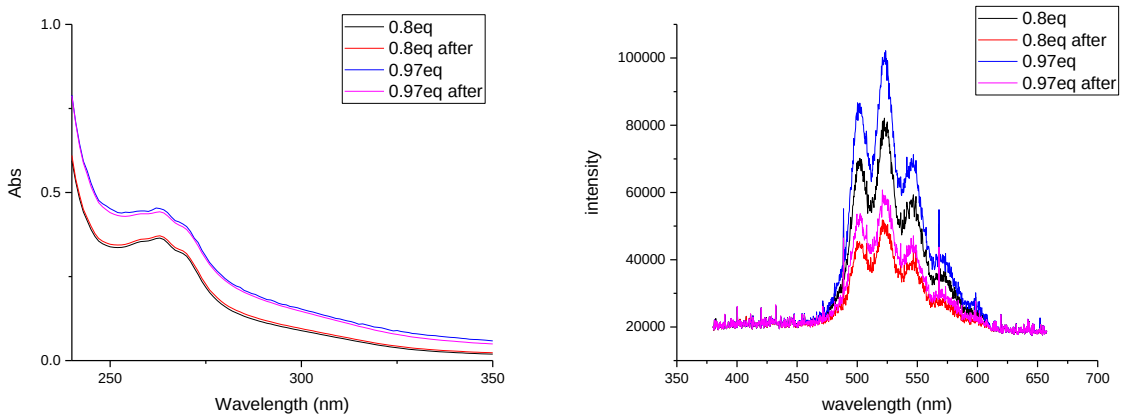

Figure 45 : Study of uranyl-L^3 complex under 430nm laser excitation, absorption measure (left); TRLFS measure (right); [L^3] = 5E-5 M, [U] 0.8 &1eq, pH 3, 0.1M NaCl.

The UO_2^{2+}could absorb light in the range of 350 to 490 nm to generate a long-lived, strongly oxidizing excited state, $*UO_2^{2+}$ (E_0 = 2.6 V),[194,195] which can be considered as a reactive oxygen-centered radical coordinated to UV. [196,197] Depending on the identity of nearby substrates, different decay routes are possible for the long-lived $*UO_2^{2+}$ ion (Fig. 38), H atom abstraction, addition to multiple bonds, oxygen atom transfer, and exciplex formation.[197–200]

Many inorganic ions quench the luminescence of uranyl in aqueous solutions.[201–203] It has been postulated that the quenching takes place according to a charge-transfer mechanism with the formation of radical-ion quenching agents. The energy levels of the quenching ions are located significantly higher than the lowest excited level of the uranyl ions,[201,202] and the observed effective quenching of the luminescence of uranyl, therefore, cannot be attributed to the transfer of energy from the excited uranyl ions to the quenching ions.

The quenching of excited uranyl ions by Hg_2^{2+}, Ti^+, Ag^+, CNS^-, CI^-, I^-, and Br^- in water, 1 mole/liter HNO_3, and 1 mole/liter H_3PO_4 takes place according to a mechanism of

intermolecular electron transfer. The complexation of the uranyl ions with anions of the medium facilitates the electron-transfer process, if the electron donors are cations, and hampers the electron-transfer process, if the donors are anions.[204] Photooxidation of substrates by $*UO_2^{2+}$ is thought to occur by both atom[199,205–208] and electron-transfer[192,201,204,209–217] processes.

Uranyl iodide complexes are known to possess charge-transfer-to-metal (CTTM) bands between 350 and 530 nm, the actual position of the bands depending upon the extent of complexation.[218] And the uranyl iodide system is any permanent change observed on photolysis.[219] In all of these systems, halide anion radicals, X_2^{*-}, have been observed by flash photolysis.[202,204,220–224]

$$*\mathbf{UO_2^{2+}} \rightarrow \mathbf{UO_2^{+}} + \boldsymbol{hv} + \Delta \qquad \text{Equation 4}$$

$$*\mathbf{UO_2^{2+}} + \mathbf{X^{-}} \rightarrow \mathbf{UO_2^{+}} + \mathbf{X^{\cdot}} \qquad \text{Equation 5}$$

$$*\mathbf{X^{-}} + \mathbf{X^{\cdot}} \rightarrow \mathbf{X_2^{*-}} \qquad \text{Equation 6}$$

$$\mathbf{UO_2^{+}} + \mathbf{X_2^{*-}} \rightarrow \mathbf{UO_2^{2+}} + \mathbf{2X^{-}} \qquad \text{Equation 7}$$

Reaction 4 includes both radiative and nonradiative decay of the excited uranyl ion.

For this study, the possible reason for the uranyl-ligand degradation at pH 3 is due to ligand degradation by uranyl with the presence of chloride ion in the solution and 430nm laser. Because of the low solubility of uranyl-ligand complex in 0.1M $NaClO_4$ solution, 0.1M NaCl solution was used as the ionic strength solution. The $*UO_2^{2+}$ which generate by the 430nm laser excitation could react with chloride and then form chloride radical by eq 5 and 6. The chloride radical could decompose organic molecules. Meanwhile $*UO_2^{2+}$ could cause the organic compound photooxidation. The decrease of UV absorption of uranyl-ligand complex is mainly due to these two reasons. The degradation compound of uranyl-ligand complex could be the complex of uranyl ion with organic monophosphonates. It is known that the complex of uranyl ion with organic monophosphonates did not show fluorescence properties. It seems that the fluorescence properties of uranyl ion with organic phosphonates depend on the structure of the ligand.[225] The fluorescence of uranyl-ligand complex decreased due to the generation of degradation compound. For the study at pH 3, only the absorption spectra before the TRLFS study will be used for the Study. The fast fluorescence spectra will be recorded for the Study. The lifetime measurement cannot be done due to the degradation of uranyl-ligand complex and non-fluorescence degradation compound.

b. study of uranyl-ligand complex at pH 7.4 in 0.1M NaCl and 0.1M $NaClO_4$

A test with uranyl-$\mathbf{L^2}$ 1:1 complex at pH 7.4 in two ionic solutions was done to determine the stability under 430nm laser excitation (Fig. 46). Owing to the benefit of non-fluorescence species of uranyl-$\mathbf{L^2}$ complex, the absorption of aromatic part didn't change in two ionic solutions which means the ligand didn't decompose under for this condition.

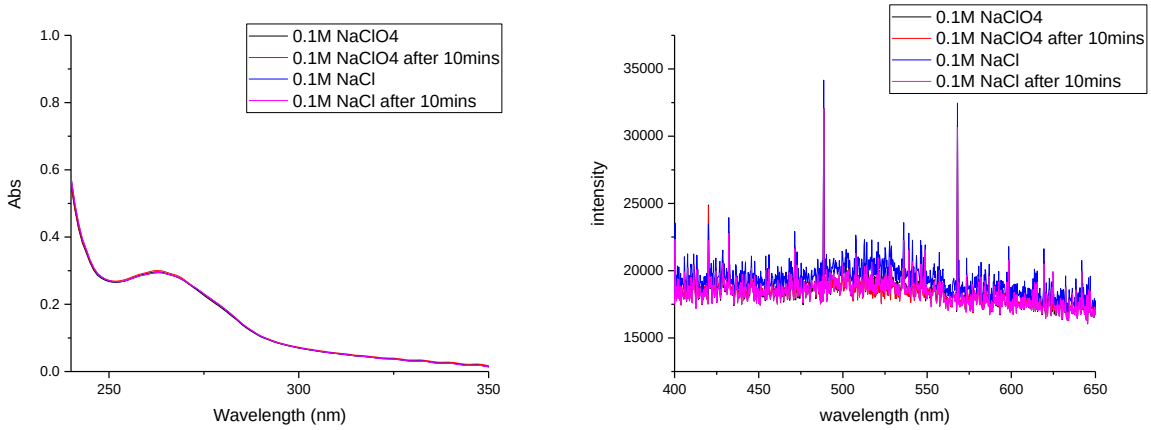

Figure 46 : Study of uranyl-L^2 1:1 complex under 430nm laser excitation, absorption measure (left); TRLFS measure (right); [L^2] = 5E-5 M, [U] = 5E-5 M, pH 7.4.

The same test with **L^3** and **L^4** was done and has the same phenomenon.

2.6 Study of uranyl-ligand complex

The Study of uranyl-ligand complex was done with the sample preparation method and experiment conditions which settled by previous test. The change over the UV absorption is mainly due to the aromatic part and amine branches. The fluorescence change is mainly due to the concentration and coordination of uranyl. Due to the problem with quenching and degradation, the lifetime measurement was not performed.

a. Study of uranyl-**L^3** complex at pH 3 in 0.1M NaCl

For the study of uranyl-**L^3** complex at pH 3, the major species of ligand alone in the solution at this condition is monophosphonate, thus the two phosphonate groups and pyridine group could provide 2 oxygen atoms and 1 nitrogen atom for the uranyl coordination. For the amine part, the proton still attach to the nitrogen at this pH, so there is a competition between the uranyl ion with hydrogen atom. For uranium alone in the solution, uranyl ion alone is the dominate species.

The absorption of aromatic part (Fig. 47 left) is increased for the Study. The evolution of the absorption ratio at 262nm is shown in figure 48 (left). The center peak position of uranyl fluorescence spectra (Fig. 47 right) is shift from 524nm (0.1M NaCl) to 522nm (0.1M NaCl). The center peak of uranyl fluorescence spectra in 0.1M $NaClO_4$ is at 524nm. The emitted intensity at 522 nm is shown in figure 48 (right).

For the first two samples, 0 and 0.2eq, the absorption of aromatic part doesn't change which means the aromatic part doesn't play a role in the coordination and the amine branches doesn't change. Due to the quenching of chloride ion, the fluorescence intensity of 0.2eq UO_2^{2+} is too low and the spectrum is noisy; it is pretty hard to identify the shift of fluorescence spectra. The uranyl may complex by chloride ion at low concentration which has been found in the previous study (Fig. 34). So for the sample with 0.2eq UO_2^{2+}, the uranyl ion might not form complex with the ligand due to the relatively low concentration at acidic condition. For the middle two samples, 0.4 and 0.6eq, the absorption at 262nm slightly increased, the shapes of the curves don't change, so the amine branches changed lot and the pyridine group might not be involved in the coordination. The fluorescence intensity at 522nm increased a lot; the shapes of the curves don't change. This means the uranyl ion is complexed by the ligand; the coordination of uranyl contains oxygen from phosphonate group. The binding mode of uranyl-**L^3** at pH 3 in this ratio range might be 2 ligands and 1 uranyl ion. The coordination of uranyl is consisting by 4 oxygen

atoms from four phosphonate groups and 1 oxygen atom from water molecular. For the last two samples, 0.8 and 1eq, the absorption at 262nm increased significantly, the shapes of the curves still don't change, so the amine branches and the pyridine group involve in the coordination. The fluorescence intensity at 522nm still increased, and the slope of fluorescence intensity at 520 nm is increased which suggest there might be a changing of binding mode. The shapes of the curves don't change. This means the uranyl ion is complexed by the ligand; the coordination of uranyl contains oxygen atoms from phosphonate group. The binding mode of uranyl-**L^3** at pH 3 in this ratio range might be 1 ligand and 1 uranyl ion. Uranyl ion is located in the pocket part of ligand. The coordination of uranyl is consisting by 2 oxygen atoms from two phosphonate groups, 2 nitrogen atoms from two amine branches and 1 nitrogen atom from pyridine group.

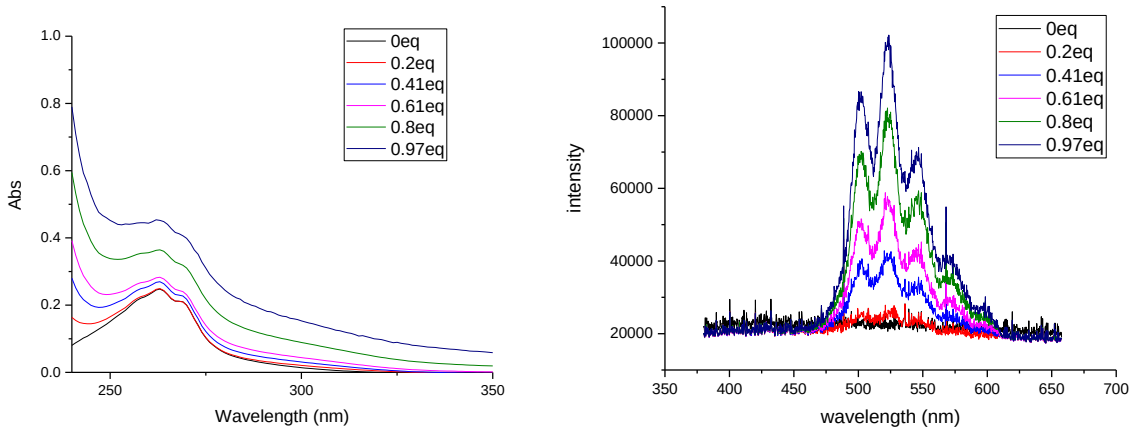

Figure 47 : Study of uranyl-L^3 complex, absorption measure (left); TRLFS measure (right); [L^3] = 5E-5 M, [U] 0-1 eq, pH 3, 0.1M NaCl.

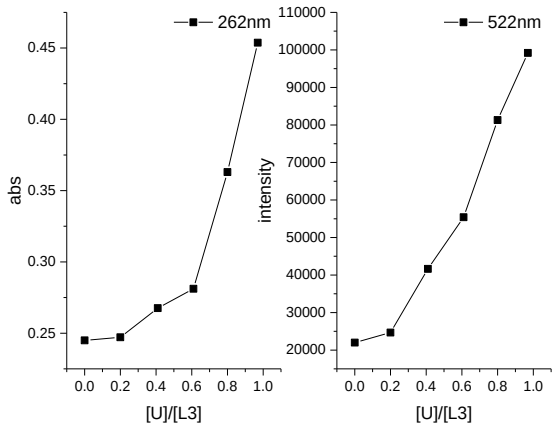

Figure 48 : Evolution of the absorption ratio at 262nm (left) and the emitted intensity at 522 nm (right) as a function of uranyl/L^3; [L^3] = 5E-5 M, [U] 0-1 eq, pH 3, 0.1M NaCl.

b. Study of uranyl-**L^4** complex at pH 3 in 0.1M NaCl

For the study of uranyl-**L^4** complex at pH 3, the major species of ligand alone in the solution at this condition is monophosphonate, thus the four phosphonate groups and pyridine group could provide 4 oxygen atoms and 1 nitrogen atom for the uranyl coordination. For the amine part, the proton is still attached to the nitrogen at this pH, so there is a competition between the uranyl with hydrogen. For uranium alone in the solution, uranyl ion alone is the dominate species.

The aromatic part absorption (Fig. 49 left) is increased for the Study. The evolution of the absorption ratio at 262nm is shown in figure 50 (left). The center peak position of uranyl fluorescence spectra (Fig. 49 right) is shift from 510nm (0.1M $NaClO_4$) to 520nm (0.1M NaCl). The center peak of uranyl fluorescence spectra in 0.1M NaCl is at 524nm. The emitted intensity at 520 nm is shown in figure 50 (right).

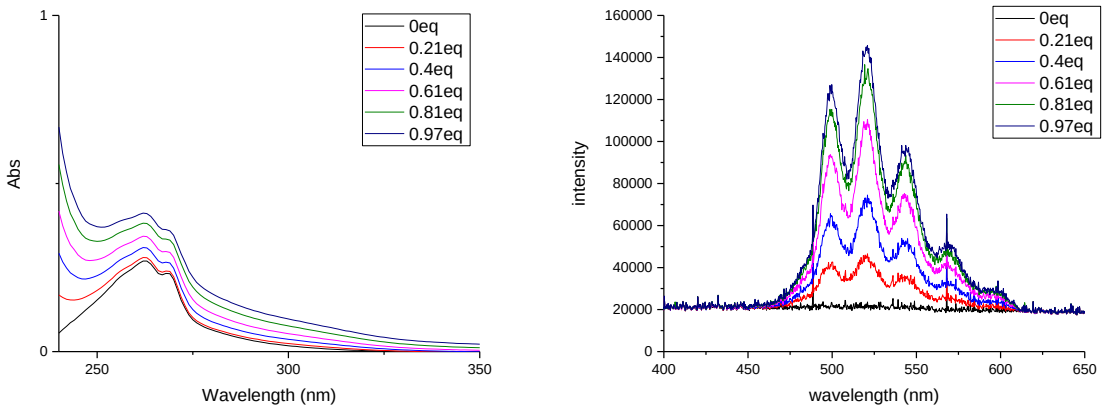

Figure 49 : Study of uranyl-L^4 complex, absorption measure (left); TRLFS measure (right); [L^4] = 5E-5 M, [U] 0-1 eq, pH 3, 0.1M NaCl.

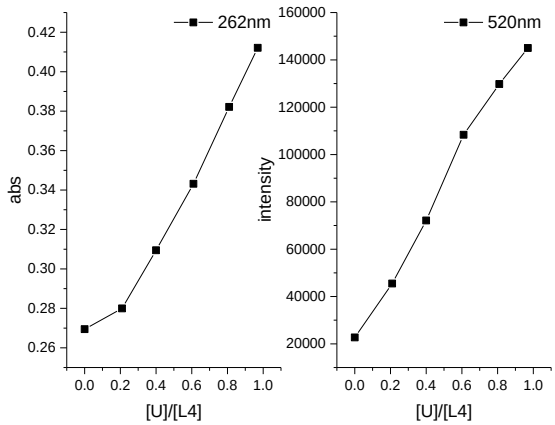

Figure 50 : Evolution of the absorption ratio at 262nm (left) and the emitted intensity at 520 nm (right) as a function of uranyl/L^4; [L^4] = 5E-5 M, [U] 0-1 eq, pH 3, 0.1M NaCl.

For the first two samples, 0 and 0.2eq, the absorption evolution of aromatic part doesn't change like the other samples which means the presence of free uranyl or that the binding is mainly between uranyl ion and phosphonate groups. For the rest, the absorption at 262nm increased significantly, the shapes of the curves still don't change, so the amine branches and the pyridine group should be involved in the coordination. The evolution of absorption at 262nm is linear which suggest the same coordination. The evolution of fluorescence intensity at 520nm is almost linear. The fluorescence of 1eq UO_2^{2+} might be affected by the degradation during the laser excitation due to the relatively high concentration of uranyl. So below 0.2eq UO_2^{2+}, the coordination of uranyl might mainly be related with the oxygen from phosphonate groups. Above 0.2eq, uranyl ion is located in the pocket part of ligand. The coordination of uranyl is consisting by 2 oxygen atoms from two phosphpnate groups, 2 nitrogen atoms from two amine branches and 1 nitrogen atom from pyridine group.

c. Study of uranyl-**L^3** complex at pH 7.4 in 0.1M $NaClO_4$

For the study of uranyl-**L³** complex at pH 7.4, the major species of ligand alone in the solution at this condition is phosphpnate group, thus the two phosphpnate groups and pyridine group could provide 2 oxygen atoms and 1 nitrogen atom for the uranyl coordination. For the amine part, the proton is still attached to the nitrogen atom at this pH, so there is a competition between the uranyl with hydrogen. For uranium alone in the solution, multispecies of uranyl hydroxide are present.

The aromatic part absorption (Fig. 51 left) is increasing for the Study and there is an evolution over the shapes of absorption spectra. The evolution of the absorption ratio at 262nm is shown in figure 52 (left). Normally uranyl ion could generate strong fluorescence at this pH. The center peak position of uranyl fluorescence spectra in 0.1M NaCl is at 525nm (Fig. 34). There is a broad intense peak of uranyl fluorescence spectra in 0.1M $NaClO_4$. The center peak position of uranyl fluorescence spectra in 0.1M $NaClO_4$ is at 522nm. (Fig. 34) But to this uranyl-**L³** complex, there is no fluorescence in each spectrum. This non-fluorescence property at 25 °C is similar to the uranyl carbonate complex $[UO_2(CO_3)_3]^{4-}$.[226,227]

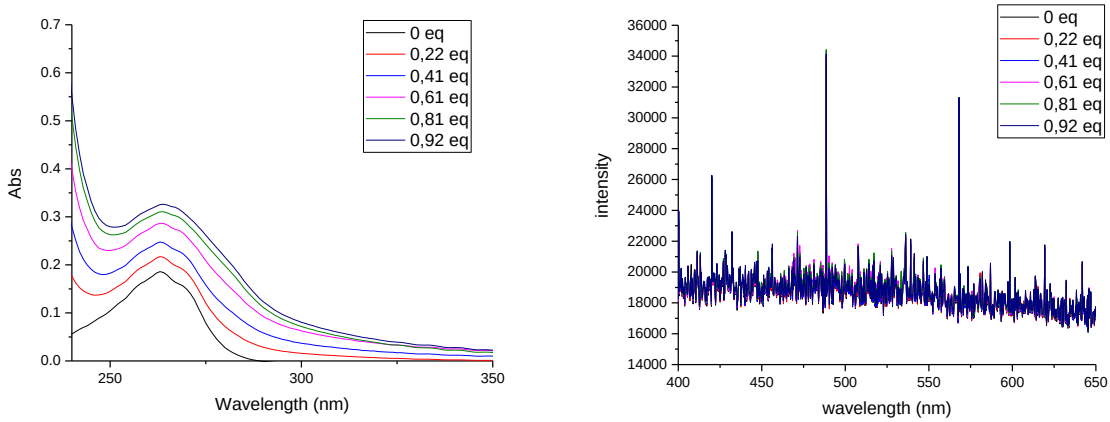

Figure 51 : Study of uranyl-L³ complex, absorption measure (left); TRLFS measure (right); [L³] = 5E-5 M, [U] 0-1 eq, pH 7.4, 0.1M $NaClO_4$.

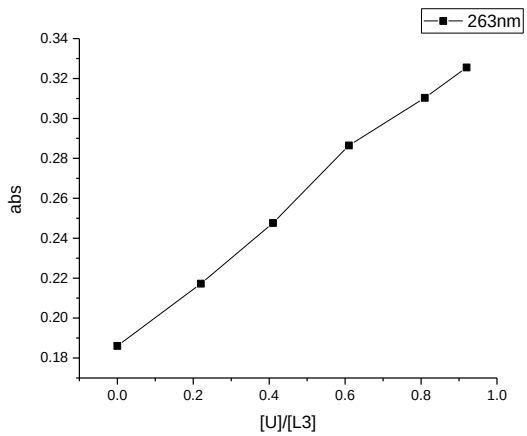

Figure 52 : Evolution of the absorption ratio at 263nm as a function of uranyl/L³; [L³] = 5E-5 M, [U] 0-1 eq, pH 7.4, 0.1M $NaClO_4$.

The evolution of absorption at 263nm is almost linear (Fig. 52). But the shape of the aromatic part is changing from a narrow peak at 263nm with a shoulder peak to a broad peak. This evolution shows the stepwise species changing of uranyl ion. And the non-fluorescence uranyl-ligand complex confirmed that there is only one binding mode. Uranyl ion is located in the pocket part of ligand. The coordination of uranyl ion is consisting by 2 oxygen atoms from

two phosphonate groups, 2 nitrogen atoms from two amine parts and 1 nitrogen atom from pyridine group.

d. Study of uranyl- **L^4** complex at pH 7.4 in 0.1M $NaClO_4$

For the study of uranyl-**L^4** complex at pH 7.4, the major species of ligand alone in the solution at this condition is phosphonate group, thus the four phosphonate groups and pyridine group could provide 4 oxygen atoms and 1 nitrogen atoms for the uranyl coordination. For the amine part, the proton is still attached to the nitrogen atom at this pH, so there is a competition between the uranyl with hydrogen. For uranium alone in the solution, multispecies of uranyl hydroxide are present.

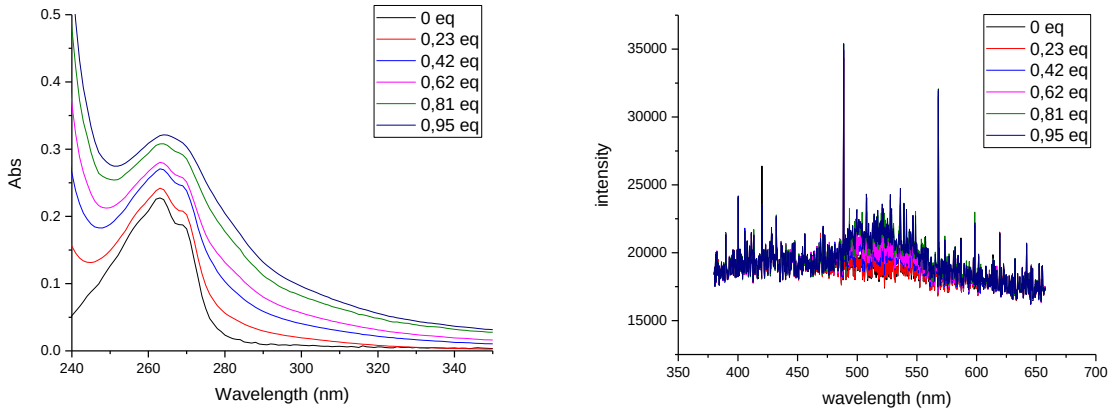

Figure 53 : Study of uranyl-L^4 complex, absorption measure (left); TRLFS measure (right); [L^4] = 5E-5 M, [U] 0-1 eq, pH 7.4, 0.1M $NaClO_4$.

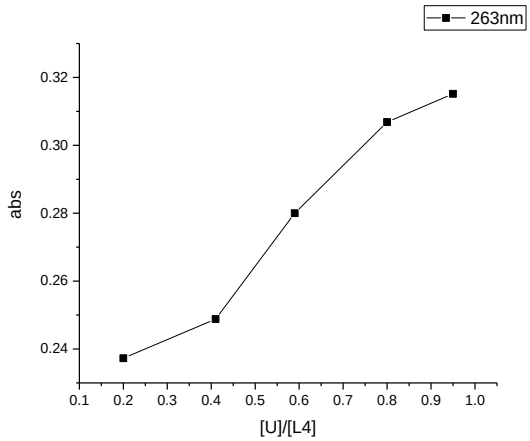

Figure 54 : Evolution of the absorption ratio at 263nm as a function of uranyl/L^4; [L^4] = 5E-5 M, [U] 0-1 eq, pH 7.4, 0.1M $NaClO_4$.

The absorption of aromatic part (Fig. 53 left) is increasing for the study and there is an evolution over the shapes of absorption spectra. The evolution of the absorption ratio at 262nm is shown in figure 54.There is non-fluorescence from the uranyl-ligand complex (Fig. 53 left) which compare to the free uranyl spectra in 0.1M $NaClO_4$. The very weak fluorescence of uranyl might reflect the presence of a very small amount of other bonding mode (Fig. 53 right).

The shape of the aromatic part is changing from a narrow peak at 263nm with a shoulder peak to a broad peak. This evolution of spectra suggests the uranyl is directly complexed by the ligand. And the non-fluorescence uranyl-ligand complex confirmed that there is only one binding mode. Uranyl ion is located in the pocket part of ligand. The coordination of uranyl is

consisting by 2 oxygen atoms from two phosphonate groups, 2 nitrogen atoms from two amine parts and 1 nitrogen atom from pyridine group.

2.7 Conclusion

At pH 3, there are two degradation paths throw the measurement. The degradation with molecular oxygen and sunlight could be minimized by prepare the sample under dark condition. But degradation with laser excitation cannot be avoided.

There are 3 steps for the uranyl-$\mathbf{L^3}$ complex study at pH 3. The uranyl is mainly complex by chloride ion in the first step (0-0.2eq). For second step (0.2-0.6eq), the major species is uranyl complex with phosphonate groups from two $\mathbf{L^3}$. The dominate species is uranyl complex with $\mathbf{L^3}$ in the pocket part for the third step (0.6-1eq).

There are 2 steps for the uranyl-$\mathbf{L^4}$ complex study at pH 3. There is mainly uranyl complex with phosphonate groups from $\mathbf{L^4}$ in the first step (0-0.2eq). For second step (0.2-1eq), the dominate species is uranyl complex with $\mathbf{L^3}$ in the pocket part.

The protonated monophosphonate organic ligands limit the complexation affinity of uranyl at low concentration. The species difference between the two slope studies is mainly due to the ligand structure difference. The steric effect of two benzyl group of $\mathbf{L^3}$ might limit the freedom of uranyl coordination.

At pH 7.4, the two degradation paths are minimized throw the measurement by non-fluorescence uranyl-ligand complex. For both ligands, uranyl ion is directly complexed with the ligand. There is only one species throughout the whole Study. The deprotonated phosphonate organic ligands are easier to form complexation with uranyl ion. The coordination environment of uranyl-ligand complex might be the same according to the non-fluorescence property.

3 IR characterization of two ligands with uranium in aqueous solution

3.1 IR spectra of ligands

Based on the species diagrams of two ligands, hydrolysis of uranium and biochemical condition of the serum, IR spectra of two ligand solutions at pH 3 (red) and 7.4 (black) were recorded.

With the help from previous study, the deprotonation happened mainly due to the phosphonate group and ternary amine unit. For phosphonate group, hydrogen phosphonate group (PO_3H^-) is the major species at pH 3 while deprotonated phosphonate group (PO_3^{2-}) is the majority at pH 7.4. The ternary amine unit is protonated under experiment condition.

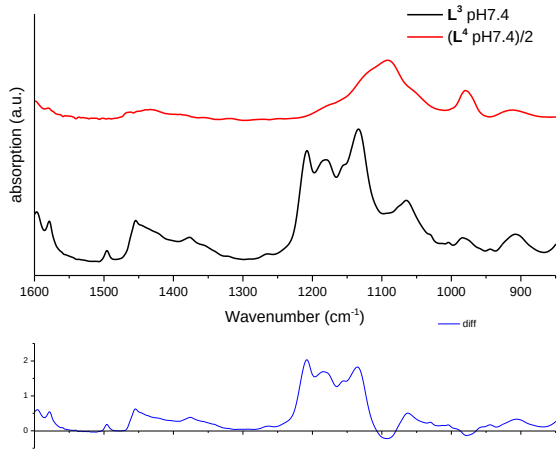

Figure 55 : FT-IR spectra of pH 3 in H_2O. Spectra of L^4 in red and L^3 in black. Difference spectra L^3 minus half L^4 (blue).

In order to determine the contribution of pyridine group and benzene fragment, it is possible to identify each peak by compare the two spectra of two ligands at the same pH. Due to the ratio difference between phosphonate group and pyridine group of two ligands, a comparison was done by normalized on the aromatic ring carbon-carbon stretching vibrations at 1580 cm^{-1}. The difference curve was done by spectra $\mathbf{L^3}$ minus half of $\mathbf{L^4}$ which aims to remove the absorption from phosphonate group.

From figure 55 above, the $\nu_{as}(P-OH)$ at 914cm^{-1} couldn't be found on the difference spectra. Thus the vibrational modes of aromatic units could be identified in the difference spectra (Fig. 55 blue). The bands at 1200cm^{-1}, 1176cm^{-1}, 1133cm^{-1} and 1000cm^{-1} reflect the pyridine backbone and benzyl group which are coherent with FT-IR spectra of 2,6-Bis(bromomethyl)pyridine and [(phenylmethyl)imino]bis(methylene)]bisphosphonic acid. Those vibration modes are out-of-plane bending vibration b_{2g}, in-plane bending vibrations b_{2g}, and C-H in-plane bending a_{1g} and C-C ring breathing a_{ig}. For the bands at 1180cm^{-1}, 1084cm^{-1} and 914cm^{-1} in the spectrum record from $\mathbf{L^4}$ at pH 3 (Fig. 55 red) are assigned to $\nu_{as}(P-O)$, $\nu_s(P-O)$, and $\nu_{as}(P-OH)$, respectively.[228] From the characteristic pattern, the symmetry of the organic phosphonate group could be identified as C_{2v} symmetry which means the monoanionic species, PO_3H^-, is the dominant species at pH 3.[229] It confirms the potentiometric titration results.

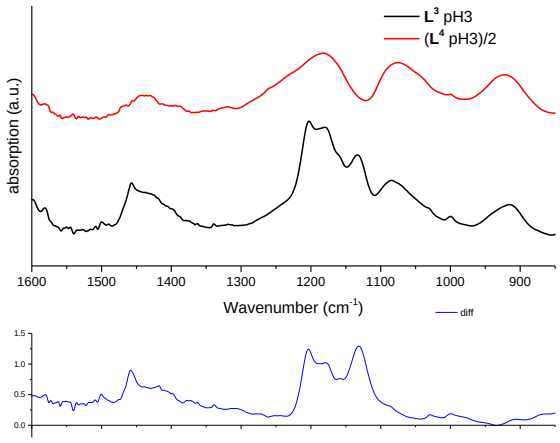

Figure 56 : FT-IR spectra of pH 7.4 in H_2O. Spectra of L^4 in red and L^3 in black. Difference spectra L^3 minus half L^4 (blue).

The same procedure was done to get the difference spectra for pH 7.4 comparison. At pH

7.4, the pyridine backbone and benzyl group have absorption at 1208cm^{-1}, 1180cm^{-1}, 1135cm^{-1} and 1062cm^{-1} in the difference spectrum (Fig. 56 blue) which shown a blue shift compared to the spectra at pH 3. From the species diagram of each ligand, it's known that the major species is phosphonate group (PO_3^{2-}). The small peak at 913cm^{-1} is due to the presence of minor species, PO_3H^-. The band at 1090 cm^{-1} and 979 cm^{-1} refer to $\nu_{as}(P-O)$, and $\nu_s(P-O)$ (Fig. 56 red)[24].

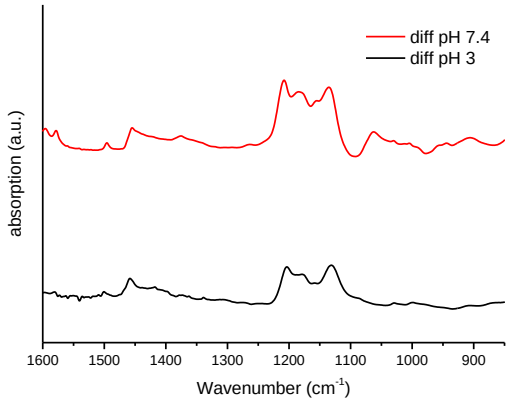

Figure 57 : FT-IR spectra of difference spectrum at pH 3(red) and 7.4(black). Difference spectra L^3 minus half L^4 at each pH.

By comparing the difference spectra **L^3** minus half of **L^4** at each pH (Fig. 57), the absorption of vibration mode of aromatic units in the middle infrared range increased with the pH increase, which the aromatic in-plane C–H bending changed.

From the potentiometric titration results of **L^4**, the protonated phosphonate group could be sensed because of the pattern of the band, namely hydrogen phosphonate group (PO_3H^-) at pH 3. At pH 7.4, the deprotonated phosphonate group (PO_3^{2-}) could be detected, since ternary amine doesn't have absorption in this range. Contributions from vibrational modes of the pyridine unit can also be neglected due to the ratio between aromatic units and phosphonate groups. In the region below 1200 cm^{-1} (Fig. 58), the distinctive spectral features at 1192 cm^{-1} (negative), 1118 cm^{-1}, 1034 cm^{-1} (negative), 981 cm^{-1}, and 932 cm^{-1} (negative) represent the deprotonation of the phosphonate groups, which provide an important spectral reference for the further study of uranyl complexation.

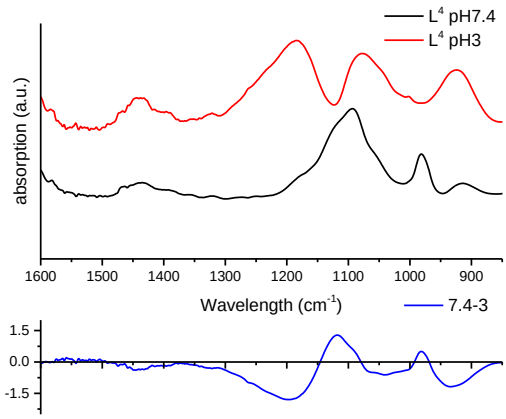

Figure 58 : FT-IR spectra of L^4 in H_2O. Spectra recorded at pH 7.4 (red) and pH 3 (black). Difference spectrum pH 7.4 minus pH 3 (blue).

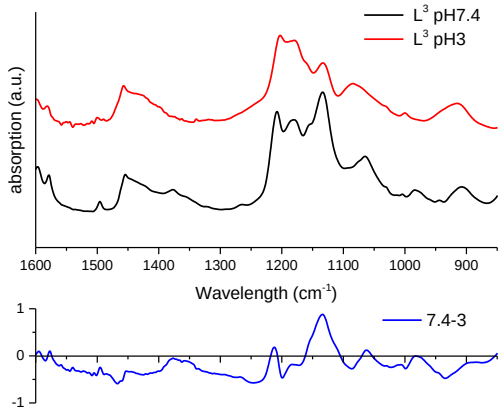

Figure 59 : FT-IR spectra of L^3 in H_2O. Spectra recorded at pH 7.4 (red) and pH 3 (black). Difference spectrum pH 7.4 minus pH 3 (blue).

Base on the study of FT-IR spectra of $\mathbf{L^4}$ and potentiometric titration of $\mathbf{L^3}$, mainly contributions from phosphonate groups are expected. It is confirmed that the aromatic in-plane C–H bending changed with pH increase from previous comparison. In the range from 1250 cm^{-1} to 900 cm^{-1} in figure 59, the modes of vibration from organic phosphonate group, benzyl group and pyridine backbone could be detected in the region. A difference spectrum (Fig 59. blue line) was calculated by using spectra at pH 7.4 minus spectra pH 3 in order to determine the changing of vibration bands due to the species variation. The distinctive spectral features at 1200 cm^{-1} (negative), 1135 cm^{-1}, 1034 cm^{-1} (negative), 980(0) cm^{-1}, and 936 cm^{-1} (negative) represent the deprotonation of the phosphonate groups. The distinctive spectral features difference between $\mathbf{L^3}$ with $\mathbf{L^4}$ is due to the vibration mode of aromatic group which is present in the same range. The distinctive spectral features at 1209 cm^{-1}, 1176 cm^{-1} (negative), 1085 cm^{-1} (negative) and 1000cm^{-1} (negative) represent the vibration mode of aromatic group, out-of-plane bending vibration b_{2g}, in-plane bending vibrations b_{2g}, and C-H in-plane bending a_{1g} and C-C ring breathing a_{ig} respectively.

3.2 IR spectra of uranyl-ligand complexation

The infrared spectroscopic tests on uranyl complexation with ligand were down to investigate the complexation mode at two pHs. Each sample in this study was prepared with same molar equivalence of uranyl and ligand base on the studies of UV-Vis absorption spectroscopy and fluorescence study. All the spectra were normalized at 1580 cm^{-1} with carbon stretching vibrations e_g.

Because the benzene groups of $\mathbf{L^3}$ are not in the coordination of uranyl, the vibration modes of benzene group have the same contribute in samples with and without uranyl. In contrast, the IR absorption of phosphonate group and pyridine group for both ligands involved in the coordination of uranyl should change significantly.

A similar symmetry of monoanionic phosphonate group in two samples was confirmed with the phosphonate groups vibration modes $\nu_{as}(P-O)$,$\nu_s(P-O)$ and $\nu_{as}(P-OH)$ for the aqueous $\mathbf{L^3}$ sample and UO_2^{2+} $-\mathbf{L^3}$ sample recorded at pH 3 (Fig. 60). The distinctive spectral features at 1201 cm^{-1}, 1178 cm^{-1}, 1156 cm^{-1}, 1069cm^{-1}, 1020cm^{-1}, 1104cm^{-1}, 997cm^{-1} and 913 cm^{-1} represent the deprotonation of the phosphonate groups and pyridine group vibration change. Positive bands at ν̌= 1201 cm^{-1}, 1156 cm^{-1},1104 cm^{-1} and 997 cm^{-1} are related with pyridine group vibration change. Positive bands at ν̌= 1178 cm^{-1}, 1069 cm^{-1}, 1020cm^{-1} and 997 cm^{-1} are assigned to $\nu_{as}(P-O)$, $\nu_s(P-O)$, $\nu_s(P-O)$ and $\nu_s(P-O)$. The band at ν̌= 913 cm^{-1} is due to $\nu_{as}(UO_2)$ mode. Thus both pyridine group and phosphonate groups are

present in the coordination of uranyl which suggests uranyl ion located in the ligand pocket with 3 nitrogens and 2 oxygens.

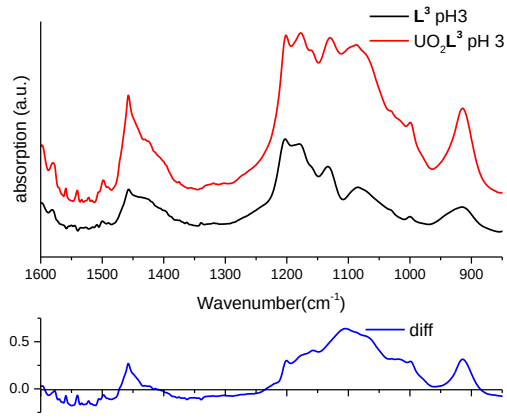

Figure 60 : FT-IR spectra of uranyl-L^3 at pH 3 in H_2O. Spectra of uranyl-L^3 in red and L^3 in black. Difference spectrum uranyl-L^3 minus L^3 (blue).

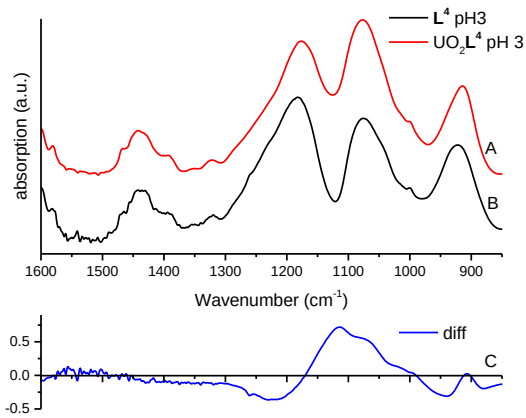

Figure 61 : FT-IR spectra of uranyl-L^4 (right) at pH 3 in H_2O. Spectra of uranyl-L^4 in red and L^4 in black. Difference spectrum uranyl-L^4 minus L^4 (blue).

A similar pattern of bands is observed in the spectrum of the aqueous $\mathbf{L^4}$ sample and UO_2^{2+} $-\mathbf{L^4}$ sample recorded at pH 3 (Fig. 61) and were assigned to the $\nu_{as}(P-O)$,$\nu_a(P-O)$ and $\nu_{as}(P-OH)$ modes of the phosphonate groups, suggesting a similar symmetry of monoanionic phosphonate group in two samples. The distinctive spectral features at 1176 cm^{-1}, 1074 cm^{-1}, 1020 cm^{-1} and 906 cm^{-1} (0) represent the deprotonation of the phosphonate groups. Because of the vibration mode at 1217 cm^{-1} is different from the $\nu_{as}(P-O)$ modes at 1176 (Fig. 61 black), there might be a pyridine vibration change which present at 1217 cm^{-1} (negative), 1114 cm^{-1}, 998(0) cm^{-1} and 940 cm^{-1} (negative). Due to the negative band of $\nu_{as}(P-OH)$ in the same range, the value is about zero for the $\nu_{as}(UO_2)$ mode at 906 cm^{-1}. Positive bands at $\check{\nu}$= 1074 cm^{-1}, 1020 cm^{-1} are related with $\nu_s(P-O)$ and $\nu_s(P-O)$. So for $\mathbf{L^4}$, it is found that the phosphonate groups are present in the uranyl coordination at pH 3. Meanwhile pyridine group might involve in the coordination of uranyl ion also.

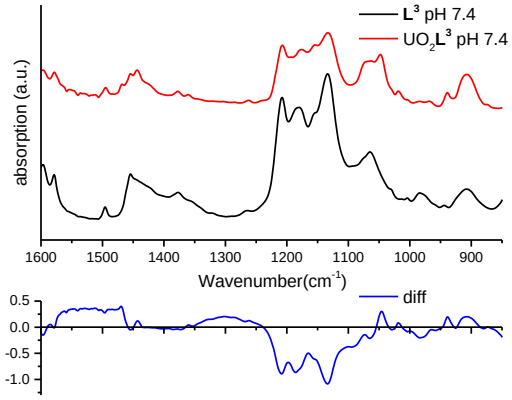

Figure 62 : FT-IR spectra of of uranyl-L³ at pH 7.4 in H₂O. Spectra of uranyl-L³ in red and L³ in black. Difference spectrum uranyl-L³ minus L³ (blue).

The distinctive spectral (Fig 62 blue) of uranyl $-\mathbf{L^3}$ at pH 7.4 has bands at 1208 cm^{-1}(negative), 1185 cm^{-1}(negative), 1134 cm^{-1}(negative), 1063cm^{-1}(negative), 1045cm^{-1}, 1003 cm^{-1}(negative), 982 cm^{-1}, 937 cm^{-1} and 907 cm^{-1}. Bands at 1208 cm^{-1} (negative), 1134 cm^{-1}(negative), 1045cm^{-1}, 1003 cm^{-1}(negative) and 937 cm^{-1} are related with pyridine group vibration change. Meanwhile bands at 1185 cm^{-1}(negative), 1063cm^{-1}(negative) and 982 cm^{-1} are assigned to the phosphonate modes, $\nu_{as}(P-O)$, $\nu_s(P-O)$ and $\nu_s(P-O)$. The band at ν̌=907 cm^{-1} is due to $\nu_{as}(UO_2)$ mode. It is the same for **L³** at pH 7.4, both pyridine group and phosphonate groups are present in the coordination of uranyl ion which suggests uranyl ion is located in the ligand pocket with 3 nitrogen atoms and 2 oxygen atoms.

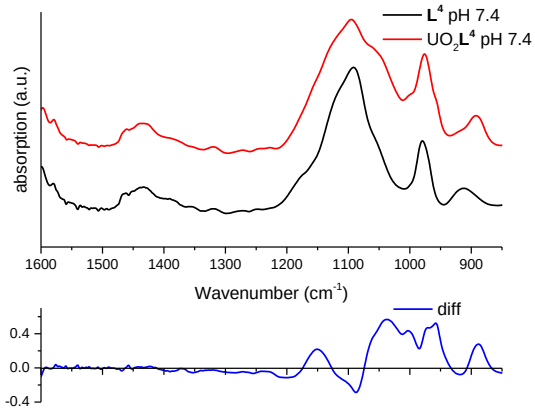

Figure 63 : FT-IR spectra of uranyl-L⁴ (right) at pH 7.4 in H₂O. Spectra of uranyl-L⁴ in red and L⁴ in black. Difference spectrum uranyl-L⁴ minus L⁴ (blue).

A similar symmetry of dianionic phosphonate group group in two samples was confirmed with the phosphonate group vibration modes. A similar pattern of bands is observed in the spectrum of the aqueous **L⁴** sample and UO_2^{2+} $-\mathbf{L^4}$ sample recorded at pH 7.4 (Fig. 63 red & black). The distinctive spectral (Fig. 63 blue) features at 1150 cm^{-1}, 1088 cm^{-1}(negative), 969 cm^{-1} and 918 cm^{-1}(negative) represent the phosphonate modes, $\nu_{as}(P-O)$, $\nu_s(P-O)$, $\nu_s(P-O)$ and $\nu_{as}(P-OH)$. Bands at ν̌= 1200 cm^{-1}(negative), 1149 cm^{-1}, 1037 cm^{-1} and 1000 cm^{-1} are related with pyridine group vibration change. The band at ν̌=888 cm^{-1} is due to $\nu_{as}(UO_2)$ mode. The large shift of $\nu_{as}(UO_2)$ mode (906 cm^{-1} to 888 cm^{-1}) is due to the negative band of $\nu_{as}(P-OH)$ in the same range. Then for **L⁴**, it is found that the phosphonate groups and pyridine group are present in the uranyl coordination at pH 7.4.

3.3 Conclusion

The FT-IR absorption comparison between each sample can be done by standardize with the aromatic C-C structural vibration. The vibration attribution of two ligands, $\mathbf{L^3}$ and $\mathbf{L^4}$, are done first with the help of difference spectrum. The vibration of phosphonate groups and pyridine group could be found in the range of 850 to 1300 cm^{-1}. But the ternary amine doesn't have absorption in the infrared range. Besides due to the coupling of phosphonate groups, amine parts and pyridine group, the FT-IR spectra are difficult to analyze.

At pH 3, phosphonate groups are involved in the uranyl coordination for both ligands. For the pyridine group, it is clearly play a role in the uranyl coordination for $\mathbf{L^3}$ which is hard to identify for $\mathbf{L^4}$.

At pH 7.4, phosphonate groups and pyridine group are involved in the uranyl coordination for both ligands.

4 Structural study of uranyl-ligand complexes

4.1 Possible structure of uranyl-ligand complexes

Previous experiments (TRLFS, UV-visible absorption spectroscopy, FT-IR) have shown that uranyl ion is located in the pocket of ligands at high equivalence above 0.6eq at pH 3. Meanwhile for pH 7.4, uranyl ion wills directly complex with ligands and located in the pocket of ligand. And due to the uranyl ligand fluorescence difference at pH 3 and 7.4, the uranyl coordinations are not the same for two pHs.

ESI-MS test was done with uranyl-$\mathbf{L^3}$ and uranyl-$\mathbf{L^4}$ at pH 7.4 to determine the complex formation. But only the fragments were found in the data. ^{15}N-NMR test was done with uranyl-$\mathbf{L^3}$ and uranyl-$\mathbf{L^4}$ at pH 3 to determine presence of nitrogen in the coordination. But the signal is too low to detect.

At pH 3, two possible structures for uranyl-$\mathbf{L^3}$ 1:1 complex are proposed. First, the possible structure is that with uranyl ion located in the pocket part of the ligand which consist 3 nitrogens and 2 oxygens. The second possibility is that where there is an extra water molecule in the coordination. Two similar uranyl coordination methods are suggested for uranyl-$\mathbf{L^4}$ complex (due to the similar structure of ligands and previous results).

At pH 7.4, two possible structures for uranyl-$\mathbf{L^3}$ 1:1 complex are proposed. First, the possible structure is that with uranyl ion located in the pocket part of the ligand which consist 3 nitrogens and 2 oxygens. The second possibility is that where there is an extra hydroxide group in the coordination. Two similar uranyl coordination methods are suggested for uranyl-$\mathbf{L^4}$ 1:1 complex (due to the similar structure of ligands and previous results).

4.2 Possible structure optimized by DFT

In order to adjust the data obtained in EXAFS, it is necessary to construct a model describing the structure of complexes between uranyl ion and ligands. Constructed structures are then optimized for energy through calculations using the Functional Theory of Density (DFT). The geometry of the systems was optimized using RECP (Relativistic Effective Core Potential) at the B3LYP level and solvation effects were introduced using a polarized continuum model (PCM). The possible structures of uranyl-ligand complexes were optimized by DFT. Many of these models were eliminated because of the steric hindrance caused by complexation in the equatorial plane, specific to uranyl ion. Other structures were discarded as unstable energy, following the processes of minimization of energy. Structures from the most

energy-efficient DFT calculations were therefore used for the adjustment of EXAFS data. Finally, the most stable energetically stable environment for uranyl which provide by ligand is composed of two oxygen atoms from monodentate phosphonate (O_{ph}), two nitrogen atoms from amine (N_{amine}), one nitrogen atom from pyridine (N_{pyr}). Besides due to the uranyl coordination difference at two pHs which confirm by UV-vis absorption study & TRLFS, two different models were built: for pH 3 (Fig. 64), a model without a water molecule in its coordination sphere and a model with the water molecule; for pH 7.4 (Fig. 65), a model without a hydroxide in its coordination sphere and a model with a hydroxide. The coordination sphere of uranyl for two ligands at pH 3 is different with or without the water molecular thus satisfying the coordination number of five or six in the equatorial plane. For pH 7.4, it is the same. The energetic optimization of the uranyl-ligand complex structures allowed us to determine the most stable.

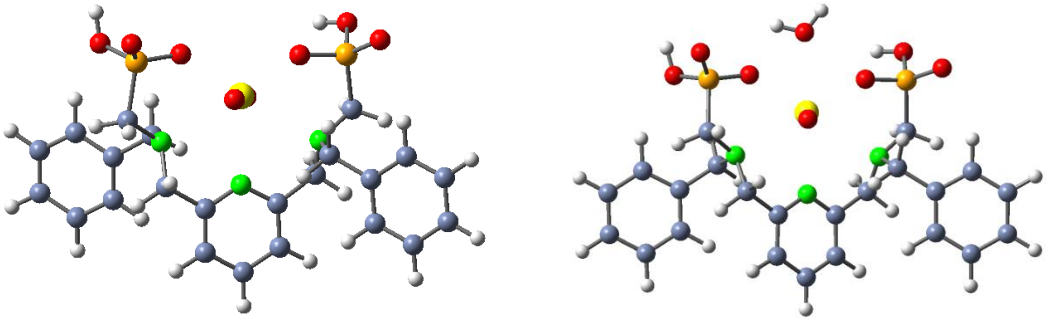

L^3/UO_2^{2+} pH=3 **L^3/UO_2^{2+} with 1 H_2O pH=3**

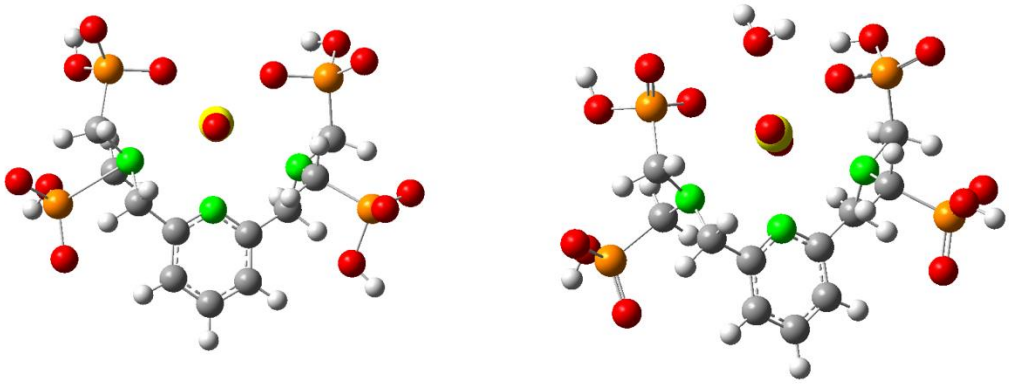

L^4/UO_2^{2+} pH=3 **L^4/UO_2^{2+} with 1 H_2O pH=3**

Figure 64 : Theoretical models optimized by DFT and electronic density of L^3 & L^4 interaction sites with uranyl at pH 3 (Oxygen: red, carbon: blue, nitrogen: light green, uranium: yellow).

distance(Å)	[L^3-U]	[L^3-U-H_2O]	[L^4-U]	[L^4-U-H_2O]
U-O_{yl}	1.79	1.78	1.79	1.78
U-O_p	2.30	2.34	2.29	2.32
U-O_{water}	~	2.72	~	2.66
U-N_{pyr}	2.87	2.75	2.59	2.72
U-N_{amine}	2.93	2.88	2.74	2.88
U-P	3.55	3.61	3.53	3.61

Table 19：Distances calculated by DFT for the four complexes

According to our calculations the ligand provides a symmetrical coordination of the uranyl ion due to the symmetrical structure of two ligands. As expected the average bond lengths of the uranyl-ligand complexes without H_2O increase in the following order (Table 19): U-O_{yl} < U-O_p < U-N_{pyr} < U-N_{amine}. For the uranyl-ligand complexes with H_2O, on the other hand, the water molecular is a little bit further to the metal center compare to the O_{yl} and O_p, which gives binding lengths that follow the order: U-O_{yl} < U-O_p < U-O_{water} <U-N_{pyr} < U-N_{amine}. These theoretical results are in agreement with the other result.[230] Both model for two ligands at pH 3 are stable in DFT calculation.

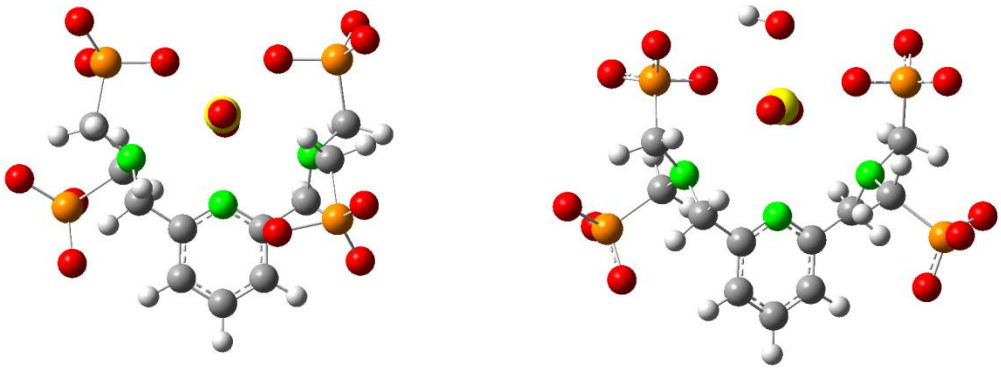

L^4/UO_2^{2+} pH=7.4 **L^4/UO_2^{2+} with OH^- pH=7.4**

Figure 65 : Theoretical models optimized by DFT and electronic density of L^4 interaction sites with uranyl at pH 7.4 (Oxygen: red, carbon: blue, nitrogen: light green, uranium: yellow).

distance(Å)	[L^4-U]	[L^4-U-OH]
U-O_{yl}	1.81	1.82
U-O_{OH}	~	2.28
U-O_p	2.23	2.31
U-N_{pyr}	2.62	3.09
U-N_{amine}	2.75	3.34
U-P	3.53	3.63

Table 20 : Distances calculated by DFT for the two complexes.

Then the DFT calculation was done only for **L^4** at pH 7.4 due to the distance similarity at pH 3 to reduce the amount of calculation. The average bond lengths of the uranyl-**L^4** complexe increase in the following order (Table 20): U-O_{yl} < U-O_p < U-N_{pyr} < U-N_{amine}. For the uranyl-**L^4**-OH complex, on the other hand, the OH^- group is much closer to the metal center, which gives binding lengths that follow the order: U-O_{yl} < U-O_{OH} < U-O_p <U-N_{pyr} < U-N_{amine}. These theoretical results are in agreement with the more covalent nature (more intense interaction) of the oxygen of the OH^- group compared to the oxygen of the water molecule. Since the OH^- ion is much closer to the metal, an increase in the U-O_{yl} and U-O_p distances is observed in the uranyl-**L^4**-OH complex relative to the uranyl-**L^4**-H_2O complex, indicating a weakening the complexation between the ligands and uranyl due to the very strong bond existing between OH and the metal center.

These structures were then used to adjust the EXAFS data and compare theoretical distances to experimental distances

4.3 EXAFS data analysis

However, a lack of information remains on the chemical function groups involved in the complexation of uranyl ion. EXAFS (Extended X-ray Fine Structure) is an X-ray spectroscopic technique that determines the composition of the coordination sphere of metals. These analyzes give us the possibility of knowing the environment of uranyl ions when they are complexed by ligands. In addition, this technique gives us the opportunity to confirm the existence of extra water molecular or hydroxide ion in the case of uranyl coordination. The effect of pH on the coordination sphere of the metal is therefore studied in this chapter for the four uranyl-ligand complexes. pH 3 and 7.4 were chosen due to the same reason. The principle of the EXAFS, the acquisition and analysis parameters as well as the details of the DFT calculations is summarized in the appendix.

4.4 EXAFS data analysis of the uranyl-ligand complex

A comprehensive structural study to determine the composition of the coordination sphere has not been conducted. Preliminary experiments of UV-vis absorption spectroscopy and TRLFS studies showed that at pH 3 and pH 7.4 the complexes between uranyl and $\mathbf{L^3}$ are largely in the majority. The changes in fluorescence property which observed in this study suggest a change in the coordination of uranyl. The measurement results of FR-IR shown the uranyl ion is located in the pocket of two ligands at 1:1 ratio. Since the presence of a single species is imperative for obtaining significant results, the EXAFS data were therefore collected at these two pHs of interest. The purpose of these experiments is to determine the composition of the coordination sphere of uranyl in these two conditions and thus to determine the impact of hydrolysis of uranyl on its complexation with the ligand.

4.4.1 Uranyl-ligand study at pH 3

The most stable adopted model at pH 3 includes two axial oxygen atoms (O_{yl}), two equatorial oxygen atoms (O_p), three equatorial nitrogen atoms (N_{pyr} & $2N_{amine}$) with or with O_{water}. The O_p atom represents the oxygen atom of the monodente phosphonate group; O_{water} represents the oxygen atom of the water. N_{pyr} atom represents the nitrogen atom of pyridine group; N_{amine} represents the nitrogen atom from amine units. An additional layer representing the phosphors atoms associated with the above-mentioned phosphonate oxygen atoms has also been taken into account.

During the adjustment procedure, the triple diffusion paths relating to the two axial oxygens of the uranyl have been taken into account. The U-P single scattering pathway and U-P-O_{ax} multiple scattering pathway were also necessary to perform the fit of the experimental data.

A Hanning adjustment window in k^3 (2; 12.9) was used and the adjustment of spectra was in R (1; 5). Adjustment parameters such as passive electron reduction factor (S_0^2) and ΔE_0 are given for each experiment. The adjustment factor R (r) and the reduced quality factor ($\chi^2_{i\ ln}$) are both provided as an indicator of the quality of the fit.

Taking into consideration the number of paths and the constraints geometric, the floating parameter number is 12 for the experiment pH 3. The fits of uranyl-ligand with 1 H_2O cannot converge. Fits of uranyl-ligand without H_2O are the best obtained. All the results of the adjustments are summarized in table 21 and table 22. The EXAFS k^3 spectra and their Fourier corresponding are shown in Figure 66.

path	R_{DFT}(Å)	N_{deg}	sigma^2(× 10−3 Å²)	R_{FIT}(Å)
U-O_{yl}	1,81	2	3,67	1,80
U-O_p	2,21	2	2,92	2,30
U-N_{pyr}	2,56	1	2,08	2,44
U-N_{amine}	2,85	2	9,93	2,96
U-P	3,62	2	14,95	3,69
U-O_{ax1}-U-U_{ax2}-U	3,63	2	7,33	3,59
U-P-O_{ax}	4,65	4	6,59	4,61

Table 21：Description of the paths used to fit the EXAFS data of the L^3-U complex determined at pH 3. S_0^2 = 1.19; ΔE_0 = 6.50 eV. R = 0.03; $\chi^2_{i\,ln}$ = 115.8.

The fitting result of **L^3**-uranyl complex is not so good. Actually this test was performed twice. There is a bubble and precipitation which formed during the sample measurement for the first time. And the U L_{III} edge k^3–weighted EXAFS spectra showed a little difference. For this reason a fast scan was implementing by decrease the accuracy and changed the position of sample to have a better reproducibility. For the uranyl-**L^4** complex, the fitting result is rather good.

Similar EXAFS spectra were obtained with the uranyl-**L^3** complex and uranyl-**L^4** complex at pH 3, which is a good indication that a unique uranyl binding site is probed under the experimental conditions used for EXAFS.

path	R_{DFT}(Å)	N_{deg}	sigma^2(× 10−3 Å²)	R_{FIT}(Å)
U-O_{yl}	1,81	2	3,87	1,81
U-O_p	2,21	2	4,04	2,32
U-N_{pyr}	2,56	1	2,92	2,50
U-N_{amine}	2,85	2	27,17	2,83
U-P	3,62	2	19,48	3,69
U-O_{ax1}-U-U_{ax2}-U	3,62	2	7,75	3,61
U-P-O_{ax}	4,65	4	7,92	4,59

Table 22 : Description of the paths used to fit the EXAFS data of the L^4-U complex determined at pH 3. S_0^2 = 1.27; ΔE_0 = 5.67 eV. R = 0.02; $\chi^2_{i\,ln}$ = 4.35.

The Fourier transforms (FT) represents a pseudo-radial distribution function of the uranium near-neighbor environment. The peaks appear at lower R values relative to the true near-neighbor distances as a result of the EXAFS phase shift, which is different for each neighboring atom (φ =0.2 to 0.5 Å).

For uranyl-**L^3** complex and uranyl-**L^4** complex at pH 3, the results show that U^{VI} has two O_{yl} atoms at a distance of 1.79 and 1.80 Å, two O_{ph} at 2.30 and 2.32 Å, one N_{pyr} at 2.44 and 2.50 Å and two N_{amine} at 2.85 and 2.85 Å. The distance between U and O_{yl} is typical for the uranyl ion.[231] The U-O_{ph} bond length is within the range of previously reported values for the oxygen atom of phosphonate groups bound to uranyl in a monodentate fashion.[145,232] These four types of atoms at equatorial plane thus could correspond to the presence of monodentate phosphonate groups and interaction with the pyridine group as deduced from the FTIR data and UV-vis absorption data. The best fit was obtained with a coordination number of two for the U-O_{ph} bond, one for N_{pyr} and two for U- N_{amine} bond, which is in accordance with the presence of two monodentate binding of the phosphonate.

The other FT components were fitted with phosphors shell P at 3.69 and 3.69 Å and

multiple scattering with U-P-O_{yl} at 4.61 and 4.59 Å. The U-P distance of 3.69 Å is consistent with a monodentate phosphonate coordination in *meta*-autunite.[233]

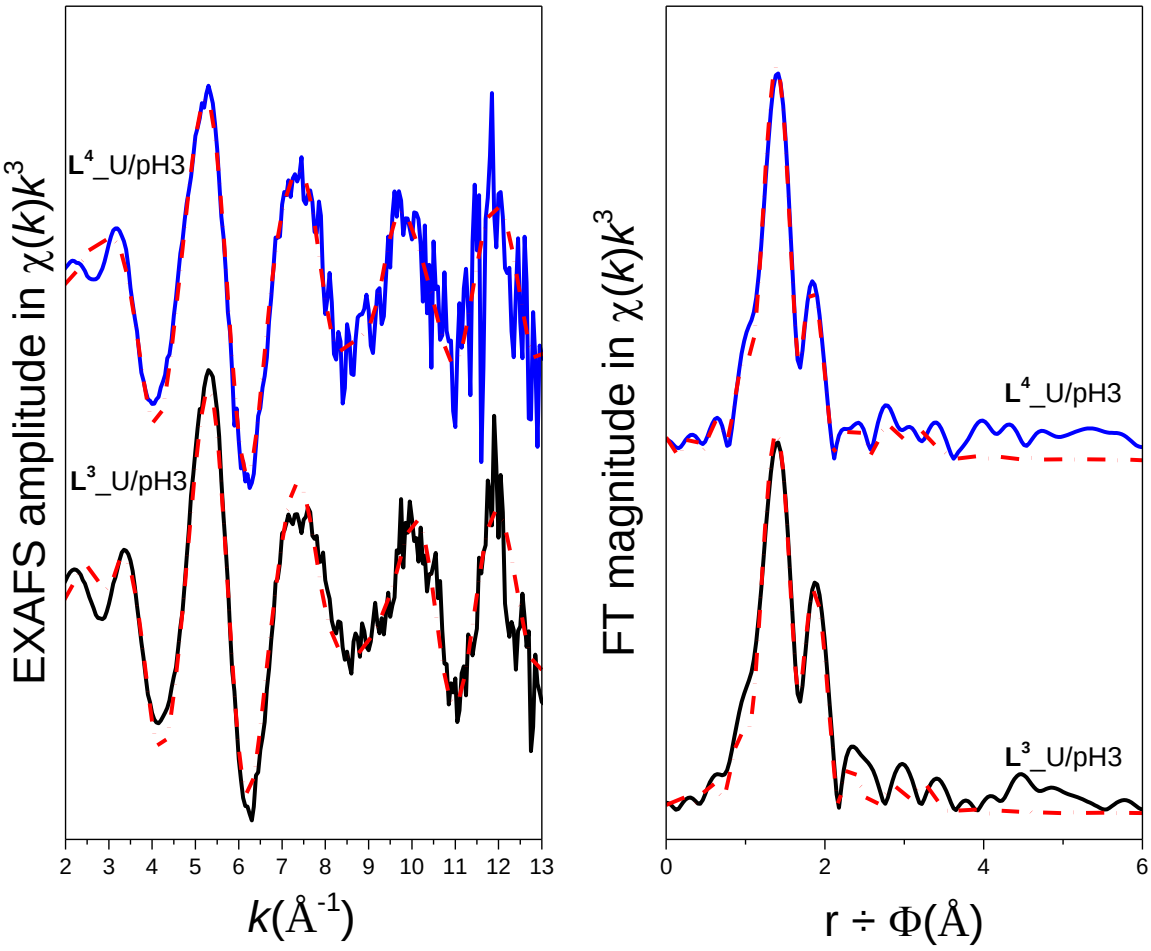

Figure 66 : U L_{III} edge k^3–weighted EXAFS spectra (left) and the corresponding Fourier transforms (right) of the L^3-U complex (lower traces) and L^4-U (upper traces) complex formed at pH 3. The experimental spectra are given in dash line and the fits are given in line.

EXAFS data collected for the uranyl-**L^3** complex and uranyl-**L^4** complex at pH 3 are consistent with a uranyl fivefold coordination at equatorial plane involving two monodentate phosphonate groups, one nitrogen atom from pyridine group and two nitrogen atoms from the amine parts. These experimental data are in line with and UV-vis absorption data, TRLFS data and FTIR data with model of uranyl-ligand without H_2O at pH 3, Figure 64, issuing from the DFT simulations. The shape of first shell of uranyl-**L^4** complex at pH 3 is slight larger than the case in **L^3**-uranyl complex. This might due to the structure difference of two ligands.

4.4.2 Uranyl-ligand study at pH 7.4

The most stable adopted model at pH 7.4 includes two axial oxygen atoms (O_{yl}), two equatorial oxygen atoms (O_p), three equatorial nitrogen atoms (N_{pyr} & $2N_{amine}$) with or with O_{OH}. The O_p atom represents the oxygen atom of the monodente phosphonate group; O_{OH} represents the oxygen atom of the hydroxide. N_{pyr} atom represents the nitrogen atom of pyridine group; N_{amine} represents the nitrogen atom from amine units. An additional layer representing the phosphors atoms associated with the above-mentioned phosphonate oxygen atoms has also been taken into account. The assignment is slightly different. O_{OH} represents the hydroxide present in the coordination sphere; the oxygen of the hydroxide was grouped together with the

oxygen of the phosphonate oxygen in the same layer because they are at roughly the same distance from the metal (resolution of EXAFS ~ 0.1 Å)).

The EXAFS data could be fit with both models with and without hydroxide well. But due to results of TRLFS study, the coordination for two pHs are not the same. Thus the model of uranyl-ligand with hydroxide was used. The paths of U-**L**^{4} complex is used in the fitting of U-**L**^{4} complex.

During the adjustment procedure, the triple diffusion paths relating to the two axial oxygens of the uranyl have been taken into account. The U-P single scattering pathway is also necessary to perform the fit of the experimental data. U-P-O_{ax} multiple scattering pathway is not used.

A Hanning adjustment window in k^3 (2; 12.9) was used and the adjustment of spectra was in R (1; 5). Adjustment parameters such as passive electron reduction factor (S_0^2) and ΔE_0 are given for each experiment. The adjustment factor R(r) and the reduced quality factor ($\chi^2_{i\ ln}$) are both provided as an indicator of the quality of the fit.

path	R_{DFT}(Å)	N_{deg}	sigma^2(× 10–3 Å²)	R_{FIT}(Å)
U-O_{yl}	1,78	2	2,78	1,81
U-O_p	2,28	2	6,97	2,37
U-O_{OH}	2,31	1	6,97	2,40
U-N_{pyr}	2,93	1	8,4	3,03
U-N_{amine}	3,24	1	9,3	3,39
U-P	3,56	1	2,81	3,81
U-O_{ax1}-U-U_{ax2}-U	3,57	2	5,55	3,62

Table 23 : Description of the paths used to fit the EXAFS data of the L^3-U-OH complex determined at pH 7.4. S_0^2 = 1.20; ΔE_0 = 7.20 eV. R = 0.01; $\chi^2_{i\ ln}$ = 5.22.

path	R_{DFT}(Å)	N_{deg}	sigma^2(× 10–3 Å²)	R_{FIT}(Å)
U-O_{yl}	1,79	2	4,02	1,82
U-O_p	2,28	2	8,2	2,28
U-O_{OH}	2,31	1	8,2	2,31
U-N_{pyr}	2,93	1	4,85	3,09
U-N_{amine}	3,24	2	10,46	3,20
U-P	3,57	1	9,14	3,59
U-O_{ax1}-U-U_{ax2}-U	3,57	2	8,03	3,63

Table 24 : Description of the paths used to fit the EXAFS data of the L^4-U-OH complex determined at pH 7.4. S_0^2 = 1.22; ΔE_0 = 3.62 eV. R = 0.01; $\chi^2_{i\ ln}$ = 27.3.

Taking into consideration the number of paths and the constraints geometric, the floating parameter number is 12 for the experiment pH 7.4. All the results of the adjustments are summarized in table 23 and table 24. The EXAFS k^3 spectra and their Fourier corresponding are shown in figure 67.

Both fitting results of uranyl-ligand complex are good. Actually this test was performed twice. There is a uranium redox reaction happened during the sample measurement for the first time for uranyl-**L**^{4} compelx at pH 7.4. The charge of uranium was decreased from 6+ to 4+. For this reason a fast scan was implementing by decrease the accuracy and changed the position of sample to have a better reproducibility.

Similar EXAFS spectra were obtained with the uranyl-**L**^{3} complex and uranyl-**L**^{4} complex at pH 7.4, which is a good indication that a unique uranyl binding site is probed under the experimental conditions used for EXAFS.

The Fourier transforms (FT) represents a pseudo-radial distribution function of the uranium near-neighbor environment. The peaks appear at lower R values relative to the true near-neighbor distances as a result of the EXAFS phase shift, which is different for each neighboring atom (φ =0.2 to 0.5 Å).

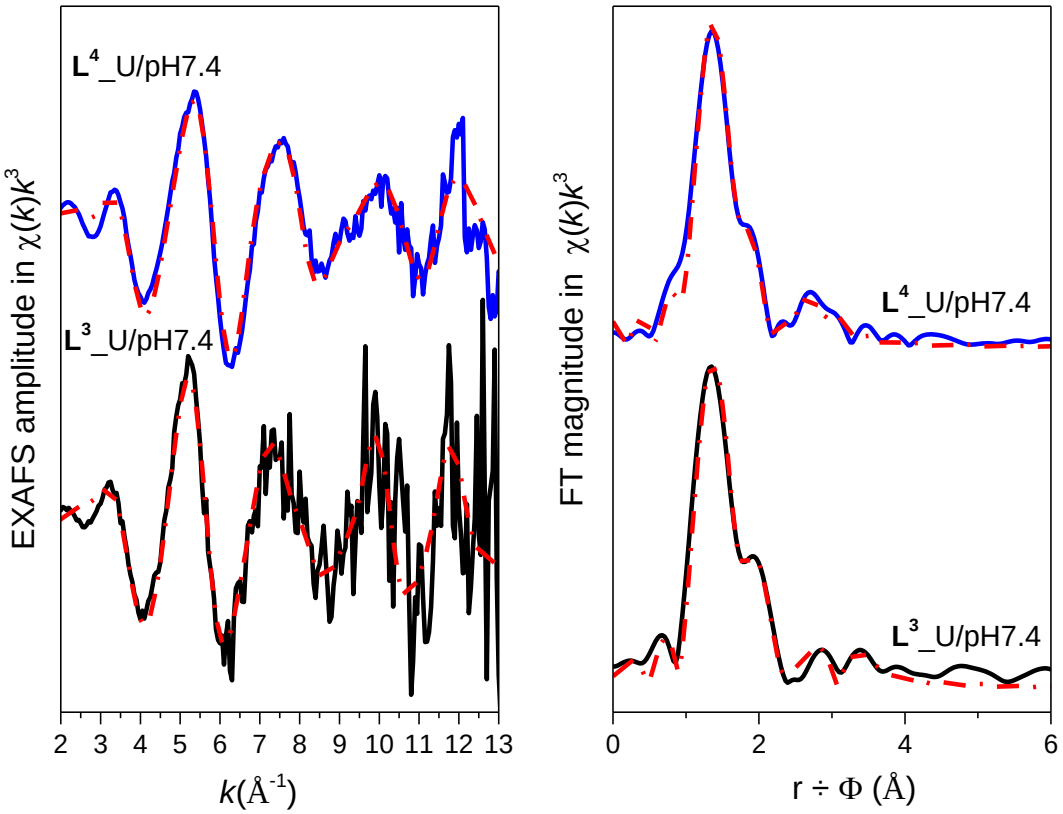

Figure 67 : U L_{III} edge k^3–weighted EXAFS spectra (left) and the corresponding Fourier transforms (right) of the L^3-U-OH complex (lower traces) and L^4-U-OH (upper traces) complex formed at pH 7.4. The experimental spectra are given in dash line and the fits are given in line.

For uranyl-**L^3** complex and uranyl-**L^4** complex at pH 7.4, fitting shows that U^{VI} has two O_{yl} atoms at a distance of 1.81 and 1.78 Å, two O_{ph} at 2.37 and 2.28 Å, one O_{OH} at 2.40 and 2.31, one N_{pyr} at 3.03 and 2.93 Å and two N_{amine} at 3.38 and 3.24 Å. The distance between U and O_{yl} is typical for a uranyl ion.[231] The U-O_{ph} bond length is within the range of previously reported values for the oxygen atom of phosphonate groups bound to uranyl in a monodentate fashion.[145,232] These five types of atoms at equatorial plane thus could correspond to the presence of monodentate phosphonate groups and interaction with the pyridine group as deduced from the FTIR data and UV-vis absorption data. The best fit was obtained with a six coordination number at equatorial plane of two for the U-O_{ph} bond, one for U-O_{OH} bond, one for U-N_{pyr} bond and two for U-N_{amine} bond, which is in accordance with the presence of two monodentate binding of the phosphonate.

The other FT components were fitted with phosphors shell P at 3.81and 3.59 Å. The U-P distance is consistent with a monodentate phosphonate coordination in *meta*-autunite.[233]

EXAFS data collected for the uranyl-**L^3** complex and uranyl-**L^4** complex at pH 7.4 are consistent with a uranyl six-fold coordination involving two oxygen atoms from monodentate phosphonate groups, one hydroxide, one nitrogen atom from pyridine group and two nitrogen atoms from the amine parts. These experimental data are in line with UV-vis absorption data, TRLFS data and FTIR data with model of uranyl-ligand with OH at pH 7.4, Figure 3.39&3.40,

issuing from the DFT simulations. Uranyl-**L^3** complex at pH 3 is slight larger than the case in uranyl-**L^4** complex. This might due to the structure difference of two ligands. The difference of U-O_{OH} bond for two uranyl-ligand complexes might result in the thermodynamic constants difference at neutral pH.

4.4.3 Comparison of uranyl-ligand study at two pHs

The EXAFS spectra and FT are not the same for two pHs, 3 and 7.4. This showed that the uranyl binding sites are not the same for two pHs, which is comparable with the TRLFS results.

For the four fitting the Debye–Waller factor σ^2 are relatively high for the path of U-N_{pyr}, U-N_{amine} and U-P. This is due to the relatively long distance compare to the oxygen atoms.

The uranyl ion is moving forward from the pyridine group from pH 3 to pH 7.4 due to the increasing of hydroxide concentration. The attraction of oxygen atom from hydroxide strongly altered the uranyl coordination, five-fold coordination at pH 3 to six-fold coordination at pH 7.4.

4.5 Conclusion

With the help of UV-vis absorption study, TRLFS study and FT-IR measurement, the possible environments of uranyl ion are proposed. Then these structures are calculated by DFT to find the stable structure. Finally the EXAFS experiment is done to determine the coordination of uranyl ion.

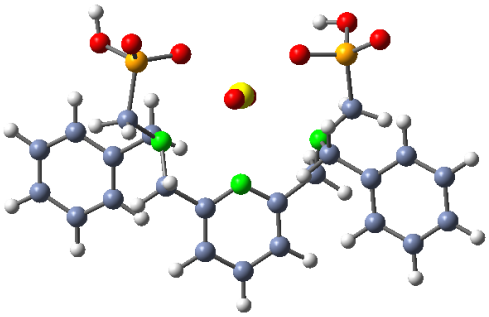

L^3/UO_2^{2+} with 1 OH pH=7.4

L^3/UO_2^{2+} pH=3

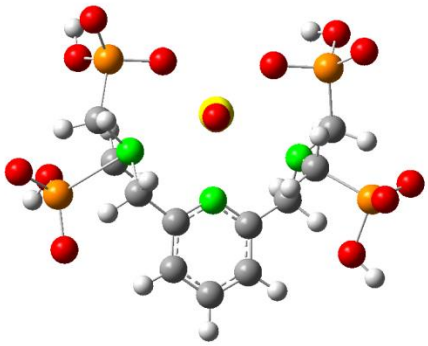

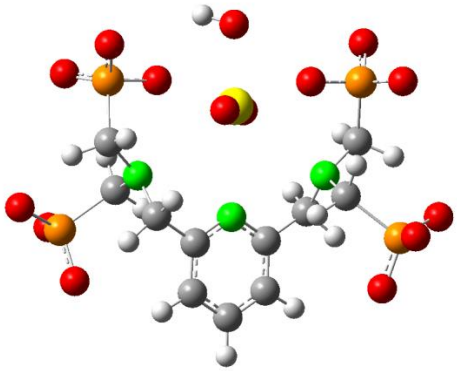

L^4/UO_2^{2+} pH=3

L^4/UO_2^{2+} with 1 OH pH=7.4

Figure 68 : Theoretical models optimized by DFT and electronic density of L^3 & L^4 interaction sites with uranyl at pH 3 and 7.4 (Oxygen: red, carbon: blue, nitrogen: light green, uranium: yellow).

For pH 3, the environments of uranyl ion are the same for both ligand, **L^3** and **L^4**. (Fig. 68) The coordination is consist by two oxygen atoms from monodentate phosphonate groups, one

nitrogen atom from pyridine group and two nitrogen atoms from the amine parts.

For pH 7.4, the environments of uranyl ion are the same for both ligand, **L**^{3} and **L**^{4}. (Fig. 68) The coordination is consist by two oxygen atoms from monodentate phosphonate groups, one hydroxide, one nitrogen atom from pyridine group and two nitrogen atoms from the amine parts.

Due to the presence of hydroxide in the coordination at pH 7.4, the uranyl ion is moving forward from the pyridine group. The stoichiometry of uranyl-ligand complexes at pH 7.4 are 1:1 within 0-1 eq uranyl.

5 Thermodynamics study by displacement titration

According to the uranyl-ligand complex fluorescence Study at pH 7.4, there is only one uranyl-ligand complex at 1:1 ratio. By using HYSS software, it is possible to estimate the stability constants of uranyl-**L**^{2} complex, uranyl-**L**^{3} complex and uranyl-**L**^{4} complex are higher than 13.3.

Due to the difficult of degradation and precipitation in 0.1M $NaClO_4$ solution of uranyl-**L**^{3} complex and uranyl-**L**^{4} complex at acidic pH, a displacement titration which developed by Dr. Taran group was done.[122,234] Sulfochlorophenol (SCP) in the figure below was use as a reference ligand, which complexes uranyl ion with a visible absorbance. The addition of a stronger ligand compare to SCP displaces the equilibrium towards the formation of UO_2L, decreases the absorbance value and changes the color of the medium. Measurements were made at 690 nm for pH = 5.5 and 7.4 or 640 nm for pH = 9.0. For our study, the titration was done at pH 7.4 (biological pH).

All experiments were carried out at room temperature in buffers with a fixed ionic strength of 0.1M prepared as follows: HEPES (for pH 7.4) (12.5 mmol) and n-Bu4N^{+}Cl^{-} (112.5 mmol) were dissolved in 1 L of Millipore quality water. [234]

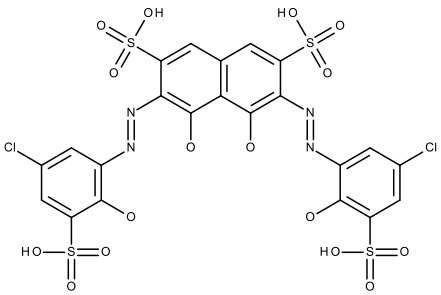

SCP

5.1 Fast screening

A fast screening was done to determine the affinity of the three ligands (Fig. 69). The protocol is followed the way which design by Dr. Taran group.[122] The detail on the procedure is written in the appendix. The test was done by measuring the displacements (%) of the uranyl-SCP complex with adding 2 eq of ligand. The affinity range was list in table 25.[122]

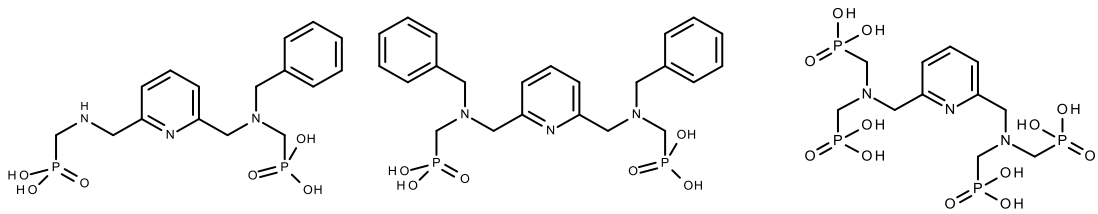

L² **L³** **L⁴**

Figure 69 : Structure of three ligands.

0-20%	15.3 > log K_{cond}
20-40%	16.2 > log K_{cond} > 15.3
40-60%	16.8 > log K_{cond} > 16.2
60-80%	17.7 > log K_{cond} > 16.8
80-100%	log K_{cond} > 17.7

Table 25 : Displacements (%) of the uranyl-SCP complex with logK_{cond} (estimates) at pH 7.4 were calculated by using the HYSS program supposing that the complex competitive uranyl-ligand is 1:1. For details on the procedure, see the appendix.

Supposing that the complex competitive uranyl-ligand is 1:1, the displacement of uranyl-SCP complex by **L²**, **L³** and **L⁴** are 86%, 17% and 2% (Fig. 70). Thus **L²** has the highest rate among the three ligands. For **L²**, the ligand complexation constants is between 16.8 and 17.7; for **L³** and **L⁴**, the constant is lower than 15.3.

Due to the low displacement of **L⁴**, the determination of the ligand complexation constants was done for **L²** and **L³**. Because uranyl ion has the same coordination for the three ligands at pH 7.4, the ligand complexation constants differences should relate with the molecular structure. Owing to the lack of one benzyl group, **L²** is an asymmetric structure ligand which might decrease the steric effect compare to **L³**. So the affinity of **L²** is higher. For **L⁴**, the two unbounded phosphonate group might weaken the ability to complex uranyl ion.

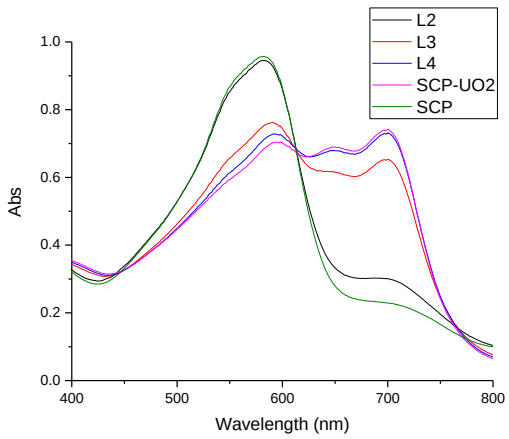

Figure 70 : Screening results of three ligands; [ligand] = 8E-5 M, [SCP] = [U] =4E-5 M, HEPES buffer=12.5 mmol, [$nBu_4N^+Cl^-$] =112.5 mmol at pH 7.4.

5.2 Determination of the ligand complexation constants

Ligand complexation constants towards uranyl ion were determined through a competitive displacement between the ligand and uranyl-SCP complex. The binding abilities for uranyl ion

with water-soluble two ligands were determined by UV spectrophotometry in aqueous media under neutral pH conditions (pH 7.4). This method is essentially based on the spectral behaviour and complexation properties of a chromophoric probe with respect to the uranyl cation.[235] The addition of a stronger ligand than SCP displaces the equilibrium towards the formation of UO2-ligand (eq 8), decreasing the absorbance value at 690 nm and changing the color of the medium. The detail on the procedure is written in the appendix.

$$SCP\text{-}UO_2 + L \rightarrow SCP + L\text{-}UO_2 \qquad \text{Equation 8}$$

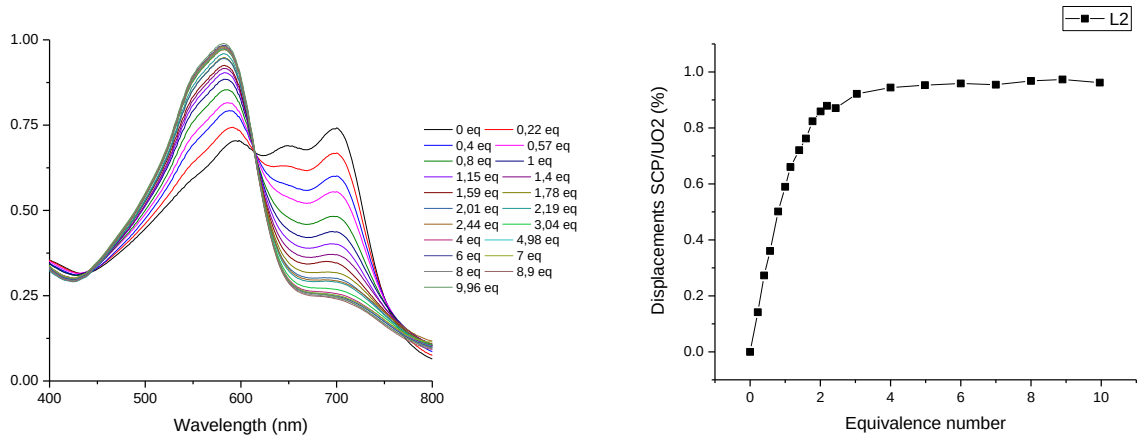

Figure 71 : Competition displacement titration of uranyl-SCP complex by L^2; [SCP] = [UO] =4e-5 M, [L^2] 0-8E-4 M, HEPES buffer=12.5 mmol, [$Bu_4N^+Cl^-$] =112.5 mmol.

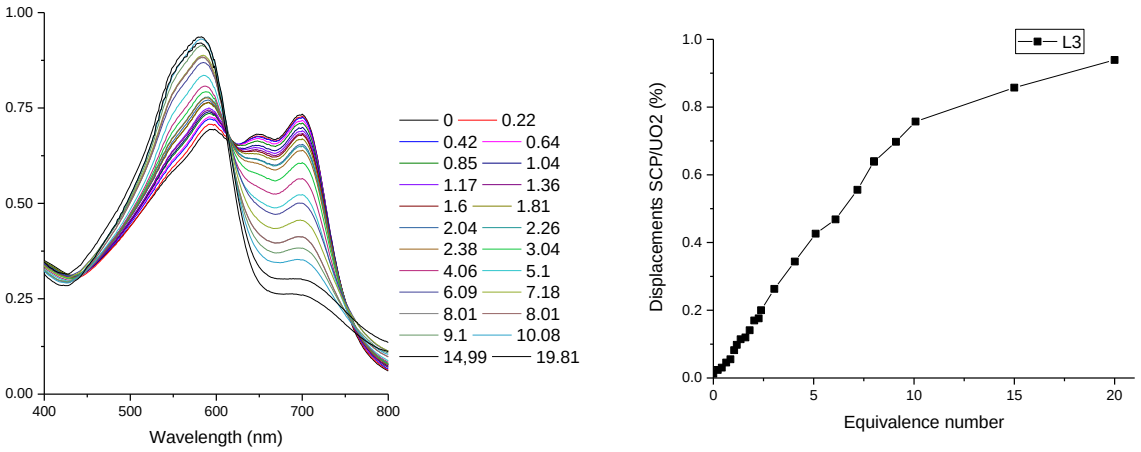

Figure 72 : Competition displacement titration of uranyl-SCP complex by L^3; [SCP] = [U] =4e-5 M, [L^3] 0-8E-4 M, HEPES buffer=12.5 mmol, [nBu_4N+Cl-] =112.5 mmol.

For **L^2**, the titration was done in the range of 0 to 10 eq due to the relatively high affinity (Fig. 71). While for **L^3**, the titration was done in the range of 0 to 20 eq (Fig. 72). The ligand complexation constant (K_{concd}) was evaluated in comparison to values of complexes K_{concd}

SCP/UO2. It appears that polyaminophosphonates ligands exhibits sufficient affinities with respect to uranium decorporation at physiological blood pH (pH 7.4). Ligand complexation constants (K_{concd}) are 17.08 for **L²** and 15.2 for **L³** at pH7.4.

A comparison was done with 5-LICAMS and 3,4,3-LI(1,2-HOPO), which are well-known ligands, which displays in vivo uranyl-removal capabilities[235,236]. The complexation constants are 17 for 5-LICAMS[237] and 16.87 for 3,4,3-LI(1,2-HOPO)[122]. Thus the polyaminophosphonates ligands, synthetized in this study, have similar complexation constants towards the two ligands which have been well studied.

6 Selectivity study with cation

Because most study on actinide biokinetics focuses on blood, three cations, Ca^{2+}, Mg^{2+} and Fe^{3+},[40] were chosen for the selectivity study. Owing to the nonfluorescence uranyl-ligand complex at neutral pH, the selectivity of the ligand was then investigated using TRLIF and UV-vis absorption experiments which consist in adding a competing metal cation (M+) in the presence of the uranyl-**L³** complex. An increase of the fluorescence signal will be observed if those metals form a new complex with **L³**. Competing metal cations, Ca^{2+}, Mg^{2+} and Fe^{3+}, have been added to the solution of the 1:1 uranyl-**L³** complex at pH 7.4. There is precipitation formed for samples with Fe^{3+}. Thus the selectivity study was done with Ca^{2+} and Mg^{2+}. The sample was prepared by fresh deionized water to minimize the possible formation of $CaUO_2(CO3)_3^{2-}$ and $Ca_2UO_2(CO3)_3^{2-}$.

For this study, the 1:1 uranyl-**L³** complex concentration is set at 5e-5 M. The concentrations of Ca^{2+} and Mg^{2+} in blood are 1.4E-3 M and 5.6E-4 M which are about 280 eq and 112 eq of uranyl-**L³** complex for each metal.

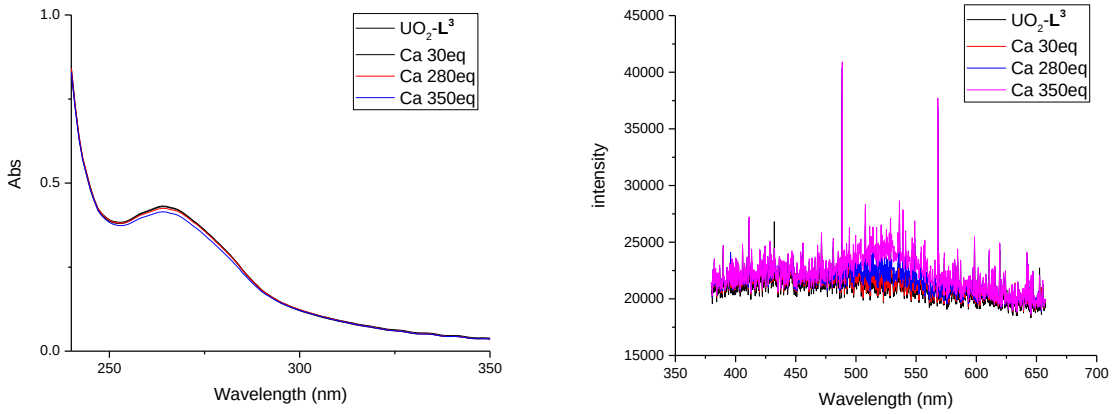

Figure 73 : Selectivity study of 1:1 uranyl-L³ complex by Ca^{2+}, absorption spectrum (left); fluorescence spectrum (right); [L³] = [U] =5E-5 M; [Ca^{2+}] =0-350 eq; [$NaClO_4$]=0.1 M.

The absorption peak (Fig. 73 left) of sample with Ca^{2+} decreased a little bit with the Ca^{2+} concentration increase. So there is a small amount of uranyl ion which is replaced by Ca^{2+}. The fluorescence intensity (Fig. 73 right) of uranyl ion also increased slightly. At 280 eq of Ca^{2+}, which is the concentration in blood, the intensity seems at zero. So the uranyl-**L³** complex presents a good stability for calcium.

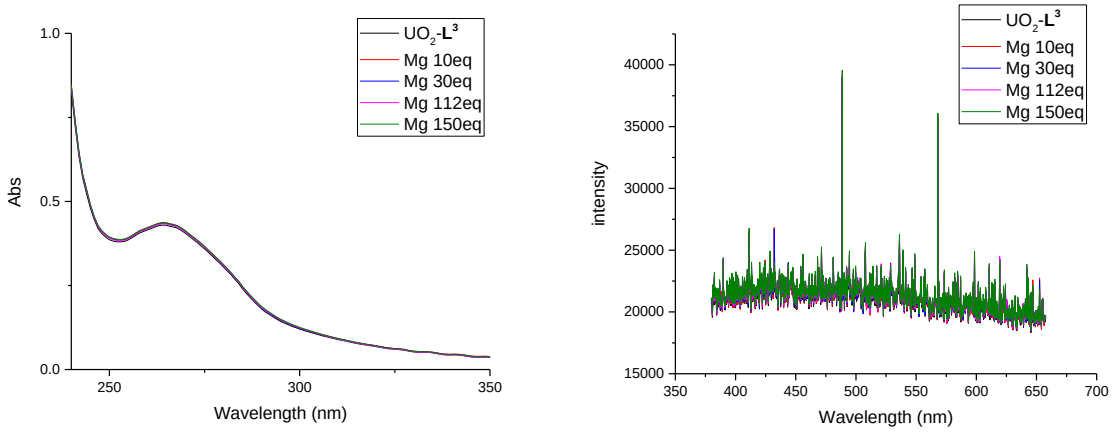

Figure 74 : Selectivity study of 1:1 uranyl-L^3 complex by Mg^{2+}, absorption spectrum (left); fluorescence spectrum (right); [L^3] = [U] =5E-5 M; [Mg^{2+}] =0-150 eq; [$NaClO_4$]=0.1 M.

The absorption (Fig. 74 left) of sample with Mg^{2+} didn't change with the Mg^{2+} concentration increase. So the uranyl ion is still in the coordination of **L^3**. The fluorescence intensity (Fig. 74 right) of uranyl ion also didn't increase. So the uranyl-**L^3** complex presents a good stability for magnesium.

7 Chelation affinity of ligand towards Calmodulin - uranyl complex

Calmodulin (CaM) is a metal protein which plays an important role in extracellular stimulus. The interaction between uranyl ion and protein has been well studied by Dr. Florian Brulfert in our lab.[149,232,238,239] .Thus the chelation affinity of ligand was done with this protein.

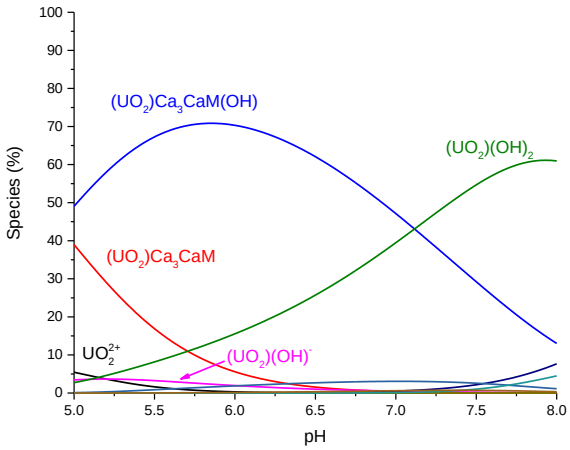

Figure 75 : Species diagram of Ca-UO_2-CaM complex from pH 5 to 8; [CaM] = [U] =5E-5 M; [Ca^{2+}] =2E-4 M; [$NaClO_4$]=0.1 M.

According to the structure of CaM, 4 times of calcium ion was used to occupy the four sites of CaM.[137–139] Due to the affinity difference of 4 sites of CaM, 1 times of uranyl ion was added to compete with calcium ion for one site. Considering hydrolysis of uranyl and stability constants of the uranyl-calmodulin complexes (Fig 75), pH 5.5 was chosen for the chelation

study due to the dominant species, $Ca_3UO_2CaM(OH)$, Ca_3UO_2CaM and $UO_2(OH)_2$. MES buffer was used to maintain the pH during the study.

Due to the multiple species of uranyl, it is better to use the nonfluorescence affinity of uranyl-ligand complex in the neutral range to overcome this difficult. For the three ligands, **L³** and **L⁴** didn't shown fluorescence after complexes with uranyl at pH 5.5 which **L²** has. Thus the **L³** was used in this study owing to the relatively high affinity and nonfluorescence property.

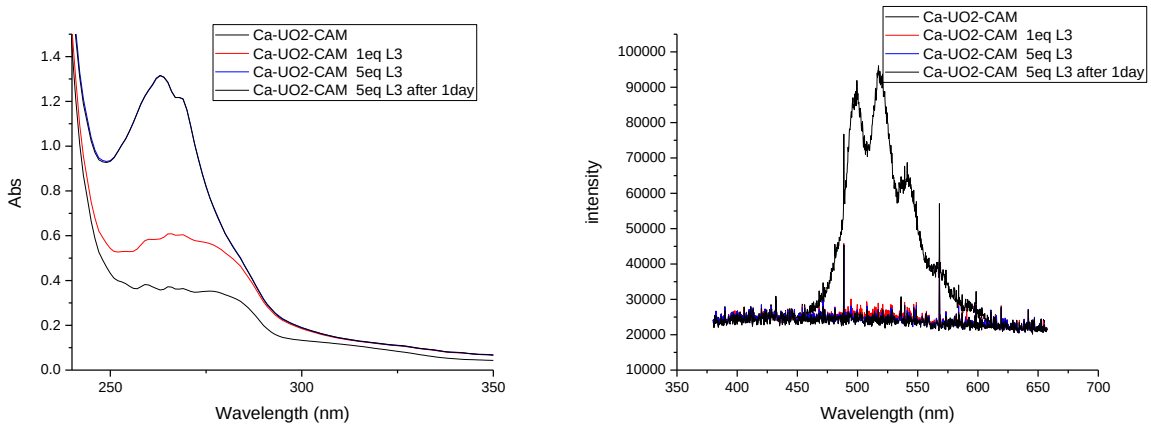

Figure 76 : Chelation study of L³ towards Ca-UO₂-CaM complex, absorption spectrum (left); fluorescence spectrum (right); [CaM] = [UO_2^{2+}] =2.5E-5 M; [Ca^{2+}] =2E-4 M; [L³]=0, 1 and 5eq ; [$NaClO_4$]=0.1 M ; [MES]= 5 mmol ; pH 5.5.

For the fluorescence spectra, an 8 nm red shift of the uranyl fluorescence spectrum was found for the Ca-UO_2-CaM complex (Fig. 76 right). The lifetime study was done with the help of lifetime reference data.[232] Three lifetimes with 0.4 µs for Ca_3UO_2CaM, 4 µs for $Ca_3UO_2CaM(OH)$ and 24µs for UO_2OH_2 were found. It confirmed the species simulation results. After adding 1eq **L³**, the sample was stirred for 10 mins, then the TRLFS measurement was done. There is no more fluorescence from uranyl which means the uranyl is almost complex by **L³**. Another 4eq was added to check the stability after 1day. Both the absorption spectra and fluorescence spectra didn't change after 1day. So the stability is pretty good. Note that then the ligand complex (for the similar bisphosphonates ligand) with Tc, the obtained complex was rapidly excreted through the kidneys and bladder after injection to mice. The fast kinetic, good stability and possible rapidly excrete of uranyl- **L³** complex provide the possible application in the chelation therapy.

Due to the absorption of CaM in the UV range, the absorption of the sample was hard to directly analyze. Because the CaM spectrum is unknown, two deconvolutions were done for Ca-UO_2-CaM complex with 1 eq and 5 eq **L³** to determine the CaM spectrum, which could further investigate the formation of uranyl ion species (Fig. 77). The deconvolution of Ca-UO_2-CaM complex with 1eq **L³** was done with 1 eq of CaM and 1 eq of uranyl-**L³** (Fig. 77 left).. The deconvolution of Ca-UO_2-CaM complex with 5 eq **L³** was done with 1 eq of CaM, 1 eq of uranyl- **L³** and 4 eq of **L³** (Fig. 77 right).

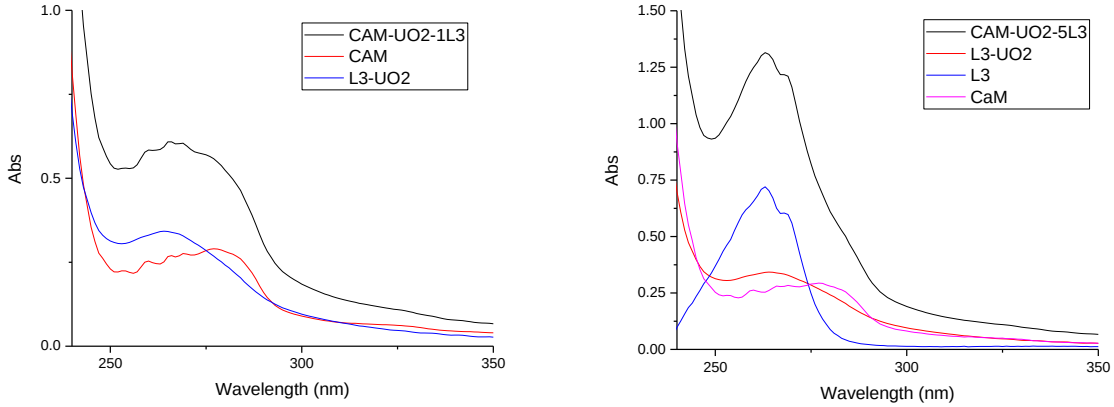

Figure 77 : Devolution study of L^3 towards Ca-UO_2-CaM complex, 1eq L^3 (left); 5eq L^3 (right). [CaM] = [U] =2.5E-5 M; [Ca^{2+}] =2E-4 M; [L^3]=0, 1 and 5eq ; [$NaClO_4$]=0.1 M ; [MES]= 5 mmol ; pH 5.5.

There is a difference on the absorption in UV range between the record UO_2-CaM spectrum with the two CaM spectra from deconvolution. The black line of CaM1 is from the deconvolution of Ca-UO_2-CaM complex with 1eq $\mathbf{L^3}$ which red line of CaM5 is for Ca-UO_2-CaM complex with 5eq $\mathbf{L^3}$ (Fig. 78). The similar spectra of CaM confirmed the CaM didn't complex with uranyl ion in these two conditions. Thus the uranyl was complexed with $\mathbf{L^3}$. This result is coherent with the fluorescence measurement.

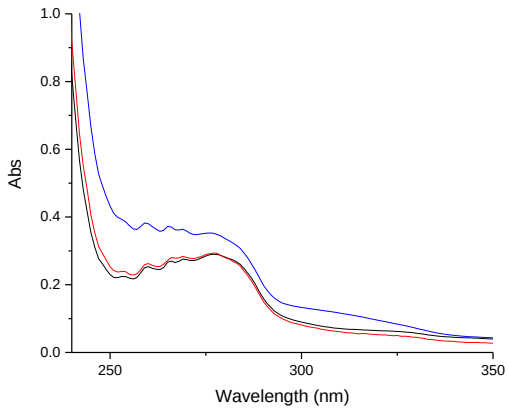

Figure 78 : Comparison of CaM spectra from two devolutions. CaM1 in black; CaM5 in red; UO2-CaM in blue.

8 Conclusion

This chapter presented the work on the structural and thermodynamic study of uranyl-ligand complex. From the structural study, it demonstrates the coordination of uranyl ion at pH 3 and 7.4 which provide by the ligand is as expected with the design. From thermodynamic study, the significant affinity of three ligands, $\mathbf{L^2}$, $\mathbf{L^3}$ and $\mathbf{L^4}$, for uranyl ion is due to the phosphonate groups and well molecular design. The uranyl- $\mathbf{L^3}$ complex shows a good stability in the presence of excess of calcium and magnesium. Especially by adding just equal mole of $\mathbf{L^3}$, the uranyl ion could be removing from calmodulin and forming complex with $\mathbf{L^3}$. Thus for these ligands the potential application as uranyl chelation agents is promising.

Combine UV-vis absorption study with TRLFS measurements allowed the preliminary

characterization of the coordination sphere of the metals in the complexation site of the protein and provided information for the experiment condition of the other study. By using FT-IR, the groups which plays a role in the coordination could be detect. Finally the DFT calculations followed with EXAFS measurements provide the accurate characterization of the coordination sphere of uranyl ion in the complexation site of the ligand. All these studies were done at two pHs, pH 3 and 7.4. The experimental / theoretical approaches proved to be very interesting for comparing the coordination properties of uranyl ion in solution at different pH on the uranyl ion coordination sphere and the stability of the uranyl-ligand complexes.

The complexation constants of uranyl-ligand complex are measured by competition displacement titration with SCP. The stability of uranyl-ligand complex with competition cation is strong enough for biochemistry condition. The chelation affinity test with protein provides a possible interaction path in the human body.

The complexation of uranyl ion with ligand is now proven and the uranyl ion coordination sphere is known, the next chapter will describe the complexation of europium, the analogue of curium, with ligand. The different structure of europium (spherical for europium and linear structure for uranyl ion) requires a different coordination with the ligand.

Chapter 4: Structural study of europium as analogue of minor actinides with polyaminophosphonates ligands

1 Thermodynamics study of europium-L^3 complex

The thermodynamic study with europium $\mathbf{L^3}$ complex was done with potentiometry first. But when the pH of europium $\mathbf{L^3}$ complex (1mM) increased to around 3.2, a precipitation occurred. Thus this measurement can't be done.

Then another test was done with UV-Vis spectroscopy to determine the formation constants. The absorption of europium $\mathbf{L^3}$ complex doesn't change, therefore it is not possible to use HypSpec software to deduce the formation constants.

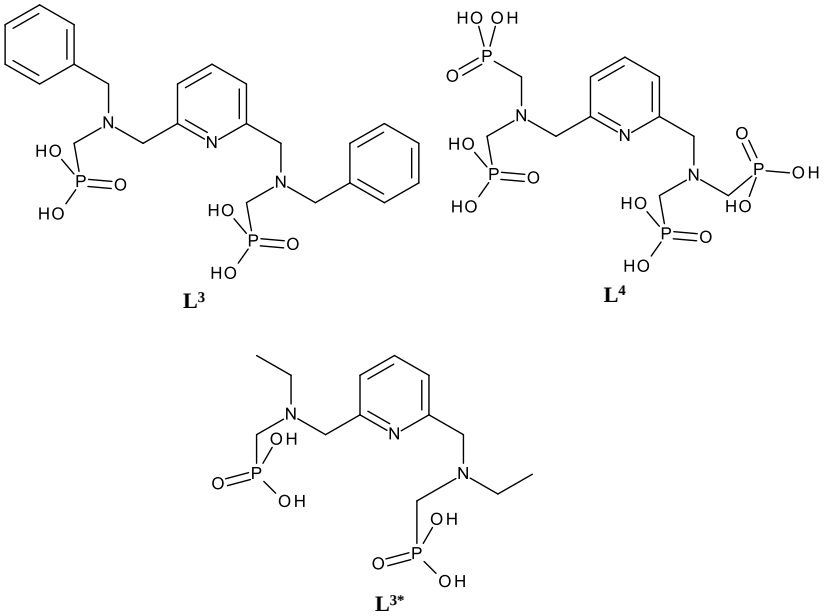

Figure 79 : Chemical structures of bis-phosphonated ligand L^3 & L^{3*} and tetra-phosphonated ligand L^4

	La	Nd	Eu	Gd	Tb	Er	Lu
$\log K_{ML^4}{}^{[b]}$	25.5(4)	27.1(3)	25.7(3)	–	29.7(6)	29.7(1)	29.3(4)
$\log K_{ML^4H}{}^{[b]}$	9.4(4)	8.8(3)	9.4(3)	–	7.6(7)	7.8(1)	7.4(6)
$\log K_{ML^4H_2}{}^{[b]}$	7.3(6)	6.6(4)	7.5(4)	–	[c]	[c]	[c]
$\log K_{ML^{2*}}$	10.14(4)	10.66(5)	–	11.22(5)	–	11.15(3)	[c]
$\log K_{ML^{2*}H}$	9.19(5)	9.35(6)	–	9.16(6)	–	9.25(4)	[c]
$\log K_{ML^{2*}H_2}$	7.42(5)	7.40(6)	–	7.21(6)	–	7.90(4)	[c]
$\mathbf{pLn}_{L^4}$	20.6	21.3	20.9	–	22.6	22.7	21.9
$\mathbf{pLn}_{L^{2*}}$	7.3	8.0	–	8.2	–	8.3	[c]

Table 26 : Thermodynamic stability constants and protonation constants for the complexes formed with ligands L^2 and L^4 and various Ln^{III} cations along the series and corresponding values of pLn. [a] pLn values are defined by pLn=-log[Ln^{III}]$_{free}$ at pH 7.0 for [Ln^{III}]=1 µm and [L]=10 µm;[240] [2] According to reference [13]. [c] Precipitationof the complexes precludes accurate determination. The hydrolysis con- stants of the free Ln^{3+} cations have been taken into account in the statistical processing (logK$_{LaOH}$=-8.83; logK$_{NdOH}$=-8.20; logK$_{EuOH}$=-7.78; logK$_{GdOH}$=-7.85; logK$_{TbOH}$=-7.66; logK$_{ErOH}$ =-7.54; log K$_{LuOH}$=-7.29).

The formation constants of similar bis-phosphonated ligand $\mathbf{L^{3*}}$ (Fig. 79) and tetra-

phosphonated ligand **L⁴** (Fig. 79) which were determined by potentiometry were listed in the table 26.[13,130] With the increasing number of terminal phosphonates groups in the ligand, the binding constants increased. The loss of two phosphonate functions leading to **L³*** resulted in the decrease of stability. Thus the loss of phosphonate groups will lead to a weak chelator ((pLn ~8).[241]

For this study, a similar trend of formation constants of **L³** with Ln^{III} could be expected due to the structure similarity of two bis-phosphonated ligand. Therefore, **L³** molecule show a weak binding affinity with Ln^{III} comparing to the **L⁴** ligand.

2 Europium/ligands interactions studied by Time-resolved laser fluorescence spectroscopy (TRLFS) and UV-visible spectroscopy

The detail of time-resolved laser fluorescence spectroscopy (TRLFS) and UV-visible spectroscopy has been described in chapter 3.

2.1 Experimental conditions selection

As for bis and tetra-phosphonated ligands, the formation of a one to one metal to ligand complex was confirmed in the other study.[130] The species diagram of europium (Fig. 80 right) is much simpler than the one of uranium. Europium hydroxide starts to form at pH 5.7.

The formation constants of europium **L⁴** complex were reported in the work of Dr. Sabah Abada by potentiometric measurements.[13] The coordination of Eu is composed by 4 oxygen atoms from phosphonate group, 2 nitrogen atoms from amine part, 1 nitrogen atom from pyridine group and 1 oxygen atom from water molecular. Therefore, the europium **L⁴** complex starts to form at really low pH (about pH 2) and H_2Eu**L⁴** species is the dominating species at pH 3((Fig. 80 left). pH 7.4 is the biological pH. Thus pH 3 and 7.4 were chosen for this study. Moreover, during the measurement, the UV-Vis absorption spectra of europium **L⁴** complex show no difference with the ligand alone at pH 3, thus pH 5 was chosen to study same dominating species, H_2Eu**L⁴**.

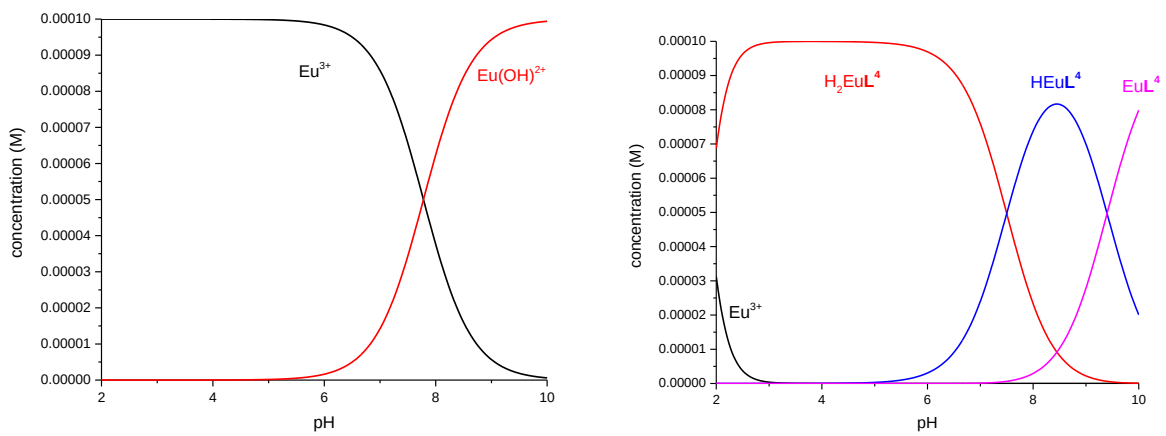

Figure 80 : Species diagram of europium ion, [Eu] = 5E-5 M in 0.1M $NaClO_4$ (left); [Eu] = [L⁴] = 1e-4 M in 0.1M $NaClO_4$ (right).

Due to the lack of formation constants of europium-**L³** complex, same pH study like europium-**L⁴** complex was done.

2.2 Study of europium-ligand complexes

Because the interaction of europium-ligand complexes is quite clear, only the comparison of europium-ligand complex with ligand alone was done. The change over the UV absorption is mainly due to the aromatic part and amine branches. The fluorescence change is mainly due to the concentration and coordination of europium. Due to the problem with TRLFS apparatus in our lab, the fluorescence measurement was not performed, only the time resolved study was done with help of Prof. Niko HILDEBRANDT of group NanoBioPhotonique at C2N lab.

a. Study of europium- $\mathbf{L^4}$ complex at pH 3 in 0.1M $NaClO_4$

For the study of europium-$\mathbf{L^4}$ complex at pH 3, the major species is the $H_2Eu\mathbf{L^4}$ species. The major species of ligand alone in the solution at this condition is monophosphonate, thus the four phosphonate groups and pyridine group could provide 4 oxygen atoms and 1 nitrogen atom for the Eu^{3+} coordination. For the amine part, the proton is still attached to the nitrogen at this pH, so there is a competition between europium ion with hydrogen. For europium alone in the solution, free europium ion alone is the dominate species.

The shapes of absorption spectra of $\mathbf{L^4}$ and europium-$\mathbf{L^4}$ complex were different (Fig. 81). But there is no shift on the absorption band. Thus, the Eu^{3+} may be only complexed by the phosphanate groups of $\mathbf{L^4}$. The lifetime of complex is 0.33 ms which means there are about 2.7 water molecules in the europium coordination.[242] It confirms the interaction of Eu^{3+} with ligand only exists in the phosphonate groups.

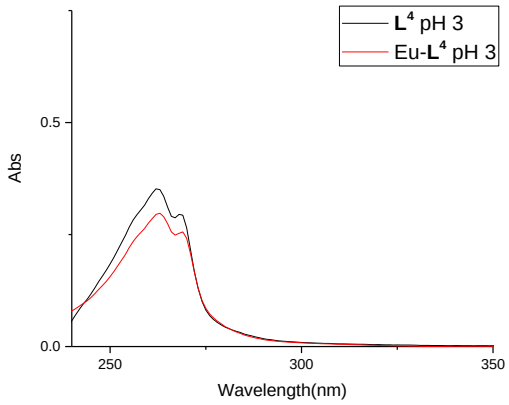

Figure 81 : Study of europium-L^4 complex, absorption measure; [Eu] = [L^4] = 1E-4 M , pH 3, 0.1M $NaClO_4$.

b. Study of europium- $\mathbf{L^3}$ complex at pH 3 in 0.1M $NaClO_4$

For the study of europium-$\mathbf{L^3}$ complex at pH 3, the major species of ligand alone in the solution at this condition is monophosphonate, thus the two phosphonate groups and pyridine group could provide 2 oxygen atoms and 1 nitrogen atom for the Eu^{3+} coordination. For the amine part, since the proton is still attached to the nitrogen at this pH, there is a competition between the europium ion with hydrogen atom. For europium alone in the solution, free europium ion alone is the dominate species.

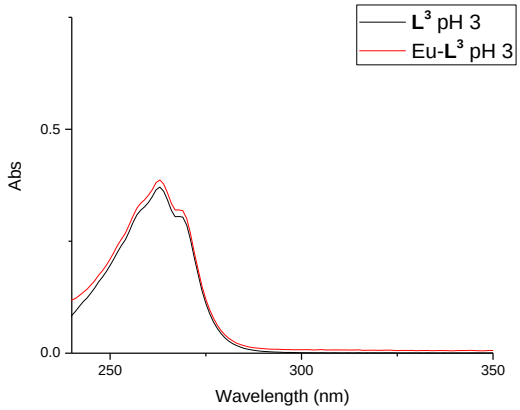

Figure 82 : Study of europium-L^3 complex, absorption measure; [Eu] = [L^3] = 1E-4 M , pH 3, 0.1M $NaClO_4$.

The shapes of absorption spectra of $\mathbf{L^3}$ and europium-$\mathbf{L^3}$ complex were different (Fig. 82). But there is no shift on the absorption band. Therefore, the Eu^{3+} may only complex with the phosphanate groups of $\mathbf{L^3}$. The lifetime of complex is 0.19 ms which means there are about 5.2 water molecules in the europium coordination. It confirms the interaction of Eu^{3+} with ligand only exists in the phosphonate groups.

c. Study of europium-$\mathbf{L^4}$ complex at pH 5 in 0.1M $NaClO_4$

For the study of europium-$\mathbf{L^4}$ complex at pH 5, the major species of complex is $H_2Eu\mathbf{L^4}$. The major species of ligand alone in the solution at this condition are monophosphonate and phosphonate group, thus the four phosphonate groups and pyridine group could provide 4 oxygen atoms and 1 nitrogen atom for the Eu^{3+} coordination. For the amine part, as the proton is still attached to the nitrogen at this pH, there is a competition between the europium ion with hydrogen atom. For europium alone in the solution, europium ion alone is the dominate species.

The shapes and absorption band of absorption spectra of $\mathbf{L^4}$ and europium-$\mathbf{L^4}$ complex were different (Fig. 83). Thus, the Eu^{3+} locates in the pocket part of $\mathbf{L^4}$. The lifetime of complex is 0.37 ms which means there are about 2.3 water molecules in the europium coordination.[242]

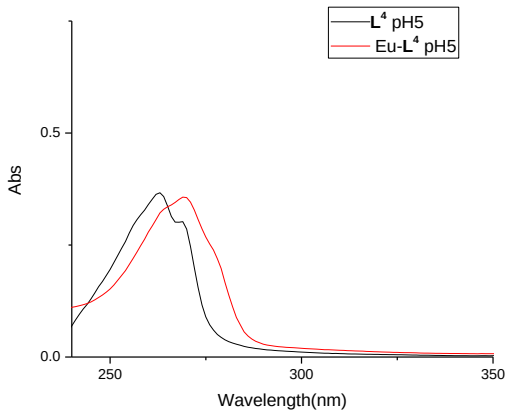

Figure 83 : Study of europium-L^4 complex, absorption measure; [Eu] = [L^4] = 1E-4 M, pH 5, 0.1M $NaClO_4$.

d. Study of europium- $\mathbf{L^3}$ complex at pH 5 in 0.1M $NaClO_4$

Due to the precipitation of 10E-4M europium-$\mathbf{L^3}$ complex at pH 7.4 in 0.1M $NaClO_4$, the test was done in 0.1M NaCl. The time resolve measurement was done with the solubilized part

of europium-**L**^{3} complex at pH 7.4 in 0.1M $NaClO_4$.

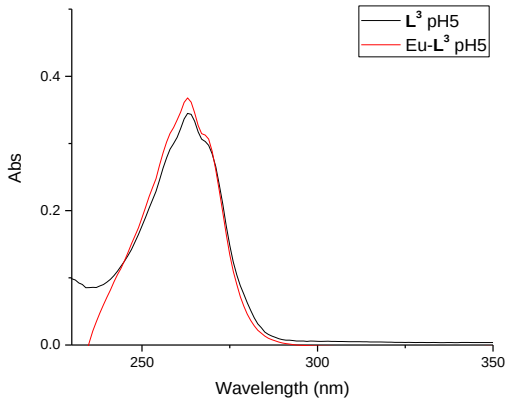

Figure 84 : Study of europium-L^{3} complex, absorption measure; [Eu] = [L^{3}] = 1E-4 M, pH 5, 0.1M $NaClO_4$.

For the study of europium-**L**^{3} complex at pH 5, the major species of ligand alone in the solution at this condition are monophosphonate and phosphonate group, thus the two phosphonate groups and pyridine group could provide 2 oxygen atoms and 1 nitrogen atom for the Eu^{3+} coordination. For the amine part, since the proton is still attached to the nitrogen at this pH, there is a competition between the europium ion with hydrogen atom. For europium alone in the solution, europium ion alone is the dominate species.

The shapes of absorption spectra of **L**^{3} and europium-**L**^{3} complex have slightly differences (Fig. 84). But there is no shift on the absorption band. Thus, the Eu^{3+} may be only complexed with the phosphanate groups of **L**^{3}. The lifetime of complex is 0.29 ms which means there are about 3.1 water molecules in the europium coordination. It confirms the europium ion is located in the pocket of ligand.

e. Study of europium-**L**^{4} complex at pH 7.4 in 0.1M $NaClO_4$

For the study of europium-**L**^{4} complex at pH 5, the major species of complex are H_2Eu**L**^{4} and HEu**L**^{4}.The major species of ligand alone in the solution at this condition is the phosphonate groups, thus the four phosphonate groups and pyridine group could provide 4 oxygen atoms and 1 nitrogen atom for the Eu^{3+} coordination. For the amine part, as the proton is still attached to the nitrogen atom at this pH, there is a competition between the Eu^{3+} ion with hydrogen. For europium alone in the solution, europium ion alone and europium hydroxide are present.

The shapes and absorption band of absorption spectra of **L**^{4} and europium-**L**^{4} complex were different (Fig. 85). Therefore the Eu^{3+} is located in the pocket part of **L**^{3}. Moreover, the spectra of europium-**L**^{4} at pH 5 and 7.4 are different. The lifetime of complex is 0.39 ms which means there are about 2.1 water molecules in the europium coordination. It confirms the strong stability constant of Eu**L**^{4} species due to encapsulating of Eu^{3+} ion by the **L**^{4} (table 26).

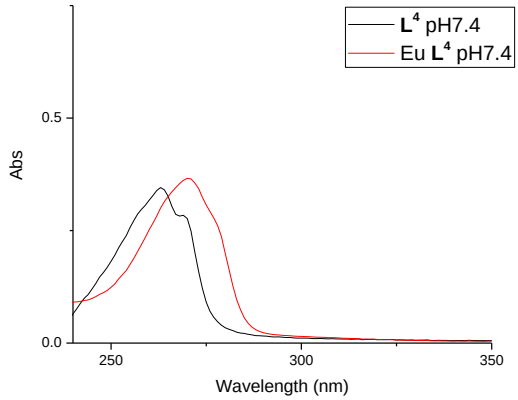

Figure 85 : Study of europium-L^4 complex, absorption measure; [Eu] = [L^4] = 1E-4 M, pH 7.4, 0.1M $NaClO_4$.

f. Study of europium-**L^3** complex at pH 7.4 in 0.1M $NaClO_4$

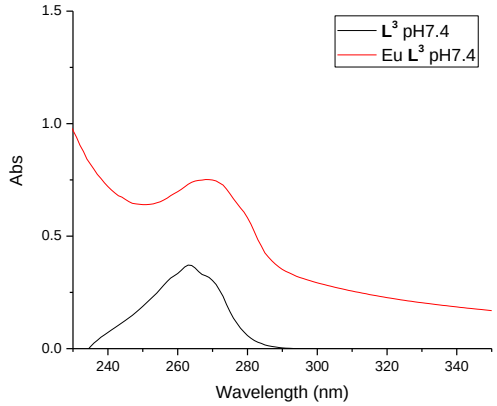

Figure 86 : Study of europium-L^3 complex, absorption measure; [Eu] = [L^3] = 1E-4 M , pH 7.4, 0.1M $NaClO_4$.

Due to the precipitation of 10E-4M europium-**L^3** complex at pH 7.4 in 0.1M $NaClO_4$, the test was done in 0.1M NaCl. The time resolved measurement was done with the solubilized part of europium-**L^3** complex at pH 7.4 in 0.1M $NaClO_4$.

For the study of europium–**L^3** complex at pH 7.4, the major species of ligand alone in the solution at this condition is the phosphonate group, thus the four phosphonate groups and pyridine group could provide 2 oxygen atoms and 1 nitrogen atom for the Eu^{3+} coordination. For the amine part, as the proton is still attached to the nitrogen atom at this pH, there is a competition between the europium with hydrogen. For europium alone in the solution, europium ion alone and europium hydroxide are present.

The shapes and absorption band of absorption spectra of **L^3** and europium-**L^3** complex changed significantly (Fig. 86). Thus the Eu^{3+} is located in the pocket part of **L^3**. Moreover, the spectra of europium-**L^4** at pH 5 and 7.4 are different. The lifetime of complex is 0.289 ms which means there are about 3.1 water molecules in the europium coordination. It confirms the relatively low stability constant of Eu**L^3** species due to the presence of 3 water moleculers in the coordination of Eu^{3+} ion .

2.3 Conclusion

For the Eu-ligand complex, based on the thermodynamic constants which are reported in

the publication, UV-vis absorption and TRLFS study were done. Because of the small changing on the absorption spectra of europium-**L³** complex with about 6 water molecules in the coordination and of europium-**L⁴** complex with about 3 water molecules in the coordination at pH 3, it seems the Eu^{3+} ion is only complex with the phosphonate groups of the ligand. But at higher pH, pH 5 and 7.4, the Eu^{3+} ion is located in the pocket part of two ligands. Thus the environments of Eu^{3+} ion are not the same for the same species $H_2Eu\mathbf{L^4}$ at pH 3 and 5.

At lower pH, the hydrogen concentration is relatively high compared to the europium concentration. The Eu^{3+} ion cannot move to the pocket part due the proton which forms hydrogen bond. Therefore, the interaction of Eu^{3+} ion with the ligand occurs only through the phosphonate groups. This could explain why there is only a small change on the absorption of the ligand but not the shape. Then at higher pH, the hydrogen concentration is lower, the Eu^{3+} ion is encapsulated by the ligand, then the hydrogen band on the nitrogen atoms of amine parts is no longer exist which affect the shape of ligand absorption, then both the shape and absorption changed.

3 IR characterization of two ligands with europium in aqueous solution

The IR spectra of ligands have been fully described in chapter 3.

3.1 IR spectra of europium -ligand complexation

Only two samples, europium-**L³** complex at pH 3 and europium-**L⁴** complex at pH 7.4 were investigated. Due to the low solubility of europium-**L³** complex, it is not possible to prepare a sample with a pH value over 3.2 at 2mM for the IR measurement. Thus pH 3 was chosen for IR study. Europium-**L⁴** complex at pH 7.4 was chosen to understand the interaction at biological pH. Each sample in this study was prepared with the same molar equivalence of europium and ligand based on the UV-Vis absorption spectroscopy and fluorescence studies. All the spectra were normalized with carbon stretching vibrations e_g at 1580 cm^{-1}.

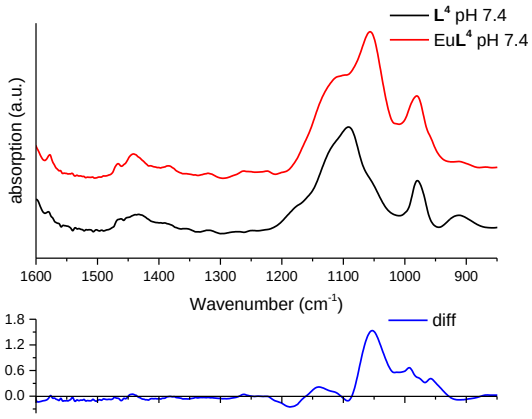

Figure 87 : FT-IR spectra of europium-L⁴ at pH 7.4 in H_2O. Spectra of europium–L⁴ in red and L⁴ in black. Difference spectrum europium-L⁴ minus L⁴ (blue).

Symmetry of dianionic phosphonate group was confirmed with the phosphonate group vibration modes (Fig. 87 black). The distinctive spectral (Fig. 87 blue) features at 1053 cm^{-1}, 975 cm^{-1}, 958 cm^{-1} and 913 (negative) cm^{-1} represent the phosphçnate modes, $\nu_{as}(P-O)$, $\nu_s(P-O)$, $\nu_s(P-O)$ and $\nu_{as}(P-OH)$. Positive bands at ν̌= 1183 cm^{-1} (negative), 1138 cm^{-1} and 992 cm^{-1} are related with pyridine group vibration change. For **L⁴**, the phosphonate groups

and pyridine group are possibly present in the Eu^{3+} coordination at pH 7.4.

The symmetry of monoanionic phosphonate group in two samples was confirmed with the phosphonate groups vibration modes (Fig. 88 black), $\nu_{as}(P-O)$,$\nu_s(P-O)$ and $\nu_{as}(P-OH)$. The distinctive spectral features (Fig. 88 blue) at 1204 cm^{-1} (negative), 1175 cm^{-1}(negative), 1152 cm^{-1}, 1036cm^{-1}(negative), 1013cm^{-1}, 998cm^{-1}, and 900 cm^{-1}(negative) represent the deprotonation of the phosphobate groups and pyridine group vibration change. Positive bands at ν= 1204 cm^{-1}, 1152 cm^{-1}, 998 cm^{-1} are related with pyridine group vibration change. Positive bands at $\check{\nu}$ = 1175 cm^{-1}, 1036 cm^{-1}, 1013 cm^{-1} are assigned to $\nu_{as}(P-O)$, $\nu_s(P-O)$ and $\nu_s(P-O)$. The negative band at $\check{\nu}$= 900 cm^{-1} is due to the displacement for hydrogen atoms by europium ion. Thus both pyridine group and phosphonate groups are changed in the coordination of Eu^{3+} which suggests Eu^{3+} strongly binds the phosphonate group and interferes with the coupling of the vibration modes of other function groups.

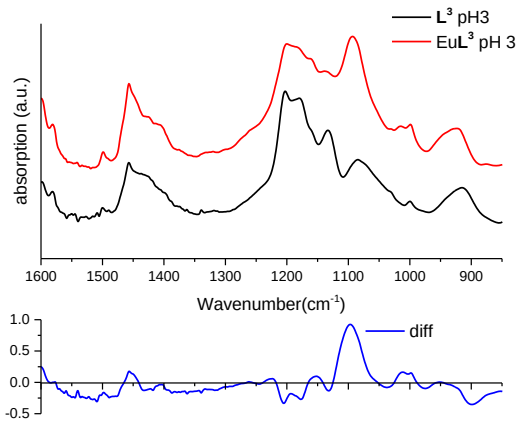

Figure 88 : FT-IR spectra of europium−L^3 at pH 3 in H_2O. Spectra of europium -L^3 in red and L^3 in black. Difference spectrum europium−L^3 minus L^3 (blue).

4 Structural study of europium-ligand complexes

4.1 Possible structure of europium-ligand complexes

Previous experiments (TRLFS, UV-visible, FT-IR) have shown that europium ion is out of the pocket of $\mathbf{L^3}$ at pH 3. Meanwhile for pH 7.4, europium will directly complex with $\mathbf{L^4}$ and located in the pocket of ligand. Thus the coordination of europium is not the same for two pHs, 3 and 7.4.

4.2 Possible structure optimized by DFT

Similar DFT calculation was done for europium-ligand complexes like the one for uranyl-ligand complexes in chapter 3.

For pH 3, the most energetically stable environment for europium with $\mathbf{L^3}$ ligand is composed of two oxygen atoms from monodentate phosphonate (O_{ph}). With the help of UV-Vis absorption study and TRLFS study and FTIR studies, a model was built for Eu-$\mathbf{L^3}$ complex with 7 H_2O at pH 3 (Fig. 89 right): 2 oxygen atoms from monodentate phosphonate (O_{ph}) and seven water molecules in its coordination sphere.

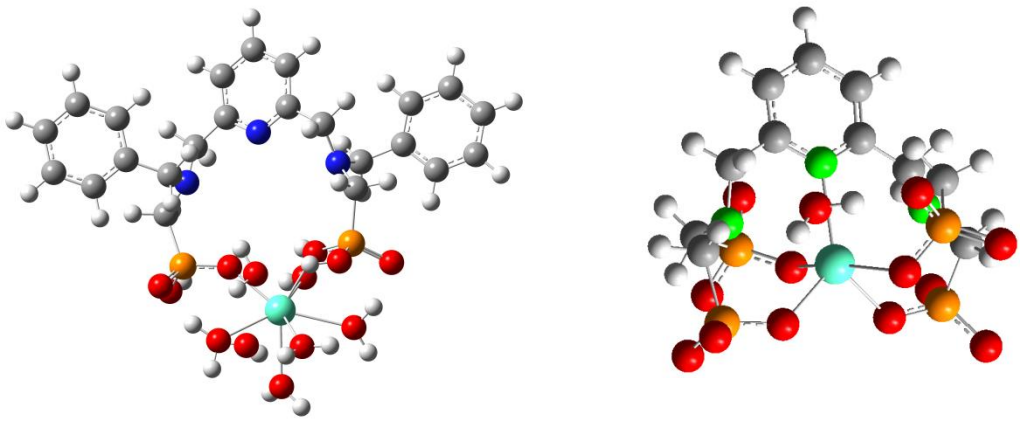

L^3/Eu^{3+} with 7 H_2O pH=3 **L^4/Eu^{3+}** with 1 H_2O pH=7.4

Figure 89 : Theoretical models optimized by DFT and electronic density of L^3/Eu^{3+} with 6 H_2O at pH=3 (right) and L^4/Eu^{3+} with 1 H_2O at pH=7.4 (left) (Oxygen: red, carbon: blue, nitrogen: light green, uranium: yellow)

For pH 7.4, the most energetically stable environment for europium with **L^4** ligand is composed of four oxygen atoms from monodentate phosphonate (O_{ph}), two nitrogen atoms from amine (N_{amine}) and one nitrogen atom from pyridine (N_{pyr}). With the help of UV-Vis absorption , TRLFS and FTIR studies, a model was built for Eu-**L^4** complex with 1 H_2O at pH 7.4 (Fig. 89 left): 4 oxygen atoms from monodentate phosphonate (O_{ph}), 1 oxygen atom from water molecule, 2 nitrogen atoms from amine (N_{amine}) and 1 nitrogen atom from pyridine (N_{pyr}).

According to DFT calculations, the ligand **L^3** shows an asymmetric coordination of the europium ion due to the presence of seven water molecules in the first coordination sphere. The models suggest the ligand provides two oxygen atoms of the phosphonate groups for the coordination. The bond lengths of Eu-**L^3** complex with 7 H_2O at pH 3 are list in table 27.

	distance(Å)
Eu-O_p	2.28 & 2.29
Eu-H_2O	2.45-2.75
Eu-P	3.55 & 3.60

Table 27 : Distances calculated by DFT for the Eu-L^3 complex at pH 3

	distance(Å)
Eu-N_{pyr}	2.66
Eu-N_{amine}	2.76 and 2.87
Eu-O_P	2.27-2.36
Eu-H2O	2.91

Table 28 : Distances calculated by DFT for the Eu-L^4 complex at pH 7.4

According to DFT calculations, the ligand **L^4** shows an asymmetric coordination of the metal ion due to the presence of a water molecule in the first coordination sphere. The models suggest the ligand provides three nitrogen atoms and four oxygen atoms of the phosphonate groups for the coordination. Two of the four methylene phosphonate groups are placed slightly above and below the plane of pyridine, while the other two remaining phosphonate groups point up and down and fold back to the Eu^{3+} ion. The bond lengths of Eu-**L^4** complex with 1 H_2O at pH 7.4 are list in table 28. The calculation result is coherent with the calculation of Gd-**L^4** complex at pH 7.[13]

4.3 EXAFS data analysis of the europium-ligand complex

A comprehensive structural study by EXAFS was done to determine the composition of the coordination sphere of europium ion. Preliminary experiments of UV-Vis absorption, TRLFS and FT-IR studies showed that the complexes between europium and ligands are mainly the f Eu-**L**^{3} species at pH 3 and Eu-**L**^{4} species at pH 7.4.

4.3.1 Eu-L^3 complex study at pH 3

During the measurement for the Eu-**L**^{3} complex at pH 3(Fig. 89 right), the precipitation has been formed. The possible reason for this phenomenon is the local pH increase because of the X-ray. Thus another Eu-**L**^{3} complex at pH 2.6 was prepared to prevent this problem. The absorption spectrum of Eu-**L**^{3} complex at pH 2.6 also has a little difference on absorption with the ligand alone at pH 2.6 which is similar with Eu-**L**^{3} complex at pH 3. The lifetime of europium at pH 2.6 is 0.15 ms which refers 6.5 water molecules in the coordination. Thus the stable adopted model at pH 2.6 should be similar with the most stable adopted model at pH 3 (Table 27). Because it is hard to distinguish the different oxygen atom with different distance for EXAFS data analysis, the EXAFS fitting of europium is different from the one of uranium in this study, a directly fitting start from the EXAFS data on different shell was done. During the adjustment procedure, two shells were taken into account, the first shell is composed by oxygen atoms; the second shell is composed by phosphorus atom. The average distances of Eu-O and Eu-P single scattering pathway were used.

A Hanning adjustment window in k^3 (2; 12.9) was used and the adjustment of spectra was in R (1; 5). Adjustment parameters such as amplitude (S_0^2) and ΔE_0 are given for each experiment. The adjustment factor R (r) and the reduced quality factor ($\chi^2_{i\,ln}$) are both provided as an indicator of the quality of the fit.

path	R_{eff}(Å)	N_{deg}	sigma^2(× 10−3 Å^2)	R_{FIT}(Å)
Eu-O$_{First\ shell}$	2.50	9	7.89	2.42
Eu-P	3.55	2	6.04	3.70

Table 29 : Description of the paths used to fit the EXAFS data of the Eu-L^3 complex at pH 3. S_0^2 = 1; ΔE_0 = 4.69 eV. R = 0.01; $\chi^2_{i\,ln}$ = 23.6

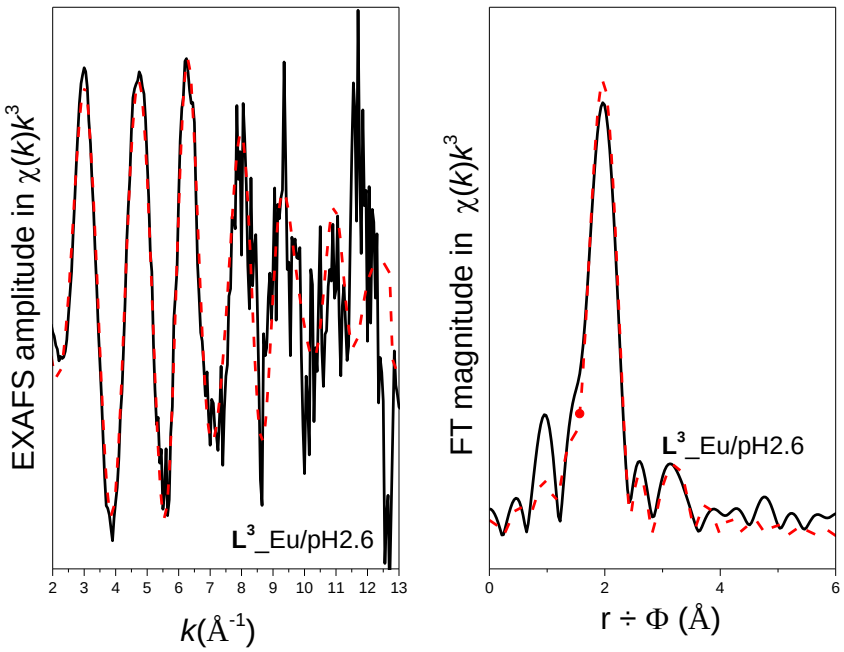

Figure 90 : Eu L$_{III}$ edge k^3–weighted EXAFS spectra (left) and the corresponding

Fourier transforms (right) of the L^3-Eu complex at pH 3. The experimental spectra are given in line and the fits are given in dash line.

The first shell coordination sphere of europium was fitted with nine oxygens to determine a mean value at 2.42 Å in agreement with literature.[243–245] As for monodentate phosphonate phosphors (3.70 Å), distance was fitted in agreement with our calculated DFT model.

4.3.2 Eu-L^4 complex at pH 7.4

The most stable adopted model at pH 7.4 (Fig. 89 left) includes four oxygen atoms (O_p), one oxygen atom (O_{water}) and three nitrogen atoms (N_{pyr} & $2N_{amine}$) in the first coordination (Table 28). The O_p atom represents the oxygen atom of the monodente phosphonate group; O_{water} represents the oxygen atom of the water. N_{pyr} atom represents the nitrogen atom of pyridine group; N_{amine} represents the nitrogen atom from amine units. An additional layer representing the phosphors atoms associated with the above-mentioned phosphonate oxygen atoms has also been taken into account.

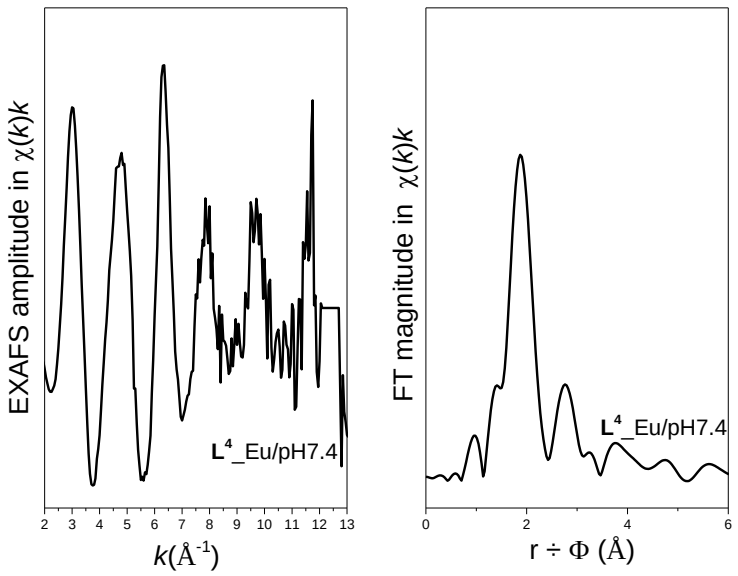

Figure 91 : Eu L_{III} edge k^3–weighted EXAFS spectra (left) and the corresponding Fourier transforms (right) of the L^4-Eu complex at pH 7.4. The experimental spectra are given in line.

Also it is hard to distinguish the different oxygen atoms and nitrogen atoms with different distance for EXAFS data analysis, a directly fitting start from the EXAFS data on different shell was done. During the adjustment procedure, two shells were taken into account, the first shell is composed by oxygen atoms and nitrogen atoms; the second shell is composed by phosphorus atom. The average distances of Eu-O&N and Eu-P single scattering pathway were used.

Unfortunately the fitting of Eu-**L^4** complex at pH 7.4 doesn't works. The first shell of europium ion could be fit with 9 atoms. Due to the strong interaction at the second shell of europium ion, not enough atoms at the second shell could satisfy the coordination.

5 Conclusion

This chapter presented the work on the structural and thermodynamic study of europium-ligand complex. Unfortunately due to the low solubility of Eu-**L^3** complex in 0.1M $NaClO_4$ solution the formation constant measurement failed with spectroscopy and potentiometry.

From the structural study by UV-vis absorption study with TRLFS measurements, it

demonstrates the coordination of europium ion at pH 3 and 5 is not the same, out of the pocket of ligand for pH 3 while in the picket of ligand for pH 5. At pH 3, the interaction of europium ion with both ligands only exists in the phosphonate groups. At pH 5 and 7.4, the europium ion is located in the pocket part of both ligands. Since the phosphonate groups and other parts of ligand couldn't provide sufficient donors for the coordination, extra water molecules from solution are compensate the coordination of europium. The possible complexation modes of Eu-$\mathbf{L^3}$ complex at pH 3 and Eu-$\mathbf{L^4}$ complex at pH 7.4 were further confirmed by FT-IR to settle down the experiment condition for EXAFS. Finally the DFT calculations followed with EXAFS measurements provide the accurate characterization of the coordination sphere of europium ion in the complexation site of $\mathbf{L^3}$ at pH 3.

Chapter 5: General conclusion

General conclusion

This thesis work is focus on the study of decorporation of actinides (U(VI) and Am/Cm(III)) based on a series of polyaminophosphonated chelating agent to target deliver these agents to the organs which retain actinides, e.g. liver, kidneys, bones. In this project, two new bis-phosphonated ligands, **L²** & **L³**, and a tetra-phosphonated ligand, **L⁴**, were synthesized easily and tested for the complexation affinities (Fig. 92). These ligands were used as the MRI contrasts or SPECT agents. By using pyridine group as the backbone, the nitrogen atom of pyridine group could be treating as an intermediate donor. A preliminary test on technetium complex with bis- and tetra-phosphonated ligands was done to reveal the bio-distribution to target organs, bone and kidneys, and fast excretion in hours. The bis-phosphonated ligands, **L²** & **L³**, could provide 2 oxygen atoms and 3 nitrogen atoms for the coordination of actinide ions, while the tetra-phosphonated ligand, **L⁴**, could provide 4 oxygen atoms and 3 nitrogen atoms. Thus the two types of ligands could satisfy the coordination of actinyl ion like UO_2^{2+}, the tetra-phosphonated pyridine ligand is more preferred to complex with actinide ion like Am/Cm(III).

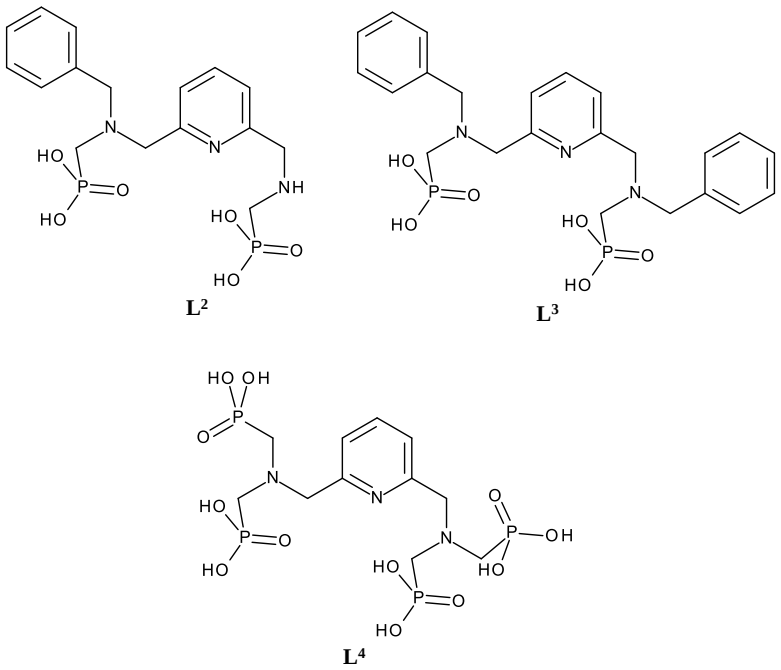

Figure 92 : Chemical structures of bis-phosphonated ligand L² & L³ and tetra-phosphonated ligand L⁴

Uranyl study:

The insufficient uranium chelation therapy for decorporation prompted us to investigate the complex of uranyl and polyaminophosphonated chelating agents in pseudo-physiological medium.

The studies with UV-Vis absorption spectrum, TRLFS and FT-IR identify the different structures of uranyl ligand complexes at at pH 3 & 7.4. The complexation site of uranyl ion in the bis- and tetra-phosphonated ligands consists two monodentate phosphonate groups, two amine parts and the pyridine group.

The EAXFS spectrum obtained was adjusted with the help of DFT calculation. For pH 3, the environments of uranyl ion are consist by two oxygen atoms from monodentate phosphonate groups, one nitrogen atom from pyridine group and two nitrogen atoms from the amine parts for both ligand, **L³** and **L⁴**. For pH 7.4, the environments of uranyl ion are consist by two oxygen

atoms from monodentate phosphonate groups, one hydroxide, one nitrogen atom from pyridine group and two nitrogen atoms from the amine parts for both ligand, $\mathbf{L^3}$ and $\mathbf{L^4}$. The only difference on the coordination of uranyl ion at two pHs is the presence of hydroxide at pH 7.4.

Ligand complexation constants (K_{concd}) are 17.08 for $\mathbf{L^2}$, 15.2 for $\mathbf{L^3}$ at pH 7.4 and in 13.3 to 15.3 for $\mathbf{L^4}$ by displacement titration method developed by Dr. Frederic TARAN. The complexation constant of $\mathbf{L^2}$ is similar with 17 for 5-LICAMS and 16.87 for 3,4,3-LI(1,2-HOPO) which are the most effective uranyl chelating agents. By combining the UV-Vis absorption spectrum and TRLFS, the strong stability of uranyl-$\mathbf{L^3}$ complex was confirmed with competition metal, Na^+, Ca^{2+} and Mg^{2+}, at pH 7.4 and with completion protein, Calmodulin, at pH 5.5.

So the bis-phosphonated ligands have strong complexation affinities and good stability with uranyl ion at biological condition due to the well design of chelating agents.

Europium as analogue of Am/Cm(III) study:

Because of the high mass activity of Am/Cm(III), Eu(III) was used as chemical analogue to perform the studies. Due to the low solubility of Eu-$\mathbf{L^3}$ complex in 0.1M $NaClO_4$, thermodynamic constant study failed.

Similar combining the UV-Vis absorption spectrum and TRLFS study was done for Eu-$\mathbf{L^3}$ complex and Eu-$\mathbf{L^4}$ complex at pH 3, 5 and 7.4. Due to the hydrogen bone on the amine parts, the Eu(III) ion is complexed with phosphonate groups of ligand at low pH, while at high pH the Eu(III) ion is located in the pocket part of ligand due the decrease of hydrogen concentration.

The EAXFS spectrum obtained was adjusted by a linear contribution of water molecules and the function goups of ligand. For Eu-$\mathbf{L^3}$ complex at pH 3, the contribution of ligand is only from the phosphonate groups. 7 water molecules is present is europium first shell. For Eu-$\mathbf{L^4}$ complex at pH 7.4, the fitting cannot be done which might due to the degradation of Eu-$\mathbf{L^4}$ complex under the X-ray.

Perspectives

This project is the first step in the development of polyaminophosphonated pyridine chelating agents for decorporation of actinides. There are still many studies to investigate and characterize.

- Formation constants of uranyl ion with $\mathbf{L^2}$, $\mathbf{L^3}$ and $\mathbf{L^4}$: the formation constant study could be done with potentiometric titration in 0.1M NaCl with Ar protection and without light;
- Formation constants of other actinides with $\mathbf{L^2}$ and $\mathbf{L^3}$ in 0.1M $NaClO_4$: the formation constants could be done with potentiometric titration in 0.1M $NaClO_4$ with other actinides. The results could give an idea about the complexation affinity of europium with $\mathbf{L^2}$ and $\mathbf{L^3}$ due to the similarity of lanthanides;
- Toxicity of polyaminophosphonated pyridine chelating agents;
- The chelation therapy by polyaminophosphonated pyridine chelating agents to sequester actinides to prevent acute effect and long-term effect;

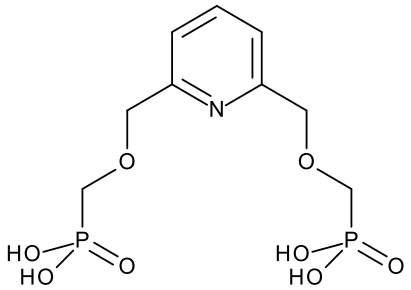

Figure 93: Chemical structures of bis-phosphonated pyridine ligand

- The synthesize of a new bis-phosphonated pyridine ligand (Fig. 93) for uranium chelating agents by replace nitrogen of amine parts by oxygen: the presence of hydroxide of uranyl coordination at pH 7.4 may depend on the 3 nitrogen atoms which can be define as intermediate donor or soft donor. By using oxygen, 4 hard donors could be in the uranyl coordination, t he stability of uranyl with new ligand might be higher.

Appendix I: materials

1 Experiment conditions

Solvents and starting materials were purchased from Aldrich, Acros and Alfa Aesar and used without further purification unless specified. IR UV-VIS TRLFS

^{1}H, ^{13}C, ^{31}P NMR spectra were recorded on Avance 300, Avance 400 and Avance 500 III HD spectrometers operating at 300, 400 and 500 MHz respectively. Chemical shifts are reported in ppm, with residual protonated solvents as internal reference.[115] The multiplicity are given as followed: s = singulet, d = doublet, t = triplet, q = quadruplet, qt = quintuplet, m = multiplet

Elemental analyses and mass spectrometry analyses were carried out by the Service Commun d'Analyses of the University of Strasbourg or by the Laboratoire de Spectrométrie de Masse BioOrganique (LSMBO, IPHC) or by the Plateforme Analytique of the Laboratoire de Reconnaissance et Procédés de Séparation Moléculaire (RePSeM, IPHC). Elemental analysis and monoisotopic masses were calculated with the chemcalc software.[246] Purifications were made on a SPOT II Interchim Flash Purification Liquid Chromatography. Distilled water was purified by ultra-pure MilliQ water.

UV-visible spectrophotometric analyzes were performed on an Agilent Technologies Cary 60 UV-vis apparatus equipped with a deuterium lamp and a tungsten lamp. The measurements were carried out in scanning mode from 200 to 800 nm (scanning speed of 3.3 nm / s).

Time-resolved laser-induced fluorescence spectroscopy (TRLFS) experiments were carried out by using a continuum R Nd:YAG laser (frequency=10 Hz, pulse duration%7ns) coupled with a Panther OPO as the excitation source. Detection was perfumed by aSpectra-Pro-300 monochromator (Acton Research Corporation) coupled with a CCD camera (Princeton Instruments). The excitation wavelength was chosen to be l=430 nm, and the laser power was about 2mJ. The emission spectra were recorded by using the WINSPEC/32 software (Princeton Instruments). The fluorescence spectra had a resolution better than 0.2 nm. The error in the fluorescence intensity was less than 5%.All fluorescence intensity measurements were carried out on non-aerated freshly prepared solutions in aquartz cell at acontrolled temperature of (20 ± 1) °C. Every measurement was repeated at least three times. The fluorescence spectra integration (λ=450–600 nm) and the fluorescence decay curves were calculated with the Origin 2016 software program (OriginLab corporation).

The infrared analyzes were carried out in attenuated total reflection mode ATR using a reflection diamond 1 coupled to a Bruker tensor spectrometer 27 equipped with a MCT detector cooled with liquid nitrogen. The measurements were carried out in scanning mode from 4000 to 600 cm^{-1} (scanning speed of 10 kHz).

2 Preparation of stock solutions

All aqueous solutions are prepared from ultra-pure MilliQ water (18 MΩ.cm-1).

- Stock solution of uranium(VI)

A commercial solution of uranium (1000 ppm, Inorganic Venture) was used for the preparation of samples analyzed by TRLFS and EXAFS.

A solution of uranium chloride (0.05M) was used for ATR-IR and EXAFS.

- Stock solution of europium(III)

The stock solution of $EuCl_3$ for potentiometry was prepared by dissolving 0.7233 mg of $EuCl_3 \cdot H_2O$ in 20 mL H_2O. Final concentration is 4.7×10^{-2} M.

The stock solution of $EuCl_3$ 0.05M for EXAFS and ATR-IR was prepared by dissolving 3.6641 mg of $EuCl_3 \cdot 6H_2O$ in 20 mL H_2O.

A commercial solution of europium (1000 ppm, Inorganic Venture) was used for the preparation of samples analyzed by TRLFS.

- Stock solution of $\mathbf{L^2}$

The stock solution of $\mathbf{L^2}$ for potentiometry was prepared by dissolving 22.83 mg of synthesized ligand in 50 mL of 0.1M $NaClO_4$ solution. Final concentration is 8.63×10^{-4} M.

The 5 mM $\mathbf{L^2}$ stock solution of was prepared by dissolving 26.451 mg of $\mathbf{L^2}$ in 20 mL H_2O

- Stock solution of $\mathbf{L^3}$

The stock solution of $\mathbf{L^3}$ for potentiometry was prepared by dissolving 25.30 mg of synthesized ligand in 50 mL of 0.1M $NaClO_4$ solution. Final concentration is 8.17×10^{-4} M.

The 5 mM $\mathbf{L^3}$ stock solution was prepared by dissolving 30.973 mg of $\mathbf{L^3}$ in 10 mL H_2O

- Stock solution of $\mathbf{L^4}$

The stock solution of $\mathbf{L^4}$ for potentiometry was prepared by dissolving 25.30 mg of synthesized ligand in 50 mL of 0.1M $NaClO_4$ solution. Final concentration is 8.17×10^{-4} M.

The 5 mM $\mathbf{L^4}$ stock solution was prepared by dissolving 31.4485 mg of $\mathbf{L^4}$ in 10 mL H_2O

- Calmoduline

Commercial calmodulin (Sigma Aldrich) was used for the preparation solutions analyzed by ITC. This protein is dissolved in a solution of HEPES at physiological pH at the desired concentration before use.

Appendix II : Experimental methods

1 Potentiometry

1.1 Preparation of solutions

All solutions were prepared with deionized water. The latter has been prepared from osmosis water which has been filtered and purified by means of anionic and cationic ion exchange columns (Fisher Bioblock Scientific type R3-83002 and M3-83006) and activated carbon columns (Fisher Bioblock Scientific type ORC-83005). The water was then boiled, and then degassed by a stream of argon that passes beforehand through a cartridge (Sigma, Oxiclear) to remove any trace of oxygen. The solutions were prepared by weighing the samples using an analytical balance (Mettler Toledo AG-245). The ionic strength was set at 0.1 M using sodium perchlorate (Merck, p.a., $NaClO_4$) and all measurements were made under standard temperature conditions (25.0 °C).

1.2 Potentiometric titrations

Potentiometric titrations of ligand $\mathbf{L^2}$ (8.63×10^{-4} M) and $\mathbf{L^3}$ (8.17×10^{-4} M) were made at using a Metrohm Basic Titrino 794 automatic titrator (Metrohm 2.794.0010) equipped with a combined glass microelectrode (Metrohm 6.0234.100, Long Life) and a 1 mL interchangeable unit (Metrohm 6.3026.110). The absolute error on the volume of the cylinder is 3µL compared to the nominal volume of 1 mL. Potentiometric titrations were carried out using the MET-PH method (Monotone, Equivalent Point) available in the Tiamo light 1.2 software (Metrohm AG Ltd, Herisau, Switzerland) with the following characteristics: increment 3 µL, maximum flow of the burette 2 mL / min, maximum signal drift 1.5 mV / min and minimum equilibrium time 500 s. To calibrate the electrode, titrate a solution of perchloric acid ($1.3\text{-}1.89\times 10^{-2}$ M, Fluka, 70%, $HClO_4$) with sodium hydroxide solution ($1.1 - 1.28\times10^{-1}$ M, BdH, AnalaR, NaOH) was carried out in a thermostated titration cell at 25.0 (2) °C (Lauda E200) under a constant argon flow, previously saturated with water vapor.

The titration of the perchloric acid solutions has been previously determined by titration colorimetric with a solution of sodium tetraborate (Fluka, puris p.a> 99.5%, $B_4Na_2O_7.10H_2O$) in the presence of methyl red (RAL reagents). The sodium hydroxide solutions (BdH, AnalaR, NaOH) were titrated with potassium hydrogenophthalate (Fluka, puriss, p.a., $C_8H_5KO_4$) in the presence of phenolphthalein. The Europium stock solution concentration was determined by complexometric titration with Titriplex III (Merck) in the presence of xylene orang. The GLEE[247] program then made it possible to obtain the electrode calibration parameters (standard electrode potential E_0/mV and slope of the electrode mV.pH^{-1}) and to check the carbonate levels of the sodium hydroxide solutions used (always <5%). Potentiometric titrations (~ 300 points collected over a pH range between 2.5 and 11.5) of the free ligands $\mathbf{L^2}$, $\mathbf{L^3}$ (V_{tot} = 10 mL, inert argon atmosphere, T = 25 °C.) were treated by the program Hyperquad 2000.[248,249] This program is based on methods of Non-Linear Least Squares Adjustment.[250] For ligands $\mathbf{L^2}$, $\mathbf{L^3}$ at least three potentiometric titrations were processed, either separately or commonly, without any significant variation in the determined values. The distribution curves of the protonated species and metal complexes were calculated using the Hyss2009 program.

The potentiometric titration of the Eu- $\mathbf{L^3}$ complex is carried out under the same experimental conditions (pH 2.5 to 11) as the free ligand, but this time in the presence of about one equivalent of Eu (III) ([L^3] tot = [Eu] tot = 1.02×10^{-4} M, pH = (1) 2.49, (2) 11). Due to the precipitation of Eu- $\mathbf{L^3}$ complex at acidic condition, it is not possible to measure the formation constants by UV-visible spectrophotometry according to pH.

2 UV-visible spectrophotometry

UV/Vis spectroscopy is routinely used in analytical chemistry for the quantitative determination of different analytes, such as transition metal ions, highly conjugated organic compounds, and biological macromolecules. Spectroscopic analysis is commonly carried out in solutions but solids and gases may also be studied.

Organic compounds, especially those with a high degree of conjugation, also absorb light in the UV or visible regions of the electromagnetic spectrum. The solvents for these determinations are often water for water-soluble compounds, or ethanol for organic-soluble compounds. (Organic solvents may have significant UV absorption; not all solvents are suitable for use in UV spectroscopy. Ethanol absorbs very weakly at most wavelengths.) Solvent polarity and pH can affect the absorption spectrum of an organic compound. Tyrosine, for example, increases in absorption maxima and molar extinction coefficient when pH increases from 6 to 13 or when solvent polarity decreases.

2.1 Titration for free ligand L^3 species

The spectrophotometric titration according to the pH was performed in order to characterize the protonated species of the free ligand $\mathbf{L^3}$ and europium complex. A volume of 40 mL of a solution of free ligand $\mathbf{L^3}$ (1.02×10^{-4} M) was added to a titration vessel (Metrohm, 6.1414.150) maintained at 25.0 (2) °C using a thermostat (Lauda E200) under a constant stream of argon, previously saturated with water vapor. After fixing the initial value of the pH at ~ 2.5 by addition of perchloric acid, the titration (pH 2.5 to 11) was carried out by adding known volumes of sodium hydroxide (0.1 M, NaOH, BdH, AnalaR) using a Metrohm Basic Titrino 794. After each base addition, an absorption spectrum (200 nm - 800 nm) was recorded automatically using a Cary 60 (Varian) spectrophotometer which equipped with a pulsed arc Xenon lamp. An optical fiber system (Hellma, 041.002-UV) connected to a Suprasil quartz immersion probe with a 10 mm optical path (Hellma, 661.500-QX) allowed in situ measurements. The processing of the data is with HypSpec.[180,181]

2.2 Displacement titration of uranyl-ligand complex

UV-visible spectrophotometric analyzes were performed on an Agilent Technologies Cary 60 UV-vis apparatus equipped with a deuterium lamp and a tungsten lamp. The measurements were carried out in scanning mode from 200 to 800 nm (scanning speed of 3.3 nm / s).

2.2.1 The solutions

0.0125 M buffers were prepared by dissolving the acid form of buffer 12.5 mmol (MES for pH = 5.5, HEPES for pH = 7.4 and CHESS for pH = 9.0) and 112.5 mmol of n-Bu_4Cl in 1L of Millipore water. The pH was adjusted to the pH meter by addition of $nBu_4N^+OH^-$- $30H_2O$.

100µM SCP Solution: 6.25 mL of 4 mM SCP stock solution were mixed in 243.75 mL of appropriate buffer.

SCP-UO_2^{2+} solution at 100 µM: 6.25 mL of stock solution of SCP at 4 mM were mixed in 242.55 mL of water and 1.2 mL of uranyl stock solution (20mM) were added. Both stock solutions were stored for 1h before use. The ligand solutions were prepared by diluting the stock solutions of 2 mM ligands with water to obtain a final concentration of 400 µM.

2.2.2 Procedure for the fast screening

In each 1 mL centrifuge tube, 100 µl of SCP-UO_2 solution (40µM) in HEPES buffer have been added, 16 µl of each ligand solution (5 mM) were added. The tubes were stored without light at room temperature for 36 hours for equilibration. The samples were read by Cary 60 UV-vis apparatus. Measurements were made at 690 nm for pH = 7.4.

2.2.3 Procedure for the titration

In each 1 mL centrifuge tube, 100 µl of SCP-UO_2 solution (40µM) in HEPES buffer have been

added, different volume of each ligand solution (5 mM) were added to reach 0 to 10 eq of ligand concentration. Samples of SCP solution, SCP-UO_2 solution and ligand solution at the same concentration are also prepared as reference. The tubes were stored without light at room temperature for 36 hours for equilibration. The samples were read by Cary 60 UV-vis apparatus. Measurements were made at 690 nm for pH = 7.4 or 640 nm.

Using the Hyss speciation program, we calculated the complexation conditional constants assuming that the complex formed L (tested) -uranyl has the stoichiometry 1: 1 in our experimental conditions.

3 Time-resolved laser fluorescence spectroscopy (TRLFS)

TRLFS is a widely used technique for the analysis of lanthanides and fluorescent actinides. It has several advantages such as speed of analysis, sensitivity (very low detection limit for uranium and europium, of the order of one µM) and selectivity (each fluorescent element is characterized by its absorption spectrum, its fluorescence spectrum and the life time of one of its emitting levels).

3.1 Principle

Luminescence is the emission of a radiation in response to absorption of energy induced by excitation. Many types of luminescence exist and are distinguished by the nature of excitation and radiative emission. Fluorescence is a form of luminescence defined by "the emission of electromagnetic radiation under the exposure of a radiation of the same type having either the same energy (resonance) or a higher energy". In the case of An or Ln, the characteristic times of the emissions are of the order of one microsecond or greater. Phosphorescence is a longer process than fluorescence that occurs after energy transfer to a higher spin state (triplet state).

Fluorescence and phosphorescence are radiative relaxation processes which take place during the transition of the electrons from the lowest vibrational level of the excited electronic state in which they are to the different vibrational levels of the ground state (Fig. 94). The electronic states giving rise to these processes are called sending levels.

Fluorescence corresponds to transitions between states of the same spin, its time scale is between 10^{-12} and 10^{-6} s. Phosphorescence is slower (typically from millisecond to second) because it involves a spin change. In the case of the An and Ln, the radiation emission is accompanied by a spin change as is the case for phosphorescence, however, the life time is lower than the life time characteristic of phosphorescence. The term luminescence seems more appropriate for the f elements; nevertheless, it is the term fluorescence which is commonly used.

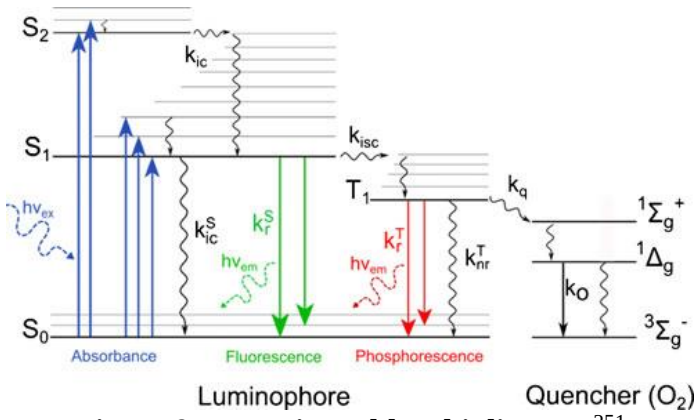

Figure 94 : Perrin–Jablonski diagram[251]

3.2 Luminescence property of europium

The emission bands corresponding to the f-f transitions of Eu (III) are narrow and of relatively low intensity. The ground state of Eu (III) is $^7F_0$. The free ion is spherical symmetry, when in solution. It undergoes a lowering of the symmetry under the influence of the ligand field (crystalline field) which induces a degeneration lift of the spectroscopic levels (Figure 95).

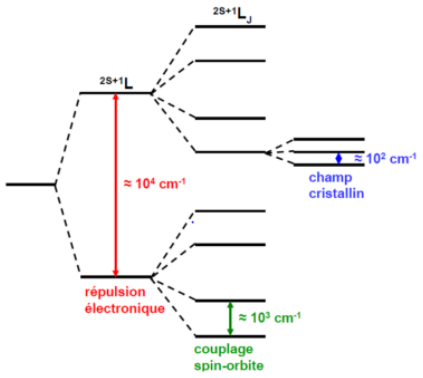

Figure 95 : Energy diagram and degeneracy lift for an Ln^{3+} ion

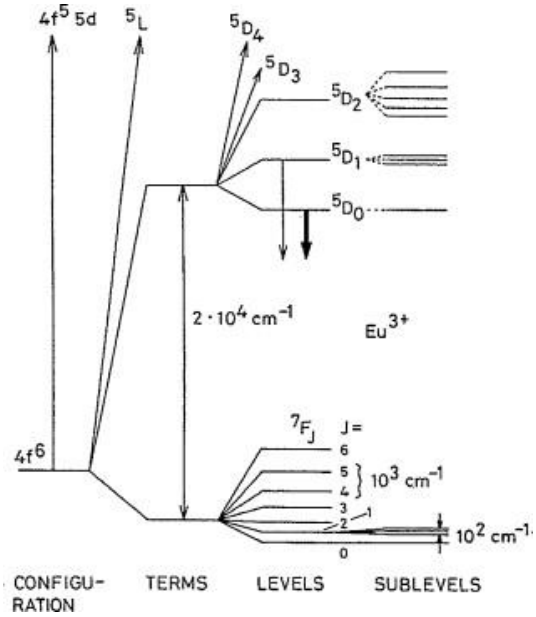

Figure 96 : Partial energy diagram of Eu^{3+} ($4f^6$) showing the relative magnitude of the interelectronic repulsion (terms), spin–orbit coupling (levels) and crystal-field effects (sublevels). The downward arrows indicate the excited states $^5D_0$ and $^5D_1$ from which luminescence occurs.[252]

4f orbitals of lanthanides are generally insensitive to disturbance generated by a ligand field; however, some transitions (hypersensitive) show great variation in intensity depending on the environment of europium. The energy levels of the Eu^{3+} ion in solution as well as the wavelengths of transitions between these same levels are shown in Figure 96 & 97.

The transition $^5D_0 \rightarrow {}^7F_2$ (616 nm) is one of those hypersensitive transitions to the environment just like the $^5D_0 \rightarrow {}^7F_4$ (698 nm) transition but to a degree less. The transition $^5D_0 \rightarrow {}^7F_0$ (579 nm) is prohibited by the selectivity rules. Therefore it has an extremely low intensity.

In this study, the europium ion was excited at 390nm.

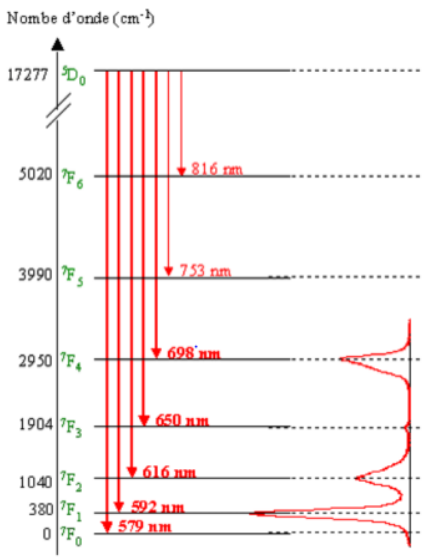

Figure 97 : Energy levels of the aqueous Eu ion (III) and associated transitions

3.3 Luminescence properties of uranium

Like europium, uranium has fluorescence properties. His energetic transitions are shown in Fig 4.4. The lifetime of uranium in solution (typically 2µs) is highly variable and depends both on temperature (a difference of 5 degrees can vary the life time of 0.5µs) but also the ionic strength and the nature of the background salt. Being subjected to hydrolysis (very low pH, several life times can be measured even if uranyl is alone in solution, the life times of hydrolyzed species of uranyl vary widely as well.

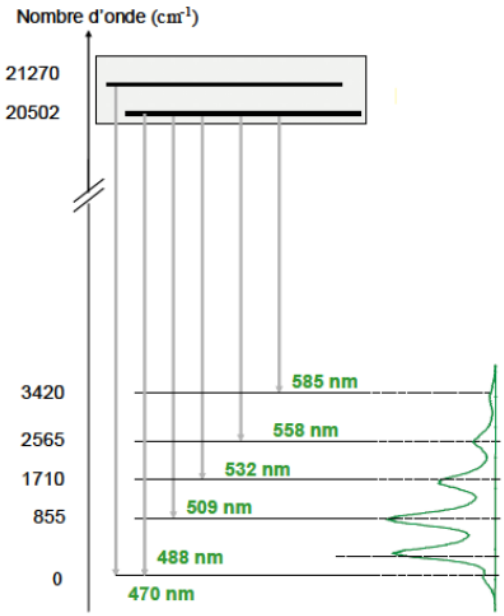

Figure 98 : Fluorescence emission of uranyl

The particular aspect of the fluorescence spectrum of uranyl is explained by the fact that each level of energy (including the ground state) is subdivided into several vibrational levels. The spectrum obtained during the fluorescence emission that accompanies the return to the ground state reflects the vibrational structure of the ground state of uranium that can be observed in figure 98.

In this study, the uranyl ion was excited at 430nm.

3.4 Instrumentation

TRLFS experiments were conducted using a laser excitation source Nd:YAG (7ns pulse at a frequency of 10 Hz with energy of 2 mJ) of the company Continuum coupled to an Optical Parametric Oscillator (OPO, Panther, Continuum). Detection is performed using a Spectra-Pro-300 monochromator (Acton Research Corporation) coupled to a CCD camera (Princeton Instruments). The beam passes through a quartz cuvette containing the solution to be analyzed before reaching the detector. A lens and mirror system focuses the fluorescence beam onto the input slot of the spectrophotometer that selects the wavelength range to be observed. The CCD camera makes it possible to adjust the various measurement parameters for the resolution in time: the delay, the gate width, the integration time and the number of spectra. Spectra are recorded using WINSPEC software (Princeton Instruments).

The excitation wavelength chosen for the measurement of uranium is 430nm and 395 nm for the measurement of europium samples.

The error on the intensity of the fluorescence is less than 5% and the resolution greater than 0.2 nm.

3.5 Samples

All fluorescent intensity measurements were conducted on samples non-aerated and freshly prepared at an ambient temperature of 25 ± 2 ° C. The pH of the solutions was adjusted using a microelectrode (semimicro, Mettler Toledo, France) and a pH meter (seven multi, Mettler Toledo, France). Samples containing uranyl were prepared at a concentration of 5×10^{-5}M ligand and a uranyl concentration from 0 to 5×10^{-5}M at fixed pH. The pH and ligand concentration are constant for the duration of the experiment and metal concentration is the only variable. MES buffer (5 mM) was only used for the preparation of uranyl-CaM solutions at pH 5.5. The pH is adjusted using NaOH and $HClO_4$ (Sigma). The europium solutions are prepared for a concentration in 5×10^{-5} M ligand and a europium concentration from 0 to 5×10^{-5} M. As with the uranyl experiment, the pH and ligand concentration are constant for the duration of the experiment and metal concentration is the only variable. The pH is adjusted using NaOH and $HClO_4$ (Sigma).

4 ATR-IR Spectroscopy

Infrared spectroscopy is a means of diagnosis allowing determine the nature of the chemical bonds present in a molecule. Indeed, experience shows that certain vibration frequencies, called "group frequencies" are characteristic of the presence of a chemical group in the molecule studied.

4.1 Principle

Infrared spectroscopy uses the ability of molecules to stretch or deform specific frequencies that correspond to discrete energy levels (vibratory or rotational modes (Fig. 99)). The electromagnetic field induced by the infrared radiation can interact with a dipole moment of a molecular entity present in the material. When the field frequency coincides with the vibration frequency of a specific mode of the molecule, the interaction created causes the vibration of certain bonds and the absorption of the energy of the corresponding excitatory wave. The frequency with which the radiation is absorbed depends on the nature of the bonds, the mass of atoms involved and the environment close to the group considered.

For a molecule to have an infrared spectrum, it must have a specific characteristic: a dipolar electric moment must change during the analysis. A heteronuclear diatomic molecule is therefore active with respect to infrared spectroscopy because its dipole moment of such a molecule changes when the bond extends or contracts. This is not the case for a homonuclear diatomic molecule because its dipole moment remains unchanged.

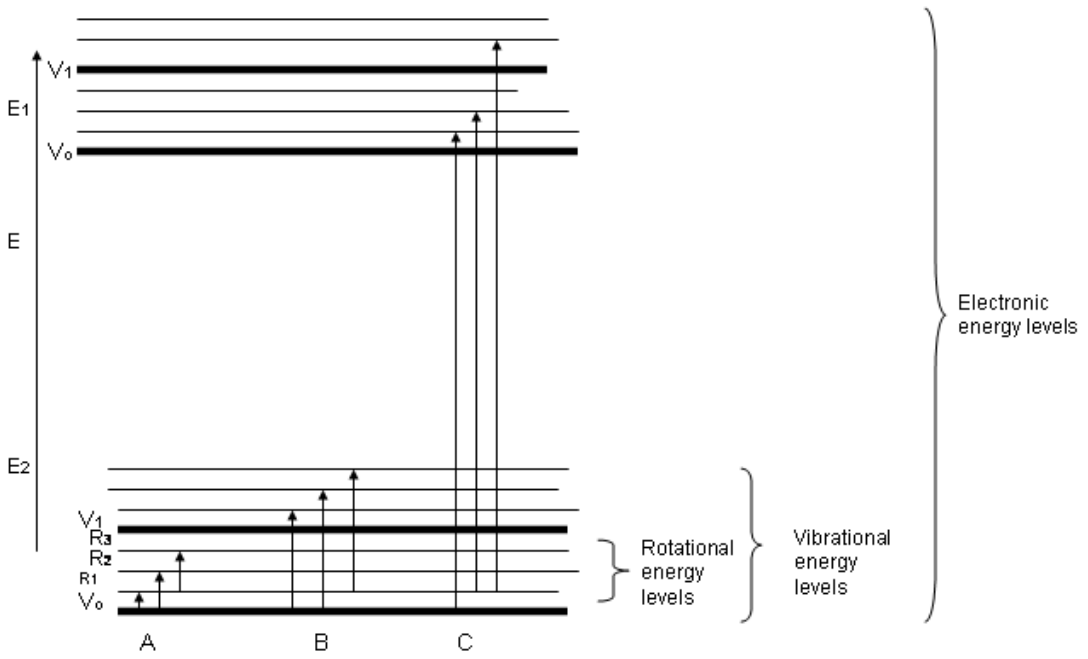

Figure 99 *:* Energy levels for a molecule.

For more complex molecules, there are two modes of vibration: stretching or elongations (symmetrical, antisymmetric) and deformations (rotation, shear, torsion ...). Stretches are present in the region of the spectrum ranging from 4000 to 1000 cm^{-1} and are generally of high intensity. The deformation vibrations are of lower intensity and are located in the 1000-600 cm^{-1} region of the spectrum and constitute the fingerprint of the molecule. The infrared spectrum of a sample is established by passing a beam of infrared light through this sample. Examination of the transmitted light indicates the amount of energy absorbed at each wave number.

4.2 General

The infrared analyzes were performed in attenuated total reflection mode (ATR) using a reflection diamond coupled to a Bruker tensor spectrometer 27 which equipped with a liquid nitrogen cooled MCT detector. The analysis was carried out in scanning mode from 4000 to 600 cm^{-1} (scanning speed of 10 kHz).

4.3 IR measurements of the uranyl-L^3 complex

The equal equivalence uranyl-$\mathbf{L^3}$ solutions (~2 mM) was prepared by increasing pH to 10 with sodium hydroxide (1 M) to solubilize the precipitation which present at acidic condition after mix the uranyl stock solution and $\mathbf{L^3}$ stock solution, then hydrochloride acid (0.1 M) and sodium hydroxide (0.1 M) were used to reach pH 3 and 7.4.

The infrared spectra of uranyl-$\mathbf{L^3}$ solutions (~2 mM) and $\mathbf{L^3}$ solution (5 mM) at two pH were recorded on a reflection ATR diamond between 4000 and 600 cm^{-1} while a wet film was formed (resolution 2 cm^{-1}, 64 sweeps per spectrum, scanning speed 10 kHz).

4.4 IR measurements of the uranyl-L^4 complex

The equal equivalence uranyl-$\mathbf{L^4}$ solutions (~2 mM) was prepared by increasing pH to 10 with sodium hydroxide (1 M) to solubilize the precipitation which present at acidic condition after mix the uranyl stock solution and $\mathbf{L^4}$ stock solution, then hydrochloride acid (0.1 M) and sodium hydroxide (0.1 M) were used to reach pH 3 and 7.4.

The infrared spectra of uranyl-$\mathbf{L^4}$ solutions (~2 mM) and $\mathbf{L^4}$ solution (5 mM) at two pH were recorded on a reflection ATR diamond between 4000 and 600 cm^{-1} while a wet film was formed (resolution 2 cm^{-1}, 64 sweeps per spectrum, scanning speed 10 kHz).

4.5 IR measurements of the Eu-ligand complex

The equal equivalence Eu-**L**^{3} solutions (~2 mM) was prepared by mixing the europium stock solution and **L**^{3} stock solution, then hydrochloride acid (0.1 M) and sodium hydroxide (0.1 M) were used to reach pH 3.

The equal equivalence Eu-**L**^{4} solutions (~2 mM) was prepared by mixing the europium stock solution and **L**^{3} stock solution, then hydrochloride acid (0.1 M) and sodium hydroxide (0.1 M) were used to reach pH 7.4.

The infrared spectra of the Eu-ligand complex solutions (~2 mM) at two pH were recorded on a reflection ATR diamond between 4000 and 600 cm^{-1} while a wet film was formed (resolution 2 cm^{-1}, 64 sweeps per spectrum, scanning speed 10 kHz).

5 Functional Theory of Density (DFT)

The foundations of density functional theory (DFT) have been laid in 1927 by Thomas and Fermi who calculated the energy of an atom by representing its kinetic energy as a function of the electron density. In this model, the n electrons dependent on 3n space coordinates are replaced by their density $\rho(\vec{r})$ which depends only on three variables. The fundamental state of this system is described by the wave function $\psi_0(\vec{r_1},\vec{r_1},\cdots \vec{r_n})$ which corresponds to a unique electronic density $\rho_0(\vec{r})$. This wave function, and the energy E_0 associated with it, are determined by the minimizing the total energy of the system. The external potential $\hat{\upsilon}_{\text{ext}}(\vec{r})$ created by the N nuclei of the system is then completely determined and thus fixes the Hamiltonian. Therefore, the number of electron n and the potential $\hat{\upsilon}_{\text{ext}}(\vec{r})$, define all properties of the ground state. The energy of the ground state can be defined as a functional of $\rho_0(\vec{r})$, which then makes it possible to determine all the properties of the ground state of the studied molecule.

Theoretical calculations performed during this thesis (Calculations done by Jérôme Roques) aim to minimize the total energy of the "metal ion-ligand" model created in order to determine which models are the most energy stable and therefore most likely to form in solution. All structures have been optimized using the DFT approach implemented in Gaussian 09. The calculations were performed using the hybrid functional B3LYP. The MWB60 Stuttgart (MWP60) have been used to describe the uranium and neptunium atoms, MWB2 for oxygen, nitrogen and carbon, and the 6-31G database for the atom. hydrogen. In order to take into account the effects of the solvent, solvation was taken into account using a dielectric continuum model for the permittivity (ε_0 = 80). The Polarizable Continuum Model (CPCM) has also been implemented in Gaussian 09.

6 EXAFS Spectroscopy

The EXAFS measurements presented in this work were carried out at the synchrotron of “Optimized Light Source of Intermediate Energy to LURE* (SOLEIL) in Saclay on the MARS line; As the samples are diluted (around the mM), the EXAFS signal comes from a fluorescence measurement. The MARS line is equipped with a high-purity 13-element germanium detector, a water-cooled Si (111) monochromator and two Pt-coated mirrors for harmonic filtering. EXAFS measurements were made at threshold L_{III} of uranium and europium. The data processing was done using the ATHENA software, and the Fourier transforms were applied via the Hanning windows using the ARTHEMIS software.

6.1 The uranyl-L^3 complex sample for EXAFS measurements

The uranyl/**L**^{3} 1/1.2 solutions was prepared by increasing pH to 10 with sodium hydroxide (1 M) to solubilize the precipitation which present at acidic condition after mix the uranyl stock solution and **L**^{3} stock solution, then hydrochloride acid (0.1 M) and sodium hydroxide (0.1 M) were used to reach pH 3 and 7.4.

6.2 The uranyl-L^4 complex sample for EXAFS measurements

The uranyl/$\mathbf{L^4}$ 1/1.2 solutions (~2 mM) was prepared by increasing pH to 10 with sodium hydroxide (1 M) to solubilize the precipitation which present at acidic condition after mix the uranyl stock solution and $\mathbf{L^4}$ stock solution, then hydrochloride acid (0.1 M) and sodium hydroxide (0.1 M) were used to reach pH 3 and 7.4.

6.3 The Eu-ligand complex sample for EXAFS measurements

The equal equivalence Eu-$\mathbf{L^3}$ solutions (~2 mM) was prepared by mixing the europium stock solution and $\mathbf{L^3}$ stock solution, then hydrochloride acid (0.1 M) and sodium hydroxide (0.1 M) were used to reach pH 3.

The equal equivalence Eu-$\mathbf{L^3}$ solutions (~2 mM) was prepared by mixing the europium stock solution and $\mathbf{L^3}$ stock solution, then hydrochloride acid (0.1 M) and sodium hydroxide (0.1 M) were used to reach pH 2.6.

The equal equivalence Eu-$\mathbf{L^4}$ solutions (~2 mM) was prepared by mixing the europium stock solution and $\mathbf{L^3}$ stock solution, then hydrochloride acid (0.1 M) and sodium hydroxide (0.1 M) were used to reach pH 7.4.

Appendix III: Thermodynamic data

The formation constants which used in this study for species calculation and stability calculation are in the table 30.

formula	log of formation constant	formula	log of formation constant
$(UO_2)(OH)$	-5,2	**HSCP**	13,3
$(UO_2)(OH)_2$	-10,3	**H_2SCP**	23,4
$(UO_2)(OH)_3$	-19,2	**H_3SCP**	31,13
$(UO_2)(OH)_4$	-33	**H_4SCP**	37,68
$(UO_2)_2OH$	**-2,7**	**HL_2**	9,5
$(UO_2)_2(OH)_2$	**-5,6**	**H_2L_2**	18,65
$(UO_2)_3(OH)_4$	-11,9	**H_3L_2**	24,82
$(UO_2)_3(OH)_5$	-15,6	**H_4L_2**	29,45
$(UO_2)_3(OH)_7$	-31	**HL_3**	9,28
$(UO_2)_4(OH)_7$	-21,9	**H_2L_3**	18,19
UO_2Ca_3CaM	18.81	**H_3L_3**	24,55
UO_2Ca_3CaMOH	13.91	**H_4L_3**	29
CaCaM	4,89	**HL_4**	11,21
Ca_2CaM	9,32	**H_2L_4**	21,5
Ca_3CaM	12,81	**H_3L_4**	29,54
Ca_4CaM	16,31	**H_4L_4**	36,03
EuL_4	25,7	**H_5L_4**	41,56
$HEuL_4$	35,1	**H_6L_4**	45,76
H_2EuL_4	42,6		

Table 30 : Formation constant which used in this study

Reference

1. Smyth, H. D. Atomic Energy for Military Purposes. *Rev. Mod. Phys.* **17,** 351–471 (1945).
2. Hamilton, J. G. The metabolism of the fission products and the heaviest elements. *Radiology* **43,** 325–343 (1947).
3. Fink, R. . Biological Studies With Polonium, Radium, and Plutonium. *Natl. Nucl. Energy Serv. Div.* **3,** (1950).
4. PAINTER, E. Clinical physiology of dogs injected with plutonium. *Nucl. Sci. Abstr.* **1,** 18 (1948).
5. Fattal, E., Tsapis, N. & Phan, G. Novel drug delivery systems for actinides (uranium and plutonium) decontamination agents. *Adv. Drug Deliv. Rev.* **90,** 40–54 (2015).
6. Services, S. Safe handling of radioactive luminous compound. *Natl. Bur. Stand. handbook.* (1941).
7. Wood, R. *et al.* Decorporation Treatment -- Medical Overview. *Radiat. Prot. Dosimetry* **87,** 51–57 (2000).
8. Portevin, A. The Scientific Background to Decorporation. *Radiat. Prot. Dosimetry* **87,** 11–17 (2000).
9. H. Henge-Napoli, E. Ansoborlo, V. C, M. *et al.* Efficacy of ethane-1-hydroxy-1, 1-bisphosphonate (EHBP) for the decorporation of uranium after intramuscular contamination in rats. *Int. J. Radiat. Biol.* **75,** 1473–1477 (1999).
10. Paquet, F. *et al.* Efficacy of 3,4,3-LIHOPO for reducing neptunium retention in the rat after simulated wound contamination. *Int. J. Radiat. Biol.* **76,** 113–7 (2000).
11. Paquet, F., Chazel, V., Houpert, P., Guilmette, R. A. & Muggenburg, B. A. Efficacy of 3,4,3-LI(1,2-HOPO) for decorporation of Pu, Am and U from rats injected intramuscularly with high-fired particles of MOX. *Radiat. Prot. Dosimetry* **105,** 521–5 (2003).
12. Abada, S. *et al.* Phosphonated chelates for nuclear imaging. *Org. Biomol. Chem.* **12,** 9601–20 (2014).
13. Abada, S. *et al.* Highly relaxing gadolinium based MRI contrast agents responsive to Mg2+ sensing. *Chem. Commun.* **48,** 4085 (2012).
14. Sherry, A. D. *et al.* Characterization of Lanthanide(III) DOTP Complexes: Thermodynamics, Protonation, and Coordination to Alkali Metal Ions. *Inorg. Chem.* **35,** 4604–4612 (1996).
15. Cacheris, W. P., Nickle, S. K. & Sherry, A. D. Thermodynamic study of lanthanide complexes of 1,4,7-triazacyclononane-N,N’,N"-triacetic acid and 1,4,7,10-tetraazacyclododecane-N,N’,N",N’’’-tetraacetic acid. *Inorg. Chem.* **26,** 958–960 (1987).
16. Ansoborlo, É. *et al.* Review of actinide decorporation with chelating agents. *Comptes Rendus Chim.* **10,** 1010–1019 (2007).
17. The Actinide User Laboratory (ActUsLab) - European Commission. Available at: https://ec.europa.eu/jrc/en/page/actinide-user-laboratory-actuslab. (Accessed: 26th June 2018)
18. Katz, J. J. & Seaborg, G. T. *Actinide and Transactinide Elements*. *The Chemistry of the Actinide and Transactinide Elements*
19. Nuclear and radiation accidents and incidents. Available at: https://en.wikipedia.org/wiki/Nuclear_and_radiation_accidents_and_incidents#cite_note-critev-10.
20. International Atomic Energy Agency. *Heavy water reactors : status and projected development.* (International Atomic Energy Agency, 2002).
21. Woodwark, D. R. Electronic Structure of Actinyl Ions. (1980).
22. Kakihana, M., Nagumo, T., Okamoto, M. & Kakihana, H. Coordination structures for uranyl carboxylate complexes in aqueous solution studied by IR and carbon-13 NMR spectra. *J. Phys. Chem.* **91,** 6128–6136 (1987).
23. Barkleit, A. *et al.* Coordination of uranium(vi) with functional groups of bacterial lipopolysaccharide studied by EXAFS and FT-IR spectroscopy. *Dalt. Trans.* **40,** 9868 (2011).
24. Li, B., Raff, J., Barkleit, A., Bernhard, G. & Foerstendorf, H. Complexation of U(VI) with highly phosphorylated protein, phosvitin. A vibrational spectroscopic approach. *J. Inorg. Biochem.* **104,** 718–725 (2010).
25. Wang, Y. *et al.* Umbellate distortions of the uranyl coordination environment result in a stable and porous polycatenated framework that can effectively remove cesium from aqueous solutions. *J. Am. Chem. Soc.* **137,** 6144–6147 (2015).
26. Neuefeind, J., Soderholm, L. & Skanthakumar, S. Experimental Coordination Environment of Uranyl(VI) in Aqueous Solution. *J. Phys. Chem. A* **108,** 2733–2739 (2004).
27. Allen, P. G. *et al.* Multinuclear NMR, Raman, EXAFS, and X-ray Diffraction Studies of Uranyl Carbonate Complexes in Near-Neutral Aqueous Solution. X-ray Structure of

[C(NH2)3]6[(UO2)3(CO3)6]·6.5H2O. *Inorg. Chem.* **34,** 4797–4807 (1995).
28. Bell, J. T. & Biggers, R. E. Absorption spectrum of the uranyl ion in perchlorate media III. Resolution of the ultraviolet band structure; some conclusions concerning the excited state of UO22+. *J. Mol. Spectrosc.* **25,** 312–329 (1968).
29. Guillaumont, R. *et al. Update on the chemical thermodynamics of uranium, neptunium, plutonium, americium and technetium*. *Chemical Thermodynamics* **5,** (2003).
30. Allen, P. G., Bucher, J. J., Shuh, D. K., Edelstein, N. M. & Craig, I. Coordination Chemistry of Trivalent Lanthanide and Actinide Ions in Dilute and Concentrated Chloride Solutions. doi:10.1021/ic9905953
31. Henderson, P. & P. Inorganic geochemistry. *Oxford, Pergamon Press. 1982. 367 p.* (1982).
32. Shannon, R. D. Revised effective ionic radii and systematic studies of interatomic distances in halides and chalcogenides. *Acta Crystallogr. Sect. A* **32,** 751–767 (1976).
33. J. L. RYAN & W. E. KEDER. *Lanthanide/Actinide Chemistry*. **71,** (AMERICAN CHEMICAL SOCIETY, 1967).
34. Johannesson, K. H., Stetzenbach, K. J., Hodge, V. F. & Lyons, W. B. Rare earth element complexation behavior in circumneutral pH groundwaters: Assessing the role of carbonate and phosphate ions. *Earth Planet. Sci. Lett.* **139,** 305–319 (1996).
35. Boniforti, R. Lanthanides, uranium, and thorium as possible simulators of the behavior of transuranics in the aquatic environment. *Sci. Total Environ.* **64,** 181–189 (1987).
36. Johansson, B. & Rosengren, A. Interpolation scheme for the cohesive energies for the lanthanides and actinides. *Phys. Rev. B* **11,** 1367–1373 (1975).
37. DOMINGO, J. Effectiveness of chelation therapy with time after acute uranium intoxication. *Fundam. Appl. Toxicol.* **14,** 88–95 (1990).
38. de Rey, B. M., Lanfranchi, H. E. & Cabrini, R. L. Percutaneous absorption of uranium compounds. *Environ. Res.* **30,** 480–491 (1983).
39. Gorden, A. E. V., Xu, J., Raymond, K. N. & Durbin, P. Rational design of sequestering agents for plutonium and other actinides. *Chem. Rev.* **103,** 4207–4282 (2003).
40. Ansoborlo, E. *et al.* Actinide speciation in relation to biological processes. *Biochimie* **88,** 1605–1618 (2006).
41. Durbin, P. W. *et al.* 237Np: oxidation state in vivo and chelation by multidentate catecholate and hydroxypyridinonate ligands. *Health Phys.* **75,** 34–50 (1998).
42. Ramounet, B., Matton, S., Grillon, G. & Fritsch, P. Early biokinetics of actinides after intravenous administration of soluble forms of Pu(IV), Np(IV) and Np(V). *J. Alloys Compd.* **271–273,** 103–105 (1998).
43. Taylor, G. N., Lloyd, R. D. & Mayst, C. W. Liver cancer induction by 239pu, 241am, and thorotrast in the grasshopper mouse, onychomys leukogaster. *Health Phys.* **64,** 141–146 (1993).
44. Taylor, D. M. The biodistribution and toxicity of plutonium, americium and neptunium. *Sci. Total Environ.* **83,** 217–225 (1989).
45. Taylor, D. M. The bioinorganic chemistry of actinides in blood. *J. Alloys Compd.* **271–273,** 6–10 (1998).
46. WHO | The world health report 2004 - changing history. *WHO* (2013).
47. Vicente-Vicente, L. *et al.* Nephrotoxicity of Uranium: Pathophysiological, Diagnostic and Therapeutic Perspectives. *Toxicol. Sci.* **118,** 324–347 (2010).
48. Van Horn, J. D. & Huang, H. Uranium(VI) bio-coordination chemistry from biochemical, solution and protein structural data. *Coord. Chem. Rev.* **250,** 765–775 (2006).
49. Durbin, P. W. in *The Chemistry of the Actinide and Transactinide Elements* **5,** 3339–3440 (Springer Netherlands, 2006).
50. Cooper, J. R., Stradling, G. N., Smith, H. & Ham, S. E. The Behaviour of Uranium-233 Oxide and Uranyl-233 Nitrate in Rats. *Int. J. Radiat. Biol. Relat. Stud. Physics, Chem. Med.* **41,** 421–433 (1982).
51. Basset, C. *et al.* Revision of the biodistribution of uranyl in serum: Is fetuin-A the major protein target? *Chem. Res. Toxicol.* **26,** 645–653 (2013).
52. Taylor, D. M. Some aspects of the comparative metabolism of plutonium and americium in rats. *Health Phys.* **8,** 673–677 (1962).
53. Taylor, D. & … J. B. Long-term biological damage from plutonium-239 and americium-241 in rats. *Univ. Utah Press Salt Lake …* (1969).
54. Choi, B. *et al.* Acute Toxicity of Arsenic in Rats and Mice. *Pathology* **15,** 323–334 (2003).
55. Leggett, R. W. & Pellmar, T. C. The biokinetics of uranium migrating from embedded DU fragments. *Journal of Environmental Radioactivity* **64,** 205–225 (2003).
56. Taylor, D. M. & Taylor, S. K. Environmental uranium and human health. *Rev. Environ. Health* **12,**

147–157 (1997).
57. Ubios, A. M., Guglielmotti, M. B., Steimetz, T. & Cabrini, R. L. Uranium inhibits bone formation in physiologic alveolar bone modeling and remodeling. *Environ. Res.* **54,** 17–23 (1991).
58. Product: Documentation of the TLVs and BEIs with Other Worldwide Occupational Exposure Values CD-ROM * 2005, Network Version: ACGIH. Available at: https://www.acgih.org/forms/store/ProductFormPublic/documentation-of-the-tlvs-and-beis-with-other-worldwide-occupational-exposure-values-cd-rom-2005-network-version. (Accessed: 2nd July 2018)
59. Lestaevel, P. *et al.* Changes in sleep-wake cycle after chronic exposure to uranium in rats. *Neurotoxicol. Teratol.* **27,** 835–840 (2005).
60. IARC Monographs- Classifications. Available at: http://monographs.iarc.fr/ENG/Classification/index.php. (Accessed: 2nd July 2018)
61. Durbin, P. W. in *Uranium · Plutonium Transplutonic Elements* 739–896 (Springer Berlin Heidelberg, 1973). doi:10.1007/978-3-642-65551-7_18
62. Mays, C. W., Lloyd, R. D., Taylor, G. N. & Wrenn, M. E. Cancer incidence and lifespan vs. alpha-particle dose in beagles. *Health Phys.* **52,** 617–24 (1987).
63. Mays, C., Taylor, G., in, R. L.-L. radiation effects studies & 1986, undefined. Toxicity ratios: their use and abuse in predicting the risk from induced cancer. *iaea.org*
64. Aub, J. C., Evans, R. D., Gallagher, D. M. & Tibbetts, D. M. An article contributed to an anniversary volume in honor of doctor Joseph Hersey Pratt: Effects of treatment on radium and calcium metabolism in the human body (Effects of treatment on radium and calcium metabolism in the human body*). *Ann. Intern. Med.* **11,** 1443–1463 (1938).
65. Voegtlin, C. & Hodge, H. Pharmacology and toxicology of uranium compounds. (1949).
66. Durbin, P. W. Lauriston S. Taylor Lecture: the quest for therapeutic actinide chelators. *Health Phys.* **95,** 465–92 (2008).
67. Schubert, J. Treatment of plutonium poisoning by metal displacement. *Science (80-.).* (1947).
68. Stone, R. Industrial medicine on the plutonium project: survey and collected papers. (1951).
69. ICRP. *Recommendations of the International Commission on Radiological Protection*. **21,** (1990).
70. ICRP. Recommendations of the ICRP. ICRP Publication 26. *Ann. ICRP* **1,** 2–3 (1977).
71. Schubert, J. Removal of Radioelements from the Mammalian Body. *Annu. Rev. Nucl. Sci.* **5,** 369–412 (1955).
72. AT, I. Effect of 2-acetylamino-1,3,4-thiadiazole-5- sulfonamide on the elimination of uranium from the organism and on the course of acute uranium poisoning. 678–687 (1968). doi:10.1056/NEJMra1103676
73. Durbin, P. W., Kullgren, B., Xu, J. & Raymond, K. N. New agents for in vivo chelation of uranium (VI): efficacy and toxicity in mice of multidentate catecholate and hydroxypyridinonate ligands. *Health Phys.* **72,** 865–879. (1997).
74. Durbin, P. W., Kullgren, B., Ebbe, S. N., Xu, J. & Raymond, K. N. Chelating agents for uranium(VI): 2. Efficacy and toxicity of tetradentate catecholate and hydroxypyridinonate ligands in mice. *Health Phys.* **78,** 511–521 (2000).
75. Sawicki, M. *et al.* Bisphosphonate sequestering agents. Synthesis and preliminary evaluation for in vitro and in vivo uranium(VI) chelation. *Eur. J. Med. Chem.* **43,** 2768–2777 (2008).
76. *Metal Chelation in Medicine*. (Royal Society of Chemistry, 2016). doi:10.1039/9781782623892
77. Sillen, L., Martell, A. & Bjerrum, J. Stability constants of metal-ion complexes.
78. MarteU, A. & Smith, R. Critical Stability Constants, Vol. 3. Other Organic Ligands. (1977).
79. Smith, R. & Martell, A. Critical stability constants. Volume 5. First supplement. (1982).
80. Smith, R. & Martell, A. Stability constants, vol. 6: second supplement. (1989).
81. Gindler, J. E. in *Uranium · Plutonium Transplutonic Elements* 69–164 (Springer Berlin Heidelberg, 1973). doi:10.1007/978-3-642-65551-7_2
82. Piskunov, E. & AG Rykov. Investigation of complex formation with diethylenetriaminepentaacetic acid. IV. Neptunium (IV). *Sov. Radiochem. Transl.)* **14,** (1972).
83. Moskvin, A. I. Correlation of the solubility products of actinide compounds with the properties of the metal ions and acid anions forming them. *Sov. Radiochem.* **13,** 299–300 (1971).
84. Mompean, F., Illemassène, M. & Perrone, J. Chemical thermodynamics of compounds and complexes of U, Np, Pu, Am, Tc, Se, Ni and Zr with selected organic ligands. (2005).
85. Durbin et al. Development of decorporation agents for the actinides. (1998).
86. Bonin, L. *et al.* Revisiting actinide–DTPA complexes in aqueous solution by CE-ICPMS and ab initio

molecular dynamics†. *RSC Adv.* **6,** 62729–62741 (2016).
87. Catsch, A. Radioactive metal mobilization in medicine. (1964).
88. Medicine, H. F.-M. in & 1960, undefined. The pharmacology of some useful chelating agents. *JB Lippincott Co, Philadelphia*
89. Hamilton, J. G. & Scott, K. G. Effect of Calcium Salt of Versene upon Metabolism of Plutonium in the Rat. *Exp. Biol. Med.* **83,** 301–305 (1953).
90. Foreman, H. The Use of Chelating Agents for Accelerating Excretion of Radioelements*. *J. Am. Pharm. Assoc. (Scientific ed.)* **42,** 629–632 (1953).
91. Foreman, H. Metal Binding in Medicine ed MJ Seven and LA Johnson. (1960).
92. Volf, V. Treatment of incorporated transuranium elements. (1978).
93. Breitenstein, B. D. & Palmer, H. E. Lifetime Follow-up of the 1976 americium accident victim. *Radiat. Prot. Dosimetry* **26,** 317–322 (1976).
94. Guilmette, R. A. & Muggenburg, B. A. Reducing the Radiation Dose from Inhaled Americium-241 Using Continuously Administered DTPA Therapy. *Int. J. Radiat. Biol.* **53,** 261–271 (1988).
95. Lloyd, R. D. *et al.* Removal of Pu and Am from Beagles and Mice by 3,4,3-LICAM(C) or 3,4,3-LICAM(S). *Radiat. Res.* **99,** 106 (1984).
96. Lloyd, R. D., McFarland, S. S., Taylor, G. N., Williams, J. L. & Mays, C. W. Decorporation of 241 Am in Beagles by DTPA. *Radiat. Res.* **62,** 97 (1975).
97. Catsch, A., Harmuth-Hoene, A., Havlicek, F. & Carpy, S. Interaction Between Chelates and Endogenous Zinc. (1968).
98. Bruenger, F. W., Kuswik-Rabiega, G. & Miller, S. C. Decorporation of aged americium deposits by oral administration of lipophilic polyamino carboxylic acids. *J. Med. Chem.* **35,** 112–118 (1992).
99. Raymond, K. N. & Smith, W. L. Actinide-specific sequestering agents and decontamination applications. *Struct. Bond. (Berlin, Ger.* **43,** 159–186 (1981).
100. Guilmette, R. A., Hakimi, R., Durbin, P. W., Xu, J. & Raymond, K. N. Competitive binding of Pu and Am with bone mineral and novel chelating agents. *Radiat. Prot. Dosimetry* **105,** 527–34 (2003).
101. Durbin, P. W. *et al.* 237Np: Oxidation state in vivo and chelation by multidentate catecholate and hydroxypyridinonate ligands. *Health Phys.* **75,** 34–50 (1998).
102. Durbin, P. W., Kullgren, B., Xu, J. & Raymond, K. N. New agents for in vivo chelation of uranium(VI): Efficacy and toxicity in mice of multidentate catecholate and hydroxypyridinonate ligands. *Health Phys.* **72,** 865–879 (1997).
103. Henge-Napoli, M. H., European Communities Radiation Protection Programme. & European Late Effects Project Group. *Decorporation of radionuclides from the human body : decorporation of the actinides, caesium and cobalt and a general medical overview*. (Nuclear Technology Pub, 2000).
104. Weitl, F. L., Raymond, K. N., Smith, W. L. & Howard, T. R. Specific sequestering agents for the actinides. 1. N,N',N'',N'''-Tetra(2,3-dihydroxybenzoyl)tetraazacyclotetra- and -hexadecanes. *J. Am. Chem. Soc.* **100,** 1170–1172 (1978).
105. Weiti, F. L., Raymond, K. N., Smith, W. L. & Howard, T. R. Synthesis, structures, and thermodynamics of complexation of cobalt (III) and iron (III) tris complexes of several chelating hydroxypyridinones. *J. Am. Chem. Soc.* **24,** 954 –967 (1985).
106. W. Durbin, B. Kullgren, J. Xu, K. N, P. Multidentate hydroxypyridinonate ligands for Pu(IV) chelation in vivo : comparative efficacy and toxicity in mouse of ligands containing 1,2-HOPO or Me-3,2-HOPO. *Int. J. Radiat. Biol.* **76,** 199–214 (2000).
107. Xu, J., Chemistry, K. R.-I. & 1999, undefined. Uranyl Sequestering Agents: Correlation of Properties and Efficacy with Structure for UO22+ Complexes of Linear Tetradentate 1-Methyl-3-hydroxy-2(1H)-pyridinone Ligands. *ACS Publ.*
108. Xu, J., Franklin, S. J., Whisenhunt, D. W. & Raymond, K. N. Gadolinium complex of tris[(3-hydroxy-1-methyl- 2-oxo-1,2-didehydropyridine-4-carboxamido)ethyl]-amine: A New Class of gadolinium magnetic resonance relaxation agents. *J. Am. Chem. Soc.* **117,** 7245–7246 (1995).
109. Xu, J., Radkov, E., Ziegler, M. & Raymond, K. N. Plutonium(IV) Sequestration: Structural and Thermodynamic Evaluation of the Extraordinarily Stable Cerium(IV) Hydroxypyridinonate Complexes [1]. *Inorg. Chem.* **39,** 4156–4164 (2000).
110. White, D. L., Durbin, P. W., Jeung, N. & Raymond, K. N. Specific sequestering agents for the actinides. 16. Synthesis and initial biological testing of polydentate oxohydroxypyridinecarboxylate ligands. *J. Med. Chem.* **31,** 11–18 (1988).
111. Durbin, P. W. *et al.* Octadentate hydroxypyridinonate (HOPO) ligands for plutonium (i.v.): pharmacokinetics and oral efficacy. *Radiat. Prot. Dosimetry* **105,** 503–8 (2003).

112. Kappel, M. J., Nitsche, H. & Raymond, K. N. Specific sequestering agents for the actinides. 11. Complexation of plutonium and americium by catecholate ligands. *Inorg. Chem.* **24,** 605–611 (1985).
113. Durbin, P. W. *et al.* Chelation of 238Pu(IV) in vivo by 3,4,3-LICAM(C): effects of ligand methylation and pH. *Health Phys.* **56,** 839–55 (1989).
114. Zhu, D., Kappel, M., acta, K. R.-I. chimica & 1988, undefined. Coordination chemistry of lanthanide catecholates. *Elsevier*
115. Stradling, G. N. Decorporation of actinides: A review of recent research. *J. Alloys Compd.* **271–273,** 72–77 (1998).
116. Dosimetry, G. S.-R. protection & 1994, U. Recent progress in decorporation of plutonium, americium and thorium. *Academic.Oup.Com*
117. Stradling, G. N. *et al.* Efficacies of LICAM(C) and DTPA for the Decorporation of Inhaled Transportable Forms of Plutonium and Americium from the Rat. *Hum. Toxicol.* **5,** 77–84 (1986).
118. Stradling, G. N. *et al.* The Efficacies of Pure LICAM(C) and DTPA on the Retention of Plutonium-238 and Americium-241 in Rats after Their Inhalation as Nitrate and Intravenous Injection as Citrate. *Int. J. Radiat. Biol.* **56,** 503–514 (1989).
119. Volf, V. & Wirth, R. Effective Chelation Therapy after Incorporation of Neptunium-239 in Rats. *Int. J. Radiat. Biol. Relat. Stud. Physics, Chem. Med.* **50,** 955–959 (1986).
120. Volf, V. Chelation therapy of incorporated plutonium-238 and americium-241: Comparison of LICAM(c), DTPA and DFOA in rats, hamsters and mice. *Int. J. Radiat. Biol.* **49,** 449–462 (1985).
121. Christophe Jacopin, *,† *et al.* Investigation of the Interaction between 1-Hydroxyethane-1,1‘-diphosphonic Acid (HEDP) and Uranium(VI). *Inorg. Chem.* **42,** 5015–5022 (2003).
122. Marcin, S. *et al.* Discovery of powerful uranyl ligands from efficient synthesis and screening. *Chem. - A Eur. J.* **11,** 3689–3697 (2005).
123. Sun, X. *et al.* In vivo behavior of copper-64-labeled methanephosphonate tetraaza macrocyclic ligands. *JBIC J. Biol. Inorg. Chem.* **8,** 217–225 (2003).
124. Guo, Y., Ferdani, R. & Anderson, C. J. Preparation and Biological Evaluation of ^{64}Cu Labeled Tyr ^{3}-Octreotate Using a Phosphonic Acid-Based Cross-Bridged Macrocyclic Chelator. *Bioconjug. Chem.* **23,** 1470–1477 (2012).
125. Synthesis, Cu (II) complexation, 64 Cu-labeling and biological evaluation of cross-bridged cyclam chelators with phosphonate pendant arms. *pubs.rsc.org*
126. Gillet, R. *et al.* A Bispidol Chelator with a Phosphonate Pendant Arm: Synthesis, Cu(II) Complexation, and64Cu Labeling. *Inorg. Chem.* **56,** 11738–11752 (2017).
127. Nchimi-Nono, K. *et al.* Activated phosphonated trifunctional chelates for highly sensitive lanthanide-based FRET immunoassays applied to total prostate specific antigen detection. *Org. Biomol. Chem.* **11,** 6493–501 (2013).
128. Abada, S., Lecointre, A., Elhabiri, M. & Charbonnière, L. J. Formation of very stable and selective Cu(II) complexes with a non-macrocyclic ligand: can basicity rival pre-organization? *Dalton Trans.* **39,** 9055–62 (2010).
129. Charbonnière, L., Mameri, S., Kadjane, P., Platas-Iglesias, C. & Ziessel, R. Tuning the Coordination Sphere around Highly Luminescent Lanthanide Complexes. *Inorg. Chem.* **47,** 3748–3762 (2008).
130. Elhabiri, M. *et al.* Importance of outer-sphere and aggregation phenomena in the relaxation properties of phosphonated gadolinium complexes with potential applications as MRI contrast agents. *Chemistry* **21,** 6535–6546 (2015).
131. Heng-Napoli, M. H. *et al.* Progress and Trends in In Vivo Chelation of Uranium. *Radiat. Prot. Dosimetry* **79,** 449–452 (1998).
132. Ubios, A., Braun, E., Physics, R. C.-H. & 1994, U. Lethality due to uranium poisoning is prevented by ethane-1-hydroxy-1, 1-biphosphonate (EHBP). *europepmc.org*
133. H. Henge-Napoli, E. Ansoborlo, V. C, M. Efficacy of ethane-1-hydroxy-1, 1-bisphosphonate (EHBP) for the decorporation of uranium after intramuscular contamination in rats. *Int. J. Radiat. Biol.* **75,** 1473–1477 (1999).
134. Racine, R. Study of the complexation mechanisms of neptunium in biological environment with a view to the development of an applicable therapeutics in the case of accidental incorporation. (2001).
135. Xia, Z. & Storm, D. R. The role of calmodulin as a signal integrator for synaptic plasticity. *Nature Reviews Neuroscience* **6,** 267–276 (2005).
136. Weiss, B., Prozialeck, W., Cimino, M., Sellinger Barnette, M. & Wallace, T. L. Pharmacological Regulation of Calmodulin. *Ann. N. Y. Acad. Sci.* **356,** 319–345 (1980).
137. Anthony-Cahill, S. J. *et al.* Molecular characterization of helix-loop-helix peptides. *Science* **255,** 979–

83 (1992).
138. American Society of Biological Chemists., G. B., Rockefeller Institute for Medical Research., H. A. & American Society for Biochemistry and Molecular Biology. *The Journal of biological chemistry. Journal of Biological Chemistry* **111,** (American Society for Biochemistry and Molecular Biology, 1935).
139. Al-Shawi, M. K., Parsonage, D. & Senior, A. E. Thermodynamic Analyses of the Catalytic Pathway of FI-ATPase from Escherichia coli. *J. Biol. Chem.* **265,** 4402–4410 (1990).
140. Klee, C. B., Crouch, T. H. & Richman, P. G. Calmodulin. *Annu. Rev. Biochem.* **49,** 489–515 (1980).
141. Williams, R. J. P. Calcium and calmodulin. *Cell Calcium* **13,** 355–362 (1992).
142. Means, R., Tash, S. & Chafouleas, G. Physiological Implications of the Presence, Distribution, and Regulation of Calmodulin in Eukaryotic Cells. *Physiol. Rev.* **62,** 1–39 (1982).
143. Klee, C. B. & Vanaman, T. C. Calmodulin. *Adv. Protein Chem.* **35,** 213–321 (1982).
144. Cheung, W. Y. Calmodulin plays a pivotal role in cellular regulation. *Science* **207,** 19–27 (1980).
145. Pardoux, R. *et al.* Modulating Uranium Binding Affinity in Engineered Calmodulin EF-Hand Peptides: Effect of Phosphorylation. *PLoS One* **7,** e41922 (2012).
146. Ye, Y., Lee, H. W., Yang, W., Shealy, S. & Yang, J. J. Probing site-specific calmodulin calcium and lanthanide affinity by grafting. *J. Am. Chem. Soc.* **127,** 3743–3750 (2005).
147. Lahrouch, F. *et al.* Polyethyleneimine methylphosphonate: towards the design of a new class of macromolecular actinide chelating agents in the case of human exposition. *Dalt. Trans.* **46,** 13869–13877 (2017).
148. Sauge-Merle, S. *et al.* Structural Analysis of Uranyl Complexation by the EF-Hand Motif of Calmodulin: Effect of Phosphorylation. *Chem. - A Eur. J.* **23,** 15505–15517 (2017).
149. Brulfert, F. *et al.* Structural Environment and Stability of the Complexes Formed between Calmodulin and Actinyl Ions. *Inorg. Chem.* **55,** 2728–2736 (2016).
150. Pible, O., Vidaud, C., Plantevin, S., Pellequer, J. L. & Quéméneur, E. Predicting the disruption by UO2 2+ of a protein-ligand interaction. *Protein Sci.* **19,** 2219–2230 (2010).
151. Montavon, G., Apostolidis, C., Bruchertseifer, F., Repinc, U. & Morgenstern, A. Spectroscopic study of the interaction of U(VI) with transferrin and albumin for speciation of U(VI) under blood serum conditions. *J. Inorg. Biochem.* **103,** 1609–1616 (2009).
152. Wang, C. Y. & Huang, L. Polyhistidine Mediates an Acid-Dependent Fusion of Negatively Charged Liposomes. *Biochemistry* **23,** 4409–4416 (1984).
153. Nemirovskiy, O., Giblin, D. E. & Gross, M. L. Electrospray ionization mass spectrometry and hydrogen/deuterium exchange for probing the interaction of calmodulin with calcium. *J. Am. Soc. Mass Spectrom.* **10,** 711–718 (1999).
154. P. A. Seeger *et al.* Neutron Resonance Scattering Shows Specific Binding of Plutonium to the Calcium-Binding Sites of the Protein Calmodulin and Yields Precise Distance Information. (1997). doi:10.1021/JA9633124
155. Pible, O., Vidaud, C., Plantevin, S., Pellequer, J. L. & Quéméneur, E. Predicting the disruption by UO22+ of a protein-ligand interaction. *Protein Sci.* **19,** 2219–2230 (2010).
156. Vidaud, C., Bourgeois, D. & Meyer, D. Bone as target organ for metals: The case of f-elements. *Chemical Research in Toxicology* **25,** 1161–1175 (2012).
157. Song, Y. Y. *et al.* Biological effects of rare earth protein complexes: influence of lanthanide ions Eu3+, Tb3+ on secondary structure of calmodulins. *Biospectroscopy* **5,** 371–7 (1999).
158. Caley, E. R. The Earliest Known Use of a Material Containing Uranium. *Isis* **38,** 190–193 (1948).
159. Dioury, F., Ferroud, C., Guy, A. & Port, M. Synthesis of an hexadentate tricyclic tetraazadiacetic ligand as precursor for MRI contrast enhancement agents. *Tetrahedron* **65,** 7573–7579 (2009).
160. Galezowska, J. & Gumienna-Kontecka, E. Phosphonates, their complexes and bio-applications: A spectrum of surprising diversity. *Coord. Chem. Rev.* **256,** 105–124 (2012).
161. Gałezowska, J. *et al.* Coordination ability of trans-cyclohexane-1,2-diamine-N,N,N',N'-tetrakis(methylenephosphonic acid) towards lanthanide(III) ions. *Dalton Trans.* 4384–94 (2006). doi:10.1039/b601941b
162. Sherry, A. D., Cacheris, W. P. & Kuan, K. T. Stability constants for Gd3+ binding to model DTPA-conjugates and DTPA-proteins: implications for their use as magnetic resonance contrast agents. *Magn. Reson. Med.* **8,** 180–90 (1988).
163. Rojas-Quijano, F. a *et al.* Lanthanide(III) complexes of tris(amide) PCTA derivatives as potential bimodal magnetic resonance and optical imaging agents. *Chemistry* **15,** 13188–13200 (2009).
164. Scheytza, H., Rademacher, O. & Reißig, H.-U. Synthesis and Structures of Novel Pyridine-Bridged

Phanes of 4,4′-Bipyridine. *European J. Org. Chem.* **1999,** 2373–2381 (1999).
165. Bj⊘rnstad, V. & Undheim, K. Cyclic Ketones in Spiroannulation. *Synth. Commun.* **39,** 1793–1800 (2009).
166. Zhang, H., Wen, X., Gan, L. & Peng, Y. Highly Efficient Asymmetric Mannich Reaction of Dialkyl α-Diazomethylphosphonates with N-Carbamoyl Imines Catalyzed by Chiral Brønsted Acids. *Org. Lett.* **14,** 2126–2129 (2012).
167. Makhloufi, A., Frank, W. & Ganter, C. Diamino- and Mixed Amino–Amido-N-Heterocyclic Carbenes Based on Triazine Backbones. *Organometallics* **31,** 2001–2008 (2012).
168. Aboussafy, C. L. & Clive, D. L. J. A Dieckmann Cyclization Route to Piperazine-2,5-diones. *J. Org. Chem.* **77,** 5125–5131 (2012).
169. Perlmutter-Hayman, B. Cooperative Binding to Macromolecules. A Formal Approach. *Acc. Chem. Res.* **19,** 90–96 (1986).
170. Ischikawa. Structure and NMR behavior complex Co with aminophosphonate.pdf. (1997).
171. Ichikawa, T. & Sawada, K. Protonation Behavior and Intramolecular Interactions of α,ω-Alkanediaminepolymethylenepolyphosphonates. *Bulletin of the Chemical Society of Japan* **70,** 829–835 (1997).
172. Union, I. *et al.* COMMISSION ON EQUILIBRIUM DATA * CRITICAL EVALUATION OF STABILITY CONSTANTS OF PHOSPHONIC ACIDS ** (IUPAC Technical Report) Critical evaluation of stability constants of phosphonic acids (IUPAC Technical Report). **73,** 1641–1677 (2001).
173. Lukeš, I., Kotek, J., Vojtíšek, P. & Hermann, P. Complexes of tetraazacycles bearing methylphosphinic/phosphonic acid pendant arms with copper(II), zinc(II) and lanthanides(III). A comparison with their acetic acid analogues. *Coord. Chem. Rev.* **216–217,** 287–312 (2001).
174. Pellegatti, L. *et al.* Pyridine-based lanthanide complexes: towards bimodal agents operating as near infrared luminescent and MRI reporters. *Chem. Commun.* 6591 (2008). doi:10.1039/b817343e
175. Polyanchuk, G. V., Shkol'nikova, L. M., Rudomino, M. V., Dyatlova, N. M. & Makarevich, S. S. X-ray diffraction structural analysis of organic complexone ligands. *J. Struct. Chem.* **26,** 586–594 (1986).
176. Wozniak, M. & Nowogrocki, G. Acidites et complexes des acides (alkyl-et aminoalkyl-) phosphoniques—IV Acides aminoalkylphosphoniques R1R2N(CH2)nCR3R4PO3H2. *Talanta* **26,** 1135–1141 (1979).
177. Kiss, T., Farkas, E. & Kozowski, H. Complexes of aminophosphonates. II. Transition metal complexes of aminophosphonic acid analogues of aspartic acid and glutamic acid. *Inorganica Chim. Acta* **155,** 281–287 (1989).
178. Guerra, K. P., Delgado, R., Lima, L. M. P., Drew, M. G. B. & Félix, V. Bis- and tris-(methylphosphonic) acid derivatives of a 14-membered tetraazamacrocycle containing pyridine: synthesis, protonation and complexation studies. *Dalt. Trans.* **0,** 1812–1822 (2004).
179. Alderighi, L. *et al.* Hyperquad simulation and speciation (HySS): A utility program for the investigation of equilibria involving soluble and partially soluble species. *Coord. Chem. Rev.* **184,** 311–318 (1999).
180. Gans, P., Sabatini, A. & Vacca, A. Determination of equilibrium constants from spectrophometric data obtained from solutions of known pH: The program pHab. *Annali di Chimica* **89,** 45–49 (1999).
181. Gans, P., Sabatini, A. & Vacca, A. Investigation of equilibria in solution. Determination of equilibrium constants with the HYPERQUAD suite of programs. *Talanta* **43,** 1739–1753 (1996).
182. Drobot, B. *et al.* Combining luminescence spectroscopy, parallel factor analysis and quantum chemistry to reveal metal speciation – a case study of uranyl(vi) hydrolysis. *Chem. Sci.* **6,** 964–972 (2015).
183. Bidoglio, G., Grenthe, I. & Eliet, V. Time-Resolved Laser-Induced Fluorescence of Uranium(VI) Hydroxo-Complexes at Different Temperatures. *Appl. Spectrosc. Vol. 54, Issue 1, pp. 99-105* **54,** 99–105 (2000).
184. Eliet, V., Bidoglio, G., Omenetto, N., Parma, L. & Grenthe, I. Characterisation of hydroxide complexes of uranium(VI) by time-resolved fluorescence spectroscopy. *J. Chem. Soc. Faraday Trans.* **91,** 2275 (1995).
185. Tondre, C., Moulin, C., Laszak, I. & Moulin, V. Time-Resolved Laser-Induced Fluorescence as a Unique Tool for Low-Level Uranium Speciation. *Appl. Spectrosc. Vol. 52, Issue 4, pp. 528-535* **52,** 528–535 (1998).
186. Moulin, C., Decambox, P. P., Moulin, V. & Decaillon, J. G. Uranium Speciation in Solution by Time-Resolved Laser-Induced Fluorescence. *Anal. Chem. J. Complexation React. Aquat. Syst. Appl. Geochem. Acta Mikrochim. Acta* **67,** 348–353 (1995).
187. Arnold, P. L., McMullon, M. W., Rieb, J. & Kühn, F. E. C-H bond activation by f-block complexes.

Angew. Chemie - Int. Ed. **54,** 82–100 (2015).
188. Bell, J. T. & Biggers, R. E. The absorption spectrum of the uranyl ion in perchlorate media: Part I. Mathematical resolution of the Overlapping band structure and studies of the environmental effects. *J. Mol. Spectrosc.* **18,** 247–275 (1965).
189. Bakac, A. & Espenson, J. H. Autoxidation of Uranium(V). Catalysis and Inhibition by Copper Ions. *Inorg. Chem* **34,** 1730–1735 (1995).
190. Wang, W.-D., Bakac, A. & Espenson, J. H. Oxidation and Reduction Reactions of Hydroperoxo Cobalt Macrocycles. *Inorg. Chem.* **34,** 4049–4056 (1995).
191. Mao, Y. & Bakac, A. Photocatalytic Oxidation of Toluene to Benzaldehyde by Molecular Oxygen. *J. Phys. Chem.* **100,** 4219–4223 (1996).
192. Wang, W.-D., Bakac, A. & Espenson, J. H. Uranium(VI)-Catalyzed Photooxidation of Hydrocarbons with Molecular Oxygen. *Inorg. Chem* **34,** 6034–6039 (1995).
193. Mao, Y. & Bakac, A. Photocatalytic Oxidation of Aromatic Hydrocarbons. *Inorg. Chem.* **35,** 3925–3930 (1996).
194. King, D. M. *et al.* Synthesis and structure of a terminal uranium nitride complex. *Science (80-.).* **337,** 717–720 (2012).
195. King, D. M. *et al.* Isolation and characterization of a uranium(VI)–nitride triple bond. *Nat. Chem.* **5,** 482–488 (2013).
196. Natrajan, L. S. Developments in the photophysics and photochemistry of actinide ions and their coordination compounds. *Coordination Chemistry Reviews* **256,** 1583–1603 (2012).
197. Burrows, H. D., Kemp, T. J. & H. D. Burrows, T. J. K. The Photochemistry of the Uranyl Ion. *Chem. Soc. Rev.* **3,** 139–165 (1974).
198. Sidhu, M. S., Singh, R. J., Sarkaria, P. & Sandhu, S. S. Effect of aromatic molecules on the photochemical reduction of the uranyl ion with triphenylphosphine. *J. Photochem. Photobiol. A Chem.* **46,** 221–226 (1989).
199. Matsushima, R. Mechanism of Quenching of the Uranyl Fluorescence by Organic Compounds. *J. Am. Chem. Soc.* **94,** 6010–6016 (1972).
200. Balzani, V., Bouetta, F. & Gandolfi, M. T. Bimolecular Electron Transfer Reactions of the Excited States of Transition Metal Complexes. *Org. Chem. Theory* 1–64 (1978). doi:10.1007/BFb0048835
201. Yokoyama, Y., Moriyasu, M. & Ikeda, S. Electron transfer mechanism in quenching of uranyl luminescence by halide ions. *J. Inorg. Nucl. Chem.* **38,** 1329–1333 (1976).
202. Burrows, H. D. & De Jesus, J. D. P. A flash photolytic study of the photo-oxidation of some inorganic anions by the uranyl ion. *J. Photochem.* **5,** 265–275 (1976).
203. Burrows, H. D., Formosinho, S. J., Da, G. M. M. & Pinto, C. F. Quenching of the luminescent state of the uranyl ion by metal ions. Evidence for an electron transfer mechanism. *J. Chem. Soc., Faraday Trans. 1* **72,** 163–171 (1976).
204. Romanovskaya, G. I., Atabekyan, L. S. & Chibisov, A. K. Role of the complexation of uranyl ions in a photochemical electron-transfer reaction. *Theor. Exp. Chem.* **17,** 221–225 (1981).
205. Sakuraba, S. & Matsushima, R. Photochemical Reactions of Uranyl Ions with Organic Compounds. I. The Mechanism of the Uranyl Ion-Photosensitized Oxidation of Lactic Acid. *Bull. Chem. Soc. Jpn.* **43,** 1950–1955 (1970).
206. Roundhill, D. M. in *Photochemistry and Photophysics of Metal Complexes* 303–320 (Springer US, 1994). doi:10.1007/978-1-4899-1495-8_8
207. Burrows, H. D. & Kemp, T. J. The Photochemistry of the Uranyl Ion. *Chem. Soc. Rev.* **3,** 139–165 (1974).
208. Rehorek, D. Photokatalytische Systeme. XIV. über den Mechanismus der Photooxydation von Alkoholen mittels Uranylnitrat. *Zeitschrift für Anorg. und Allg. Chemie* **443,** 255–264 (1978).
209. Mao, Y. & Bakac, A. Uranyl-sensitized photochemical oxidation of naphthalene by molecular oxygen. Role of electron transfer. *J. Phys. Chem. A* **101,** 7929–7933 (1997).
210. Khudyakov, I. V. & Buchachenko, A. L. Unusual Uranium Isotope Effect Induced by Photolysis of Uranyl Salts in Micelles. *Mendeleev Commun.* **3,** 135–136 (1993).
211. Burrows, H. D. *et al.* The photochemical reaction between uranyl nitrate and azulene. *J. Photochem. Photobiol. A Chem.* **68,** 279–287 (1992).
212. Billing, R., Zakharova, G. V., Atabekyan, L. S. & Hennig, H. Luminescence quenching of *[UO2F4]2− in aqueous solutions by anions. *J. Photochem. Photobiol. A Chem.* **59,** 163–174 (1991).
213. Burrows, H. D. Electron transfer from halide ions to uranyl(2+) excited-state ions in aqueous solution: formation and decay of dihalide radical anions. *Inorg. Chem.* **29,** 1549–1554 (1990).

214. Buchachenko, A. L. & Khudyakov, I. V. The photochemistry of uranyl: spin selectivity and magnetic effects. *Russ. Chem. Rev.* **60,** 555–567 (1991).
215. Rosenfeld-Gruenwald, T. & Rabani, J. Quantum yield and electron-transfer reaction of the lowest excited state of uranyl ion. *J. Phys. Chem.* **84,** 2981–2985 (1980).
216. Marcantonatos, M. D. Dual luminescence of uranyl and self-quenching in aqueous acidic solution. *Inorganica Chim. Acta* **26,** 41–46 (1978).
217. Sergeeva, G. I., Chibisov, A. K., Levshin, L. V. & Karyakin, A. V. A flash photolysis study of photochemical reactions of uranyl ions. *J. Photochem.* **5,** 253–264 (1976).
218. Ryan, J. L. & Jørgensen, C. K. Electron transfer and 5f→6f transitions in uranium(iv), neptunium(iv), plutonium(iv) hexahalides. *Mol. Phys.* **7,** 17–29 (1964).
219. J. K. S. Wan, , E. A. Schuck, , J. K. Foote, and, J. N. P. J. the Formation of Tributyliodoammonium Iodide I N the Uranyl Photosensitized Reaction With Tetrabutylammonium Iodide. *J. Pet. Technol.. SAGE. Ind. Eng. Chern. M. v. Sta~kelb. H. R. MULLER. Z. Elektrochern* **4,** 1734–25 (1964).
220. Golub, D., Cohen, H. & Meyerstein, D. Kinetics and mechanism of single electron oxidations of the tervalent uranium ion, U3+(aq), by free radicals in aqueous solutions. *J. Chem. Soc. Dalt. Trans.* **0,** 641–644 (1985).
221. Cohen, H., Slama-Schwok, A., Rabani, J., Watts, R. J. & Meyerstein, D. Trication in Aqueous Solutions: A Pulse Radiolytic Study. *J. Phys. Chem* **89,** 2465–2467 (1985).
222. *Journal of inorganic and nuclear chemistry.* (Pergamon Press).
223. Neta, P., Huie, R. E. & Ross, A. B. Rate Constants for Reactions of Inorganic Radicals in Aqueous Solution. *J. Phys. Chem. Ref. Data* **17,** 1027–1284 (1988).
224. Lierse, C., Sullivan, J. C. & Schmidt5, K. H. Contribution from the Rates of Oxidation of Selected Actinides by Cl2. *Inorg. Chem* **26,** 1408–1410 (1987).
225. Geipel, G. Some aspects of actinide speciation by laser-induced spectroscopy. *Coord. Chem. Rev.* **250,** 844–854 (2006).
226. Bernhard, G. *et al.* Uranyl(VI) carbonate complex formation: Validation of the Ca2UO2(CO3)3(aq.) species. *Radiochim. Acta* **89,** 511–518 (2001).
227. Bernhard, G., Geipel, G., Brendler, V. & Nitsche, H. Uranium speciation in waters of different uranium mining areas. *J. Alloys Compd.* **271–273,** 201–205 (1998).
228. Tejedor-Tejedor, M. I. & Anderson, M. A. Protonation of Phosphate on the Surface of Goethite As Studied by CIR-FTIR and Electrophoretic Mobility. *Langmuir* **6,** 602–611 (1990).
229. Wei Jiang, *,† *et al.* Elucidation of Functional Groups on Gram-Positive and Gram-Negative Bacterial Surfaces Using Infrared Spectroscopy. (2004). doi:10.1021/LA049043+
230. Catalano, J. G. & Brown, G. E. Analysis of uranyl-bearing phases by EXAFS spectroscopy: Interferences, multiple scattering, accuracy of structural parameters, and spectral differences. *Am. Mineral.* **89,** 1004–1021 (2004).
231. Thompson, H. A., Brown, G. E., Parks, G. A., Brown Jr, G. E. & Parks, G. A. XAFS spectroscopic study of uranyl coordination in solids and aqueous solution. *Am. Mineral.* **82,** 483–496 (1997).
232. Sauge-Merle, S. *et al.* Structural Analysis of Uranyl Complexation by the EF-Hand Motif of Calmodulin: Effect of Phosphorylation. *Chem. - A Eur. J.* **23,** 15505–15517 (2017).
233. Merroun, M. L. *et al.* Complexation of uranium by cells and S-layer sheets of Bacillus sphaericus JG-A12. *Appl. Environ. Microbiol.* **71,** 5532–43 (2005).
234. Migianu-Griffoni, E. *et al.* Design and synthesis of new polyphosphorylated upper-rim modified calix[4]arenes as potential and selective chelating agents of uranyl ion. *Tetrahedron* **65,** 1517–1523 (2009).
235. Braun, O., Contino, C., Ansoborlo, E. & Pucci, B. Original articles Development of an in vitro test for screening of chelators of uranium. *Analusis* **27,** 65–68 (1999).
236. Wang, L. *et al.* A biocompatible method of decorporation: Bisphosphonate-modified magnetite nanoparticles to remove uranyl ions from blood. *J. Am. Chem. Soc.* **128,** 13358–13359 (2006).
237. Leydier, A. *et al.* Sequestering agents for uranyl chelation: new calixarene ligands. *Tetrahedron* **64,** 11319–11324 (2008).
238. Brulfert, F. thesis Mécanisme d'interaction des actinides avec une protéine : la calmoduline. (2016).
239. Brulfert, F. *et al.* Enzymatic activity of the CaM-PDE1 system upon addition of actinyl ions. *J. Inorg. Biochem.* **172,** 46–54 (2017).
240. Harris, W. R., Carrano, C. J. & Raymond, K. N. Spectrophotometric determination of the proton-dependent stability constant of ferric enterobactin. *J. Am. Chem. Soc.* **101,** 2213–2214 (1979).
241. Fitzsimmons, P., acta, S. J.-I. chimica & 1996, undefined. Helical hexaazamacrocyclic ligands

containing pyridyl and (+ or−)-trans-diaminocyclohexyl groups: effect of ligand constraints upon metal ion binding. *Elsevier*

242. Beeby, A. *et al.* Non-radiative deactivation of the excited states of europium, terbium and ytterbium complexes by proximate energy-matched OH, NH and CH oscillators: an improved luminescence method for establishing solution hydration states. *J. Chem. Soc. Perkin Trans. 2* **0,** 493–504 (1999).
243. Suib, S. L., Zerger, R. P., Stucky, G. D., Morrison, T. I. & Shenoy, G. K. The coordination environment of Eu(III) ions in hydrated A and Y zeolites as determined by luminescence lifetime and EXAFS measurements. *J. Chem. Phys.* **80,** 2203–2207 (1984).
244. Safi, S. *et al.* Thermodynamic and Structural Investigation of Synthetic Actinide-Peptide Scaffolds. *Inorg. Chem.* **55,** 877–886 (2016).
245. Runde, W., Pelt, C. Van, Compounds, P. A.-J. of A. and & 2000, undefined. Spectroscopic characterization of trivalent f-element (Eu, Am) solid carbonates. *Elsevier*
246. Patiny, L. & Borel, A. ChemCalc: A building block for tomorrow's chemical infrastructure. *J. Chem. Inf. Model.* **53,** 1223–1228 (2013).
247. Boucher, L. J. Advanced Inorganic Chemistry, Fifth Edition (Cotton, Albert F.; Wilkinson, Geoffrey). *J. Chem. Educ.* **66,** A104 (1989).
248. Pearson, R. G. Hard and soft acids and bases, HSAB, part 1: Fundamental principles. *J. Chem. Educ.* **45,** 581 (1968).
249. Pearson, R. G. Hard and soft acids and bases, HSAB, part II: Underlying theories. *J. Chem. Educ.* **45,** 643 (1968).
250. Gans, P. *Data fitting in the chemical sciences*. (Wiley, 1992).
251. Quaranta, M., Borisov, S. M. & Klimant, I. Indicators for optical oxygen sensors. *Bioanal. Rev.* **4,** 115–157 (2012).
252. Bünzli, J. claude G. The europium(III) ion as spectroscopic probe in bioinorganic chemistry. *Inorganica Chim. Acta* **139,** 219–222 (1987).

Résumé

1 Introduction générale

Lors de l'utilisation militaire et industrielle de l'uranium enrichi au milieu du XXe siècle, les propriétés de l'uranium, du plutonium et de la plupart des produits de fission n'ont pas été bien étudiées. Un grand nombre de matières radioactives produites au cours de cette période peuvent être considérées comme équivalentes à des tonnes de radium. Ainsi, avec le développement de l'industrie nucléaire, notamment les accidents industriels (Mayak, Tchernobyl, Fukushima), la manipulation et l'accumulation des actinides conduisent à considérer la dispersion, le devenir et les effets sanitaires de ces matières radioactives.

Pour ce projet, nous nous concentrons sur les ligands de chélation de synthèse pour l'uranium et l'américium/curium en utilisant l'europium comme analogue chimique.

La décorporation est la méthode dédiée à l'élimination des éléments radioactifs et toxiques qui ont été incorporés dans les organes cibles du corps humain. Les principaux traitements utilisés dans les thérapies de décorporation ont été énumérés dans le tableau 1 concernant la contamination par les actinides. Cependant, en réalité, cette stratégie se heurte à de nombreux obstacles : souvent difficiles à transférer à l'organe cible, difficiles à retirer des éléments radioactifs et toxiques déposés dans l'organe cible, liés à la complexité d'un organisme vivant. En pratique, un très bon ligand in vitro peut être totalement inefficace, et parfois même nocif, dans les évaluations in vivo.

Type d'incorporation	Traitement
Inhalation	Lavage pulmonaire Chélation sanguine (iv, ip, im)
Ingestion	Pansement gastrique Purge de précipitation
Blessé	Lavage Excision chirurgicale, Pansement Chélation sanguine (iv, ip, im)

Tableau 1：Principaux traitements utilisés dans les traitements de décorporation selon le type d'incorporation. iv, intraveineux ; ip, intrapéritonéal ; im, intramusculaire.

Ainsi, pour mieux comprendre et étudier les méthodes efficaces d'élimination des actinides déposés dans le corps humain, trois aspects fondamentaux liés à cette question doivent être étudiés : les propriétés chimiques et physiques des actinides (uranium et américium/curium dans cette étude) ; la toxicologie des actinides (uranium et américium/curium dans cette étude) ; les contre-mesures après contamination (chélation thérapeutique dans cette étude).

Les éléments actinides sont les 15 éléments chimiques de numéros atomiques 89 à 103 qui sont des éléments métalliques naturels ou artificiels. Le premier de ces éléments actinides est l'actinium et le dernier le lawrencium. La production de ces radionucléides provient principalement des accélérateurs, de la nucléosynthèse, de la mise au point d'armes nucléaires, de la désintégration des isotopes et des centrales nucléaires civiles. Les propriétés chimiques des éléments actinides sont régies par leurs sous-couches électroniques les plus externes. Les actinides sont les éléments de transition qui remplissent la sous-couche 5f. Il existe donc des propriétés uniques pour l'actinide :

- Tous les isotopes d'actinides sont radioactifs ;
- Les rayons des actinides et des cations actinides sont les plus grands ;
- Plusieurs des éléments actinides ont un grand nombre d'états d'oxydation.

Du point de vue biologique, les actinides sont en fait les éléments chimiques qui n'ont aucun effet essentiel ou bénéfique sur la vie. En raison de leur radioactivité (radiotoxique) et de leur comportement chimique (chimio-toxique), les actinides sont considérés comme toxiques. Cependant, à des niveaux environnementaux normaux, cette toxicité pourrait être gérée par le corps humain lui-même, par excrétion et/ou rétention du métal sous une forme biochimiquement inactive. Mais les essais d'armes nucléaires et l'exploitation industrielle des actinides avec des actinides, principalement

l'uranium et le plutonium, soulèvent des questions sociétales et environnementales en raison du risque de pollution et de contamination humaine. Par conséquent, la nécessité de comprendre les comportements des actinides chez l'homme est essentielle pour élucider leurs mécanismes de toxicité. Dans ce cas, la demande d'agents thérapeutiques chélateurs de l'actinide est également urgente.

Selon ces modes de contamination, la voie biologique des actinides sera différente. Il existe quatre voies d'entrée principales et quatre voies d'excrétion des actinides dans l'organisme.

Principales voies d'entrée : inhalation, ingestion, blessure et peau.

Principales voies d'excrétion : expiration, excrétion d'excréments, excrétion d'urine et transpiration.

Après une contamination externe ou interne, les actinides solubilisés pourraient être distribués aux organes cibles par la circulation sanguine. L'uranium, qui est sous forme de $[UO_2]^{2+}$ et l'américium/curium, qui sont sous forme d'Am^{3+} et de Cm^{3+}, sont transférés de préférence aux tissus du squelette, du foie et des reins et sont retenus à ces organes cibles. En raison de la chimio-toxicité et de la radiotoxicité de ces éléments, l'effet aigu sur la santé pourrait causer la mort et l'effet à long terme pourrait entraîner cancer, anémie et nécrose.

Afin de limiter les dommages séquentiels aux organes en favorisant l'excrétion des actinides, des agents chélatants ont été utilisés à cette fin. L'acide diéthylènetriaminepentaacétique (DTPA) présente une affinité particulière pour les actinides(IV), et il est actuellement utilisé en clinique en cas de contamination. Les polyphosphonates (HEDP) sont également utilisés dans les cliniques pour la décorporation de l'uranium(VI). Le 3,4,3-Li(1,2-HOPO), dérivé du sidérophore, a montré de fortes affinités pour les actinides (III), (IV), (V) et (VI). Avec le développement des agents chélatants, plusieurs propriétés de ceux-ci mettent en évidence une forte affinité et sélectivité envers les actinides, une faible toxicité, un taux d'excrétion élevé.

Les agents de décorporation sont toxiques en raison de la nature du ligand et de la grande quantité injectée pour le traitement par chélation dans un milieu biologique. Les éléments essentiels tels que le fer et le calcium sont également chélatés tout comme les actinides compte tenu de la concentration des éléments essentiels. Par conséquent, la conception de ces édifices moléculaires est nécessaire et concerne plusieurs aspects importants: 1) distribuer les agents chélatants aux organes cibles ; 2) excréter le complexe de l'élément toxique cible avec les agents chélatants par l'urine ou la bile ; 3) haute sélectivité et affinité de liaison avec l'élément toxique cible sur l'autre ion métallique pour diminuer la quantité totale des agents chélatants qui ont été injectés. Les ligands polyaminophosphonates de cette étude ont été initialement conçus pour l'imagerie par résonance magnétique (IRM) et la tomographie par émission monophotonique (TEMP). D'après l'étude SPECT sur le complexe de ligands ^{99m}Tc, une grande quantité de ^{99m}Tc avec quatre groupes de ligands phosphonés pourrait être rapidement excrétée et une partie du complexe s'accumule dans les tissus osseux après 4 h. Alors que pour le ^{99m}Tc avec deux groupes de ligands phosphonés, grâce au caractère plus lipophile, on trouvait une excrétion rapide et une rétention beaucoup moins importante dans les articulations. Les lanthanides pourraient former une liaison étroite avec quatre ligands de groupes phosphonates ayant des constantes de haute stabilité similaires à celles du DOTP, l'analogue phosphoné du DOTA. La coordination des lanthanides par le ligand des quatre groupes phosphonates est composée de 1’atome d'azote du groupe pyridine, 2 atomes d'azote des groupes amine, 4 atomes d'oxygène des groupes phosphonates et 1 atome d'oxygène des molécules d'eau. De plus, deux des groupes méthylène-phosphonate se trouvent près de ce plan du fragment pyridyle et forment une coordination au plan équatorial, les deux autres groupes méthylène-phosphonate sont placés au-dessus et au-dessous du plan moyen du fragment pyridyle. En raison de la similitude du complexe de ligands actinides avec le complexe de ligands ^{99m}Tc et le complexe de ligands lanthanides, nous avons supposé que la bio-distribution et l'excrétion possible de quatre groupes phosphonates ligands et deux groupes phosphonates ligands auraient des comportements similaires avec le complexe du ^{99m}Tc avec les ligands. Grâce à cette structure moléculaire, une sélectivité et une affinité élevées avec les actinides pourraient être atteintes. Par conséquent, l'application potentielle au traitement par chélation devrait être prometteuse.

Ce projet de thèse est une étude préliminaire sur les ligands polyaminophosphonates, une série de ligands conçus pour les agents de contraste IRM et SPECT, pour chélater les actinides qui se déposent dans les organes cibles afin d'augmenter leur excrétion.

Ce travail de doctorat s'est concentré sur la synthèse de ligands polyaminophosphonates et sur l'étude de la structure et de l'affinité de la forme complexe avec l'uranium(VI) et l'europium(III) comme analogue de l'américium/curium(III). La sphère de coordination de ces cations a été observée par spectroscopie UV-visible, TRLFS, FT-IR et EXAFS (Extended X-Ray Absorption Fine Structure). L'étude d'affinité a été réalisée par spectroscopie UV-visible et dans le cas des complexes europium, une mesure potentiométrique a été également réalisée. Enfin, la spectroscopie UV-visible et le TRLFS ont été utilisées pour tester d'une part la stabilité du complexe de ligand uranyle avec certains ions métalliques dans des conditions biologiques et d'autre part pour révéler l'interaction entre le système ternaire, ion uranyle/ligand/calmoduline.

Ce projet s'est déroulé comme suit :

- Synthétiser des ligands polyaminophosphonates capables de complexer l'uranium (VI) et l'europium (III) dans un milieu biologique.
- Caractériser les structures du complexe du ligand uranyle formé par les ligands polyaminophosphonates synthétisés. Estimer les affinités de ces complexes de ligands uranyle par rapport au 5-LICAMS et au 3,4,3-LI(1,2-HOPO), qui ont une bonne application dans le traitement par chélation. L'étude des mécanismes de compétition avec le complexe et le ligand d'uranyle calmoduline et avec le complexe et le ligand d'uranyle ligand et l'ion métallique de compétition
- Caractériser les structures de l'europium (comme analogue de américium/curium) complexe ligand formé par des ligands polyaminophosphonates synthétisés.

2 Synthèse de ligands polyaminophosphonates

Le ligand pour le contraste de l'IRM qui a fait l'objet d'études approfondies est un candidat prometteur. Ces ligands, de masse moléculaire comprise entre 300 et 600, pourraient fournir une coordination 7-8 pour le lanthanide et avoir une affinité de complexation vraiment forte. De plus, l'excrétion du complexe de ligands métalliques est assez rapide, de quelques heures à quelques jours. La toxicité est relativement faible.

Parmi tous les ligands de contraste de l'IRM, les ligands polyaminophosphonates ont été choisis pour cette étude. La synthèse des ligands polyaminophosphonates a été développée par le groupe de Loïc Charbonniaire de l'IPHC. L'idée principale est d'utiliser des groupes phosphonés ayant un caractère de base dure et une charge négative élevée pour fonctionnaliser les positions 2 et 6 de la pyridine. De cette façon, la stabilité du complexe uranyle-ligand pourrait être augmentée.

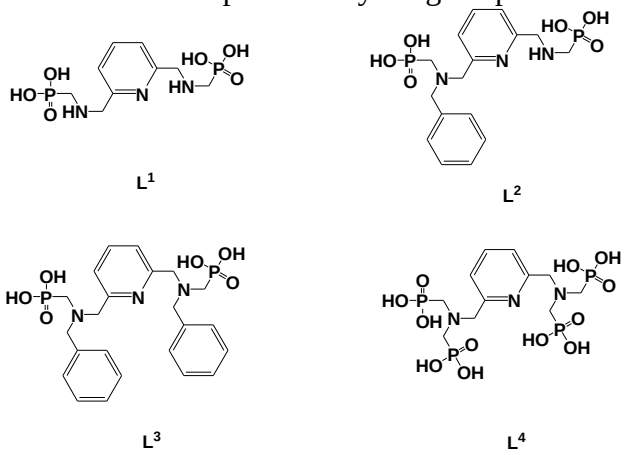

Figure 1 : Structure chimique des ligands L^1, L^2, L^3 et L^4.

Pour obtenir les ligands polyaminophosphonates **L^1-L^3** (Figure 1), il faut une synthèse préalable de la plateforme pyridinique **1** qui porte les bras phosphonates (Figure 2). Les précurseurs des bras phosphonés sont les composés **3** et **5** (Figure 2).

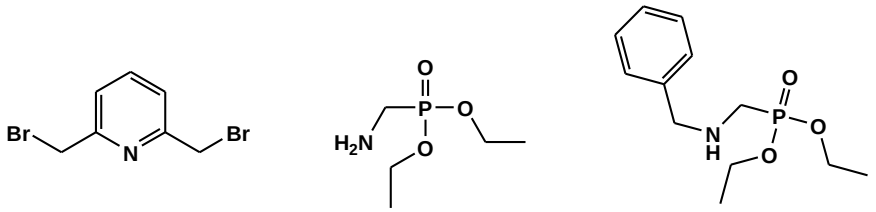

1 **3** **5**

Figure 2 : Structure chimique des précurseurs.

La synthèse du ligand bis-phosphoné $\mathbf{L^1}$, $\mathbf{L^2}$ et $\mathbf{L^3}$ (Schéma 1) a été adaptée à partir de préparations connues de ligand pyridine phosphoné. $\mathbf{L^2}$ et $\mathbf{L^3}$ ont été obtenus par bromation de la 2,6-dihydroxyméthylpyridine **1** disponible dans le commerce avec PBr_3 à 0 °C, donnant 2,6-dibromométhylpyridine (95%). Le diéthyl ((benzylamino)méthyl)phosphonate **3** a été obtenu à partir de benzylamine en deux étapes (schéma 1). On a ajouté du formaldéhyde à une solution agitée de benzylamine pour obtenir de la 1,3,5-Tribenzylhexahydrotriazine **2** (91%). Le composé **3** désiré (42%) a été synthétisé par réaction avec du diéthylphosphite. La réaction N-alkylation de 1 avec 3 a donné naissance au composé bisphosphoné **4** (79%) qui a donné le ligand $\mathbf{L^1}$ (9%), $\mathbf{L^2}$ (13%) et $\mathbf{L^3}$ (52%) après hydrolyse des groupes phosphonates par 6M HCl.

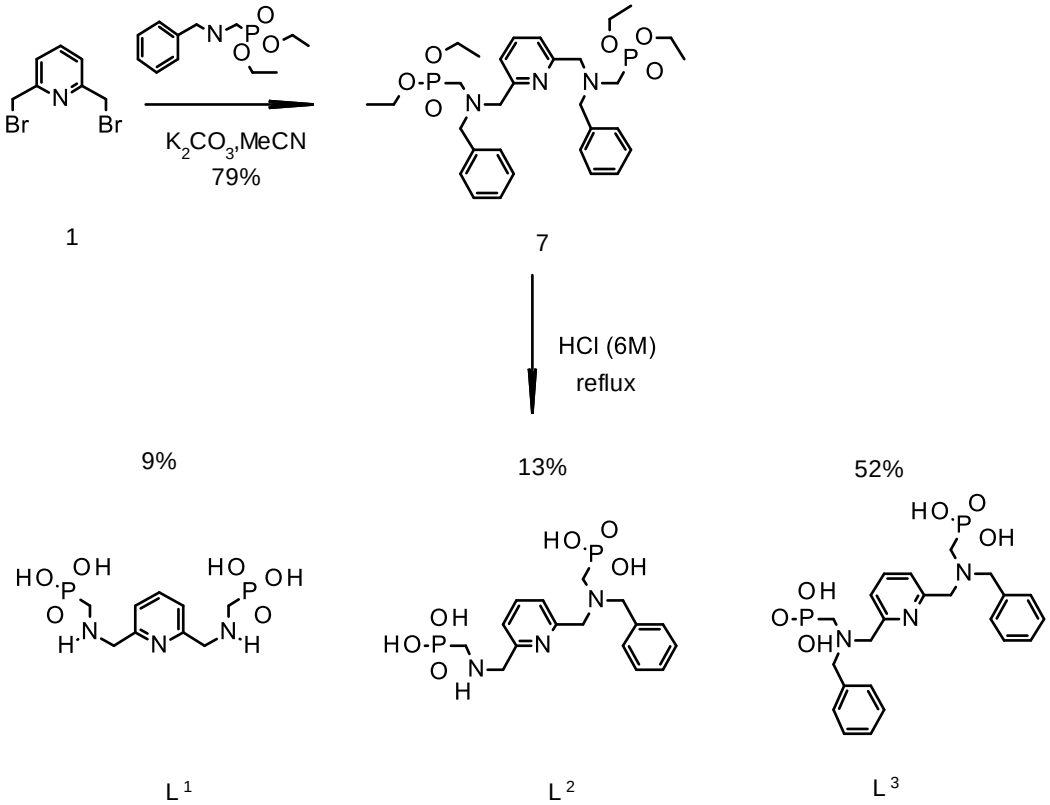

Schéma 1 : Voie synthétisée des ligands bisphosphonate.

3 Étude structurale et thermodynamique de l'uranyle avec des ligands polyaminophosphonates

Après la caractérisation du ligand, l'étude d'interaction de l'uranyle et des ligands a été réalisée à pH 3 et 7,4.

L'étude du complexe uranyle- $\mathbf{L^3}$ se déroule en 3 étapes à pH 3, l'uranyle étant principalement complexé par ion chlorure dans la première étape (0-0,2eq). Pour la deuxième étape (0,2-0,6eq), l'espèce principale est le complexe uranyle avec des groupes phosphonates de deux L3. L'espèce dominante est le complexe d'uranyle avec $\mathbf{L^3}$ dans la partie interne du ligand pour la troisième étape

(0,6-1 éq.).

L'étude du complexe uranyle- **L^4** se déroule en deux étapes à pH 3 : il s'agit principalement d'un complexe uranyle avec des groupes phosphonates de **L^4** dans la première étape (0-0,2eq). Pour la deuxième étape (0,2-1 éq), l'espèce dominante est le complexe uranyle avec **L^4** dans la partie poche.

Les ligands organiques monophosphonates protonés limitent l'affinité de complexation de l'uranyle à faible concentration. L'effet stérique de deux groupes benzyle de **L^3** pourrait limiter la liberté de coordination avec l'uranyle.

Pour le complexe uranyle-ligand 1:1, les environnements de l'ion uranyle sont les mêmes pour les deux ligands, **L^3** et **L^4**. La coordination se compose de deux atomes d'oxygène provenant de groupes phosphonates monodentés, d'un atome d'azote provenant du groupe pyridine et de deux atomes d'azote provenant des parties amine.

A pH 7,4, les deux voies de dégradation sont minimisées par la mesure par le complexe uranyl-ligand non-fluorescent. Pour les deux ligands, l'ion uranyle est directement complexé avec le ligand. Il n'y a qu'une seule espèce dans toute l'étude. Les ligands organiques phosphonates déprotonés sont plus faciles à complexation avec l'ion uranyle. L'environnement de coordination du complexe uranyle-ligand peut être le même selon la propriété de non-fluorescence.

Pour le complexe uranyle-ligand 1:1, les environnements de l'ion uranyle sont les mêmes pour les deux ligands, **L^3** et **L^4**. La coordination se compose de deux atomes d'oxygène provenant de groupes phosphonates monodentés, un hydroxyde, un atome d'azote provenant du groupe pyridine et deux atomes d'azote provenant des parties amine. En raison de la présence d'hydroxyde dans la coordination à pH 7,4, l'ion uranyle se déplace en avant du groupe pyridine. La stoechiométrie des complexes uranyle-ligand à pH 7,4 est de 1:1 à 0-1 éq uranyle.

Les constantes de complexation des ligands (Kconcd) sont 17,08 pour **L^2** et 15,2 pour **L^3** à pH 7,4. Une comparaison a été effectuée avec le 5-LICAMS et le 3,4,3-LI(1,2-HOPO), qui sont des ligands bien connus et qui présentent des capacités d'élimination de l'uranyle *in vivo*. Les constantes de complexité sont 17 pour le 5-LICAMS et 16,87 pour le 3,4,3-LI(1,2-HOPO). Ainsi, les ligands polyaminophosphonates, synthétisés dans cette étude, ont des constantes de complexation similaires aux deux ligands cités. Le complexe uranyle- **L^3** présente une bonne stabilité face au calcium et au magnésium. Le test d'affinité par chélation avec les protéines a montré que l'ion uranyle a été soustrait de la calmoduline par 1eq **L^3** en 15 minutes, ce qui permet d'envisager des applications potentielles de décorporation d'uranium.

Les ligands bis-phosphonés ont donc de fortes affinités de complexation et une bonne stabilité avec l'ion uranyle dans des conditions biologiques grâce à la bonne conception des agents chélatants.

4 Étude thermodynamique de l'europium avec des ligands polyaminophosphonates

En raison de l'activité massique élevée de l'Am/Cm(III), Eu(III) a été utilisé comme analogue chimique pour effectuer les études. En raison de la faible solubilité du complexe Eu- **L^3** dans 0,1M $NaClO_4$, l'étude de la constante thermodynamique a échoué.

Une combinaison similaire du spectre d'absorption UV-Vis et de l'étude TRLFS a été réalisée pour le complexe Eu- **L^3** et le complexe Eu- **L^4** à pH 3, 5 et 7,4. En raison de l'hydrogène sur les parties amines, l'ion Eu(III) est complexé avec des groupes phosphonate de ligand à faible pH, tandis qu'à pH élevé, l'ion Eu(III) est situé dans la partie interne du ligand en raison de la diminution de la concentration en hydrogène.

Le spectre EAXFS obtenu a été ajusté en utilisation la contribution de molécules d'eau et de groupes fonctionnels de ligands. Pour le complexe Eu- **L^3** à pH 3, la contribution du ligand provient uniquement des groupes phosphonates. Pour le complexe Eu-**L^4** à pH 7,4, il n'a pas été possible de procéder à l'ajustement, ce qui pourrait être dû à la dégradation du complexe Eu-**L^4** sous le faisceau.

5 Perspectives

Ce projet est la première étape dans le développement d'agents chélatants polyaminophosphonés

à base de pyridine pour la décorporation des actinides. Il reste encore beaucoup d'études à étudier et à caractériser.

- Constantes de formation de l'ion uranyle avec **L²**, **L³** et **L⁴**: l'étude de la constante de formation pourrait être réalisée par titrage potentiométrique dans 0,1M NaCl avec protection Ar et sans lumière;

- Constantes de formation d'autres actinides avec **L²** et **L³** dans 0,1M NaClO4 : les constantes de formation pourraient être réalisées par titrage potentiométrique dans 0,1M $NaClO_4$ avec d'autres actinides. Les résultats pourraient donner une idée de l'affinité de complexation de l'europium avec **L²** et **L³** en raison de la similitude des lanthanides ;

- Toxicité des agents chélatants polyaminophosphonés à base de pyridine ;

- Le traitement par chélation au moyen d'agents chélatants à base de pyridine polyaminophosphonée pour séquestrer les actinides afin de prévenir les effets aigus et les effets à long terme ;

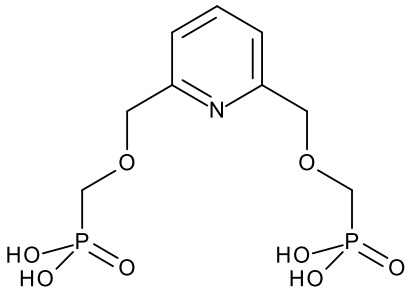

Figure 3 : Structures du ligand pyridine bis-phosphoné

- La synthèse d'un nouveau ligand pyridine bis-phosphoné (Figure 3) pour les agents chélatants de l'uranium par remplacement de l'azote des parties amines par l'oxygène : la présence d'hydroxyde de coordination uranyle à pH 7,4 peut dépendre des 3 atomes d'azote qui peuvent être définis comme donneur intermédiaire ou donneur mou. En utilisant de l'oxygène, 4 donneurs durs pourraient être dans la coordination uranyle. La stabilité de l'uranyle avec le nouveau ligand pourrait ainsi être plus élevée.

Titre : Etudes thermodynamiques et structurales des interactions entre les actinides et des ligands à base de phosphonate

Mots clés : Thermodynamique; Structure; Actinides; Ligands à base de phosphonate; Chelation ; Décorporation

Résumé: En cas d'accidents nucléaires (Tchernobyl, Fukushima) ou d'exopsition à de l'uranium appauvri dans des zones de conflit, la décontamination est nécessaire pour réduire au mieux les conséquences de l'ingestion de radionucléides. Après une contamination externe ou interne, les actinides solubilisées sont distribués dans les organes cibles (squelette, foie, tissus, reins, etc.) *via* la circulation sanguine. Compte tenu de cette dispersion, la chélation de ces radionucléides par des ligands biologiques est une méthode efficace de décorporation pour favoriser l'excrétion de ces métaux déposés et ainsi réduire les risques pour la santé.

En raison du faible taux de distribution dans les organes cibles (os, foie, reins) de l'acide diéthylènetriaminepentaacétique (DTPA), des agents de chélation ont été synthétisés et testés *in vitro* ou *in vivo*. Dans ce projet, plusieurs ligands polyaminophosphonates, (conçus à l'origine pour être des agents de contraste), ont été synthétisés selon leurs propriétés de bio-distribution, de leurs groupes fonctionnels, de leur potentiel site de coordination et de leur lipophilie. Des études structurales et thermodynamiques ont ensuite été effectuées sur les complexes entre l'uranium (VI) et l'europium (III) (comme analogue de l'américium (III) et curium (III)) et les ligands polyaminophosphonates. La sphère de coordination de ces cations a été observée par spectroscopie UV-visible, TRLFS, FT-IR et la spectroscopie d'absorption X (EXAFS). L'étude de l'affinité a été réalisée par spectroscopie UV-visible. Enfin, les spectroscopies UV-visible et TRLFS ont été utilisées d'une part pour tester la stabilité du complexe ligand/uranyle en présence d'un ion métallique et d'autre part pour étudier le système ternaire : ion uranyle/ligand/calmoduline.

Ces résultats ont permis de mieux comprendre les mécanismes de chélation et d'évaluer l'affinité chimique de ces ligands polyaminophosphonates pour l'uranium (VI) et l'europium (III). Cela devrait ainsi aider à la conception de nouveaux agents de chélation de plus en plus efficaces du point de vue de la décorporation.

Université Paris-Saclay
Espace Technologique / Immeuble Discovery
Route de l'Orme aux Merisiers RD 128 / 91190 Saint-Aubin, France

Title : Thermodynamic and structural investigations on the interactions between actinides and phosphonate-based ligands

Keywords : Thermodynamic; Structural; Actinides; Phosphonate-based ligands; Chelation; Decorporation

Abstract : For exposed person who suffers from contamination of nuclear accidents (Chernobyl, Fukushima) or depleted uranium in war zones, decontamination is required to reduce the sequence damage of radionuclide intake. After an external or internal contamination, the solubilized actinides could be distributed to the target organs (skeletal, liver, kidneys tissues, etc.) *via* the bloodstream. Actinides are radio-toxic and chemo-toxic elements. Considering the dispersion, fate and health effect of the actinides, chelation therapy is an effective decorporation method to promote the excretion of deposited actinides to reduce the health risk.

Due to the defect on weak distribution rate to the target organs (bone, liver, kidneys) of diethylenetriaminepentaacetic acid (DTPA) which currently used in clinics, plenty chelation agents were synthesized and tested *in vitro* or *in vivo*. In this project, several polyaminophosphonates ligands, a series ligand originally designed for MRI contrast and SPECT agents, were synthesized according to the properties of ligand bio-distribution, functional groups, coordination site and lipophilic. Then the structural and thermodynamic studies were done with the complexes between metal ion such as uranium(VI) and europium(III) (as americium/curium(III) analogue), and polyaminophosphonates ligands. The sphere of coordination of these cations was observed by UV-visible spectroscopy, TRLFS, FT-IR and Extended X-Ray Absorption Fine Structure (EXAFS). The affinity study was done with UV-visible spectroscopy. Finally, the UV-visible spectroscopy and TRLFS were used to test the stability of uranyl ligand complex with competition metal ion in biological conditions and to reveal the interaction between the ternary system, uranyl ion/ligand/calmodulin. These results allow to better understand the chemical affinity and possible chelation mechanism of the polyaminophosphonates ligands for the above actinides and therefore to promote the design of new chelation agents.

Université Paris-Saclay
Espace Technologique / Immeuble Discovery
Route de l'Orme aux Merisiers RD 128 / 91190 Saint-Aubin, France